#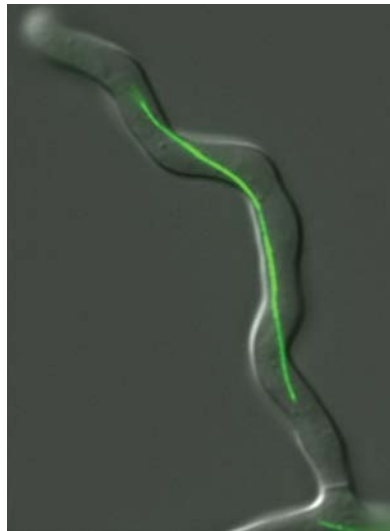 On the role of the kinesin-3 motor protein UncA and the role of different microtubule populations in the filamentous fungus *Aspergillus nidulans*

Zur Erlangung des akademischen Grades eines

DOKTORS DER NATURWISSENSCHAFTEN

(Dr. rer. nat.)

Fakultät für Chemie und Biowissenschaften

Karlsruher Institut für Technologie (KIT) - Universitätsbereich

genehmigte

DISSERTATION

von

Dipl. Biol. Nadine Zekert

aus

Damaskus - Syrien

Die vorliegende Arbeit wurde in der Zeit vom 01. September 2006 bis 30. Dezember 2009 im institut für Angewandte Biowissenschaften, Abteilung Mikrobiologie des Instituts für Technologie Karlsruhe (KIT) unter der Betreuung von Herrn Prof. Dr. Reinhard Fischer durchgeführt.

Tag der Abgabe der Arbeit: 24. Oktober 2011

Ich versichere, dass ich meine Dissertation mit dem Titel "On the role of the kinesin-3 motor protein UncA and the role of different microtubule populations in the filamentous fungus *Aspergillus nidulans*" selbständig, ohne unerlaubte Hilfe angefertigt und mich dabei keiner anderen als der von mir ausdrücklich bezeichneten Quellen und Hilfen bedient habe.

Die Dissertation wurde in der jetzigen oder einer ähnlichen Form noch bei keiner anderen Hochschule eingereicht und hat noch keinen sonstigen Prüfungszwecken gedient.

Karlsruhe,   den 24. 10. 2011

Nadine Zekert

Im Rahmen dieser Dissertation entstanden folgende Publikationen:

A)   Original publication

Zekert, N.*, Enke, C.*, Veith, D.*, Schaaf C., Konzack, S., Fischer, R. (2007): *Aspergillus nidulans* Dis1/XMAP215 protein AlpA localizes to spindle pole bodies and microtubule plus ends and contributes to growth directionality
* Equal contribution
Eukaryotic Cell **6, 555-562.**

Zekert, N. & Fischer, R. (2009): The *Aspergillus nidulans* kinesin-3 UncA motor moves vesicles along a subpopulation of microtubules.
Molecular Biology of the Cell **20, 673-684.**
(To InCytes from the MBC selection & Journal Cover 15.01.09)

Zekert, N.*, Veith, D.*, Fischer, R. (2010): Interaction of the *Aspergillus nidulans* MTOC component ApsB with gamma-tubulin and evidence for a role of a subclass of peroxisomes in the formation of septal MTOCs
* Equal contribution
Eukaryotic Cell **9, 795-805.**

B)   Review

Fischer, R., Zekert, N. & Takeshita, N. (2008): Polarized growth in fungi – interplay between the cytoskeleton, positional markers and membrane domains
Molecular Microbiology **68, 813-826.**

Pour mes anges, Papa et Maman,

TABLE OF CONTENT

I.   Abbreviations

alcA(p)	alcohol dehydrogenase promoter
APS	Ammonium persulfate
BiFC	Bimolecular Flourescence Complementation Assay
BSA	Albumine bovine Fraction V
CM	Complete medium
DAPI	4',6-Diamidino-2-phenylindole
DIG	Digoxygenin
EDTA	Ethylenediamine tetraacetic acid
gpd(p)	Glycerinaldehyde-3-Phosphate-Dehydrogenase promoter
HA	Hemagglutinin epitope
IPTG	Isopropyl-β-D-thiogalactopyranoside
LB	Luria-Bertani-Medium
MM	Minimal medium
MTOC	Microtubule Organizing Centre
OM	Osmotic medium
PAGE	Poly-Acrylamid-Gel-Electrophoresis
PEG	Polyethylene glycol
PH	Pleckstrin-Homology Domain
PTS	Peroxisomal Targeting Sequence
RNase	Ribonuclease
TAE	Tris-Acetate-EDTA
TBS-T	Tris-Buffered Saline-Tween 20
TE	Tris-EDTA
TEMED	N, N, N', N'-Tetramethylene diamine
WT	Wild-type
X-Gal	5-Brom-4-chlor-3-indoxyl-β-D-Galactoside

II.   Summary

The extremely polarized growth form of filamentous fungi imposes a huge challenge on the cellular transport machinery, as proteins and lipids required for hyphal extension have to be continuously transported to the growing tip. The transport depends on the actin and the microtubule (MT) cytoskeleton along with their associated motor proteins, myosin, kinesin and dynein. *Aspergillus nidulans* contains eleven different kinesins, two of which (named UncA and UncB) belong to the kinesin-3 family (formerly Unc-104). Previously it was shown that *A. nidulans* conventional kinesin (kinesin-1), KinA, is required for vesicle transportation and normal hyphal growth, and the kinesin-7, KipA, for the maintenance of hyphal polarity. Here it was found that the *A. nidulans* kinesin-3 motor protein UncA transports vesicles along microtubules (MTs) and is required for hyphal extension. Most surprisingly, UncA-dependent vesicle movement occurred along a subpopulation of MTs. The second kinesin-3 member, UncB, localized to nuclei, MTs and septa in a cell-cycle dependent manner, but the exact role of UncB remained still unclear.

The MT cytoskeleton is not as rigid and uniform as the name implies, but is characterized by its dynamic instability. In addition, MTs can be made up of different tubulin isoforms and can be post-translationally modified. MT modifications, such as acetylation or polyglutamylation are evolutionarily old "inventions" and occur in primitive eukaryotes such as *Giardia lamblia*, whereas detyrosination appeared later during evolution. Although many modifications were discovered more than 20 years ago, their cellular functions are not well understood yet. Here, it was discovered that in the filamentous fungus *A. nidulans* at least two different MT populations exist. A UncA^{rigor} mutated protein with a point mutation at the ATPase site of the motor has been created. The UncA^{rigor} still binds MTs but cannot move along them. Hyphae of *A. nidulans* consist of multinucleated compartments, in which a few MT bundles run along the longitudinal axis of the hyphae. GFP labelled UncA^{rigor} decorated a single MT bundle, which remained intact during mitosis, while other cytoplasmic MTs were depolymerised. Mitotic spindles were not labelled with GFP-UncA^{rigor} but reacted with a specific antibody against tyrosinated alpha-tubulin. This antibody did not label the stable MTs outside the mitotic nuclei suggesting that these MTs are detyrosinated. UncA appears to bind preferentially to detyrosinated MTs. In contrast, conventional kinesin (kinA) and kinesin-7 (KipA) did not show a preference for certain MTs. This is the first example for different MT subpopulations in filamentous fungi and the first example for the preference of a kinesin-3 motor for detyrosinated MTs.

The modified MT connects all nuclei and septa along the hyphal axis. In order to understand better the organization of *A. nidulans* MTs, the origin of MTs, the MT organizing centers (MTOC) have been studied. Eukaryotic cells assemble MTs from distinct points in

the cell. In the fungus *A. nidulans*, localization studies revealed that not only spindle-pole bodies (SPB) act as MTOCs, but also that MTOCs are located at septa. Septum-associated MTOCs (sMTOCs) are also very active. Previously a novel MTOC-associated protein, ApsB (*Schizosaccharomyces pombe* Mto1), has been identified, whose absence affected MT formation from sMTOCs more than from SPBs, suggesting different organization of the two protein complexes. Here, it was shown that sMTOCs share at least two further components, gamma-tubulin and GcpC (*S. pombe* Alp6) with SPBs and that ApsB physically interacts with gamma-tubulin. In addition, it was discovered that ApsB interacts with the Woronin body protein HexA and is targeted to a subclass of peroxisomes via a PTS2 peroxisomal targeting sequence. The PTS2 motif was necessary for function, but could be replaced by a PTS1 motif at the C-terminus of ApsB. Those results suggest an interesting novel function of a subclass of peroxisomes involved in MT organization.

II. Zusammenfassung

Das extreme polare Wachstum von filamentösen Pilzen ist eine große Herausforderung für das zelluläre Transportsystem, da kontinuierlich Proteine und Lipide für die Hyphenverlängerung zur wachsenden Spitze transportiert werden müssen. Der Transport ist von Aktin und dem Mikrotubuli (MT) Zytoskelett mit den assoziierten Motorproteinen, Myosin, Kinesin und Dynein abhängig. *Aspergillus nidulans* besitzt elf verschiedene Kinesine, von denen zwei (UncA und UncB) zur Kinesin-3 Familie (zuvor Unc-104) gehören. Zuvor wurde gezeigt, dass das *A. nidulans* Kinesin-1 KinA für den Vesikeltransport und damit für schnelles Hyphenwachstum benötigt wird. Das Kinesin-7 KipA ist für die Bestimmung der Wachstumsrichtung wichtig. In dieser Arbeit wurde herausgefunden, dass das *A. nidulans* Kinesin-3 Motorprotein, UncA, Vesikel entlang von MT transportiert und ebenfalls für das Hyphenwachstum benötigt wird. Erstaunlicherweise findet die UncA-abhängige Vesikelbewegung entlang einer Subpopulation von MT statt. Das zweite Kinesin-3 Motorprotein, UncB, lokalisiert Zellzyklus-abhängig in Zellkernen, entlang von MTs und an Septen. Die exakte Rolle von UncB und die Funktion der interessanten, dynamischen Lokalierung des Proteins sind noch nicht abschliessend geklärt.

Das MT Zytoskelett ist nicht so starr und einheitlich wie der Name vermuten lässt, sondern ist durch seine dynamische Instabilität charakterisiert. Zusätzlich können MT aus unterschiedlichen Tubulinisoformen aufgebaut sein und post-translational modifiziert werden. MT-Modifizierungen, wie Acetylierung oder Polyglutamierung sind alte „Erfindungen" in der Evolution und finden bereits in primitiven Eukaryoten wie *Giardia lamblia* statt. Dagegen taucht die Detyrosinierung erst später in der Evolution auf. Obwohl viele Modifizierungen vor mehr als 20 Jahren entdeckt wurden, ist ihre zelluläre Funktion bis heute noch nicht vollständig verstanden. In dieser Arbeit wurde gezeigt, dass in *A. nidulans* mindestens zwei verschiedene MT Populationen existieren. Ein UncA^rigor mutiertes Protein wurde durch Einführung einer Punktmutation an der ATPase Stelle des Motors hergestellt und in *A. nidulans* eingebracht. UncA^rigor kann zwar an MT binden, sich aber nicht an ihnen entlang bewegen. Die mehrkernigen Kompartimente der Hyphen von *A. nidulans* werden ihrer Länge nach von einer kleinen Anzahl von MT-Bündeln durchquert. Nur an einem dieser MT-Stränge konnte GFP-markiertes UncA^rigor nachgewiesen werden. Dieses Bündel blieb auch während der Mitose intakt, während andere cytoplasmatische MT depolymerisierten. Die Mitosespindeln wurden nicht mit GFP-UncA^rigor dekoriert, sie reagierten jedoch mit einem spezifischen Antikörper gegen tyrosiniertes alpha-Tubulin. Dieser Antikörper wiederum reagierte nicht mit den MT, die während der Mitose im Cytoplasma intakt blieben. Diese Ergebnisse deuten darauf hin, dass UncA bevorzugt an detyrosinierte MT bindet. Im

Gegensatz dazu zeigen sowohl konventionelles Kinesin (KinA) als auch Kinesin-7 (KipA) keine Präferenz für bestimme MT. Dies ist das erste Beispiel für das Vorhandensein von verschiedenen Subpopulationen von MT in filamentösen Pilzen und zugleich der erste Hinweis auf die Spezifität eines Kinesin-3 Motors gegenüber detyrosinierten MTs.

Die modifizierten MT verbinden alle Zellkerne und Septen einer Hyphe. Zum besseren Verständis des Aufbaus und der Organisation der MT wurden die MT-organisierenden Zentren (MTOCs) untersucht. In *A. nidulans* gibt es MTOCs nicht nur am Spindelpolkörper (SPB), sondern auch an den Septen. Diese Septum-assoziierten MTOCs (sMTOCs) sind auch sehr aktiv. In vorangegangenen Versuchen wurde das Protein ApsB (*Schizosaccharomyces pombe* Mto1) als ein neues MTOC-assoziiertes Protein beschrieben. ApsB hat einen größeren Einfluss auf die Bildung von MTs an Septen als auf deren Entstehung an den SPB. Dies lässt darauf schließen, dass es sich um unterschiedliche Proteinkomplexe handelt, die teilweise getrennt voneinander reguliert werden. In dieser Arbeit wurden zwei weitere Komponenten gefunden, die sowohl in sMTOCs als auch in den SPB vorkommen: gamma-Tubulin und GcpC (*S. pombe* Alp6). Außerdem wurde eine direkte Interaktion von ApsB mit gamma-Tubulin nachgewiesen. Zusätzlich konnte gezeigt werden, dass ApsB mit dem Woronin body Protein HexA interagiert und aufgrund seiner PTS2 (peroxisomal targeting sequence) in Peroxisomen importiert wird. Das PTS2 Motiv war für die Funktion des Proteins notwendig, konnte jedoch durch ein PTS1 Motiv am C-Terminus von ApsB ersetzt werden. Diese Ergebnisse deuten auf eine bisher unbekannte Population der Peroxisomen hin, die an der Mikrotubuli-Entstehung beteiligt ist.

III. Introduction

Polarized cell growth and division are essential processes of living organisms (Macara & Mili, 2008). In single cell yeasts, such as *Saccharomyces cerevisiae* and *Schizosaccharomyces pombe*, polarized growth is restricted to certain times during the cell-cycle, whereas in filamentous fungi, such as *Aspergillus nidulans* or *Neurospora crassa*, cell extension is a continuous and indefinite process (Pringle *et al.*, 1995; Riquelme *et al.*, 2003; Snell & Nurse, 1994). Microtubules (MTs) play fundamental roles in cell growth and division, together with filamentous actin (F-actin) and their associated motor proteins, kinesin, dynein and myosin. Together they provide the cell with a dynamic network called cytoskeleton. *A. nidulans* and other filamentous fungi have served as model organisms for many genetic, biochemical and cell biological approaches, providing keys for the understanding of MT function and the organization of different cytoskeletal-related processes. Since hyphal extension in filamentous fungi depends on the continuous synthesis of cell wall and on a continuous fusion of vesicles with the membrane, microtubules and actin, which serve as tracks for vesicles, have to be oriented properly in the cell **(Figure III. 01)**.

The control of fungal filamentous growth is important to prevent infections or to protect food from fungal spoilage. Thus, a detailed understanding of polarized growth may lead to the identification of targets for new antifungal drugs or fungicides. A second important aspect is that filamentous fungi are widely used in biotechnology. It is assumed that heterologously-produced hydrolytic enzymes are secreted through the same machinery as the enzymes required for polarized growth (Pel *et al.*, 2007; Seiler *et al.*, 1997). The understanding of the molecular components might help to increase the production of secreted enzymes or open up new accesses for the production of heterologous proteins.
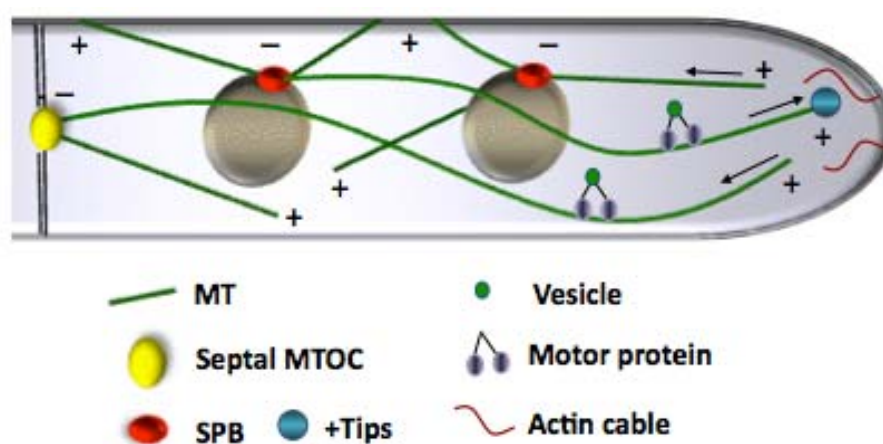
Figure III. 01. Scheme of microtubule organization in the hyphal tip of *A. nidulans*

To gain further insights into the filamentous growth network and dynamics, the role of the MT cytoskeleton and several kinesins have been studied, and their interplay with other proteins has been investigated in our laboratory. It becomes clear that many proteins and structures act together to maintain polarized growth in filamentous fungi.

1.   **The microtubule cytoskeleton**

Microtubules are hollow tubes composed of a lattice of $\alpha\beta$-tubulin heterodimers. They are 25 nm in outer diameter with a 17 nm interior space diameter (Hawkins *et al.*, 2009). Different models were developed to explain the way in which tubulin heterodimers polymerize a MT. The most popular models are the "template model" and the "protofilament model". In the template model the basis is made by a ring structure of 13 γ-tubulins where $\alpha\beta$-heterodimers bind and polymerize MTs (Oakley *et al.*, 1990; Zheng *et al.*, 1995), whereas in the protofilament model γ-tubulin build a short helix with short filament, and tubulin heterodimers stack end-to-end to form protofilaments. 13 protofilaments bind laterally to form sheets that are rolled into a tube (Erickson & Stoffler, 1996; Hirose & Amos, 2007; Meurer-Grob *et al.*, 2001). MTs grow and shrink in a tread-milling manner if they are polymerized *in vitro*. In contrast, MTs are rather stable at the minus end *in vivo* and are dynamic mainly at the plus end where the $\alpha\beta$-tubulins can be added or removed, this exhibits alternating rounds of growth and shrinkage (Desai & Mitchison, 1997; Fischer *et al.*, 2008; Mitchison & Kirschner, 1984). The elongation rate depends on the concentration of $\alpha\beta$-tubulin dimers in the cell. Both tubulin subunits contain a GTP bound, the one of α subunits is stable whereas the one of β subunits can undergo hydrolysis and causes MT catastrophe (Heald & Nogales, 2002; Nogales *et al.*, 1998).

All tubulin genes were first discovered in *A. nidulans* (Morris *et al.*, 1979; Oakley, 2004; Sheir-Neiss *et al.*, 1978). *A. nidulans* harbors two α-tubulins (*tubA*, *tubB*), two β-tubulins (*benA*, *tubC*) and one γ-tubulin (*mipA*) **(Table III. 01)**. Mutations in *tubA* were identified as suppressors of a temperature sensitive benA mutation (Oakley *et al.*, 1987). Molecular disruption of the *tubA* gene leads to a mitotic block in vegetative cells (Doshi *et al.*, 1991), while disruption of the other α-tubulin gene, *tubB*, leads to a block in meiosis (Kirk & Morris, 1991). *tubA* encodes the major vegetative tubulin protein while *tubB* is highly expressed during sexual development, so the most likely reason for the differences in phenotype is differential expression, rather than any major functional difference (Kirk & Morris, 1993). The *ben*A gene encodes two β-tubulin polypeptides and is expressed preferentially (Sheir-Neiss *et al.*, 1976; Sheir-Neiss *et al.*, 1978) and the other β-tubulin gene (tubC) plays a specialized but non-essential role in conidiation (May *et al.*, 1985; Weatherbee

et al., 1985). Suppressor analysis of the *benA33* mutation uncovered a new member of the tubulin superfamily, *mipA* or γ-tubulin (Weil *et al.*, 1986), which defines a completely new class of tubulin (Oakley & Oakley, 1989). γ-tubulin has crucial roles in MT organization (determines both the location and polarity of MT initiation) and mitosis (Oakley *et al.*, 1990, Oakley, 1992), and is an important gene for MT organizing centers (MTOC), where it forms the basis of a high molecular weight complex known as the γ-tubulin ring complex (γTuRC) that provides a template for MT assembly (Horio *et al.*, 1991; Joshi *et al.*, 1992; Liang *et al.*, 1996; Martin *et al.*, 1997; Stearns *et al.*, 1991).

Table III. 01. Tubulin members of *A. nidulans*, *S. cerevisiae*, *S. pombe* and *U. maydis*.

Tubulin	*A. nidulans*	*S. cerevisiae*	*S. pombe*	*U. maydis*
α-tubulin	TubA, TubB	Tub1, Tub3	Nda2, Tub1 (Atb2)	Tub1 (UM01221)
β-tubulin	BenA, TubC	Tub2	Nda3 (Ben1)	UM05828, UM10558
γ-tubulin	MipA	Tub4	Gtb1 (Tug1)	Tub2 (UM03803)

The research on the cytoskeleton and cytoskeleton-dependent processes in general but also in fungi was largely stimulated through the discovery of the green fluorescent protein, which enabled direct observations of the dynamic processes. In order to analyze MTs, α-tubulin was fused to GFP. The role of mitotic MTs is mostly conserved, whereas the role of cytoplasmic MTs depended on cell type. In *S. cerevisiae* interphase cells, short MTs are attached to nuclei and their growth and shrinkage dynamics causes short-distance movement of the nuclei. During mitosis, cytoplasmic MTs mediate MT-cortex interactions and lead to pulling of nuclei into the budding neck, allowing the divided nuclei to be properly distributed in mother and bud cells (Hoepfner *et al.*, 2000). In *S. pombe,* interphase cells contain several cytoplasmic MTs, which span the entire cell. They serve as tracks to deliver so called cell-end markers and determine growth directionality (Tran *et al.*, 2001; Chang, 2001; Sawin & Nurse, 1998) **(Figure III. 02)**. The dimorphic fungus *Ustilago maydis* grow as a haploid yeast-like cell or as a filamentous dikaryotic hypha. This makes the organization of the microtubule cytoskeleton in *U. maydis* more complex than that in *S. cerevisiae*, and reminiscent of that observed in *S. pombe*. In *U. maydis* yeast-like cells, astral microtubules, and cytoplasmic microtubule are nucleated toward the bud and mother cell and support nuclei migration and positioning (Fink *et al.*, 2006; Straube *et al.*, 2003). In the hyphae, the majority of MTs are orientated with their plus ends toward the growing tips, some MTs are orientated with their plus ends toward the basal end of the apical cell (Schuchardt *et al.*, 2005). Secretion vesicles and other cargoes are transported along these polarized

microtubules and are required for normal cell morphogenesis in *U. maydis* (Steinberg *et al.*, 2001).

In the filamentous fungus *A. nidulans* MTs are quite inflexible structures and their orientation probably mainly depends on the shape of the cell. Hence, the bundles of MTs are mostly aligned parallel to the growth axis and their number ranges from 3 to 8 (resembles *U. maydis* MTs in the filamentous growth shape). *A. nidulans* MTs extend with a speed of about 14 μm per min, reach the cortex, pause for some time and undergo catastrophe. Subsequently, MTs shrink with a speed of about 30 μm per min and they may either depolymerize all the way to the MTOC or rescue occurs and they may recommence elongation again (Han *et al.*, 2001) **(Figure III. 02)**. Slightly different values were obtained in the group of B. Heath (Sampson & Heath, 2005). They found that short MT fragments were able to slide towards the hyphal tip.

MTs in *A. nidulans* are required for nuclear migration and positioning as in *S. cerevisiae* (Fischer and Timberlake, 1995; Suelmann *et al.*, 1998; Veith *et al.*, 2005). Also interphase MTs play a role in signalling polarity information to the hyphal tips as described in *S. pombe* (Konzack *et al.*, 2005; Takeshita *et al.*, 2008). Furthermore, MTs in filamentous fungi play crucial role in vesicle transportation (Fischer *et al.*, 2008). In summary, filamentous fungi may thus combine strategies used by *S. cerevisiae* and *S. pombe* in novel ways to establish and maintain polarized growth and to generate cell shape (Banuett *et al.*, 2008).
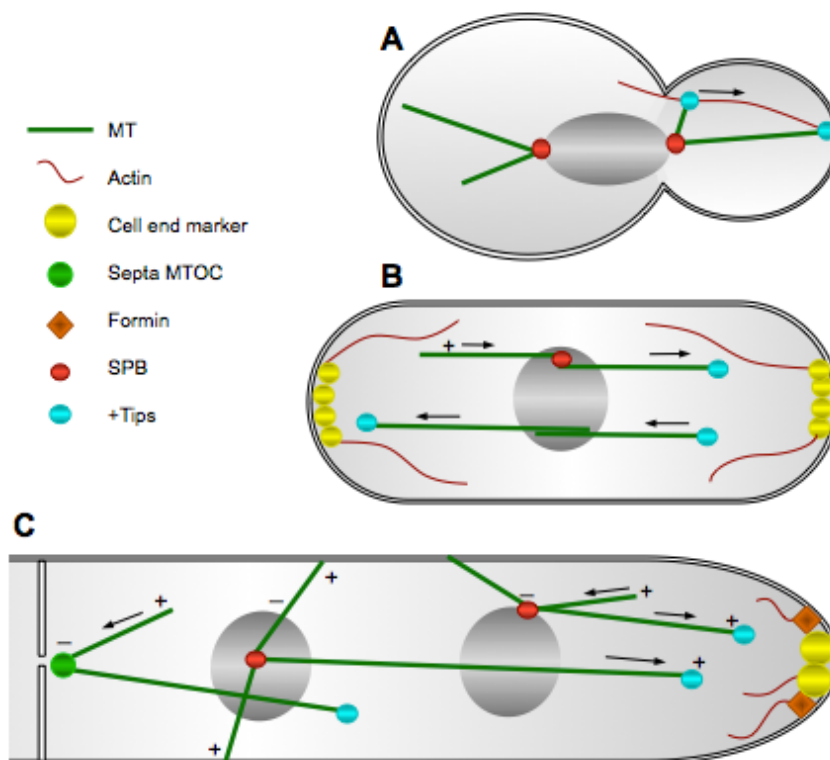
Figure III. 02. Scheme of the MT and actin cytoskeleton in *S. cerevisiae*, *S. pombe* and *A. nidulans*. (A) In *S. cerevisiae*, actin cables capture MT plus ends and thereby regulate MT localization and shrinkage to orientate the mitotic spindle. (B) Interphase MTs in *S. pombe.* (C) In *A. nidulans*, tip of hyphae in interphase cell. See text for details.

1.1. Origin of microtubules

In most higher eukaryotic cells, MTs distribute radially, and are nucleated from a perinuclear centrosome or microtubule organizing centre (MTOCs) with their plus ends facing the cell periphery (Keating & Borisy, 1999). γ-tubulin is a characteristic and necessary component of MTOCs. In higher eukaryotes γ-tubulin forms a 2.2 MDa ring complex (γ–TuRC) that consists of 5 to 7 γ–TuSC (two γ -tubulin units with GCP2 and GCP3 proteins, GCP=<u>G</u>amma-tubulin <u>C</u>omplex <u>P</u>rotein) associated with three other proteins (GCP4, GCP5 and GCP6) **(Table III. 02)** (Xiong & Oakley, 2009). The γ–TuRC measures 25 nm in diameter and associates with different proteins to form the MTOC with three plaque structures (outer-, inner- and intermediate-plaque) (Kilmartin, 1994). The intermediate plaque embeds into membranes and nucleates MTs whereas both the inner and outer-plaques contain a γ–TuRC besides different other proteins (Aldaz *et al.*, 2005).

In *S. cerevisiae*, the MTOC is localized in the nuclear envelope and called spindle pole body (SPB) (Jaspersen & Winey, 2004). Only few MTs are found in interphase cells and they disassemble as the mitotic spindle is formed. *S. pombe* has both the SPB and perinuclear MTOCs (Sawin & Tran, 2006). In the filamentous fungus *A. nidulans* two different MTOCs (SPBs and sMTOCs associated with septa, which will be discussed in this study) are responsible for the formation and maintenance of cytoplasmic MTs (Veith *et al.*, 2005) **(Figure III. 02)**.

Table III. 02. Some MTOC proteins, which were studied in this work

MTOC protein	*A. nidulans*	*S. cerevisiae*	*S. pombe*	*U. maydis*
GCP2	GCPB (AlpC)	Spc97	Alp4	UM01474
GCP3	GCPC (AlpB)	Spc98	Alp6	UM00950
γ-tubulin-complex subunit	ApsB	?	Mod20	?

Many evidence have already proposed that microtubule polymerization in *A. nidulans* is initiated at septa. Using the kinesin motor KipA as MT plus-end associated protein, Konzack *et al.* found that the cytoplasmic area close to septa acts as active microtubule organizing centre (MTOC) (Konzack *et al.*, 2005). Furthermore, Veith *et al.* identified a novel MTOC associated protein, ApsB and localized it to the spindle pole bodies and to septa (Veith *et al.*, 2005). The presence of septal MTOCs is similar to the equatorial MTOC in *S. pombe*, but there is no evidence for such organelles in *S. cerevisiae* or the *S. cerevisiae*-related filamentous fungus *Ashbya gossypii* (Lang et al., 2010a; Lang et al., 2010b). Given that MTOCs are generally comprised of a large protein complex with gamma-tubulin as one

characteristic member, this study anticipated that MT polymerisation at septa also requires a protein complex (Xiong & Oakley, 2009). In this work, the presence of gamma-tubulin at septal MTOCs (sMTOCs) and the physical interaction between gamma-tubulin and ApsB was shown for the first time. Surprisingly, ApsB was associated with peroxisomes in the cytoplasm, which proposed that ApsB defines a new class of peroxisomes involved in MTOC function.

1.2. Proteins at the microtubule plus end and the microtubule lattice

Understanding the regulation of MT formation and their dynamics is one of the main foci of recent research. Proteins called plus end tracking proteins (+TIPS) **(Table III. 03)**, because they associate and remain at growing MT plus ends, regulate MT dynamics and are very important for MT-cortical interactions (Akhmanova & Hoogenraad, 2005; Xiang, 2006). In *yeast S. cerevisiae*, the interaction of microtubule plus ends with the cell cortex play crucial roles in positioning the mitotic spindle, whereas in *S. pombe* those interactions support signaling of polarity information to the cell cortex **(Figure III. 02)** (Nelson, 2003). In *S. cerevisiae* mitotic cells, the +Tip protein Kar9 directs one SPB towards the bud by linking astral MTs to the actin cytoskeleton through the interaction with the class-V myosin Myo2 **(Figure III. 02)** (Yin *et al.*, 2000; Hwang *et al.*, 2003).

One interesting question is why MTs stop growing when they reach the cell ends instead of bending around the cortex. At least two +TIPs, Tip1 (CLIP-170) and Mal3 (EB1 in higher eukaryotes) are involved in this regulation in *S. pombe*. Phenotypic analyses suggest that these proteins are important for suppressing MT catastrophe (Brunner & Nurse, 2000; Busch & Brunner, 2004). In Δ*tip1* cells, MTs initiate catastrophe anywhere the MT plus ends contact the cortex, and in Δ*mal3* cells, MTs undergo catastrophe even before they reach the cortex (Beinhauer *et al.*, 1997). As a result, these mutants have shorter MT bundles. Also Tea1 (TeaA in *A. nidulans*) plays a role in regulating MT dynamics: in Δ*tea1* mutants, some MTs fail to stop growing and curve around the cell end (Mata & Nurse, 1997). Dynein is a prominent example of a MT plus-end associated protein that localizes to the MT tip and hitchhikes with the growing filament to the cell periphery. Once at the cortex, dynein is activated and pulls the attached MT towards the cortex. This leads to translocation of the nucleus (Maekawa *et al.*, 2003; Maekawa & Schiebel, 2004; Schuyler & Pellman, 2001; Sheeman *et al.*, 2003).

MT function and dynamics are not only determined by the plus and minus end, but also by the filament lattice, which in higher eukaryotes can be decorated with a number of different microtubule-associated proteins (MAPs), which in turn may control the activity of associated motor proteins (Baas *et al.*, 1994; Baas & Qiang, 2005; Cassimeris & Spittle,

2001). One of the MAPs was discovered in *Xenopus* and named XMAP215 (Gard & Kirschner, 1987). Similar proteins, which are meanwhile classified in the Dis1/XMAP215 family, exist in eukaryotes from yeast to plants and humans (Ohkura *et al.*, 2001). Common to all of them is their association with MTs and the presence of TOG domains and HEAT repeats. XMAP215 proteins have a prominent MT-stabilizing function (Kinoshita *et al.*, 2002).

In *S. cerevisiae* it was nicely shown that the Dis1/XMAP215 protein Stu2 binds to tubulin heterodimers and associates to the MT plus end, where it appears to be responsible for the loading of tubulin dimers to the growing end (Al-Bassam *et al.*, 2006). This activity may explain the Stu2 stabilization activity of MTs in living cells. Besides the MT stabilization activity of Dis1/XMAP215 proteins, DdCP224, the *Dictyostelium discoideum* homologue, is involved in MT-cortex interactions. There is evidence that this contact is mediated by cortical dynein with which DdCP224 is able to physically interact (Hestermann & Graf, 2004). The Dis1/ XMAP215-like protein AlpA in *A. nidulans* localizes at the spindle pole bodies and at MT plus ends. A drastic reduction of the MT array and reduced MT dynamics was observed in a corresponding deletion strain. Hyphae of this strain grew in curves, suggesting that AlpA is also involved in the determination of growth directionality (Enke *et al.*, 2007). Most +Tips and MAPs movements are powered by protein machines called protein motors.

Table III. 03. Conserved +Tips of *A. nidulans*, *S. cerevisiae*, *S. pombe* and *U. maydis*.

+Tips	*A. nidulans*	*S. cerevisiae*	*S. pombe*	*U. maydis*
CLIP-170	ClipA	Bik1	Tip1	Clip1
APC	-	Kar9	-	-
EB1	AN2862	Bim1	Mal3	Peb1
XMAP215	AlpA	Stu2	Alp14	UM06328

2.   Molecular motors

Three types of motor proteins are known, myosins, which use actin filaments as track, dynein and kinesin, which move along microtubules. Protein motors transport various cargoes including membranous organelles, protein complexes and mRNA, drive cell locomotion and division and allow organisms to move and fuse. Important and unexpected roles for protein motors are newly discovered as the involvement in higher brain function, tumor suppression and developmental patterning (Hirokawa *et al.*, 2009). Motor defects can also result in developmental, cardiovascular and neuronal diseases or can be even lethal (Vale & Milligan,

2000). In filamentous fungi protein motors are essential for polarized growth, morphogenesis, cytoskeletal organization and dynamics (Schliwa & Woehlke, 2003).

In order to perform their work in the cell, motor proteins have special structures: one region of the protein binds to a filament (F-actin or microtubules), hydrolyses ATP and exerts force onto the filament, while other regions are responsible for achieving the different cellular functions such as attachment to cargo for transport or anchoring for force generation. They coordinate the hydrolysis of ATP with binding to, and movement along, a filament and thus convert the chemical energy derived from ATP hydrolysis directly into mechanical work. The ability of motor proteins to transport such a wide array of cargo is in part due to the fact that the tail domains are quite divergent from one another. This allowed them to evolve into adaptors, linking themselves to cargo through interactions with receptor proteins on the cargo surface (Karcher *et al.*, 2002). Here I give a short introduction for the three types of motor proteins.

2.1. Myosin

Myosins are a large family of diverse mechanoenzyme which, upon interaction with actin filaments, convert energy from ATP hydrolysis into mechanical force (Hasson & Mooseker, 1995). They are involved in muscular contraction, cytokinesis, short-range membrane-vesicle transport and a host of other cellular processes. Myosins of three families (myosins-I, -II and -V) are conserved in yeast **(Table III. 04)**. Actin cables are nucleated from the bud tip to the mother cell during bud growth and one myosin-V, Myo2, transports vesicles and other organelles, such as the Golgi, mitochondria, vacuoles and peroxisomes (Pruyne *et al.*, 2004). Some mRNA molecules such as *ASH1* are transported by another myosin-V, Myo4 (Bobola *et al.*, 1996; Shepard *et al.*, 2003). In *S. pombe*, a new daughter cell grows at the previous cell end in a monopolar manner, and then initiates growth at the previous cell division site in a bipolar manner. This phenomenon is named NETO (new end take-off) (Mitchison & Nurse, 1985). Actin cables grow towards the growing cell ends, only towards the old ends before NETO and towards both ends after NETO, and Myo52, a myosin-V, is responsible for polarized secretion of vesicles along actin cables and hence membrane enlargement and secretion of cell wall-synthesizing enzymes (Montegi *et al.*, 2001; Mulvihill *et al.*, 2006; Win *et al.*, 2001). Although in filamentous fungi, the function of myosin-V is largely unclear, these myosins are required for filamentous growth and pathogenicity in *U. maydis* and *C. albicans* (Schuchardt *et al.*, 2005; Weber *et al.*, 2003; Woo *et al.*, 2003).

Myosin-I functions in endocytosis associated by actin patche formation (Kim & Flavell, 2008), and Myosin-II functions in cytokinesis by shrinking actomyosin-ring (Pollard, 2009).

Table III. 04. Myosins of *A. nidulans*, *S. cerevisiae*, *S. pombe* and *U. maydis*.

Myosin subfamily	*A. nidulans*	*S. cerevisiae*	*S. pombe*	*U. maydis*
Myosin-I	MyoA (AN1558)	Myo3, Myo5	Myo1	Myo1
Myosin-II	AN4706	Myo1	Myo2, Myo3	Myo2
Myosin-V	AN8862	Myo2, Myo4	Myo51, Myo52	Myo5
Myosin-XVII	CsmA, CsmB	-	-	Mcs1

2.2. Microtubule dependent motor proteins

Microtubules and their dynamics are, in principle, able to create force and transport cargoes (attached to the growing end) in a cell. However, at least two classes of motor proteins have evolved that mediate fast MT-dependent movement within the cell. These are the minus-end directed dynein and the plus-end directed kinesin, although some kinesins can also move in a minus-end mode. Both motor classes are characterized by a motor domain in which ATP is hydrolyzed (Hirokawa, 1998).

2.2.1. Dynein super-family

The first MT associated motor protein is dynein, which is a large protein complex **(Table III. 05)**. Cytoplasmic dynein consists of two ~500 kDa dynein heavy chains (DHCs), several ~74 kDa intermediate chains (DICs), four 50-60 kDa light intermediate chains (DLICs) and several 6-22 kDa light chains (DLCs) (Bowman *et al.*, 1999; Holzbaur & Vallee, 1994; King *et al.*, 1998; Yamamoto & Hiraoka, 2003). DHC, the motor unit of dynein, contains an ATP binding catalytic site (Asai & Koonce, 2001; King, 2000; Yamamoto & Hiraoka, 2003). DLICs, DICs and DLCs are probably involved in binding to different structures and regulate motor activity. Cytoplasmic dynein requires dynactin for its functions (Allan, 1996; Gill *et al.*, 1991; Schroer & Sheetz, 1991). Dynactin is a protein complex that comprises two distinct structural components: a short, actin-like filament and a projecting sidearm (Eckley *et al.*, 1999; Schafer *et al.*, 1994). The actin-like filament consists of a polymer of the actin-related protein Arp1 and several attached proteins. The sidearm consists of a dimer of p150*Glued*, which contains distinct binding sites for microtubules, DIC and Arp1 (Karki & Holzbaur, 1995). Dynactin is proposed to mediate the interaction of cytoplasmic dynein with cellular structures and/or to regulate dynein motility (King & Schroer, 2000; Yamamoto &

Hiraoka, 2003). Dynactin also affects the ATPase activity of dynein by changing its phosphorylation state (Kumar *et al.*, 2000).

Table III. 05. Dynein and regulators of *A. nidulans*, *S. cerevisiae*, *S. pombe* and *U. maydis*.

Dynein	*A. nidulans*	*S. cerevisiae*	*S. pombe*	*U. maydis*
DHC	NudA	DYN1 (DHC1)	Dhc1	Dyn1, Dyn2
DIC	NudI	PAC11	Dic1	UM04598
DLIC	NudN	DYN3	Dil1	UM03459
DLC	NudG, RobA, TctexA	DYN2 (SLC1)	Dlc2, Dlc1	UM04651
Dynactin				
P150_Glued_	NudM	NIP100	Ssm4	Dya1
Arp1	NudK	ACT5	Arp1	UM11692
Dynein regulators				
LIS1	NudF	PAC1	?	Lis1
Num1 (cortical anchor)	ApsA	NUM1	Mcp5	?
NUDC	NudC	?	SPBC19F8	?
NUDE	NudE	NDL1	?	?

Cytoplasmic dynein has various roles in nuclear migration and organelle transport in fungi (Xiang & Fischer, 2004; Yamamoto & Hiraoka, 2003). Fungi contain a single cytoplasmic dynein (Yamamoto & Hiraoka, 2003), its role in nuclear migration has been best studied in *S. cerevisiae*. Dynein mediates the contact of astral MTs to the cortex and slides the MTs on the contact sites by moving along the MTs towards the minus end. Consequently, the nucleus moves to the bud neck and the opposing pulling forces along the cell axis contribute to spindle pole separation (Bloom, 2001; Yamamoto & Hiraoka, 2003). In filamentous fungi, dynein mediates organelle and vesicle transport (Xiang & Plamann, 2003). In *N. crassa*, dynein is involved in retrograde transport of vesicles and a dynein mutant showed defects in the organization and stability of the Spitzenkörper (Riquelme *et al.*, 2002; Seiler *et al.*, 1999). In *U. maydis*, it functions in endoplasmic reticulum (ER) organization and endosome transport (Wedlich-Söldner *et al.*, 2002a; Wedlich-Söldner *et al.*, 2002b). Moreover, dynein and its regulator accumulated at MT plus ends within the hyphal tips possibly ensure that endosomes reach the tips and contribute to tip growth by endocytic membrane recycling (Lenz *et al.*, 2006).

2.2.2. Kinesin super-family

Kinesins are microtubule-stimulated ATPases that share a variably conserved ~350 amino acid "motor domain" that contains binding sites for microtubules and adenine nucleotides (Bloom & Endow, 1995; Bloom, 2001; Goldstein, 2001; Hirokawa, 1998). Kinesin moves mostly toward the microtubule plus end and many of them have two catalytic subunits, whereas others contain just one single motor domain (Hirokawa, 1998). Kinesins are very diverse, they are found as monomers or heterodimers. The motor localizes to the N- terminal, C- terminal or can be intermediary. The processivity, directionality and the forms differ too.

According to the latest nomenclature, kinesins are grouped into 14 families (kinesins 1–14) and one orphan family (Lawrence *et al.*, 2004). The number of kinesins in fungi ranges from six in *S. cerevisiae* to nine in *S. pombe* and 10 and 11 in *N. crassa* and *A. nidulans,* respectively (Rischitor *et al.*, 2004; Schoch *et al.*, 2003) **(Table III. 06)**. Mammals contain about 45 kinesin genes, 38 of which are expressed in brain tissue, and many of these motors are likely to be involved in transporting distinct cargoes in axons and dendrites (Miki *et al.*, 2001). Even the protozoal parasite *Giardia* contains 25 kinesins (Vale, 2003). Five kinesins of *A. nidulans*, kinesin-1 (KinA), kinesin-7 (KipA), kinesin-8 (KipB) and in this work, kinesin-3 (UncA and UncB), have been studied in our group.

Some of those kinesins was shown to be involved in mitosis, whereas three kinesin families (1, 3 and 7) are involved in polarized growth. Kinesin-1 or conventional kinesin is currently probably the best-studied molecular motor (Schliwa & Woehlke, 2003). ATP hydrolysis causes a small conformational change in a globular motor domain that is amplified and translated into movement with the aid of accessory structural motifs. Additional domains outside the motor unit are responsible for dimerization, regulation and interactions with other molecules. The activity of conventional kinesin is required for vesicle transportation toward the hyphal tips and thereby for normal fungal hyphal extension. *N. crassa* and *A. nidulans* members of the kinesin-1 family play important roles in filamentous growth, probably in the transportation of vesicles, roles in nuclear positioning were also observed (Requena *et al.*, 2001; Seiler *et al.*, 1997). However, additional functions were reported, for example, defects on mitochondrial distribution were observed in kinesin-1 mutants of *N. crassa* and *Nectria haematococca,* and defective vacuolar distribution was found in the corresponding *U. maydis* mutant (Lehmler *et al.*, 1997). Members of the kinesin-1 family do not exist in *S. cerevisiae*, whereas in *S. pombe* such a kinesin functions in Golgi membrane recycling (Brazer *et al.*, 2000). Hence, it appears that kinesin-1 can bind to different cargoes and, thus, be involved in different cellular processes.

Table III. 06. Kinesins of *A. nidulans*, *S. cerevisiae*, *S. pombe*, *N. crassa*, *U. maydis*, *C. albicans* and *A. gossypii*.

Kinesin Subfamilies	*A. nidulans*	*S. cerevisiae*	*S. pombe*	*N. crassa*	*U. maydis*	*C. albicans*	*A. gossypii*
Number of Kinesin	11	6	9	10	10	6	6
Kinesin-1 (KHC)	KinA	-	Klp3	KHC	Kin1	-	-
Kinesin-3 (Unc104)	UncA, UncB	-	-	Nkin2, Nkin3	Kin3	Ca019.1115-1	-
Kinesin-4 Chromokinesin	AN6875	-	-	Nc06832	Kin4	-	-
Kinesin-5 (BimC)	BimC	Cin8, KIP1	Cut7	Nc00927	Kin5	Ca019.712	ACR010Cp ACR228Cp
Kinesin-6 (MKLP1)	An3124	-	Klp9	Nc05180	Kin6	-	-
Kinesin-7 (CENP-E)	KipA	KIP2	Tea2	Nc02626	Kin7a, Kin7b	Krp	ACR145W-p
Kinesin-8 (Kip3)	KipB	KIP3	Klp5, Klp6	Nc06144	Kin8	Ca019.735	AER441C-.p
Kinesin-10	An3721	-	-	Nc05028	-	-	-
Kinesin-11	-	-	-	-	-	Ca019.1273-0	ADR145Cp
Kinesin-14/ Ncd	KlpA	Kar3	Pkl1, Klp2	Nc04581	Kin14	AY182242.1	AGR253-Wp
Orphan Kinesin	An3970	Smy1	Klp8	-	Kin9	-	-

Members of the kinesin-7 family (Kip2 in *S. cerevisiae*, Tea2 in *S. pombe,* KipA in *A. nidulans*) are used to deliver proteins to the MT plus ends. Kip2 transports Bik1 (CLIP-170), Kar9 and dynein (Carvalho *et al.*, 2004), while Tea2 transports Tip1 (CLIP-170) and Tea1 (for cell polarity) (Browning *et al.*, 2000; 2003; Busch *et al.*, 2004). KipA is not essential for ClipA (CLIP-170) and TeaA transport, likewise, dynein accumulation at the MT plus end is independent of KipA but depends on KinA (Zhang *et al.*, 2003). Surprisingly, kinesin-7 family kinesins in *U. maydis* have no critical role in polarized growth (Schuchardt *et al.*, 2005). Other kinesins with a role in polarized growth are those of the kinesin-3 family (will be discussed).

Kinesin-8 family members play different roles. In our group it was shown that *A. nidulans* KipB has a role in MT depolymerization and spindle positioning during synchronized mitosis (Rischitor *et al.*, 2004). The kinesin-8 (Kip3) of *S. cerevisiae* is involved in nuclear migration and spindle positioning especially in the absence of dynein (Cottingham

& Hoyt, 1997; Cottingham *et al.*, 1999; DeZwaan *et al.*, 1997; Heil-Chapdelaine *et al.*, 2000; Miller *et al.*, 1998). Two other kinesin-8, Klp5 and Klp6, were characterized in the yeast *S. pombe*. Deletion of Klp5 or Klp6 causes MT stabilization and impairs meiosis and mitosis (West *et al.*, 2002). Both kinesins are also required for normal chromosome movement in prometaphase (West *et al.*, 2001). It was suggested that members of this family are likely to conduct a conserved and important function in all fungal species (Schoch *et al.*, 2003). An overview of different kinesin families and subfamilies is shown in **(Table III. 06)**.

In this work, roles of the Unc104-related kinesins (kinesin-3), UncA and UncB, will be discussed in detail. Our understanding of vesicle and organelle transport towards the tip is still quite limited and it seems that different motors play different roles in different fungi.

2.2.2.1. The Unc-104 (kinesin-3) family

The Kif1/Unc-104 family has been renamed into the kinesin-3 family (Lawrence *et al.*, 2004; Wickstead & Gull, 2006). This plus-end directed motor harbors the motor domain in the N-terminus (N-type), a pleckstrin homology domain (PH) for the binding of membranous cargoes at the C-terminus and a forkhead-associated domain (FHA) for protein-protein interactions (Klopfenstein *et al.*, 2002). In contrast to the majority of dimeric kinesins, most Kin-3 kinesins are monomeric motors (Okada & Hirokawa, 1999; Okada & Hirokawa, 2000), but a lysine-rich loop in KIF1A binds to the negatively charged C-terminus of tubulin and compensates for the lack of a second heavy chain, allowing KIF1A to move processively like a dimeric motor (Okada & Hirokawa, 1999; Okada & Hirokawa, 2000). Al-Bassam suggests a structural basis for Unc104 regulation of motility by reversible dimerization (Al-Bassam *et al.*, 2003; Vale, 2003) **(Figure III. 03)**. However, very recent data suggest that KIF1A is only able to undergo ATP-dependent processive motility in the dimeric form (Hammond *et al.*, 2009).

Unc-104 was first discovered in *Caenorhabditis elegans* shortly after the discovery of conventional kinesin (Otsuka *et al.*, 1991). Mutations in *unc-104* caused uncoordinated and slow movement of corresponding mutants. The motor is required for synaptic vesicle transport (Hall & Hedgecock, 1991). Later, the motor was also discovered in mouse due to sequence similarities of cDNAs from a library of murine brain (Okada *et al.*, 1995). The motor is associated with certain vesicles of the neuron, which transport synaptic vesicle proteins. Other protein motors from the Unc104/KIF1 family were found to transport mitochondria (Nangaku *et al.*, 1994) or vesicle from Golgi apparatus to the endoplasmic reticulum (Dorner *et al.*, 1998). The motor activity was measured in gliding assays and movement was measured at 1.2 µm per sec, the fastest kinesin with anterograde movement at the time. It was observed that Kif1A apparently only binds to special vesicles and is only required for the anterograde transportation of certain synaptic proteins.

S. cerevisiae does not contain a member of the kinesin-3 family. However, this motor family was characterized in *Dictyostelium discoideum*, *U. maydis, N. crassa,* and *Thermomyces lanuginosus* (Pollock et al., 1999; Rivera et al., 2007). In *N. crassa* one kinesin-3 motor, Kin2, is involved in mitochondrial distribution (Fuchs & Westermann, 2005). The kinesin-3 family contains also a unique fungal subgroup of "truncated" proteins, which do not have FHA and PH domains and may constitute a new subfamily (Schoch *et al.*, 2003). Although the structure of the protein is very different from other kinesin-3 family members, it is very interesting that in *N. crassa* Kin3 can rescue the lack of Kin2 (Fuchs & Westermann, 2005). In *U. maydis* a kinesin-3 motor is required for endosome movement (Steinberg, 2007). Deletion of *kin-3* reduces endosome motility to 33%, and abolishes endosome clustering at the distal cell pole and at septa. It was proposed that dynein and Unc104 counteract on endosomes to arrange them at opposing cell poles (Wedlich-Söldner *et al.*, 2002b). Recently, Schuchardt *et al.* showed that Kin-3 may also be required for exocytosis, because acid phosphatase secretion was lowered to 50 % in *kin-3* deletion strains (Schuchardt et al., 2005). In filamentous fungi it has been shown recently that not only exocytosis but also endocytosis is important for polarized growth (Araujo-Bazan *et al.*, 2008; Fischer *et al.*, 2008; Taheri-Talesh *et al.*, 2008; Upadhyay & Shaw, 2008).

If we accept the model of long-distance MT-dependent vesicle transportation and subsequent accumulation in the Spitzenkörper and actin dependent short-distance transportation from the VSC towards the surface, one interesting yet open question is whether different motor proteins (kinesin, dynein and myosin) are always attached to the vesicles or whether they associate with the vesicles as required. However, no information was available how endosomes are transported in *A. nidulans*. In this study two members of the kinesin-3 family were identified in *A. nidulans* and one of them, UncA, was studied in detail and gives evidence that UncA is associated with endosomes and other vesicles and transports them surprisingly along a subpopulation of microtubules.
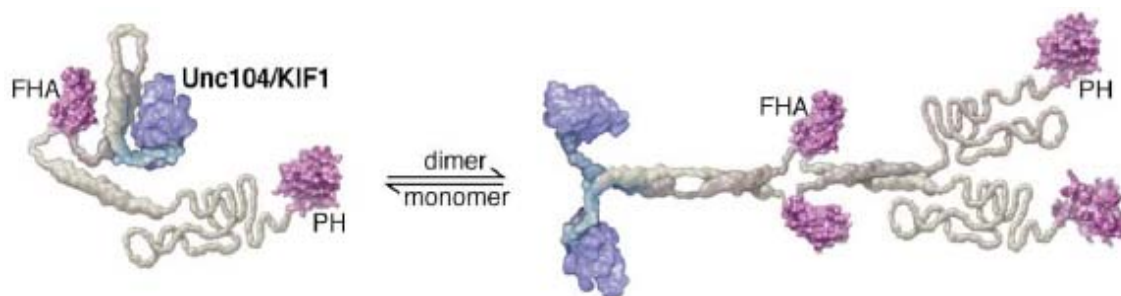
Figure III. 03.   The Unc104/KIF1 motor can exist as a monomer and dimer, as indicated by the equilibrium. The motor catalytic domains are displayed in blue, mechanical amplifiers in light blue, and tail domains implicated in cargo attachment are shown in purple. From Vale, 2003.

IV. Results

To gain insights into the organization and function of *Aspergillus nidulans* kinesins, the genomic DNA database was analysed at Cereon Genomics LLC (Cambridge, USA), and sequences of putative kinesin motors were retrieved. Two of them encoded polypeptides with high homology to the Kinesin-3 family, called UncA and UncB respectively. Those two kinesins were studied in this work.

1.   UncA and UncB isolation

A. nidulans harbors eleven different kinesins, including UncA and UncB, which are members of the Kinesin-3 family (formerly called Unc-104 family) (Galagan *et al.*, 2005; Rischitor *et al.*, 2004). According to the Broad Institute gene database (http://www.broadinstitute.org/), the *uncA* gene (AN7547) locates at chromosome IV and the *uncB* gene (AN6863) at chromosome I. The predicted structures of the two genes were confirmed through amplification of small cDNAs and subsequent sequencing. The *uncA* gene was disrupted by an intron of 75 bp length located between amino acids 21 and 22 of the open reading frame, and the *uncB* open reading frame by an intron of 52 bp after amino acid position 120 of the open reading frame. The protein sequences of both proteins were analyzed with the SMART program (http://smart.embl-heidelberg.de) and besides the kinesin motor domains in both proteins, a forkhead association (FHA) and a pleckstrin homology (PH) domain were identified in UncA **(Figure IV. 01, A and Figure IV. 03, A)**.

1.1. UncA structure and relatedness analysis

The UncA protein is comprised of 1631 amino acids, with a calculated molecular mass of 182.7 kDa. The predicted motor domain starts two amino acids downstream of the start codon, and consists of 361 amino acids. One of the ATP-binding motifs (P-loop) is located between amino acids 111 and 118 (GQTGSGKS). The C-terminal half of the motor domain displays the highly conserved regions termed switch I (NETSSR), between amino acids positions 224 and 229 and switch II (DLAGSE), between amino acids 261 and 266, which are involved in nucleotide-binding (ATP). Two microtubule-binding motifs were found, MT1 (RDLL) starting at amino acids 170 and MT2 (VPYRDS) starting at amino acids 312 (Song *et al.*, 2001). The motor domain is connected to the tail via a conserved neck linker, which ends with a conserved proline (KNHAVVNEDP). This domain is adjacent to the conserved

catalytic core. The neck linker may regulate a monomer to dimer motor transition (Al-Bassam *et al.*, 2003) **(Figure IV. 01, B)**.

A characteristic feature of this class is the presence of a forkhead-association domain (FHA) located downstream of the motor domain between amino acids 496 and 596. The FHA domain is proposed to be involved in signaling and protein-protein interactions of kinesins (Westerholm-Parvinen *et al.*, 2000). It mediates protein–protein interactions in a variety of proteins by binding to a phosphothreonine motif (Durocher *et al.*, 2000; Durocher & Jackson, 2002). In addition, between the catalytic core and the FHA domain are two predicted helices capable of weak intermolecular coiled-coil (CC) interactions (neck CC and CC1) (Al-Bassam *et al.*, 2003; Okada *et al.*, 1995; Pierce *et al.*, 1999). The two helices are separated by an unstructured region (20–50 residues) that may serve as a flexible hinge (termed the neck hinge). This sequential arrangement of the catalytic core, neck linker, helix–hinge–helix, and the FHA domain is characteristic of Unc104/KIF1-type motors from unicellular organisms (such as *Giardia*) to man (Vale, 2003). Another coiled coil domain (CC2) is located after the FHA domain between amino acids 748 and 823. It has been suggested that intramolecular FHA–CC2 interaction negatively regulates KIF1A activity by inhibiting MT binding and dimerization of KIF1A. This points to a novel role of the FHA domain in the regulation of kinesin motors (Lee *et al.*, 2004). The FHA-CC2 interactions are mediated by a linker connecting the FHA domain and the CC2 domain. The linker is apparently long enough to allow intramolecular interaction. This predicted structure may limit the flexibility that is required for its function as a hinge. Recent study has shown that mammalian kinesin-3 motors are dimeric in vivo and move by processive motility upon release of auto-inhibition via two inhibitory mechanism, first, the FHA and CC2 domains inhibit the interaction of KIF1A with microtubules, as mentioned before. Second, the CC1 domain blocks processive motility by interference with the formation of dimeric motors (Hammond *et al.*, 2009).

The C-terminus of UncA exhibited very low sequence similarity to the corresponding regions of other Kin-3 family proteins, besides the FHA domain, a pleckstrin homology domain (PH) exists from amino acids positions 1509 to 1615. The (PH) domain has previously been reported in Unc104 related kinesins in *C. elegans* where it has been proposed to bind lipids and lipid rafts. The potential of UncA to make clusters, in order to dock onto membrane cargoes, has been discussed for providing a trigger for membrane transport (Klopfenstein *et al.*, 2002) **(Figure IV. 01, B)**.

A UncA

B
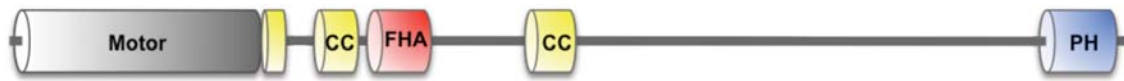
```
ATG GCG CCA GGA GGT GGT GGA AAC ATT AAG GTG GTG GTG AGA GTG CGG CCG TTC AAC AGC CGA G   gtgagtaaaggacagcctgctgtgttta
 M   A   P   G   G   G   G   N   I   K   V   V   V   R   V   R   P   F   N   S   R   E

cctaccaccaggggcgttaagagactgatgaatgccttgaattatag  AA ATT GAA CGG GGG GCA AAA TGT ATT GTG CAG ATG AAA GAC AGT CAA ACG
                                                   I   E   R   G   A   K   C   I   V   Q   M   K   D   S   Q   T

ATC CTC ACG CCG CCG CCC GGA GCT GAA GAG AAA TCG CGA AAA GGT GGA AAC AAG GCT GCT GCT GAA GGG CCA AAG ACG TTT GCT TTT
 I   L   T   P   P   P   G   A   E   E   K   S   R   K   G   G   N   K   A   A   A   E   G   P   K   T   F   A   F

GAT AGG TCG TAT TGG TCT TTC GAC AAG AAG GCT CCC AAC TAT GCC GGT CAG GAT AAT CTC TTC TCG GAC TTG GGT GTT CCG CTT TTG
 D   R   S   Y   W   S   F   D   K   K   A   P   N   Y   A   G   Q   D   N   L   F   S   D   L   G   V   P   L   L

GAT AAT GCC TTC CAG GGC TAC AAC AAC TGT ATT TTC TAC GGT CAG ACC GGT TCG GGA AAG TCT TAC TCG ATG ATG GGA TAC GGC
 D   N   A   F   Q   G   Y   N   N   C   I   F   A   Y   G   Q   T   G   S   G   K   S   Y   S   M   M   G   Y   G

AAG GAG TAT GGT GTG ATC CGC CGG ATT TGT CAG GAT ATG TTT GAG CGC ATA CAA GAG ATA CAA AAC CTC ACC TGC ACG
 K   E   Y   G   V   I   P   R   I   C   Q   D   M   F   E   R   I   R   K   I   Q   E   D   K   N   L   T   C

ACG GTG GAG GTC TCG TAT CTG GAA ATC TAT AAC GAG CGG GTT CGT GAC TTG CTC AAC CCG TCG AAT AAA GGC AAC CTG AAA GTC CGT
 T   V   E   V   S   Y   L   E   I   Y   N   E   R   V   R   D   L   N   P   S   N   K   G   N   L   K   V   R

GAA CAC CCG TCT ACA GGT CCC TAT GTC GAA GAC CTT GCC AAA CTC GCC GTT CGC TCT TTT GAG GAA ATA GAG AAC TTA ATG GAC GAG
 E   H   P   S   T   G   P   Y   V   E   D   L   A   K   L   A   V   R   S   F   E   E   I   E   N   L   M   D   E

GGA AAC AAA GCG CGA ACT GTT GCT GCC ACG AAC ATG AAC ACG TCT AGT CGA TCA CAC GCC GTG TTT ACG TTG ATG CTT ACA CAG
 G   N   K   A   R   T   V   A   A   T   N   M   N   E   T   S   S   R   S   H   A   V   F   T   L   M   L   T   Q

AAA CGA CAT GAT GCA GAG ACA AGC ATG GAT ACG AAA GTG TCG AGA ATC AGT CTG GTC GAT CTT GCG GGT TCA GAG CGA GCG AAC
 K   R   H   D   A   E   T   S   M   D   T   K   V   S   R   I   S   L   V   D   L   A   G   S   E   R   A   N

TCG ACT GGA GCC ACC GGT GCT AGG TTG AAG GAA GGA GCT GAA ATC AAC AGA TCA CTT TCT ACG GGA CGT GTC ATT GCA GCT CTG
 S   T   G   A   T   G   A   R   L   K   E   G   A   E   I   N   R   S   L   S   T   L   G   R   V   I   A   A   L

GCG GAT GCG GCT TCT GGA AAG AAA AAG GGA AAG CAG GTG CCG TAC CGT GAT TCA GTA CTT ACG TGG TTG CTA AAG GAC TCT CTT GGA
 A   D   A   A   S   G   K   K   K   G   K   Q   V   P   Y   R   D   S   V   L   T   W   L   L   K   D   S   L   G

GGA AAT TCT ATG GCC ATC GCC ATC TCG CCG GTA TCA CCT GCC GAT ATT AAC TTC GAC GAG ACT CTT AGC ACT TTA CGT TAT GGC GAC
 G   N   S   M   A   I   A   A   I   S   P   A   D   I   N   F   D   E   T   L   S   T   L   R   Y   A   D

TCT GCG AAG CGC ATC AAG AAC CAC GCT GTT GTC AAC GAG GAC CCC AAC GCG CGG ATG ATC AGA GAA CTC AAG GAC GAG CTG GCA CAG
 S   A   K   R   I   K   N   H   A   V   V   N   E   D   P   N   A   R   M   I   R   E   L   K   D   E   L   A   Q

TTA CGA GCG AAG CTT GGC GGT GGT GCA GCA GGC GGC GCG ACG GCA GGG GCA GCA GGC GGG GTG GTG GCA GAC GAA GTA TAT CCT CCA
 L   R   A   K   L   G   G   G   A   A   G   G   A   T   A   G   A   A   G   G   V   V   A   D   E   V   Y   P   P

GAC ACG CCT ATG GAA AAG CAA ATG GTC TCT ATA CAG CAG CCA GAC GGT ACC ATT AAG AAA GTG AGC AAG GCG GAG ATT GTG GAA CAG
 D   T   P   M   E   K   Q   M   V   S   I   Q   Q   P   D   G   T   I   K   K   V   S   K   A   E   I   V   E   Q

CTG AAC CAA AGC GAG AAG TTA TAC AAG GAT CTT AAC CAA ACT TGG GAA GAG AAA TTG ATC AAG ACC GAA CAG ATC CAC AAA GAG CGT
 L   N   Q   S   E   K   L   Y   K   D   L   N   Q   T   W   E   E   K   L   I   K   T   E   Q   I   H   K   E   R

GAA GCG GCT CTG GAA GAG CTT GGT ATC AGT ATT GAG AAG GGA TTT ATC GGT TTG AGT ACA CCG AAA AAG ATG CCG CAT TTA GTC AAT
 E   A   A   L   E   E   L   G   I   S   I   E   K   G   F   I   G   L   S   T   P   K   K   M   P   H   L   V   N

TTG AGC GAT GAC CCG TTG CTA GCA GAA TGT CTA GTA TAT AAC CTA AAA CCG GGA GTC ACT CAC GTC GGA AAT ATG GAT CAA GGA AAT
 L   S   D   D   P   L   L   A   E   C   L   V   Y   N   L   K   P   G   V   T   H   V   G   N   M   D   Q   G   N

CAC GTC GAG ATC AGA TTG AAC GGC TCC AAG ATC TTA GCT GAT CAC TGC AAG TTC GAA AAT GTG GAT AAC GTC GTT ACA ATC CTG CCC
 H   V   E   I   R   L   N   G   S   K   I   L   A   D   H   C   K   F   E   N   V   D   N   V   V   T   I   L   P

AGC GAG GGG GCT GCA GTC ATG GTC AAT GGA GTG CGC GTC GAC AAG CCC AAG CGG TTA AAG AGT GGT TAT CGC ATC ATC TTG GGT GAC
 S   E   G   A   A   V   M   V   N   G   V   R   V   D   K   P   K   R   L   K   S   G   Y   R   I   I   L   G   D

TTT CAT ATC TTT CGA TTC AAT CAC CCC CAG GAA GCA AGG GCT GAA CGA GTA GAA CAA AGC TTA CTC CGC CAT TCC GTT ACG ACT AGC
 F   H   I   F   R   F   N   H   P   Q   E   A   R   A   E   R   V   E   Q   S   L   L   R   H   S   V   T   T   S

CAG CTT GCC TCC CCT GCG CCG AAA GCT CAG AGA AAC GTT AGC GAT TTG GAC TGG GAT TCA AGA ACG TCT GAT
 Q   L   A   S   P   A   P   G   K   A   H   E   R   N   V   S   K   A   S   D   L   D   W   D   S   S   R   A   D

TCT CCA ATG GGT TTC CAA CGT GGG AGA GAG TCG GAC TGG TTT TAT GCG CGT CGT GAA GCT GTG AGC GCG GGG ATG GAT CCG GAT AGG
 S   P   M   G   F   Q   R   G   R   E   S   D   W   F   Y   A   R   R   E   A   V   S   A   G   M   D   P   D   R

CTT GCT CAT ATG CCT GAT GAT GAG CTC GAT GCT CTG TTC GAG AAT GTA CAG AAC GTT AGG GCA AAC CGC CGT GGG TTA TTG GAG AAT
 L   A   H   M   P   D   D   E   L   D   A   L   F   E   N   V   Q   N   V   R   A   N   R   R   G   L   L   E   N

GAA GAA GAC TCG GAT TCC TTA AGT TCA TAT CCG ATT CGC GAT AAG TAT ATG TCC AAT GGT ACT ATT GAC AAC TTT TCC TTG GAC ACG
 E   E   D   S   D   S   L   S   S   Y   P   I   R   D   K   Y   M   S   N   G   T   I   D   N   F   S   L   D   T

GCC ATC ACA ATG CCA GGG ACA CCT CGC CAC GGC GAT GAG GAT GCC ACC CTG CAG TCG GTG CGT CAG GAT ATG CAA CGA CAG TTA GAG
 A   I   T   M   P   G   T   P   R   H   G   D   E   D   A   T   L   Q   S   V   R   Q   D   M   Q   R   Q   L   E

CGA CAG AAA GAG CAG TAT CTG GAT AAG CTA AGG GAA TCG GAA GCG TCC CCG AGT CAA GGC ATC GAC GAA TTG CGG TCT GAA AAG GCC
 R   Q   K   E   Q   Y   L   D   K   L   R   E   S   E   A   S   P   S   Q   G   I   D   E   L   R   S   E   K   A

CGC ATG GAG GAT GCT CTT CGA GTA GCA AAA GAA GAA TAC GAA GAG CAA CTT CGA AAG CAA AAA GAA GCG TTT GAG ACG CAT ATG AAG
 R   M   E   D   A   L   R   V   A   K   E   E   Y   E   E   Q   L   R   K   Q   K   E   A   F   E   T   H   M   K

GCA CTT GGT CAC CCA GTG CCA AGA ATC TAC GAG AAT GGT TAC TCA AAG TTG TCC CCC AGG GAG CTA GAG ATT GAA AAC TCA GTT TTC
 A   L   G   H   P   V   P   R   I   Y   E   N   G   Y   P   K   L   S   P   R   E   L   E   V   A   R   S   V   F

CGA CAC TGG TCT CAG CAA AAT TAT GTC CGC ATG GCC GAA AAG GTT TTG CAG CAT GCT TCG CTG CTA AAG GAG GCC CAG GTC ATG AGC
 R   H   W   S   Q   Q   N   Y   V   R   M   A   E   K   V   L   Q   H   A   S   L   L   K   E   A   Q   V   M   S

CAT ATA ATG GAT AAG AAC GTC GTC TTC CAG TTC TCG ATT GTT GAC CAT GGA CAT AAC ATG GCA TCG TCG TAC GAT CTT GTT CTG AAT
 H   I   M   D   K   N   V   V   F   Q   F   A   I   V   D   H   G   H   N   M   A   S   S   Y   D   L   V   L   N

GGC ATT TCT GGA GAC GAG GAT ATC ATA CTT GAT GAT GCC AAA AAG CCT TGT GTT GCT GTT CGT GTC ATG GAT TTC AAA CAA TGT GTC
 G   I   S   G   D   E   D   I   I   L   D   D   A   K   K   P   C   V   A   V   R   V   M   D   F   K   Q   C   V

ATC CAT CTT TGG TCT ATC GAA AAG CTC CAA CGC CGT GTT CAG AGG CAA CTG CAC CAG TAC ATT GAC AGG CCG GAC TAC ATT
 I   H   L   W   S   I   E   K   L   Q   R   R   V   Q   A   M   R   Q   L   H   Q   Y   I   D   R   P   D   Y   I
```

```
CAG CAC TTT AAG CTT GAA AAC CCG TTC TCC GAG CCA TGC TCG CCT CAG TAC TCT CTT GTA GGT GAC GCT GAC ATT CCG CTC ACA GCT
 Q   H   F   K   L   E   N   P   F   S   E   P   C   S   P   Q   Y   S   L   V   G   D   A   D   I   P   L   T   A

GTA TTC GAG ACG CGA GTT CAG GAC TTT TCG GTT GAT GTC ATC TCA CCC TAT ACA CAG GGT GTG GTC GGT ATC ATA CGA CTG TCC TTG
 V   F   E   T   R   V   Q   D   F   S   V   D   V   I   S   P   Y   T   Q   G   V   V   G   I   I   R   L   S   L

GAA CCA TCG TCG GCG CAG GCG CCG TCG TCT ACG CTC AAA TTC AAC GTT GTC ATG CGT GAC ATG GCC GGC TTT GCT GAG TGG GAG GGA
 E   P   S   S   A   Q   A   P   S   S   T   L   K   F   N   V   V   M   R   D   M   A   G   F   A   E   W   E   G

ACG GAT GTG CAC GCC CAG TTG TTT GTA CCA GGC ATC TCT GAA GAA GGT GGT GCA ACC ACA ACA CAG ATG ATT AGC GGT TTT AAT GAG
 T   D   V   H   A   Q   L   F   V   P   G   I   S   E   E   G   G   A   T   T   T   Q   M   I   S   G   F   N   E

ACA CCG GTC CGT TTC GAG AGT GTC CAC AGC ATG AGC TTG CCG CTT ACC AGT CCG CGC AAT GCA GCC CTT AAG ATT TGT GTC TAT GCG
 T   P   V   R   F   E   S   V   H   S   M   S   L   P   L   T   S   P   R   N   A   A   L   K   I   C   V   Y   A

CGT GTG ACC ACA ATG CAT CTT GAT AAG CTC CTT AGC TGG GAT GAC ATG CGC GAC TTA GCG GAG CAA GGG GCC CAG GAC CAA AAG ACG
 R   V   T   T   M   H   L   D   K   L   L   S   W   D   D   M   R   D   L   A   E   Q   G   A   Q   D   Q   K   T

CCA CGT ATC GCT GAA TCA GAG TAC TTT TCG GAA GAA AGA CAT GAC GTT TTC GCA AGG CTC CAG GTA CTG GAG ATG ACT GAA ACG GGT
 P   R   I   A   E   S   E   Y   F   S   E   E   R   H   D   V   F   A   R   L   Q   V   L   E   M   T   E   T   G

GAC TAC CTG CCT GTG GAG GTG GTG CAA AAC AGC CCT ACT GAA GTA GGC ACA TAT CAG CTC CAT CAA GGT CTT CAG CGC CGA ATC TCG
 D   Y   L   P   V   E   V   V   Q   N   S   P   T   E   V   G   T   Y   Q   L   H   Q   G   L   Q   R   R   I   S

GTG AAT CTC ACC TAT AGC TCA ACG GAA GCT CTT CCC TGG GAC GAT TTG ACG AAT ATT CGA GTT GGT TCT GTG CGG CTG CTG GAT CCA
 V   N   L   T   Y   S   S   T   E   A   L   P   W   D   D   L   T   N   I   R   V   G   S   V   R   L   L   D   P

TGG GGC AAG ATA CCC GAC GAC CTT CAG ACT CCG GAT GTT CCT CTA AAG TTC ATT CAA GAG CCC ATG GTG AAG GAC AAT GCC GAT
 W   G   K   I   P   D   Q   D   L   Q   T   P   D   V   P   L   K   F   I   Q   E   P   M   V   K   D   N   A   D

GGA ACG TCC AAC ATC ACT CTT GTA GGC CAA TGG GAC TCC AGC TTA CAT AAC TCG CTA CTC CTG GAC CGG GTG ACT CCG GAA AAG TAC
 G   T   S   N   I   T   L   V   G   Q   W   D   S   S   L   H   N   S   L   L   L   D   R   V   T   A   E   K   Y

CGC GTG CAA GTA ACG GTC AGA TGG GAT CTC CAG TCT TCA CGC TTG CAG GAC CCT GTG TCG TTC GAG ATC GAC CTG ACG CTC CAA GTG
 R   V   Q   V   T   V   R   W   D   L   Q   S   S   R   L   Q   D   P   V   S   F   E   I   D   L   T   L   Q   V

CAG GGG CGG ACG TAT ATA CGC CCG CAA TCG ATG TTC AAG AAC TTC TTT AGT ACC ACA CGC GTT GTG CAC TCT ACG GTC CGT ATG TAT
 Q   G   R   T   Y   I   R   P   Q   S   M   F   K   N   F   F   S   T   T   R   V   V   H   S   T   V   R   M   Y

TCT GTT GCG GTA CGT CCA GTG TCT GCA AAG CGC GCC GCA GAC CTC TGG CGT ATG AAT ACA CAG AAT GAC TAT GTG AAA GGC GAG GAG
 S   V   A   V   R   P   V   S   A   K   R   A   A   D   L   W   R   M   N   T   Q   N   D   Y   V   K   G   E   E

TTC CTG ACC AAG TGG GCT CCG AGA AAG GTC TCG CTT GTT CGT GAC TAT ATC ACC TCT CGC CGA CGG CGC AGG CGT ATT GCA GAG CTT
 F   L   T   K   W   A   P   R   K   V   S   L   V   R   D   Y   I   T   S   R   R   R   R   R   R   I   A   E   L

AAC GCT GCG AAA GGC GCA CTT AGC GCA AAT AGC CTC ACT GTC GCC TCG CCC CCA CGG AGT GGA AGG TCA ACC CCC CTT CGC GCT CAG
 N   A   A   K   G   A   L   S   A   N   S   L   T   V   A   S   P   P   R   S   G   R   S   T   P   L   R   A   Q

GAG CCT GAT CGC AGA GTC AAA CTG CTT CAA AAA TAC GTT GAC CTG TGG ACC GCA AGA ACC GAT CCC ATC GAT GTG ATT CTG ATT CGA
 E   P   D   R   R   V   K   L   L   Q   K   Y   V   D   L   W   T   A   R   T   D   P   I   D   V   I   L   I   R

GAC AAT ACG GAG CCC CCA GCA CGT GGC GCA GCG TTT GCG TCT CGA GGA AAG AGT CCG TCA AGC AAT AAT ACG AAC GAT AAT GAA GAG
 D   N   T   E   P   P   E   R   G   A   A   F   A   S   R   G   K   S   P   S   S   N   N   T   N   D   N   E   E

CAG GGT TCA CTC ACG CCG CGG TTC TAC GCT ACC GTT CAA ACT CTC CCG AAG AAT CCT TCC GCG TCT AAA ACT GGG TAT CTG TTA ATG
 Q   G   S   L   T   P   R   F   Y   A   T   V   Q   T   L   P   K   N   P   S   A   S   K   T   G   Y   L   L   M

CCT GAC GAT ACC TAC ACG CAC TGG GCA CGG CGG TTC GTT GAA CTT CGG CTG CCG TAC CTG CAT ATC TAT TCT GTC CCG GAA GGC GAC
 P   D   D   T   Y   T   H   W   A   R   R   F   V   E   L   R   L   P   Y   L   H   I   Y   S   V   P   E   G   D

GAA ATT AAC GCA ATC AAC CTC CGC AAT GCG CGA GTC GAC CAT GCG CCT GAT TTC GCC AGA CTT CTC GAC GGC CCC GGA GCT GAT GGG
 E   I   N   A   I   N   L   R   N   A   R   V   D   H   A   P   D   F   A   R   L   L   D   G   P   G   A   D   G

TCA TCT CAG GGG CGG CCT AAT GTG TTT GCA GTG TAC GGT CCG CAG AAC ACG TTC CTC TTC GCG GCG CGG ACA GAG GCT CAG AAG GTT
 S   S   Q   G   R   P   N   V   F   A   V   Y   G   P   Q   N   T   F   L   F   A   A   R   T   E   A   Q   K   V

GAA TGG ATC TTG AAG ATC GAT GAG ACT TAT TTC AGC AAT AAC GCA CCT CGA GCG GGA GCG ACG ACC AAC AGG TCC GGG AGA TGA
 E   W   I   L   K   I   D   E   T   Y   F   S   N   N   A   P   R   A   G   A   T   N   R   S   G   R   *
```

Figure IV. 01. Analysis of *A. nidulans* kinesin *uncA*. (A) Domain prediction for the UncA protein. The UncA (1631 amino acids) protein sequence was analyzed with the SMART program (http://smart.embl-heidelberg.de) and besides the kinesin motor domain, a forkhead association (FHA) and a pleckstrin homology (PH) domains have been identified in UncA. **(B)** Open reading frame of the UncA protein. The *uncA* gene is 4968 bp long and a 75 bp long intron (lower-case letters) at amino acid position 65, has been determined. The kinesin motor domain (labelled in gray) 6-361 aa, ATP-binding motifs (labelled in yellow): P-loop from amino acid (aa) 111 to 118, switch I from aa 224 to 229 and switch II from aa 261 to 266, respectively. Microtubule binding motifs (labelled in yellow): MT1 starts at aa 170 and MT2 at aa 312, the neck linker after the motor domain (labelled with bright gray), two coiled coil domains (labelled with yellow) at aa positions 371 to 481 (including the neck CC and CC1) and 748 to 823 (including CC2), FHA domain (labelled with red) between aa 496-596 and a PH domain (labelled with blue) between aa 1508 and aa 1616.

Relatedness analysis of UncA with other Kinesin-3 proteins was done using Vector NTI, and a phylogenetic tree was constructed **(Figure IV. 02, A)**. Comparison between the kinesin-3 sequences revealed 60% homology with *N. crassa* Nckin2 (48% Identity), 48.1% with *U. maydis* Kin3 (34% identity)*,* and 46.5% with *C. elegans* Unc104 (28% identity), but 80.8% homology with *A. oryzae* BAE60207 (74% identity), and 88.1% with *A. fumigatus* XP-755805 (80% identity). Both, homology and identity between the proteins are even much higher when only the motor domains are compared **(Figure IV. 02, B)**.

A
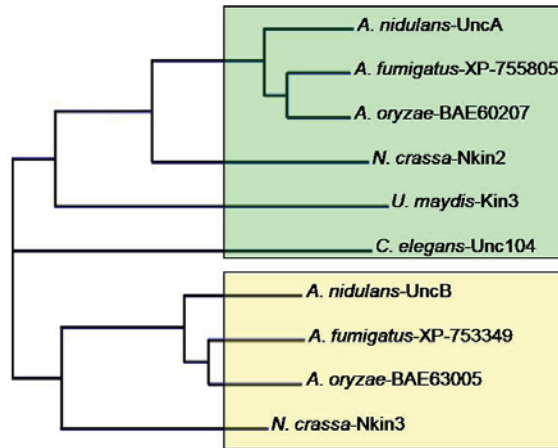
B
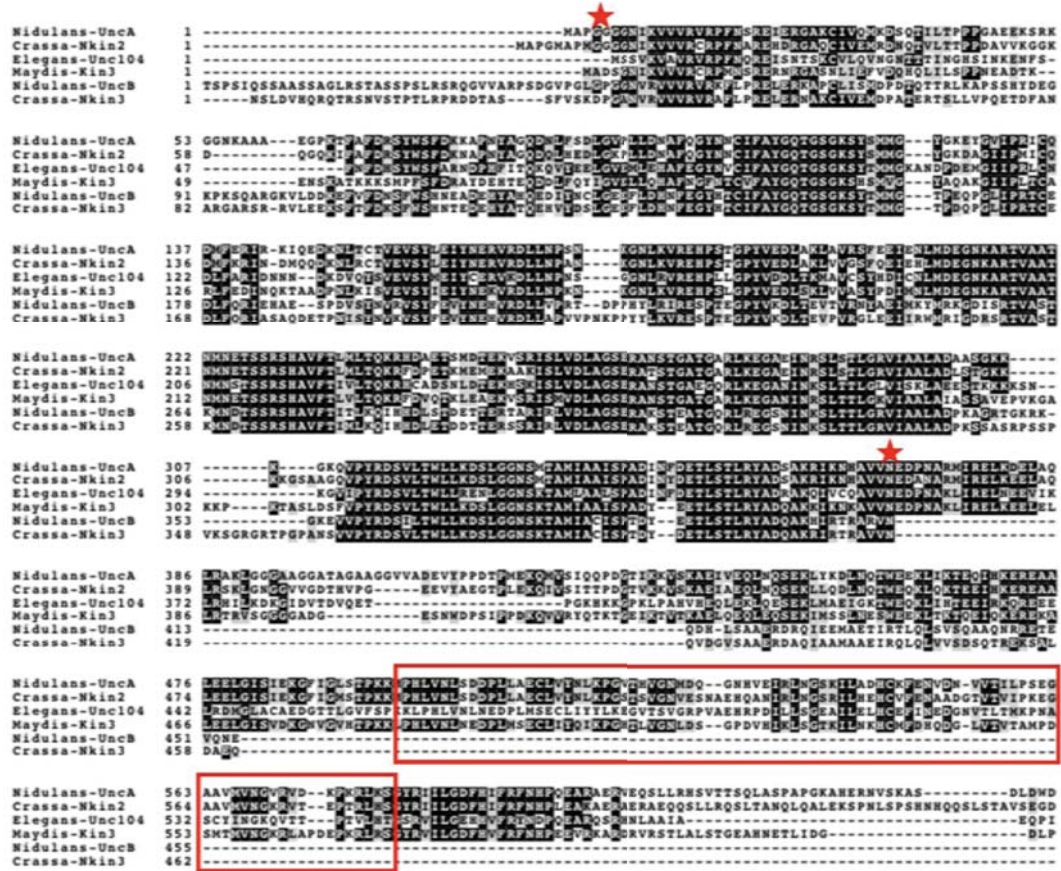
Figure IV. 02. UncA and UncB relatedness analysis with other kinesins of the kinesin-3 family.
(A) The relatedness analysis was done with Clustal W using standard parameters. UncB groups with the fungal-specific subclass as indicated by yellow shading. **(B)** Alignment of *A. nidulans* UncA and UncB (An7547.2 and An6863.2 respectively) motor domain and the FHA (red frame) domains with homologous sequences from *N. crassa* (Nkin2 and Nkin3), *C. elegans* (Unc104), and *U. maydis* (Kin3)*.* The alignment was done with Clustal W and Boxshade with a window size of 5. The red asterisks mark the borders of the motor domain.

1.2. UncB structure and relatedness analysis

The derived UncB protein is comprised of 671 amino acids, with a calculated molecular mass of 75 kDa. The motor domain starts 104 amino acids downstream of the initiation codon, and consists of 356 amino acids. The ATP-binding motif (P-loop) starts at amino acid 212 (GQTGSGKS). The C-terminal half of the motor domain displays the highly conserved regions termed switch I (NDTSSR), at amino acid 326 and switch II (DLAGSE) at amino acid 363, which are involved in nucleotide-binding (ATP). Two microtubule-binding motifs were found, MT1 (RDLL) starts at amino acid position 268 and MT2 (VPYRDS) at amino acid 417. The N-terminal region before the motor domain starts with a short sequence of 104 amino acids and contains 2 low complexity regions, whose function is not yet known **(Figure IV. 03, A and B)**.

Comparison of full-length UncB with other Kin-3 proteins revealed 56.4% homology with *N. crassa* Nckin3 (49% identity), 83% with *A. oryzae* BAE63005 (76% identity) and 75% with *A. fumigatus* XP-753349 (68% identity). The values are much higher when only the motor domains are compared **(Figure IV. 02, A and B)**.

The 195 amino acid long C-terminal part outside the motor domain exhibits very low sequence similarity to the corresponding regions of related proteins **(Figure IV. 02, A and B)**. It contains coiled coil regions, which may regulate a monomer to dimer transition **(Figure IV. 03, A and B)**. Recently, Adio and Woehlke shows a direct comparison of the monomeric Nkin3 with its dimeric full-length counterpart and suggest that the heads of the wild-type NcKin3 motor are strictly coupled via the neck domain, and that the dimeric structure is required for proper detachment after one ATPase cycle (Adio & Woehlke, 2009).

To get more insights into the function of both proteins, deletion strains of *uncA*, *uncB,* and *uncA*/*uncB* double deletion strains were constructed (see below).

A   UncB

B

```
ATG TAC CAT CAC TTT ATC CGT CGC CAA CGA GAA ATC GTC GCT CAA CTT GAA CAG ACA TTG TCA GAT CAC GGT GAA GAG ATG GCG CTG
 M   Y   H   H   F   I   R   R   Q   R   E   I   V   A   Q   L   E   Q   T   L   S   D   H   G   E   E   M   A   L

GAC CCT CGC TTC TAT CAC CAT CTC GGC CCC GGC ATC GGA TCT GGT TCG CAG TCT TCG GCT TCG CTG TCG GGG TTA TCT TCG GCG ACG
 D   P   R   F   Y   H   H   L   G   P   G   I   G   S   G   S   Q   S   S   A   S   L   S   G   L   S   S   A   T

GGA ATC ACG AGC CCA TCT ATA CAA TCG TCT GCT GCT TCT TCT GCC GGC TTG CGG TCA ACT GCT TCT AGT CCA TCC CTA CGG TCA CGA
 G   I   T   S   P   S   I   Q   S   S   A   A   S   S   A   G   L   R   S   T   A   S   S   P   S   L   R   S   R

CAA GGC GTT GTT GCC AGA CCT TCT GAT GGC GTC CCG GGC CTC GGT CCT GGA GGA AAT GTT CGT GTC GTT GTA AGA GTG CGG AAG TTT
 Q   G   V   V   A   R   P   S   D   G   V   P   G   L   G   P   G   G   N   V   R   V   V   V   R   V   R   K   F

CTG CCG AGA G   gtacgtgcagccagtttgatggacatgaaagctaatatgatttatggttcag   AG CTC GAG CGC AAG GCA CCA TGT TTG ATT TCA ATG
 L   P   R   E                                                            L   E   R   K   A   P   C   L   I   S   M

GAT CCG GAT ACA CAG ACG ACG AGG CTA AAG GCA CCG AGC TCC CAC TAT GAC GAA GGG AAA CCG AAA TCG CAG GCG CGC GGG AAA GTG
 D   P   D   T   Q   T   T   R   L   K   A   P   S   S   H   Y   D   E   G   K   P   K   S   Q   A   R   G   K   V

CTG GAC GAT AAG GAA TTC GTA TTC GAT AAT TCA TTC TGG TCA CAC AAC GAG GCA GAC GAA CAT TAT GCC CAC CAG GAG GAT ATC TAT
 L   D   D   K   E   F   V   F   D   N   S   F   W   S   H   N   E   A   D   E   H   Y   A   H   Q   E   D   I   Y

AAC TGT CTA GGA GAG GAG TTT CTA GAC CAC AAT TTT GAA GGT TAC CAC ACG TGT ATC TTC GCA TAC GGT CAA ACA GGT TCT GGT AAG
 N   C   L   G   E   E   F   L   D   H   N   F   E   G   Y   H   T   C   I   F   A   Y   G   Q   T   G   S   G   K

AGT TAT ACT ATG ATG GGA ACT CCT GAG CAG CCC GGC TTG ATC CCG CGG ACA TGC GAG GAT TTA TTC CAA CGA ATT GAA CAC GCC GAG
 S   Y   T   M   M   G   T   P   E   Q   P   G   L   I   P   R   T   C   E   D   L   F   Q   R   I   E   H   A   E

TCT CCG GAT GTC AGC TAT AAC GTT CGC GTC TCC TAT TTT GAA GTC TAC AAC GAG CAT GTA CGC GAC TTG CTG GTT CCT CGA ACT GAC
 S   P   D   V   S   Y   N   V   R   V   S   Y   F   E   V   Y   N   E   H   V   R   D   L   V   P   R   T   D

CCG CCT CAT TAT CTT CGA ATT CGA GAA TCA CCT ACT GAG GGG CCG TAT GTG AAA GAT CTT ACC GAA GTC ACA GTC CGG AAC TAT GCA
 P   P   H   Y   L   R   I   R   E   S   P   T   E   G   P   Y   V   K   D   L   T   E   V   T   V   R   N   Y   A

GAG ATC ATG AAG TAC ATG CGC AAA GGC GAT ATA TCA CGC ACC GTT GCT AGC ACT AAG ATG AAT GAT ACG TCC TCG CGG TCA CAT GCC
 E   I   M   K   Y   M   R   K   G   D   I   S   R   T   V   A   S   T   K   M   N   D   T   S   S   R   S   H   A

GTT TTC ACG ATC ACA CTG AAG CAG ATC CAC CAT GAT CTC TCT ACA GAC GAG ACA ACA GAA CGC ACA GCG CGC ATT CGC CTT GTC GAT
 V   F   T   I   T   L   K   Q   I   H   H   D   L   S   T   D   E   T   T   E   R   T   A   R   I   R   L   V   D

CTC GCT GGT TCT GAA AGA GCC AAA TCC ACC GAA GCT ACG GGT CAG CGA CTG CGC GAG GGA TCT AAT ATC AAC AAA TCT CTT ACC ACT
 L   A   G   S   E   R   A   K   S   T   E   A   T   G   Q   R   L   R   E   G   S   N   I   N   K   S   L   T   T

TTG GGT AGA GTT ATT GCG GCT CTT GCC GAC CCC AAA GCA GGA CGG ACG GGT AAA CGG AAG GGA AAG GAA GTT GTT CCT TAC CGT GAC
 L   G   R   V   I   A   A   L   A   D   P   K   A   G   R   T   G   K   R   K   G   K   E   V   V   P   Y   R   D

TCA ATC CTC ACA TGG TTA TTG AAA GAC AGT CTT GGG GGT AAC TCA AAA ACG GCT ATG ATT GCC TGT ATC TCG CCC ACA GAT TAT GAA
 S   I   L   T   W   L   L   K   D   S   L   G   G   N   S   K   T   A   M   I   A   C   I   S   P   T   D   Y   E

GAA ACA CTC TCC ACG CTA CGC TAC GCT GAC CAG GCG AAG CAT ATC CGC ACG CGC GCG AGA GTT AAT CAA GAT CAT CTG TCC GCT GCT
 E   T   L   S   T   L   R   Y   A   D   Q   A   K   H   I   R   T   R   A   R   V   N   Q   D   H   L   S   A   A

GAG CGT GAC CGA CAG ATC GAA GAA ATG GCG GAG ACT ATC CGC ACG CTC CAG CTC AGC GTC AGC CAA GCT GCG CAG AAT CGC CGA GAG
 E   R   D   R   Q   I   E   E   M   A   E   T   I   R   T   L   Q   L   S   V   S   Q   A   A   Q   N   R   R   E

ACC GAG GTC CAG AAT GAA CGG CTT GAA GAG TAT CAG CAG CAG GTG GAG AAG CTT CAG CGG CTC ATG GAG GAG AAC AAG ATG GTT AGT
 T   E   V   Q   N   E   R   L   E   E   Y   Q   Q   Q   V   E   K   L   Q   R   L   M   E   E   N   K   M   V   S

GAA TGC AAA ATC AGG CAG CTG CAG ACC GAG AAC GAA GCG CTA CGC AAC CAC CTA AAG CTG GCT TTG GAT AGC TTA AAG AAT CCT ATT
 E   C   K   I   R   Q   L   Q   T   E   N   E   A   L   R   N   H   L   K   L   A   L   D   S   L   K   N   P   I

CCT CCA GTG ACA ATC GAG AAG GCT CTC AGC GAC GTT GAT ATT CCA GAC GAG GAG CAG CCG ATC GAC GAG CAG CAG CCG GGC TCT CCT
 P   P   V   T   I   E   K   A   L   S   D   V   D   I   P   D   E   E   Q   P   I   D   E   Q   Q   P   G   S   P

ACT TCG GGA GCA GAA ACA GAG CCG GAT CTA ATT TGG GAA GAC GAG AAC CTC CCA CCC GAC ACA AGC GAG TTA GAA GCC CAA GAA ATG
 T   S   E   A   E   T   E   P   D   L   I   W   E   D   E   N   L   P   P   D   T   S   E   L   E   A   Q   E   M

CAG GCA ACA ATG GAG AAT CTT TTG GGC GAT CTC GAT GTC TTC AAG AGA AAG CTG GCT ACA GAC CAC GAA CGC TTT GGT GCA AGT CGA
 Q   A   T   M   E   N   L   L   G   D   L   D   V   F   K   R   K   L   A   T   D   H   E   R   F   G   A   S   R

AAA CAC GAG GGC CGC AAA AGA CGG CGG GCT CTT GGG GAC ATC TTG GGG AAC TGA
 K   H   E   G   R   K   R   R   R   A   L   G   D   I   L   G   N   *
```

Figure IV. 03. Analysis of the A. *nidulans* kinesin *uncB*. (A) Domain prediction for the UncB protein. The UncB (671 amino acids) protein sequence was analyzed with the SMART program (http://smart.embl-heidelberg.de) and besides the kinesin motor domain, a short tail consisting of multiple coiled coil motifs was identified. **(B)** The UncB open reading frame has 2065 bp and a predicted intron with 52 bp (lower-case letters) at amino acid position 120. The motor domain (labelled in gray) spans between 104-473 aa, the ATP-binding motifs (labelled in yellow): P-loop at aa 212-219, switch I at aa 326-331 and switch II at aa 363-368 respectivly, microtubule binding motif (labelled in yellow): MT1 at aa 268-271 and MT2 at aa 417-422, two low complexity regions (labelled with blue) at aa positions 40 to 73 and 97 to 114, two coiled coil domains (labelled with yellow) at aa positions 482 to 564 and 615 to 643.

2.   Deletion of *uncA* and *uncB*

2.1. Deletion of *uncA*

The *uncA*-open reading frame was deleted in the *uncA* wild-type strain TN02A3 with *pyroA* as selection marker, and the deletion event was confirmed by diagnostic PCR and Southern blot **(Figure IV. 04)**. The flanking regions of *uncA* were amplified by PCR using genomic DNA and the primers UncA-LB-fwd and UncA-LB-*Sfi*I-rev for the upstream region of *uncA*, and UncA-RB-*Sfi*I-fwd with UncA-RB-rev for the downstream region. In a three-fragment ligation, the *pyroA*-gene obtained from plasmid pNZ12 was ligated between the two *uncA*-flanking regions, resulting in vector pNZ13. The deletion cassette was amplified with the primers UncA-LB-fwd and UncA-RB-rev, and the resulting PCR product was transformed into the pyro-auxotrophic *A. nidulans* strain TN02A3 **(Figure IV. 04)**.
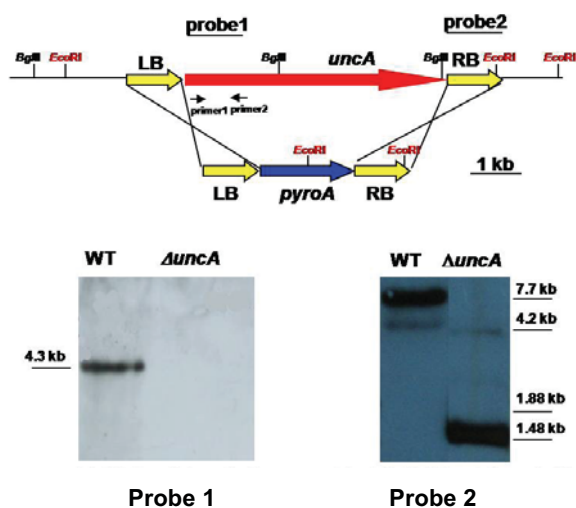
Figure IV. 04. Deletion of *uncA*. Scheme of the deletion procedure and corresponding Southern blots. DNA was digested with *Bgl*II (left) and with *Eco*RI (right). The probes are indicated above.

One of the strains (SNZ9) was used for further analysis and the construction of *uncA*-deletion strains in other genetic backgrounds. Colonies of this strain grew slower than wild-type colonies and appeared more compact **(Figure IV. 05)**.
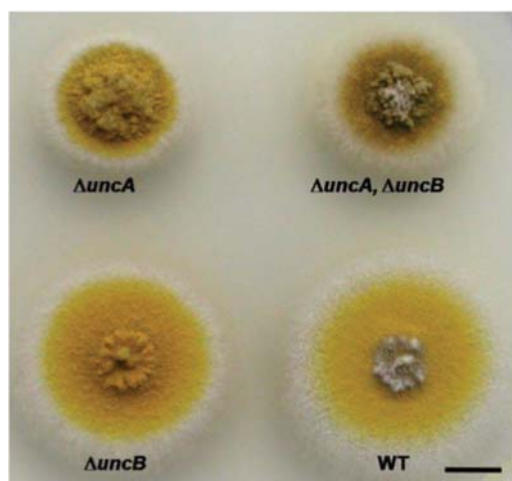
Figure IV. 05. Phenotype of an *uncA*, an *uncB,* and a double-deletion strain. Growth of the strains SNZ27 (*ΔuncA*), SNZ15 (*ΔuncB*), SNZ29 (*ΔuncA, ΔuncB*), and RMS011 on minimal medium for 3 days. Scale bar 1 cm.

The coupling of the observed phenotypes with the gene-deletion event was confirmed by crosses and by down-regulation of *uncA* through the inducible *alcA* promoter **(see below, Figure IV. 15)**.

Comparison of organelle distribution as nuclei (visualized with Dsred-StuA in SNZ21), mitochondria (visualized with GFP-tagged mitochondria in SNZ20) or the organization of the microtubule cytoskeleton (visualized with GFP-alpha tubulin in SNZ-SI40) shows no differences to wild-type strain **(Figure IV. 06)**.
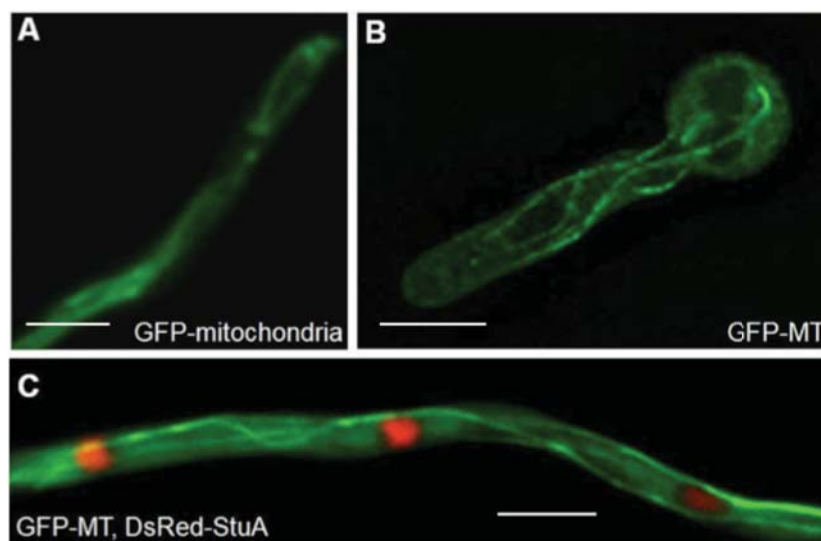
Figure IV. 06. Observation of mitochondria (A), microtubules (B), and microtubules with nuclei (C) in an *uncA*-deletion strain. GFP or DsRed were used for the visualization. Strains are SNZ20 in (A), SNZ-SI40 in (B) and SNZ21 in (C). Scale bar 5 μm.

However, an increased number of branches in *ΔuncA* strain was noticed at 37°C. At higher temperature a slight curved hyphal phenotype similar to the phenotype of cell end marker mutants was observed (Takeshita *et al.*, 2008) **(Figure IV. 07)**.
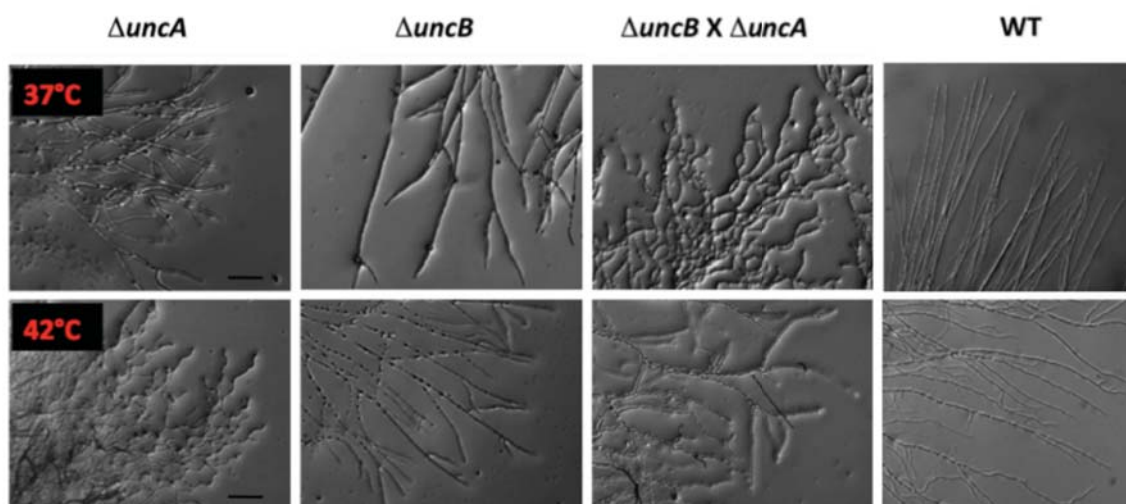
Figure IV. 07. Phenotype of *ΔuncA*, *ΔuncB*, and a double-deletion strain at 37°C and 42°C. Strains SNZ27 (*ΔuncA*), SNZ15 (*ΔuncB*), SNZ29 (*ΔuncA, ΔuncB*), and RMS011 (WT) were grown on minimal medium with glycerol as carbon source for 2 days. Scale bar 25 μm.

To test if the *uncA*-deletion strain showed this curved phenotype because of mislocalization of the cell end marker TeaA, a *uncA*-deletion strain with a mRFP1-TeaA and GFP-alpha tubulin was constructed. Suprisingly, neither TeaA nor the microtubules displayed any defect in the tip compartment in comparison to wild-type **(Figure IV. 08)**.
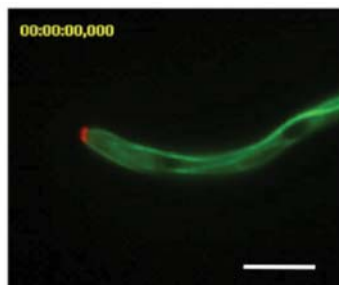
Figure IV. 08. Observation of the cell end marker mRFP1-TeaA with GFP-microtubules in an *uncA*-deletion strain (SNZ43). Scale bar 5 μm.

2.2. Deletion of *uncB*

The *uncB*-open reading frame was deleted using the same strain (TN02A3) as for the *uncA* deletion with *pyr4* as selection marker. The *uncB*-flanking regions were amplified by PCR using genomic DNA and the primers uncB_LB_fwd and uncB_LB_*Sfi*I_rev for the upstream region of *uncB*, and uncB_RB_*Sfi*I_fwd with uncB_RB_rev for the downstream region. The two *uncB*-flanking regions were ligated upstream and downstream of the *pyr4* marker in pCS1, generating pNZ5. This plasmid was cut with *Eco*RI and *Bgl*II, generating a fragment containing *pyr4* flanked by *uncB* sequences. This fragment was transformed into the uracil-auxotrophic strain TN02A3 **(Figure IV. 09)**.
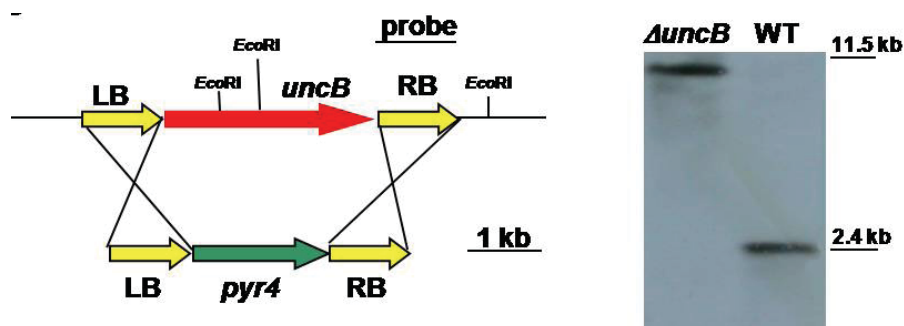
Figure IV. 09. Deletion of *uncB*. Scheme of the deletion procedure and corresponding Southern blot. DNA was digested with *Eco*RI. The probe is indicated

Transformants were screened by PCR for the homologous integration event. Single integration of the construct was confirmed by Southern blotting **(Figure IV. 09)**. One of the strains (SNZ3) was used for further analysis and the construction of *uncB*-deletion strains in other genetic backgrounds. Colonies of this strain grew like wild-type colonies **(Figure IV. 05)**. Septum formation and branching was also similar to the wild-type at 37°C

and at 42°C (**Figure IV. 07**). No difference to wild-type with respect to nuclear distribution (sNZ25) or microtubule organization (sNZ62) was observed (**Figure IV. 10**).
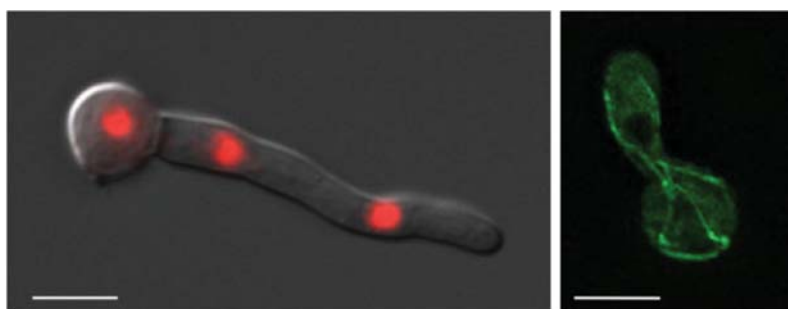
Figure IV. 10. Observation of nuclei (left), and microtubules (right) in an *uncB*-deletion strain. DsRed-StuA or GFP-alpha tubulin was used for visualization. Strain sNZ25 (left) and sNZ62 (right). Scale bars 5 μm.

In order to investigate whether UncA and UncB are functionally related, an *uncA/uncB* double-deletion strain was genetically created generating SNZ29 **(Figure IV. 05)**. It displayed the same compact growth phenotype as the *uncA*-deletion mutant at 37°C and at 42°C **(Figure IV. 07)**. The analysis of nuclear and mitochondrial distribution, the organization of the MT cytoskeleton revealed no difference in comparison to the wild-type. This was unlike the situation in *N. crassa* (Fuchs & Westermann, 2005).

2.3. Analysis of genetic interactions between UncA and other motor proteins

To see if the deletion of *uncA* causes a more severe phenotype in the absence of other motor proteins involved in polarized growth, an *uncA/kinA* (conventional kinesin) and an *uncA/nudA* (heavy chain of dynein) double-deletion mutant were constructed **(Figure IV. 11).**
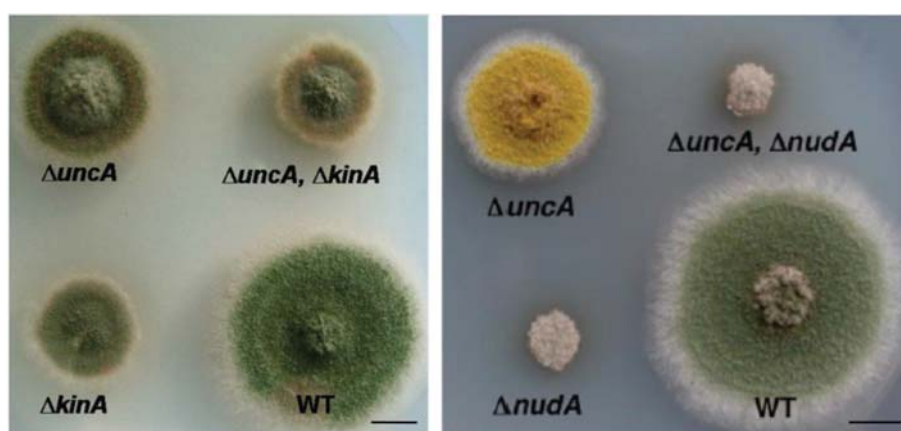
Figure IV. 11. Comparison of colony growth of different mutants as labeled. Left picture shows the deletion strains of *uncA* (SNZ9) and conventional kinesin, *kinA* (AnKin26) in comparison to the double deletion strain (SNZ36) and a wild-type (TN02A3). Right picture compares the colony phenotypes of the *uncA*-deletion strain (SNZ27) and the dynein-deletion strain (*ΔnudA*) (XX60) and the corresponding double-deletion (SNZ63). Colonies were grown for 3 days on glucose minimal medium at 37°C. Scale bars 1 cm.

The growth defects of these strains were comparable to the growth defect of stains with single mutations in either *kinA* or *nudA*, respectively. No additional phenotype was observed.

2.4. Analysis of the cell wall of *uncA* and *uncB* mutant strains

Because of the compact phenotype of *uncA* mutant strains and in order to test the integrity of the cell wall, especially in the tip compartment, Calcofluor white (CFW) and Congo red (CR) were used. CFW and CR contain two sulfonic-acid groups. Both exert antifungal activities when they are solubilized and their sulfonic-acid groups are negatively charged. As CFW preferentially stains chitin in the cell wall of fungi, it (and by analogy CR) is thought to interfere with the cell wall assembly by binding to chitin and to nascent chitin chains, thereby inhibiting the assembly enzymes that connect chitin to β-1,3-glucan and β-1,6-glucan. As a result, the cell wall becomes weakened. The addition of CFW or CR to growing fungal cells results in cell wall-related morphological changes, such as swelling or lysis of hyphal tips. The cell wall-weakening effect of CFW and CR activates the cell wall stress response (Levin, 2005). It also induces increased deposition of chitin in the cell wall. As CFW and CR are believed to bind to chitin, these compounds also directly counteract the cell wall stress response itself.

Testing for altered susceptibility to CFW and CR is commonly used in fungi to identify mutants with cell wall defects. Some mutants with lowered chitin levels in their walls become more resistant to CFW and CR. Most of the cell wall mutants, however, have more chitin in their walls than wild-type cells, because of activation of the cell wall stress response, and become more sensitive to CFW and CR. Not all mutants with a CFW-hypersensitive phenotype display increased chitin levels, indicating that the chitin level in the cell wall is not the only factor determining CFW sensitivity. Increased susceptibility to CFW or CR is indicative of cell wall defects in mycelial fungi such as *A. nidulans* (Shaw & Momany, 2002).

The concentration of CFW or CR to be used in susceptibility assays depends on several parameters. Both, the size of the inoculum and the fungal species to be tested. The preferred way to determine CFW or CR susceptibility is to inoculate a concentration series of asexually derived conidiospores (in the case of mycelial fungi) in the form of spots on plates containing CFW and CR. The concentrations of CFW or CR used for *Aspergillus* vary between 50 and 1,000 μg/ ml (Damveld *et al.*, 2005; Ram & Klis, 2006). Sensitivity to CFW and CR in this case is determined by comparing the extent of colony formation between parental and mutant strains on the control plate (CM medium) and the plates containing CFW or CR both with a concentration of 75 μg/ ml. A slightly increased sensitivity was observed in the *uncA*/*uncB* double mutant strain **(Figure IV. 12)**.
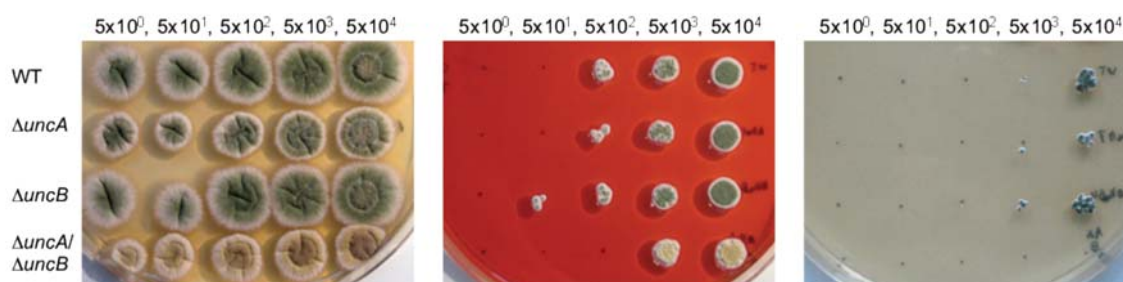
Figure IV. 12. Susceptibility of *A. nidulans* mutants to CFW (75 μg/ ml) or CR (75 μg/ ml). Ten-fold dilutions, starting at 5 x 10^4 spores, were spotted on complete medium plates buffered with 100 mM MES-NaOH (pH 6.0; left), or similar plates containing CR (75 μg/ ml; middle) or CFW (75 μg/ ml; right). Pictures were taken after 3 d of growth at 30°C. The strains used are the wild-type (TN02A3) parental strain, the *uncA* knockout strain, the *uncB* knockout strain and the *uncA* / *uncB* double deletion strain as indicated.

2.5. Amylase secretion in *uncA* deletion strain

Filamentous growth depends on the continuous delivery of secretion vesicles to the growing surface, where protein secretion mostly occurs. A structure unique to filamentous fungi, the Spizenkörper (SPK) is located in the growing hyphal tip. It is an aggregate of vesicles which are further transported to the plasma membrane (Gierz & Bartnicki-Garcia, 2001). Secretion of glucoamylase was studied in *A. niger* and was mainly observed at the hyphal tip (Gordon *et al.*, 2000a; Gordon *et al.*, 2000b). The same machinery is used for the secretion of other hydrolases and different enzymes involved in cell wall biosynthesis.

Because endocytosis and exocytosis are related machineries, and because *uncA*-deletion had an effect on hyphal extension, the protein secretion potential was studied. The amylase was used as a marker enzyme. The amylase activity was measured by determining the concentration of released glucose in surface and submerged cultivation with 2% starch as carbon source (te Biesebeke *et al.*, 2005) **(Figure IV. 13 and IV. 14)**. In the case of the solid media, Gram's Iodine was used for staining the remaining starch in the agar plate. The diameter of the produced halo was used as a measure for the secretion potential. Similar halos were surrounding both *uncA*-deletion and WT strains **(Figure IV. 13)**.
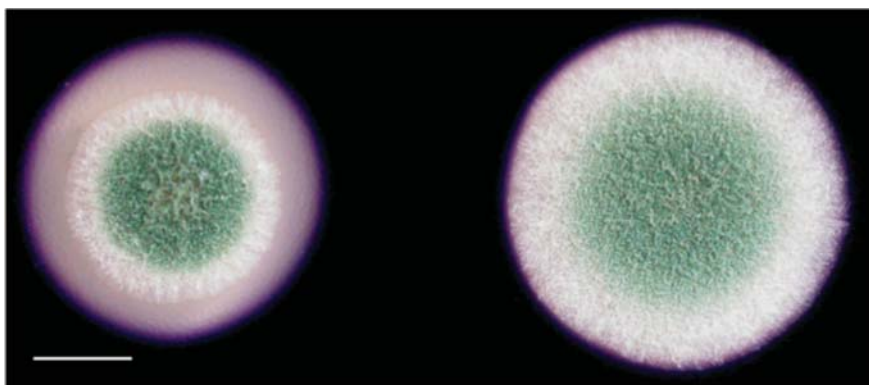
Figure IV. 13. Gram's Iodine staining of the remaining starch in surface cultivation of Δ*uncA* and wild-type strains of *A. nidulans*. The same number of spores was inoculated on 2% starch solid medium. Strains used in this assay are: *uncA*-deletion strain (left), and TN02A3 (right). Scale bar 1 cm.

The same number of spores was added per ml medium in both surface and submerge cultivations. During surface cultivation, glucose concentrations liberated from the substrate were lower than 0.03 mmol/l. In submerged cultivations, the glucose concentrations were maximal 0.35 mmol/l. Apparently, during submerged cultivation, an excess of glucose was liberated from the substrate, whereas the glucose concentrations in surface cultivation remained low at all time points. However, the situations in the *uncA*-deletion strain and the WT strain were similar **(Figure IV. 14)**. Confirming that the halos shown in **(Figure IV. 13)** are similar and that the occurred secretion at the branches of *uncA*-deletion strain is sufficient to recover the loss of vesicle secreted at the tip.
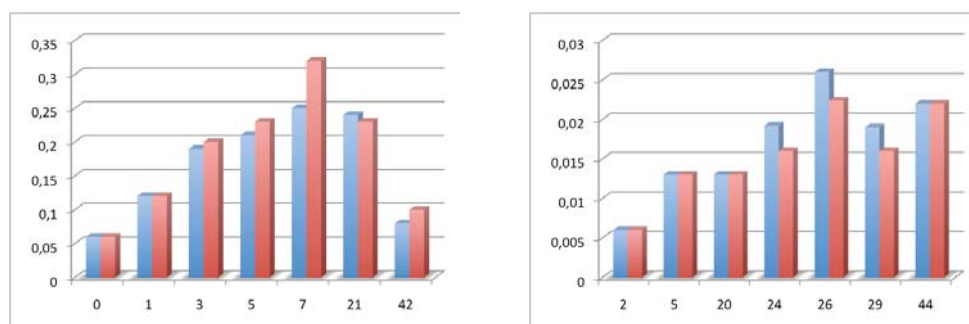
Figure IV. 14. Glucose concentration measured in (left) submerged and (right) surface cultivation of Δ*uncA* and wild-type strains of *A. nidulans*. Spores were inoculated in 2% starch liquid media (left) and 2% starch solid media (right). Glucose concentration (mmol/l, Y axes) measured in the growth medium of submerged cultivation and in the extracts of surface cultivation at the time points indicated (hours, X axes). Blue is Δ*uncA* and red is WT.

3.   Localization of UncA

3.1. UncA localizes to fast moving spots

The UncA protein was visualized by fusion with a fluorescent protein (GFP or mRFP1 in the vector pMCB17apx). To create an N-terminal GFP fusion construct of UncA, a 0.9-kb N-terminal fragment of UncA (starting from ATG) was amplified from genomic DNA, with the primers uncA_*Asc*I_fwd1 and uncA_*Pac*I_rev1. The *Asc*I-*Pac*I fragment was subcloned into the corresponding sites of pCMB17apx, yielding pAS3, where GFP-UncA was under the control of the *alcA*-promoter (de-repressed with glycerol, induced with threonine, repressed with glucose). To create an N-terminal mRFP1 fusion construct of UncA, the GFP *Kpn*I-*Asc*I fragment from pAS3 was substituted by mRFP1 from pDM8, yielding pNZ9.

After homologous integration of the construct at the *uncA* locus, the 0.9-kb fragment becomes duplicated and the full-length *uncA*-open reading frame is fused to GFP and is under the control of the *alcA* promoter. The *uncA-GFP* strain (SNZ2), in which plasmid pAS3 is homologously integrated, grew like the *uncA*-deletion strain when grown on glucose medium and like wild-type when grown on glycerol or threonine medium, showing that the GFP fusion protein was fully functional **(Figure IV. 15)**.
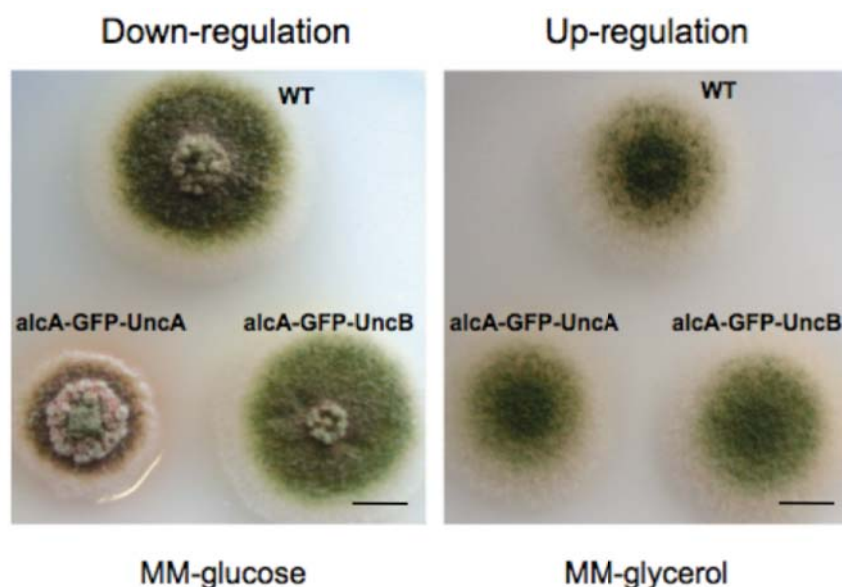
Figure IV. 15. Up- and downregulation of GFP-UncA and GFP-UncB fusion constructs. Colonies were grown on minimal medium with glucose (downregulation) or minimal medium with glycerol (de-repression). The GFP-UncB strain behaves always like the WT, whereas the GFP-UncA strain shows a compact growth phenotype when grown on glucose medium. Scale bar 1 cm.

Under inducing conditions GFP-UncA was visible as fast moving spots and accumulated sometimes at the tips of the hyphae **(Figure IV. 16, A; movie IV. 01)**. They moved into two

directions with speeds of up to 6 μm/sec. The GFP signal at the tip looked like an accumulation of dynamic vesicles.
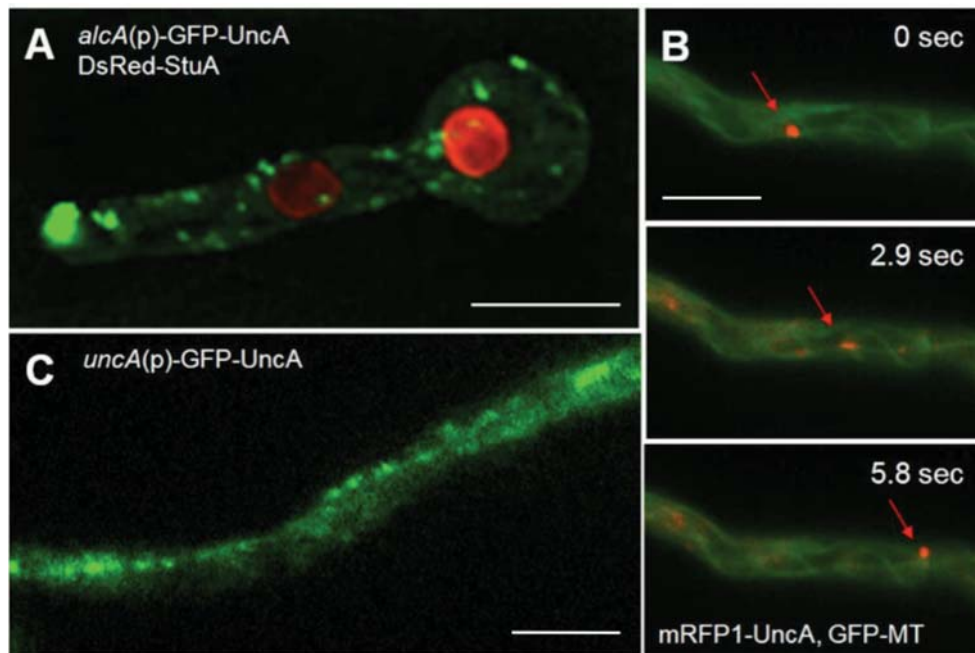
Figure IV. 16. Localization of UncA. (A) UncA was labeled with GFP and nuclei with DsRed, UncA was under the control of the *alcA* promoter (SNZ4). **(B)** Movement of UncA along microtubules. Time-lapse analysis of mRFP1-UncA in a strain with GFP tagged microtubules (SNZ26). One spot (indicated with the arrow) was focused and followed over time. The time between the exposures of the pictures is indicated. **(C)** GFP-UncA expressed under the natural promoter (SNZ74). A pearl-string like arrangement of the signal is visible. Scale bars 5 μm.

After addition of the microtubule-destabilizing drug benomyl, vesicle movement in the hyphae and at the tip stopped (**Figure IV. 17)**, suggesting microtubule-dependent movement. This finding was supported by co-localization of GFP-labelled microtubules with mRFP1-labelled UncA **(Figure IV. 16, B; movie IV. 02)**.
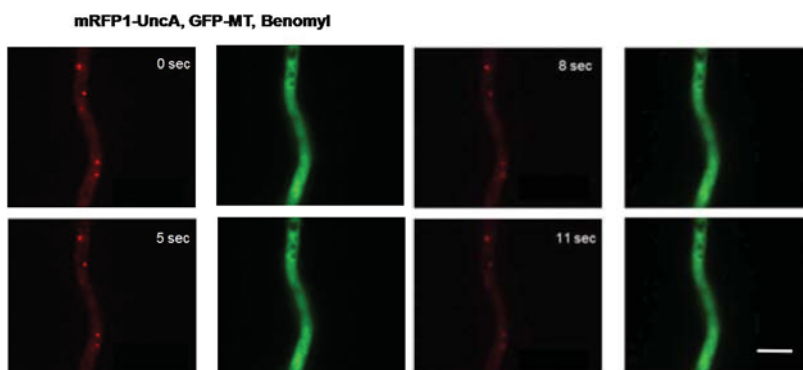
Figure IV. 17. Effect of benomyl on UncA movement. Hyphae of SNZ26 were incubated with 2.5 µg/ml benomyl for 10 min. mRFP1-UncA spots did not move during the 11 seconds observation time. Microtubules (GFP) were disassembled under these conditions. Strain sNZ26. Scale bars 5 μm.

To exclude the possibility that the observed localization was due to the artificial expression of the GFP-UncA fusion protein (glycerol as carbon source for the de-repression of the *alc*A promoter), the *alcA* promoter was replaced with a 1.5-kb DNA fragment derived from the

putative *uncA* promoter. The putative promoter was amplified from genomic DNA with the primers UncA_nat(P)_*EcoR*I_fwd and UncA_nat(P)_*Kpn*I_rev, digested with *EcoR*I and *Kpn*I, and the two fragments were ligated with *EcoR*I-*Kpn*I–digested pAS3, yielding pNZ-SI49. This construct was transformed into TN02A3. One strain with a homologous integration event at the *uncA* locus was selected for further analysis (SNZ74) **(Figure IV. 18)**.
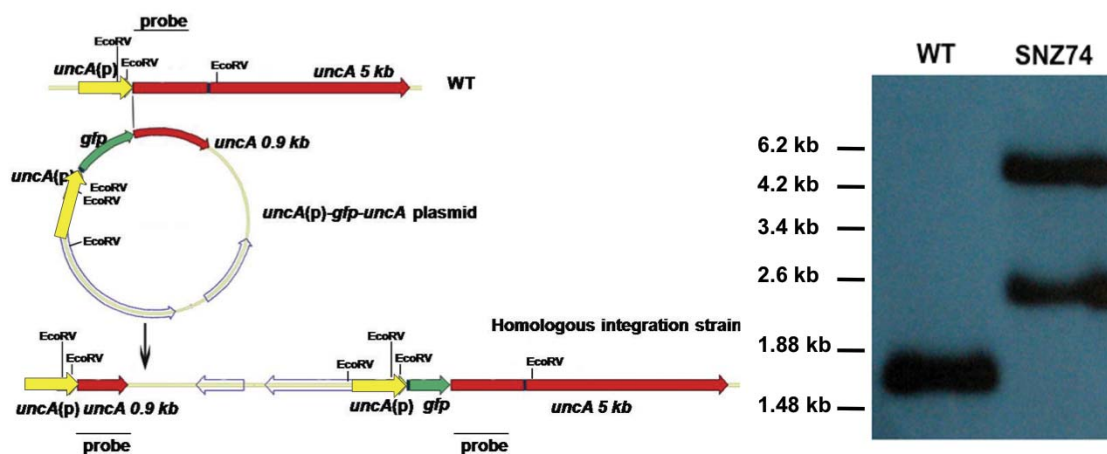
Figure IV. 18. Expression of GFP-UncA under the control of the natural promoter. Scheme of the construct and the integration event (left) and the corresponding Southern blot to show integration at the locus (right). Probe is indicated.

The strain appeared like wild-type, suggesting functionality of the UncA-GFP fusion protein. Although the GFP signal was weaker than in the previous strains, small moving spots were clearly visible in the microscope **(Figure IV. 16, C)**. These results suggested that in the above-described experiments moderate overexpression with glycerol in the medium did not cause artefacts and/or mislocalization of the protein. Interestingly, the GFP-UncA protein appeared to prefer essentially one track in the cell **(Figure IV. 16, C; movie IV. 01)**.

3.2. UncA is involved in vesicle transport

Because a role of UncA in mitochondrial movement - as it was observed in *N. crassa* - was excluded, and because Kin-3 of *U. maydis* localizes to early endosomes, the association of UncA with endosomes was analyzed. To this end, the plasma membrane in *A. nidulans* strain (SNZ74, *uncA(p)::GFP::uncA*) was stained with the membrane-selective fluorescent vital dye FM4-64 (Peñalva, 2005). FM4-64 was used at a concentration of 10 µM in the medium. Coverslips were incubated for 1-2 min and washed. After internalization of the membrane early endosomes were visible. The movement of the corresponding vesicles resembled the movement of GFP-UncA **(movie IV. 03).** However, co-localization of the red FM4-64 and the green UncA signal proved to be difficult because of the high speed of the structures.

This technical obstacle was overcome by generating a rigor variant of UncA by changing glycine residue 450 to glutamate. This modification of the P-loop allows binding of the motor to the microtubules but not their dissociation (Nakata & Hirokawa, 1995). The movement of FM4-64 labelled vesicles was reduced and co-localization with GFP-UncA^{rigor} was observed in some cases **(Figure IV. 19, A)**.
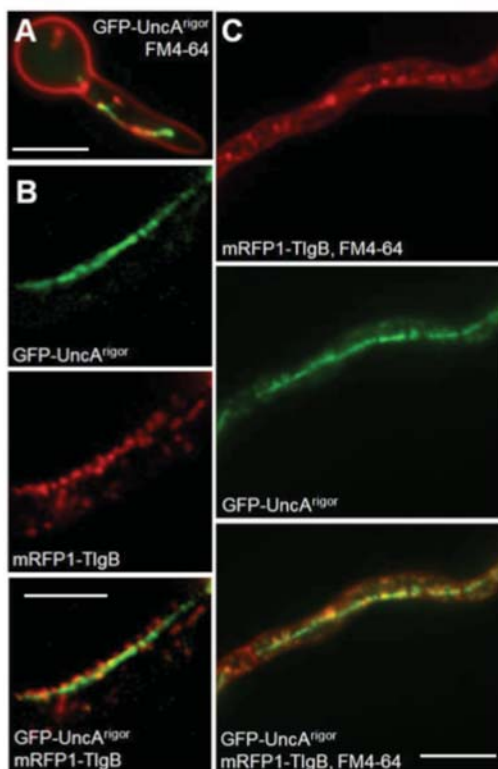
Figure IV. 19. Co-localization of endosomes with UncA. (A) FM4-64 stained endosomes in the GFP-UncA^{rigor} strain (SNZ14). **(B)** Co-localization of mRFP1-TlgB and GFP-UncA^{rigor} (SNZ69). **(C)** Co-localization of mRFP1-TlgB and FM4-64 with GFP-UncA^{rigor}. Scale bars 5 μm.

Quantification was impossible, because of the alignment of the vesicles to a continuous structure. The fact that not all GFP signals co-localized with FM4-64 suggested that UncA is not only associated with early endosomes but also with other vesicles. It also shows that early endosomes are not homogenous. As a further proof for the binding of UncA to endosomes, a *S. cerevisiae* Tlg2 homologue was tagged with mRFP1 in *A. nidulans* and named TlgB. TlgB was used as a marker as it was used before for endosome labelling in *A. oryzae* (Kuratsu *et al.*, 2007). *S. cerevisiae* Tlg2 localizes to trans-Golgi and endosomes (Gurunathan *et al.*, 2002; Holthuis *et al.*, 1998).

The *tlgB* gene (or AN2048) is localized to chromosome VII and displays 39.9% homology to the *S. cerevisiae* Tlg2 protein. Tlg2 belongs to the group of syntaxin-like t-SNARE protein, and harbors a Syntaxin domain between amino acid positions 66 and 174 and a t-SNARE domain in the C-terminal part, between amino acid position 234 and 301 **(Figure IV. 20, A and B)**. Syntaxins are a family of receptors for intracellular transport of vesicles. Target membranes are identified by specific members of the syntaxin family. The t-SNARE (target soluble N-ethylmaleimide-sensitive factor (NSF) attachment protein (SNAP)

receptor proteins) belongs to SNAREs, which normally localize to distinct membrane compartments of the secretory and endocytic trafficking pathway, and contribute to the specificity of intracellular membrane fusion processes.

A   TlgB

B

```
ATG TGG CGG GAC CGC ACC AAT CT  gtacttaccgaccttgccttgtatatgcgcctctcaacgggtttatgctaacacctgtcctctcgcag  T TAC
M   W   R   D   R   T   N   L                                                                                         Y

ATC TCC TAC CGT CAG TCA TTT ACC CAT CAC CCC GCA AAG AAG CCG CGA TAC CTC GGA ACA CCC AAT GGC TTC TCC GAC GTA
I   S   Y   R   Q   S   F   T   H   H   P   A   K   K   P   R   Y   L   G   T   P   N   G   F   S   D   V

GCG TCA CAA TCT GAA GAA AGT CGG CGG CTT ATA TCT GAA TCC ACG GGG ATT GAC GAC GAT GGC GAT GCG ATC ATT GAG ATG
A   S   Q   S   E   E   S   R   R   L   I   S   E   S   T   G   I   D   D   D   G   D   A   I   I   E   M

GAT GTG CTC CCG CCA CGC TGG GTC GAT GTG CAG GAG GAT GTG ACG GAC TTA CTC GCG GAC ATT GCA CAG AAG TCG GCC CAG
D   V   L   P   P   R   W   V   D   V   Q   E   D   V   T   D   L   L   A   D   I   A   Q   K   S   A   Q

CTA GAT AAG CTG CAC CAC AAG CAC CTC TTA CCG GGA TTC GGC GAT GAG GAA GTA CGA AAG CAA GAC GAG CGT GTT ATT GAA
L   D   K   L   H   H   K   H   L   L   P   G   F   G   D   E   E   V   R   K   Q   D   E   R   V   I   E

CGG TAT ACG CAA GAA ATT ACA CGC GGC TTC CAT GAG TGT CAA AAG CTT GTC AAG CGC ATA GAG GTT ATG GTA CAT GAA GCC
R   Y   T   Q   E   I   T   R   G   F   H   E   C   Q   K   L   V   K   R   I   E   V   M   V   H   E   A

AAA CAG CAA GGG GGG GTG AGT AGC GGA GAT GAA ACC ATG GCC AAG AAC ATT CAG ATA TCA CTT GCA TCG AGG GTA CAA GAA
K   Q   Q   G   G   V   S   S   G   D   E   T   M   A   K   N   I   Q   I   S   L   A   S   R   V   Q   E

GCC AGT GCT CAG TTC AGG AAG AAA CAA AGC AAT TAT TTA AAG A gtatgttgaagggtttgtcgctgctcctagacggccagtcagctaacgt
A   S   A   Q   F   R   K   K   Q   S   N   Y   L   K   K

atgtgtcattag AG CTA CGA GGT CTT GAA GAT ACG GCC TCA CAA TTC GAT CGT TCT ACT ACG CCA ATG CAG AAT CCG TAT ACA
              L   R   G   L   E   D   T   A   S   Q   F   D   R   S   T   T   P   M   Q   N   P   Y   T

GAT CCG TCA TTA ATG GAG TCC GAT GCC GAT AAG TCC TTC TCG CAA ACC ACC CTG ATG CAG ACG ACA CAG CGG ATG ACC GGC
D   P   S   L   M   E   S   D   A   D   K   S   F   S   Q   T   T   L   M   Q   T   T   Q   R   M   T   G

CAA AAC GAT GCC GCA ATC CTA CAA CGA GAG CGG GAG ATC AAC GAC ATT GCC AAA GGA ATC ATC GAA CTA TCT GAT ATT TTC
Q   N   D   A   A   I   L   Q   R   E   R   E   I   N   D   I   A   K   G   I   I   E   L   S   D   I   F

CGC GAG CTA CAG GCA ATG GTC ATC GAC CAA GGT ACA ATG CTG GAT CGC ATA GAC TAC AAT GTG GAG AGA ATG AAC ACC GAT
R   E   L   Q   A   M   V   I   D   Q   G   T   M   L   D   R   I   D   Y   N   V   E   R   M   N   T   D

GTT CAA GCA GCC CAG AAG GAA CTC AAT GTG GTA TGT CTC ACA ACC CTA CTG GCG GGC ATA CAA TCT ATA GAG CTC GAA AAC
V   Q   A   A   Q   K   E   L   N   V   V   C   L   T   T   L   L   A   G   I   Q   S   I   E   L   E   N

TAA acatctaactcaggcgactaactaccaacggcgtaccacaaagcgcaaataattcttcttttgatccttctggtggtggggatgataattatcctcctcgtt
*
aagccgaagaaacatgaatcatctgaacctgcgccgcctcctacccaaccagaaaatctaccgcctggcctacgccgcgaggttttgaaatagcatataggcgtcc

aaggtcaccttcattgacgcgagttgcaaggagcgagtgggttgatcctgatatatatcgataa
```

Figure IV. 20. Analysis of A. *nidulans tlgB*. (A) Domain prediction for the TlgB protein. The TlgB (318 amino acids) protein sequence was analyzed with SMART program (http://smart.embl-heidelberg.de). **(B)** The open reading frame has 1083 bp and two predicted introns (small letter case letters) after amino acid position 8 with 68 bp, and after amino acid position 186 with 61 bp.

The *A. nidulans tlgB* full-length coding region was cloned downstream of mRFP1 using the same approach as for UncA. Thus a N-terminal mRFP1 fusion construct of *tlgB* was created. The primer set used for TlgB was Tlg2_nidulans_AscI_fwd and Tlg2_nidulans_PacI_rev. The PCR fragment was cloned into pCR2.1-TOPO and subsequently into pDM8 (*pyroA* as selection marker), yielding pNZ58. The plasmid was integrated into the genome of SNZ14 (GFP-UncA[rigor]). Fluorescence microscopy revealed again partial co-localization between UncA-GFP and mRFP1-TlgB **(Figure IV. 19, B)**. This strain was again treated with FM4-64. Because in *S. cerevisiae* Tlg1 and Tlg2 endocytic vesicles were only transiently labelled with FM4-64 (Holthuis *et al.*, 1998), it was anticipated that the combination of FM4-64 and TlgB-mRFP1 would stain all GFP-UncA[rigor] labelled endosomes **(Figure IV. 19, C)**. Indeed

more co-localization was detected but still some GFP signals did not localize at the same place as the red signals, again indicating that UncA is associated not only with early endosomes.

Similar to TlgB, the same molecular techniques were used to detect the *A nidulans* syntaxin-like t-SNARE protein *tlgA* (An8171), *S. cerevisiae tlg1* homologue, but many big vacuoles and vesicles were stained with this marker, that's why *tlgB* was preferred for the last experiment.

3.3. UncA cooperates with dynein in vesicle transportation

In order to study if the observed movement of FM4-64 labelled vesicles was due to UncA or another motor activity, vesicle behaviour (stained with FM4-64) was studied in *uncA*-, *kinA*-, and *nudA*-deletion strains **(Figure IV. 21; movies IV. 04 - IV. 08)**. Although UncA and KinA move towards the MT plus ends and dynein towards the MT minus ends, their movement may occur into both directions in hyphae because MTs have a mixed orientation.

It was clearly visible that the movement changed dramatically when UncA or dynein were absent or non-functional, respectively. Long distance movement as observed in wild-type was largely reduced in 28 out of 37 hyphae. In nine hyphae one or two vesicles were observed moving long distances (2 min observation time). In addition to the reduced motility, an accumulation of vesicles was observed in the dynein mutant at the hyphal tip, suggesting that dynein is required for retrograde transportation **(Figure IV. 21)**.
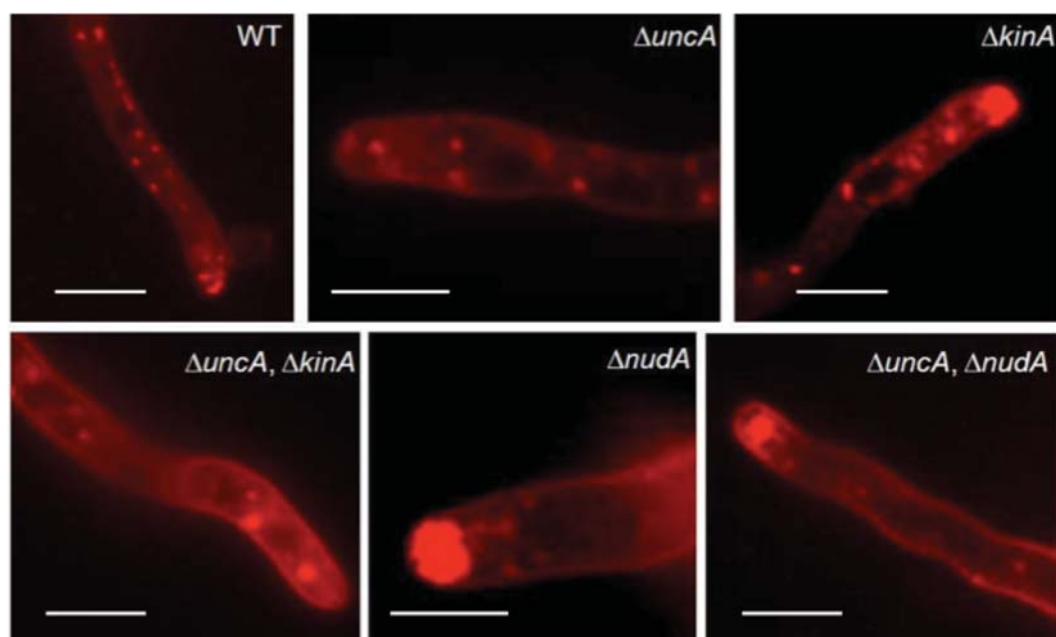
Figure IV. 21. FM4-64 staining in the strains indicated in the pictures. The strains were the same as described in the legend for (Figure IV. 11). FM4-64 staining was done as described above. Scale bars 5 μm.

In the double mutant Δ*nudA*/Δ*uncA* the defect in vesicle movement was the same as in the dynein single mutant. In the *kinA*-deletion strain, long-distance vesicle movement occurred, and vesicle accumulation was visible at the hyphal tip. The effect was not as strong as in the dynein mutant. This observation can be explained with the fact that the accumulation of dynein at the microtubule plus end, and thereby its transportation to the tip zone, depends on conventional kinesin (Zhang *et al.*, 2003). Hence, the observed defect of vesicle movement in the *kinA* mutant is probably due to the lack of dynein at the tip. A double mutant between Δ*kinA* and Δ*uncA* displayed a similar phenotype as the Δ*uncA* deletion with some more accumulated vesicles at the tip **(Figure IV. 21)**.

3.4.   UncA localizes to a subpopulation of microtubules

In the above-described experiments a rigor mutation in the UncA motor was found to reduces the movement of the vesicles and most surprisingly, the GFP-UncA[rigor] signal was aligned along a rod-like structure in the cell **(Figure IV. 19)**. To generate this rigor variant of UncA, the glycine residue 450 was changed to glutamate using QuikChange XL site-directed mutagenesis kit (Stratagene, Heidelberg, Germany). The used oligonucleotides were UncA_P-Loop_Gly_fwd and UncA_P-Loop_Gly_rev and plasmid pAS3 was the template for this amplification to yield plasmid pNZ15. The strain TN02A3 was transformed and searched for transformants in which pNZ15 was homologously integrated at the *uncA* locus. Among 12 transformants, two (one named SNZ14) displayed the *uncA*-deletion phenotype under both repressing and inducing conditions **(Figure IV. 22)**.
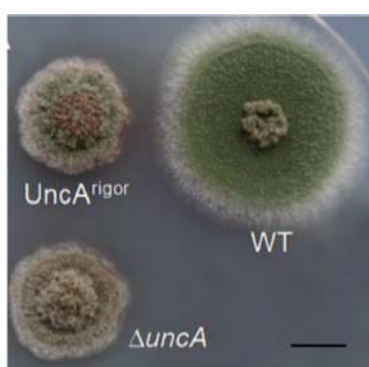
Figure IV. 22. The colony of an *uncA*[rigor] mutant shows the same phenotype as an *uncA*-deletion strain. Scale bar 1 cm.

PCR and Southern blot analysis confirmed that the construct was integrated at the *uncA* locus in both transformants. The PCR fragments were sequenced to confirm the mutagenesis event. The GFP-UncA[rigor] signal in SNZ14 was very nicely aligned along a rod-like structure in the cell **(Figure IV. 23)**.
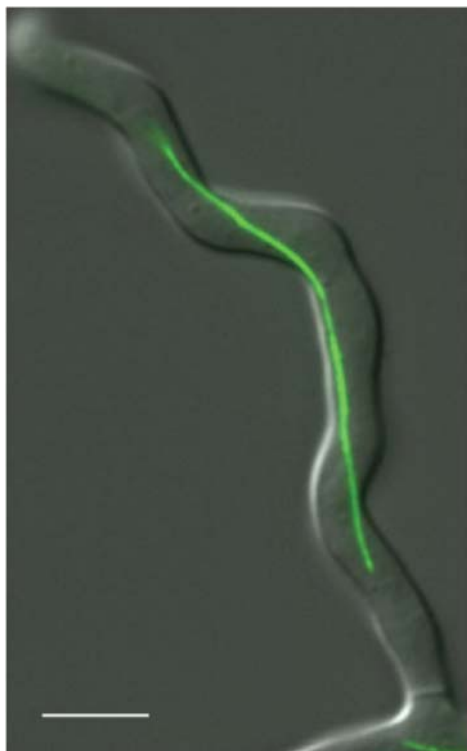
Figure IV. 23. Localization of UncA^{rigor} along a single microtubule. GFP-UncA^{rigor} localizes to a rod-like structure in a hyphal compartment. Scale bar 5 μm.

To determine the nature of this rod, the morphology of this structure was compared with the structure of mitochondria and the microtubule cytoskeleton (MT) by making double stainings. SNZ14 was transformed with mRFP1 targeted to mitochondria or with the mRFP1-KipB fusion protein for decoration and visualization of MTs. Co-localization occurred only in the case of UncA with MT, suggesting that this rod represents MTs (or a bundle of MTs), **(Figure IV. 24)**. To further prove this, the strains were treated with Cytochalasin A, 2 μg/ml for 10 min (in the case of Mitochondria) and with benomyl, 2.5 μg/ml for 10 min (in the case of MT). The rod of UncA^{rigor} disassembled only in the presence of benomyl, but its disassembling rate was much slower than other cytoplasmic MT bundles, indicating that this MT bundle is more stable than other MTs.
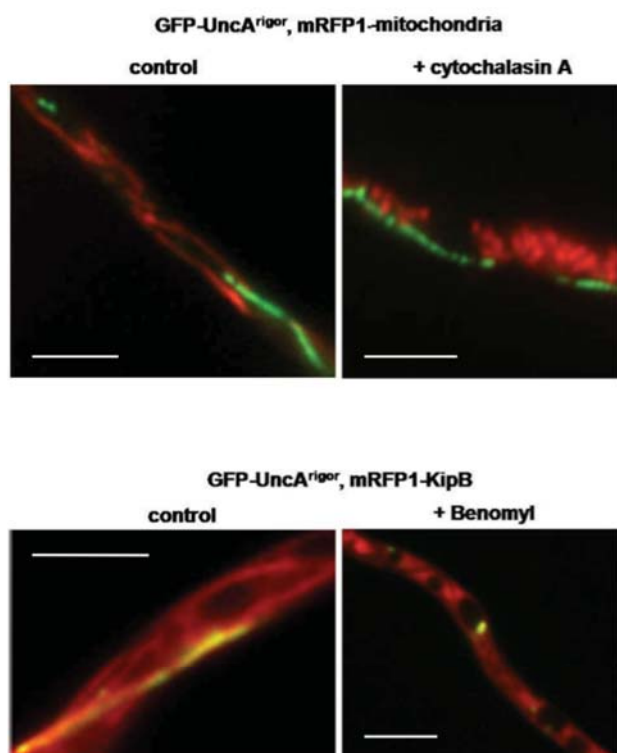
Figure IV. 24. Comparison of GFP-UncA^{rigor} with the morphology of mitochondria (stained with mRFP1) in the absence and presence of cytochalasin A. And with the morphology of microtubule (stained with mRFP1-KipB) in the absence and presence of Benomyl. Upper panel: Cytochalasin A was used at a final concentration of 2 μg/ml (Sigma) from a stock solution of 100 mg/ml in dimethyl sulfoxide (DMSO), and incubated for 10 min. **Lower panel:** Localization of GFP-UncA^{rigor} in the absence and presence of benomyl (final concentration 2.5 μg/ml, from a stock solution of 1 mg/ml in ethanol, 10 min incubation time). Scale bars 5 μm.

 In order to analyze this phenomenon further, the MTs were stained by secondary immunofluorescence and compared with the observed rod structure stained with mRFP1-UncA[rigor]. Indeed, the red rod represented a subpopulation of MTs, because many other MTs were clearly visible beside the one decorated by UncA[rigor] (**Figure IV. 25)**.

            Using UncA as a nice marker for this population of MTs, the occurrence in different developmental stages was analyzed. The GFP-UncA labelled rod-like structure was found already in conidiospores as well as in young germ tubes and older hyphal compartments. This suggests that the occurrence of this MT population is independent of the growth phase of the hyphae.
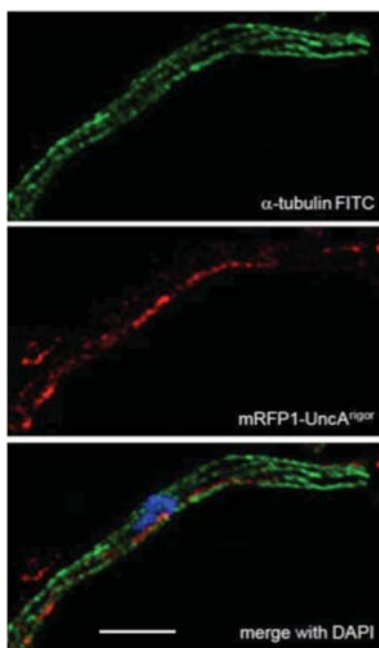
Figure IV. 25. Immunostaining of mRFP1-UncA[rigor] hyphae with anti-alpha-tubulin antibodies and FITC labeled secondary antibodies. Tip compartment of a mRFP1- UncA[rigor] strain (SNZ54) stained with anti-alpha-tubulin antibodies (DM1A) and FITC-labeled secondary antibodies. Nuclei were stained with DAPI. **Upper panel:** FITC fluorescence; middle panel: mRFP1 fluorescence; **lower panel:** overlay with the DAPI channel. Scale bar 5 μm.

 In addition, the behaviour of this rod was observed during mitosis. This is in agreement with previous observations that not all microtubules are disassembled during nuclear division and indicates different stabilities of different microtubules (Veith *et al.*, 2005). UncA appears to associate with the more stable MTs. Mitotic spindle MTs were not labelled with mRFP1-UncA[rigor].

        To analyze the observed specificity of the UncA motor protein, the presence of post-translational modifications of tubulin in *A. nidulans* was studied **(see Figure V. 02, page 76)**. One modification is the addition of glutamate residues near the carboxy-terminus of alpha and beta-tubulin. Using specific antibodies (Monoclonal antipolyglutamylated tubulin, clone B3, Sigma) for immunostaing and western blot experiments, MTs weren't visualized. It is possible, that these antibodies do not recognize the *A. nidulans* modified tubulin. However, it is more likely that this modification does not exist in *A. nidulans*. The same was true for the analysis of acetylated MTs. Another modification is a reversible removal of a terminal

tyrosine residue of alpha tubulin. In *A. nidulans* the C-terminus of alpha tubulin ends with glutamate and tyrosine. Monoclonal anti-tyrosine tubulin (clone TUB-1A2, Sigma) antibodies were used against the tyrosinated form of alpha tubulin. These antibodies stained cytoplasmic and mitotic MTs **(Figure IV. 26, A)**.
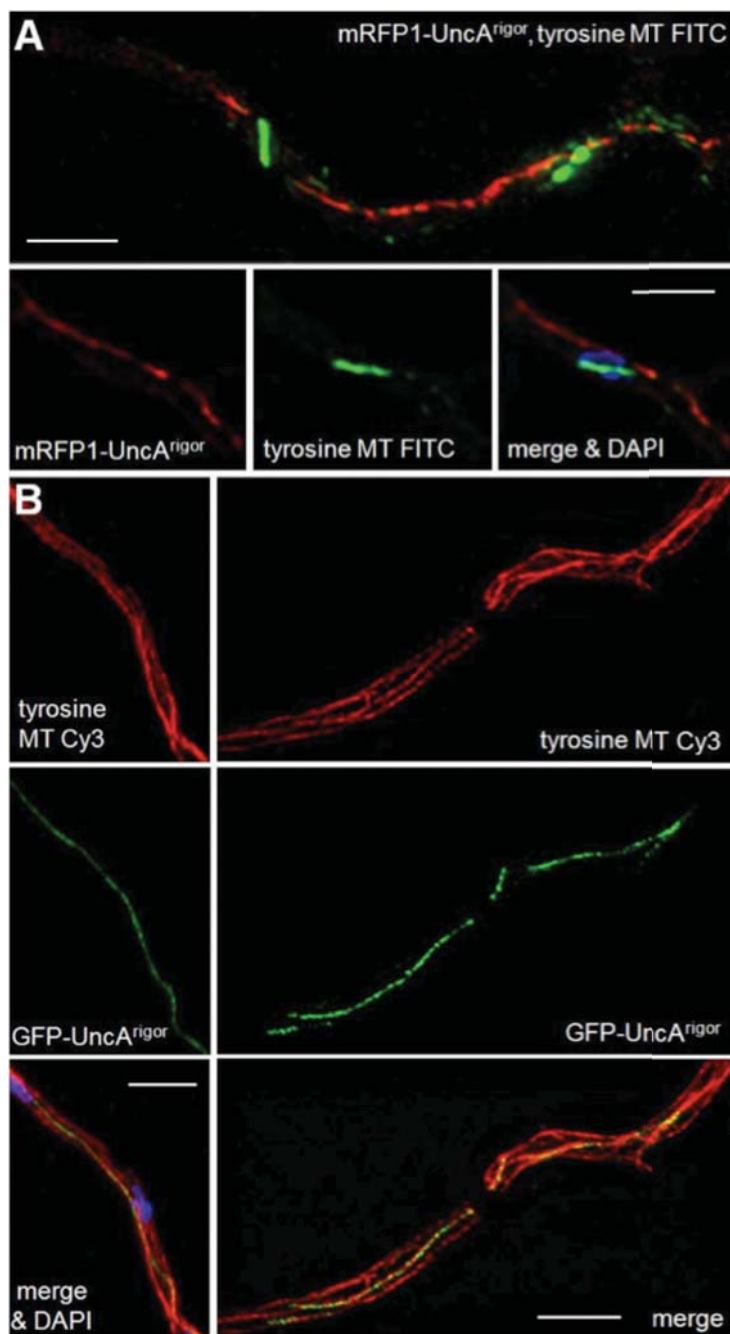

Figure IV. 26. Immunostaining of mRFP1-UncA[rigor] hyphae with antityrosinated tubulin antibodies and FITC labeled secondary antibodies. (A) Hyphal compartment during mitosis. mRFP1-UncA[rigor] localizes to one MT in the cytoplasm but not to the two mitotic spindles, which are decorated with the green fluorescent FITC antibodies. The lower row of three pictures shows a second example and demonstrates that the anti-tyrosine antibody does not stain any microtubule in the cytoplasm (middle panel). Right panel: overlay of the mRFP1, the FITC and the DAPI channel. **(B)** Co-localization of GFP-UncA[rigor] and tyrosinated microtubules labeled with Cy3 secondary antibodies in interphase. Upper panel: Cy3 channel, middle panel: GFP channel; lower panel: overlay of the two channels with the DAPI channel. Scale bars 5 μm.

In interphase cells, all MTs were stained with the antibody, including the MT characterized by GFP-UncA[rigor] **(Figure IV. 26, B)**. However, in mitotic cells, the mRFP1-UncA[rigor] rod was clearly visible and was not stained with the anti-tyrosin tubulin antibody **(Figure IV. 26, A)**. In comparison, the mitotic spindle was stained. From this, it was concluded that UncA binds preferentially to detyrosinated MTs. In interphase cells tyrosinated and detyrosinated MTs

appear to exist in parallel in one MT bundle. During mitosis the tyrosinated cytoplasmic MT depolymerises and the detyrosinated one remains. If UncA^{rigor} cannot label the spindle because of the existence of nuclear envelop and if mitosis can occurs with only detyrosinated tubulin have to be further studied.

3.5.   KinA and KipA localize to all microtubules

In order to test whether the observed behaviour of the UncA motor protein is specific for UncA, the results to the binding of kinesin rigor variants of kinesin-1 (conventional kinesin, KinA), kinesin-7 (KipA) and kinesin-8 (KipB) were compared (Konzack *et al.*, 2005; Requena *et al.*, 2001; Rischitor *et al.*, 2004; Seiler *et al.*, 1997) **(Figure IV. 27)**. To construct a KinA^{rigor} plasmid, a GFP-KinA plasmid was generated at first using the primer set KinA_ATG_Asc1_fwd and KinA_1324bp_Pac_rev to amplify a 1.3-kb *kinA* fragment. The PCR fragment was cloned into pCMB17apx (pyroA as selection marker), yielding plasmid pCS2-NZ. This plasmid was used as a template to create the KinA^{rigor} plasmid using primer KinA_Rigor_P-Loop_for and KinA_Rigor_P-Loop_rev and the QuikChange XL site-directed mutagenesis kit (Stratagene, Heidelberg, Germany) to change glycine residue 97 to glutamate. In the case of KipA and KinA no specificity to different microtubules was found **(Figure IV. 27, A B)**. Simultaneous visualization of KinA^{rigor} and UncA^{rigor} confirmed the specificity of UncA **(Figure IV. 27, C)**.
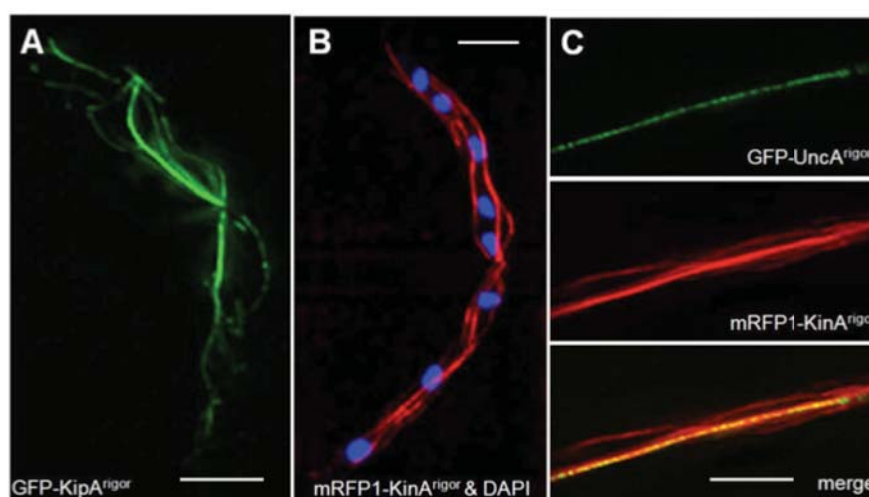
Figure IV. 27. Comparison of the localization of three kinesin motor proteins in the rigor state. (A) GFP-KipA^{rigor}. **(B)** mRFP1-KinA^{rigor} overlaid with the DAPI channel. **(C)** Co-localization of GFP-UncA^{rigor} (upper panel) with mRFP1-KinA^{rigor} (middle panel). The lower panel shows the overlay. Scale bars 5 μm.

Kinesin-8 had been already studied in a previous paper and did not show a preference for certain microtubules **(Figure IV. 24)** (Rischitor *et al.*, 2004).

Another interesting observation was made during the experiment procedure. It was noticed that KinA[rigor] did not decorate microtubules, stained with the anti-tyrosine tubulin antibody, at the very tip of the hypha **(Figure IV. 28)**. Currently, there is no explanation for this phenomenon.
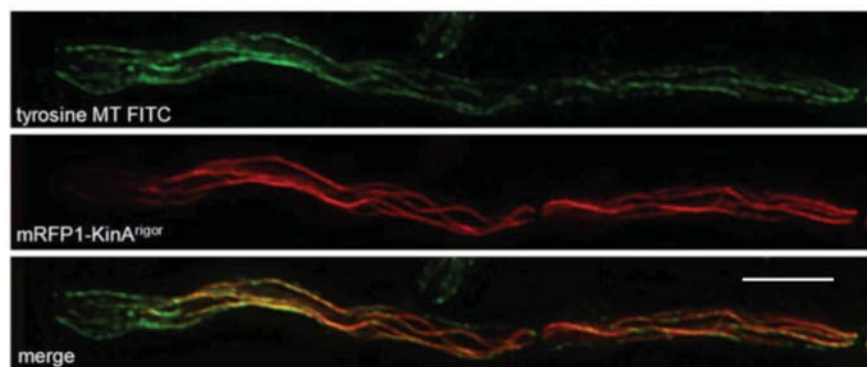
Figure IV. 28. Immunostaining of mRFP1-KinA[rigor] hyphae with antityrosinated tubulin antibodies and FITC labeled secondary antibodies. Co-localization of mRFP1-KinA[rigor] and tyrosinated microtubules in interphase. upper panel: FITC channel, middle panel: mRFP1-KinA[rigor], lower panel: overlay. Scale bar 5 μm.

Those results suggest for the first time that post-translational modifications of microtubules exist in filamentous fungi, or at least in *A. nidulans*. Hence it postulates the existence of the tubulin tyrosination and detyrosination cycle **(Figure IV. 29)**.
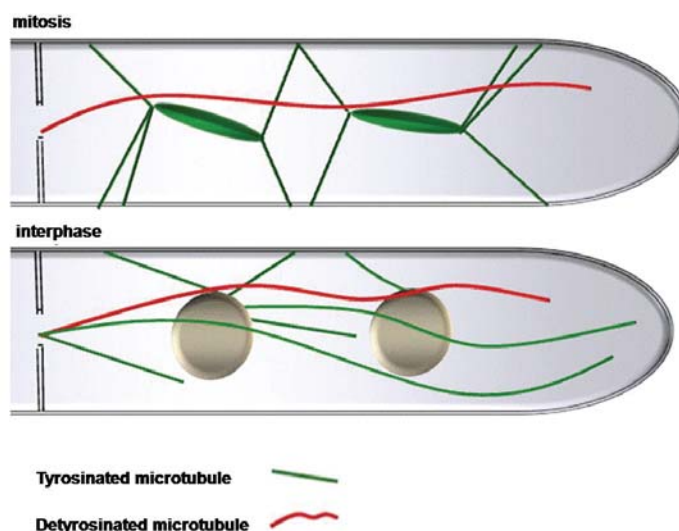
Figure IV. 29. Proposed model for the arrangement of tyrosinated and detyrosinated microtubules during mitosis and during interphase in *A. nidulans*. For details refer to the Discussion section.

Some questions still have to be answered:
- From which MTOC do the putative detyrosinated MTs generate? SPB or sMTOC?
- Do MT modification enzymes, such as tubulin tyrosine ligase and tubulin tyrosine carboxypeptidase, exist in filamentous fungi?
- How does the plus end of detyrosinated MTs look like?

4.   The origin of detyrosinated microtubules

4.1. Putative detyrosinated microtubules connect SPBs and septal MTOCs

MTs are polymerized from nuclear- and from septal-MTOCs. To analyze from where detyrosinated MTs originate, the distribution of GFP-UncA^{rigor} was analyzed in combination with labeled nuclei, MTs and MTOCs. An UncA^{rigor}-decorated bundle spanned the entire hyphal compartment. It connected all nuclei with each other and linked them to the septa. Some nuclei appeared pear-like with the elongated region attached to the MT, indicating that those nuclei were actively pulled **(Figure IV. 30, A)**. In order to visualize the co-localization pattern between MTOCs, MTs and the UncA^{rigor} MT bundle in more detail, a GFP-TubA strain containing mRFP1-UncA^{rigor} was constructed. The UncA^{rigor} signal decorated one main MT bundle in the compartment (as mentioned before). This bundle was very stable (as indicated with benomyl-test in page 41) and connected all MTOCs with each other during interphase, whereas all other dynamic cytoplasmic MTs were not decorated with UncA^{rigor}. Those results suggest that uncA^{rigor} chooses the stable MT bundles as tracks **(Figure IV. 30, B).**
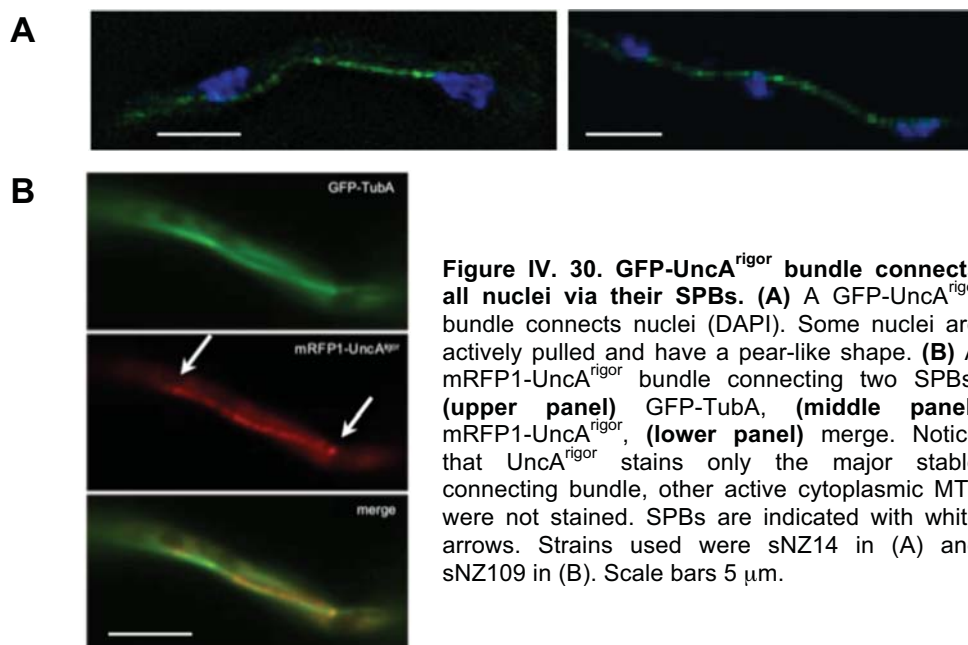

Figure IV. 30. GFP-UncA^{rigor} bundle connects all nuclei via their SPBs. (A) A GFP-UncA^{rigor} bundle connects nuclei (DAPI). Some nuclei are actively pulled and have a pear-like shape. **(B)** A mRFP1-UncA^{rigor} bundle connecting two SPBs. **(upper panel)** GFP-TubA, **(middle panel)** mRFP1-UncA^{rigor}, **(lower panel)** merge. Notice that UncA^{rigor} stains only the major stable connecting bundle, other active cytoplasmic MTs were not stained. SPBs are indicated with white arrows. Strains used were sNZ14 in (A) and sNZ109 in (B). Scale bars 5 μm.

This study has shown that mitotic spindles were not decorated with UncA^{rigor}, although it still decorates one MT bundle in the cytoplasm during mitosis **(Figure IV. 31, A)**. Those observations suggest that during mitosis UncA could still transports vesicles along the stable detyrosinated MT bundles as a track. Further observations in a GFP-α-tubulin strain revealed

that the stable MT bundles depolymerize toward septal MTOCs and take longer time to do this than the other tyrosinated microtubule bundles which depolymerize very fast **(Figure IV. 31, C; movie IV. 09)**.

In order to test the hypothesis of vesicle transport during mitosis, UncA movement was followed in mitotic cells. GFP-UncA spots were fast moving and some of them formed pearl-like structures similar to UncA behavior during interphase. Mitotic nuclei were observed with DsRed-StuA. This fusion protein is released from nuclei during mitosis, thus the disappearance of the nuclear staining indicates the mitotic state. UncA-spots were permanently moving during mitosis **(Figure IV. 31, B, left; movie IV. 10)** just like after mitosis when daughter nuclei appeared again **(Figure IV. 31, B, right; movie IV. 10)**.
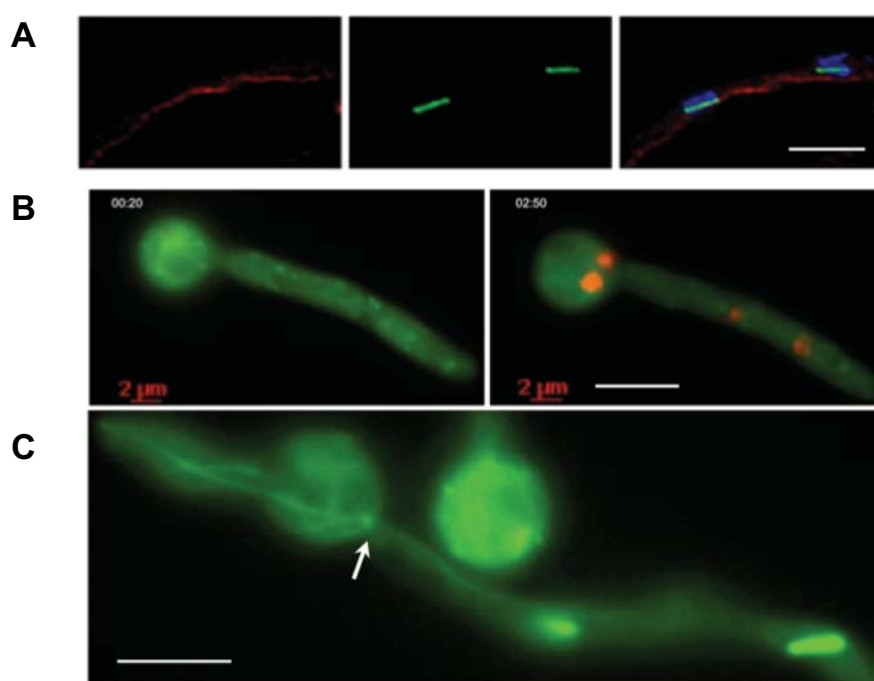
Figure IV. 31. Detyrosinated MTs exist outside the nucleus during mitosis. (A) Immunostaining with anti Tyr-tubulin antibodies (Hyman *et al.*) of the mRFP1-UncA^{rigor} strain (left). Nuclei were stained with DAPI (right). **(B)** GFP-UncA was still able to move toward the tip during mitosis, a pearl-string phenomenon was observed (left), after 2 min daughter nuclei were observed via staining with DsRed-StuA (right). **(C)** GFP-TubA confirms the hypothesis that stable detyrosinated MT bundles connect sMTOC during mitosis (arrow). Strains are sNZ54 in (A), sNZ4 in (B) and sNZ77 in (C). Scale bars 5 μm.

One interesting result was that UncA^{rigor} was not totally immobile, after MT depolymerization UncA^{rigor}-spots were able to move partially and a GFP-UncA signal accumulation was observed at MT minus ends (the MTOCs) **(Figure IV. 32, A)**. The same phenomenon was detected when the *alcA* promoter was replaced with the 1.5-kb putative *uncA* promoter. In this strain only the *uncA*(p)-GFP-UncA^{rigor} accumulations were visible, whereas the rods were very hardly observed **(Figure IV. 32, B)**. Those results confirm that UncA^{rigor} localizes to one MT bundle composed of different MTs, and that those MTs originate from nuclear SPB and

from septal MTOC, and when they depolymerize UncA signals accumulate at the different MTOCs **(movie IV. 11)**.
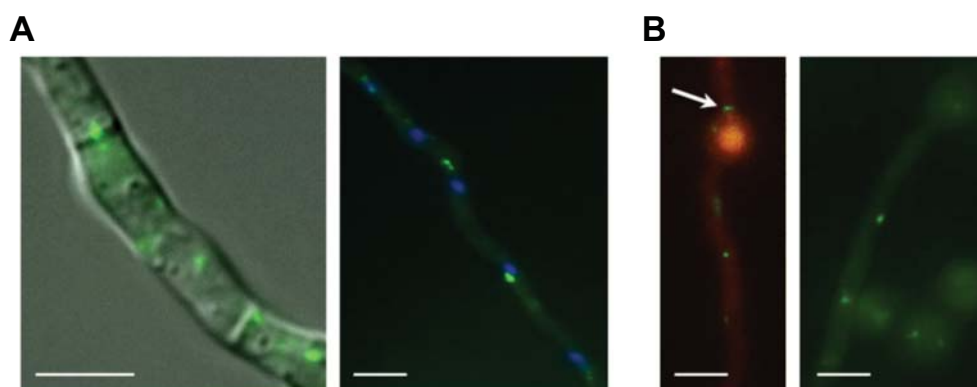

Figure IV. 32. GFP-UncA^{rigor} localizes to SPBs and to sMTOCs after MT depolymerization. (A) GFP-UncA^{rigor} under the control of *alcA*(p) after MT depolymerization. The GFP signal was observed at sMTOC (left) and at SPBs (right). Nuclei were stained with DAPI. **(B)** GFP-UncA^{rigor} under the control of the native promoter. The GFP signal was found at septa (left, arrowhead) and the SPB (right). Strains used were sNZ14 in (A) and sNZ110 in (B). Scale bars 5 μm.

Because sMTOCs appeared to play an important role in the fomation of the stable MTs during mitosis, I studied in the following the organization of sMTOC and tried to find out if any differences in protein composition or structure makes it different than the nuclear SPB.

4.2. Identification of gamma-tubulin and AlpB^{Alp6} at septal MTOCs

Previously was showen that *A. nidulans* ApsB localized at SPBs and at septa, suggesting the presence of MTOCs at septa (Veith *et al.*, 2005). Unfortunately, the most important protein of MTOCs, gamma-tubulin has not been identified at septa before. Here, for the first time a very weak signal at septa was detectable, when gamma-tubulin was expressed from its own promoter and fused to GFP **(Figure IV. 33)**. In *S. pombe* it has also been reported that gamma-tubulin was present at non-nuclear MTOCs in very low amounts and is thus not easy to detect (Sawin *et al.*, 2004).

        To obtain *in vivo* protein expression levels, the proteins were expressed under the corresponding natural promoters. The *apsB* promoter (1.33-kb) was amplified from genomic DNA using primers apsB_nat(p)_AvrII_fwd and apsB_nat(p)_KpnI_rev, cloned instead of alcA(p) in pDV21 giving pNZ-SI37 (*apsB(p)::GFP::apsB),* transformed in TN02A3 giving SNZ59. The gamma-tubulin promoter (1.16-kb) was amplified from genomic DNA using primers Gamma_tub_nat(p)_EcoRI_fwd and Gamma_tub_nat(p)_BsiwI_rev, cloned instead of alcA(p) in pNZ17 giving pNZ-SI36 (*γtubulin(p)::GFP::γtubulin$^{1.8}$*), transformed in TN02A3 resulting in SNZ61. pMCB17apx was used as the basic vector for tagging the proteins with GFP and pDM8 for tagging with mRFP1.
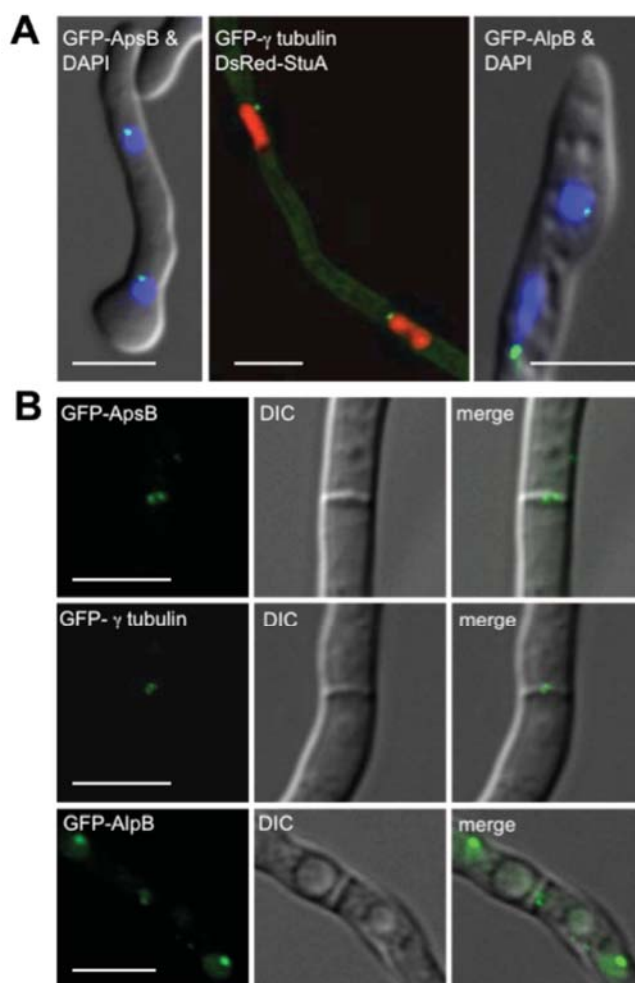
Figure IV. 33. Gamma-tubulin and AlpB localize to septal MTOCs. **(A)** GFP-ApsB, GFP-gamma-tubulin and AlpB[Alp6]-GFP localize to the SPBs. Nuclei are stained with DsRed-StuA (NLS) or DAPI. **(B)** Localization of the same GFP-tagged proteins to the septal pore (two spots in the center). Fluorescence image (left), DIC and merge (right). Strains used: GFP-ApsB (SNZ59), GFP-gamma-tubulin (SNZ61) and AlpB[Alp6]-GFP (SNZ-SH80). All proteins were expressed from their natural promoters. Scale bars 5 μm.

To further elucidate the composition of septal MTOCs, the *A. nidulans* genome was searched for a homologue of *S. pombe* Alp6 and identified the open reading frame AN4867 (968 amino acids in length) with 35 % identity to Alp6, located on chromosome III. This gene was named *alpB* **(Figure IV. 35)**.

The AlpB protein comprises the SPC97/SPC98 domain located between amino acid position 270 and 752 **(Figure IV. 34, A and B)**, and belongs to a family of spindle pole body protein components such as Spc97, Spc98 and gamma-tubulin. In *S. cerevisiae*, it has been shown that gamma-tubulin forms a stable complex with Spc97 and Spc98 (Vinh *et al.*, 2002).

A

SPC97/SPC98

B

```
ATG TCA AGT CGG CAC CAT GTA CGT CCA CGT CGC ATC GAT GAC GCC CTT TCG CAG CTT GTC GAC TCT CTC GCT CCC CCA CTG CCT CCG
 M   S   S   R   H   H   V   R   P   R   R   I   D   D   A   L   S   Q   L   V   D   S   L   A   P   P   L   P   P

TCC GCC GTC ACC GAC GAA TAT TCG GAC GAC GCC GAA GAA GCC CTA GCT GCA GCG GAG GCA GAA TAT CAC CAA CGC CTC CTC GAC CAT
 S   A   V   T   D   E   Y   S   D   D   A   E   E   A   L   A   A   A   E   E   Q   Y   H   Q   R   L   L   D   H

GCG TGG CGT ACT ATA GAC AGC CAT GCA AAC TTA GCC GAC AAC CCA GCT GCA CCG TCT GGG AGT TTG GGT ATT GGC CGC CGA GGA AGC
 A   W   R   T   I   D   S   H   A   N   L   A   D   N   P   A   A   P   S   G   S   L   G   I   G   R   R   G   S

CTA ACG GGT GCA ACA GGG GCA GAG AGT ATC AAT AAC GCG GCG GAT ATG ATT AAG CGG AAG CTG CTA CGC GAA AAT GAA AGT CCC GAT
 L   T   G   A   T   G   A   E   S   I   N   N   A   A   D   M   I   K   R   K   L   L   R   E   N   E   S   P   D

AAG GCT GTC CGG TTC TCG AAT CTC TAT TCG CGT CTG TTG ACG CAG CCT GTG CTG TCG CAG AAA TGG GGA ATA CTA TAC TTA CTC TAT
 K   A   V   R   F   S   N   L   Y   S   R   L   L   T   Q   P   V   L   S   Q   K   W   G   I   L   Y   L   L   Y

CGA CTA TCG AGG ACG GAG AAC GCT GAG AGC TTC ACA TAC GAC GAT GAA AGG CCA CGC AGT CCG CTG ATG GAC CAG TCC AAA TTA CAA
 R   L   S   R   T   E   N   A   E   S   F   T   Y   D   D   E   R   P   R   S   P   L   M   D   Q   S   K   L   Q

AGA ATG CTT GTA AAG GAG CAA AGA ATG GGG GGC AGG GTG GCG GCG AGT TCG GAG GAT GAT GGC CCA GCC GTT AGC TCA TCA GCA TCT
 R   M   L   V   K   E   Q   R   M   G   G   R   V   A   A   S   S   E   D   D   G   P   A   V   S   S   S   A   S

CAG ATG GCT GCG CGG GTC GAA CGG AAG GCT TCA CTG CGG CGA ACA GAG GAC AAG GAA AGG GAA AGG AAT CGA GAT GCG GAG CAT GGA
 Q   M   A   A   R   V   E   R   K   A   S   L   R   R   T   E   D   K   E   R   E   R   N   R   D   A   E   H   G

TCT GCG CCG GAG CGG CTG CGC ATG AGT CGT CAA AAC GCA CCC TTT GAC GGA CAT GGA GAG AAT GGA GAG CAG GAA AGG ATG
 S   A   P   E   R   L   R   M   S   R   Q   N   A   P   F   D   G   H   G   E   K   N   E   E   Q   E   R   M

ACA CAA TGT GGT GAA TCA GGA CTT TTG CGT GAC TTG CCT TTC AAC CTA CAG GGT CTG TCC TCA TCT GAT ATG CAG TTC ATG TCA ACT
 T   Q   C   G   E   S   G   L   L   R   D   L   P   F   N   L   Q   G   L   S   S   S   D   M   Q   F   M   S   T

TCT ACA CTC AAG TTA CCT CCG ACA CTA CCT CTT CCT ATG GTG TCT CTC CTA AAT ACG CTA GCT GAG CCG TGT CTG CTA TAT CGC GGT
 S   T   L   K   L   P   P   T   L   P   L   P   M   V   S   L   L   N   T   L   A   E   P   C   L   L   Y   R   G

CTT TCT GCT TTT GTT GAA AGC AGT GAC GGG GGT CTC GTC AGT CAG AGT CTG CGG GCA GCT CTT TCG GCA CTT CGT TCT TAC CTA
 L   S   A   F   V   E   S   S   D   G   G   L   V   S   Q   S   L   R   A   A   L   S   N   E   L   R   S   Y   L

GGA TTG GTA GCG ACG CTC GAA GGT GAG ATT CGC AGG GCG CTG GCT GCG CCT GAA GAA TCG CCT GGT TCT AAA AGT GGT GTG ACG TTG
 G   L   V   A   T   L   E   G   E   I   R   R   A   L   A   A   P   E   E   S   P   G   S   K   S   G   V   T   L

AAA AGA TGC GTT GTT TGG ACA CGA GAT GCG ACT ATG GCG TTG CGT TTG ATG AGT TTA ATT GTT GAG GAG GCT CAG A gtaagtgcatctc
 K   R   C   V   V   W   T   R   D   A   T   M   A   L   R   L   M   S   L   I   V   E   E   A   Q   K

attccttctgtttcgattgctctgacttttatcaggcaagaaaggaggtcaattagtgtccctgatccatggcttttccacatcacacggagatccttttgtgtgtaattttgca

g AA AAA CTT CTC ACG CAC GTA ACG AAG CCG TTC TAC GGT ATG CTG CGG CTC TGG ATT TAC GAT GGC GAG CTC TCA GAC CCG TAC
   K   L   L   T   H   V   T   K   P   F   Y   G   M   L   R   L   W   I   Y   D   G   E   L   S   D   P   Y

AAA GAG TTC TTC GTC GTG GAA CCG GAG GTC AGG CCT AGT ACA GAT CCA CGA CGC ATT GCA ACT AGT GTA TGG GAG GAC AAA TAC AAA
 K   E   F   F   V   V   E   P   E   V   R   P   S   T   D   P   R   R   I   A   T   S   V   W   E   D   K   Y   K

CTC GAA GAC GAT ATG GTG CCT TCG ATC ATT ACC AAG GAA TTC GCT AAA AAA GTA TTC CTT ATT GGA AAG TCT CTT AAC TTC ATC CGA
 L   E   D   D   M   V   P   S   I   I   T   K   E   F   A   K   K   V   F   L   I   G   K   S   L   N   F   I   R

TAT GGC TGT GGC GAT TCT GGT TGG GTG GAG GCC TAC TCG AAG GAG GCC TCC AAA GAG CTG CGT TAT GGT GAC ACG GCC AGT CTC GAA
 Y   G   C   G   D   S   G   W   V   E   A   Y   S   K   E   A   S   K   E   L   R   Y   G   D   T   A   S   L   E

ACC TCA ATT GAT GAA GCA TAT AAG ACA ACA ATG GCA CGA TTA ATC CAC CTA ATG GAC GAA AAA TTC AAG CTA TTT GAT CAC CTT CAT
 T   S   I   D   E   A   Y   K   T   T   M   A   R   L   I   H   L   M   D   E   K   F   K   L   F   D   H   L   H

GCG CTA AAG AAG TAT TTG CTG CTG GGC CAA GGC GAC TTC ATC GCT TTA CTC ATG GAA TCA TTG GCA TCA AAT CTT GAT CGT CCC GCA
 A   L   K   K   Y   L   L   L   G   Q   G   D   F   I   A   L   L   M   E   S   L   A   S   N   L   D   R   P   A

AAC TCA CAA TAC CGT CAC ACG CTG ACT GCA CAG TTG GAA CAT GCT ATC CGC GCT TCT AAT GCA CAA TAT GAC TCG CAA GAT GTC CTT
 N   S   Q   Y   R   H   T   L   T   A   Q   L   E   H   A   I   R   A   S   N   A   Q   Y   D   S   Q   D   V   L

CGA CGT TTG GAC GCT ATG CTC GAC TGT AGT CAT GGC GAG ATC GGT TGG GAT TGT TTC ACT CTT GAA TAC AAG ATC GAC GCA CCA
 R   R   L   D   A   R   M   L   E   L   S   H   G   E   I   G   W   D   C   F   T   L   E   Y   K   I   D   A   P

GTG GAT GTG GTG ATT ACA CCA TGG GGC TCT ACG CAA TAT CTC AAA GTC TTC AAT TTC CTA TGG CGC GTG AAG CGC GTC GAG TTC TCC
 V   D   V   V   I   T   P   W   G   S   T   Q   Y   L   K   V   F   N   F   L   W   R   V   K   R   V   E   F   S

TTG GGC AGC ACA TGG CGA CGT TGC ATG ACT GGC GCC AGA GGG GTC CTA GGC AGC GTT GAC GAC AAA GTT GGC GCT GAT TGG AAG CGT
 L   G   S   T   W   R   R   C   M   T   G   A   R   G   V   L   G   S   V   D   D   K   V   G   A   D   W   K   R

GCA TGC GTC ATC GCA GAG ATG ATT CAT TTT GTC TGC CAA TTA TAC TAT ATC CTC TTC GAG GTC ATT GAG TCC AGT TGG GAT
 A   R   C   V   I   A   E   M   I   H   F   V   C   Q   L   Q   Y   Y   I   L   F   E   V   I   E   S   S   W   D

CAA CTG CAG GCG TCT ATT TGC AAG CCG GGG TGT ACG CTT GAC GAC CTA ATA GAA GCT CAT ACC AAG TAC CTC AAC TCT ATC ACA CAC
 Q   L   Q   A   S   I   C   K   P   G   C   T   L   D   D   L   I   E   A   H   T   K   Y   L   N   S   I   T   H

AAG GGT CTT CTA GGC TCA TCC TCA ACA AAG ACT ACT GGC AAG CAG GAA GAA GGC TTC CTA GCT CAG CTA CAT CAC ATT TTA AAA ATA
 K   G   L   L   G   S   S   S   T   K   T   T   G   K   Q   E   E   G   F   L   A   Q   L   H   H   I   L   K   I

ATG CTG GCC TAC AAG GAC GCG GTT GAC GGA TTG TAC TCG TTT TCT GTC GCA GAA TTC ACT CGA CGG CAA GAG CTA AGC GCA AAG ATT
 M   L   A   Y   K   D   A   V   D   G   L   Y   S   F   S   V   A   E   F   T   R   R   Q   E   L   S   A   K   I

GAG ACG CAA GCT ACT CAG GGT CAG TGG GGA GTC TCA GAG CGC GAC CTC CTT TCT TCC CGA CAC AAG CAA GAG CTC GCC TCC
 E   T   Q   A   T   Q   G   Q   W   G   V   S   E   R   D   L   L   S   S   R   H   S   Q   A   Q   R   L   A   S

GCA TCC TCG TCA TTT TCT ATC ACA CCA AAT GTC GGA TCT GGA GCC GAT GGA GTC GCT ACG CCT TCT TCT CTT GCA AAC CAC GAC CTC
 A   S   S   F   S   I   T   P   N   V   G   S   G   A   D   G   V   A   T   P   S   S   L   A   N   H   D   L

TCC GCG GAC GAC CAT ATG CTT CCA TCC CTC CGA ACT CGC CTC CGT GAC CTC TCA GTG GAG TTT CGT TCA CGG TTG AAC GTC CTC CTC
 S   A   D   D   H   M   L   P   S   L   R   T   R   L   R   D   L   S   V   E   F   R   S   R   L   N   V   L   L

GGC GAC CTA GCC TAC CAG CCT GAC GTA GAT ATG CGA TTT TTG GGT GTC GTT ATG AAC TTT AAC GAA GTC TAT GAG CCT GTG CGG AGA
 G   D   L   A   Y   Q   P   D   V   D   M   R   F   L   G   V   V   M   N   F   N   E   V   Y   E   P   V   R   R

CGA AGA GCC ACA GGT ACT AGC TCT CGA GAT AAA GAG CGG GAG CGG GGA CGA GCA AGG CGG AAA GCA CCA CCA CAA TCA GGA GGA ACA
 R   R   A   T   G   T   S   S   R   D   K   E   R   E   R   E   R   A   R   R   K   A   P   P   Q   S   G   G   T

GAG ACG CAA TCT CAA GCG AAA AAG GAA AAG AAG GAT TCG ACT GAG CAA TAG
 E   T   Q   S   Q   A   K   K   E   K   K   D   S   T   E   Q   *
```

Figure IV. 34. Analysis of the *A. nidulans* spindle pole body protein encoding gene *alpB*. (A) Domain prediction for the AlpB protein. The AlpB (968 amino acids) protein sequence was analyzed with the SMART program (http://smart.embl-heidelberg.de), **(B)** Open reading frame of the AlpB protein. *alpB* is 2901 bp long and has one intron (lower-case letters) at amino acid position 403. The SPC97/SPC98 domain located between amino acids position 270 and 752 (shaded in gray).

In order to localize AlpB, a C-terminal GFP fusion protein expressed from the native promoter was constructed as follows. AlpB AN4867 was amplified via fusion PCR using primers Alp6_mitte_fwd and Alp6_linker_rev to amplify the C-terminal fragment of AlpB without the stop codon, and primer Alp6_RB_link_fwd and Alp6_RB_rev to amplify the right border of AlpB. The two PCR products were fused to a *GFP-pyrG* PCR cassette (kindly provided by S. Osmani, Ohio State University, US) to generate a 5.5-kb fusion PCR product using the primer Alp6_Nprimer_fwd and Alp6_Nprimer_rev. The fusion PCR product was transformed into the *A. nidulans* strain SO451 giving SNZ-SH80 (*alpB(p)::alpB::GFP*). As expected the strain showed that AlpB localized to SPBs at nuclei but also to sMTOC, indicating that the two MTOCs share also this protein **(Figure IV. 33)**.
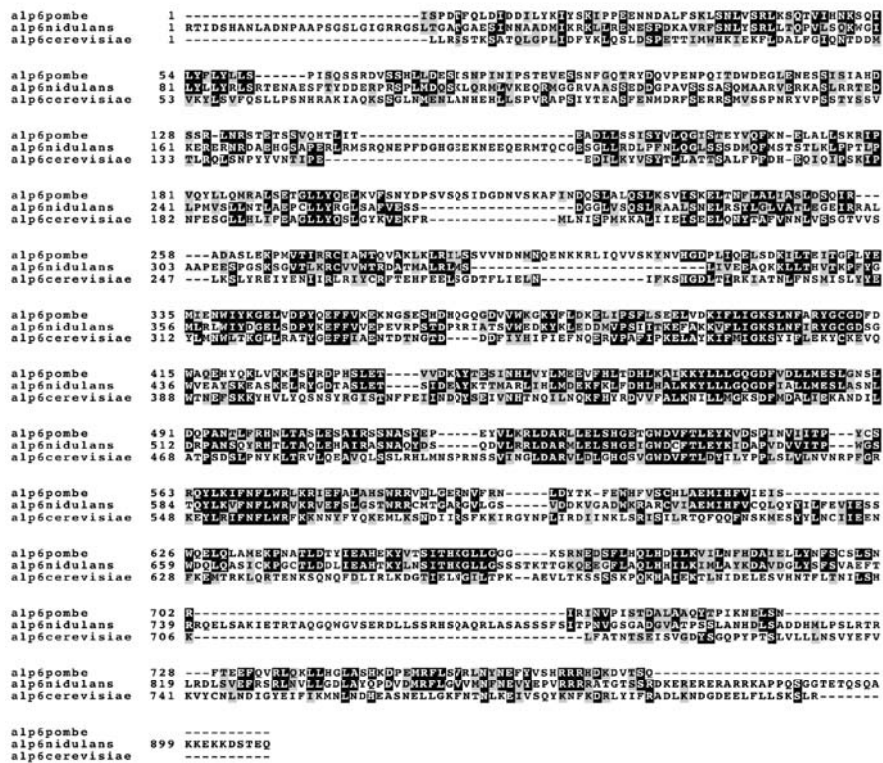
Figure IV. 35. AlpB relatedness analysis with other SPC97/SPC98 proteins. Alignment of *A. nidulans* AlpB (AN4867) with homologous sequences from *S. cerevisiae* SPC98 (25% identity) and *S. pombe* Alp6 (37% identity). The alignment was done with Clustal W and Boxshade with a window size of 5.

The *A. nidulans* genome was also searched for a homologue of *S. pombe* Alp4 and identified open reading frame AN5873 (876 amino acids in length) with 43 % identity to Alp4, located to chromosome I. This gene was named *alpC*. The AlpC protein has the SPC97/SPC98 domain too.

To visualize AlpC, an N-terminal fusion construct with GFP was created. In this experiment, AlpC shows nuclear localization but no specific co-localization with MTOCs.

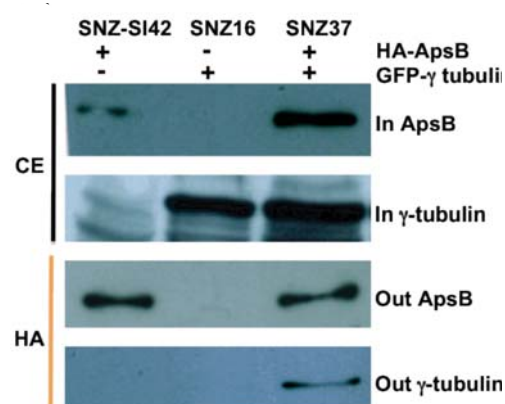## 4.3. Interaction of ApsB with gamma-tubulin

Next, ApsB was shown not only to co-localize but also to interact with gamma-tubulin. To this end the bimolecular fluorescence complementation system (BiFC) was applied. ApsB full-length was fused with the N terminal part of YFP and gamma tubulin full-length with the C-terminal part of YFP. For the BiFC system the eYFP was split at position 460bp-462bp, using the ATG as start codon for the YFP^C half. Each YFP half was amplified and PCR fragments were used to replace GFP2-5 of pMCB17apx-apsB (Veith *et al.*, 2005) giving pDV7 (YFP^N) and pDV8 (YFP^C). Full-length *apsB*$^{3.2}$ (3.2-kb) was taken from pDV21a and cloned into pDV7 giving pDV22b (*alcA(p)::YFP^N::apsB*$^{3.2}$), and full-length *γtubulin*$^{1.8}$ was amplified using primers Gamma_tub_Asc_fwd and Gamma_tub_Pac_rev, cloned into pDV8 giving pDV50 (*alcA(p)::YFP^C::γtubulin*$^{1.8}$). For the BiFC analysis pDV22 and pDV50 were combined and transformed into GR5 resulting in SNZ11. The cloned gene length is indicated as exponents: e.g. *apsB*$^{3.2}$ (3.2-kb). Corresponding *A. nidulans* strains showed a YFP signal at nuclei and at septa **(Figure IV. 36, A)**.
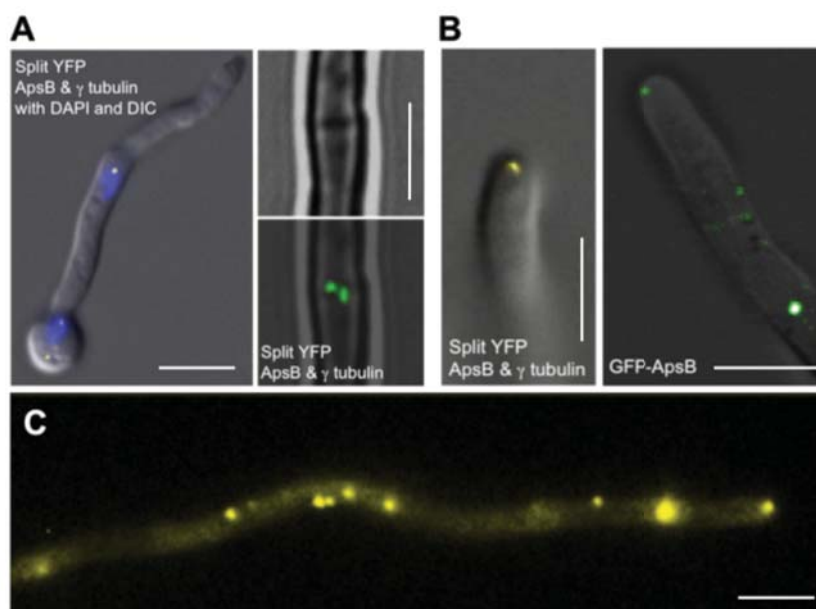
Figure IV. 36. Interaction of ApsB with gamma-tubulin. (A) Bimolecular-fluorescence-complementation assay (BiFC) of ApsB and gamma-tubulin (SNZ11). Fluorescent signals, indicating an interaction between ApsB and gamma-tubulin, were found at the SPBs (left), and to the centre of septal pores as two spots (right). Upper image is DIC and lower image is merge of a fluorescent picture with the upper DIC picture. **(B)** Fluorescent signals of interacting ApsB with gamma-tubuin (BiFC) and of GFP-ApsB in the hyphal tip. **(C)** ApsB-gamma-tubulin interaction (BiFC) in the cytoplasm. Some spots were highly mobile. Scale bars 5 μm.

Interestingly, a fluorescence signal at the tip of all actively growing hyphae was also found **(Figure IV. 36, B)**. Previously, ApsB has already been found at the tip and growing MTs were also described to originate from the tip in some cases (Konzack *et al.*, 2005). Gamma-tubulin alone was not visible at the tip probably due to the high cytoplasmic background. Some cytoplasmic spots were also observed, as shown before for ApsB alone (Veith *et al.*, 2005) **(Figure IV. 36, C)**.

The ApsB-gamma-tubulin interaction result was confirmed with Co-IP using hemagglutinin (HA)-ApsB and GFP-gamma tubulin tagged proteins. Gamma-tubulin was detected in the precipitate obtained with anti-HA antibodies. The resulting band confirmed the interaction between ApsB and Gamma-tubulin **(Figure IV. 37)**.

Figure IV. 37. Interaction of ApsB with gamma-tubulin. Confirmation of the ApsB-gamma-tubulin interaction by co-immunoprecipitation. SNZ37 (*alcA(p)::apsB::3xHA; alcA(p)::GFP::γtubulin$^{1.8}$*) was used for this assay, and SNZ-SI 42 (*alcA(p)::3xHA::apsB$^{3.2}$*) and SNZ16 (*alcA(p)::GFP::γtubulin$^{1.8}$*) were the control strains. Anti-HA antibodies (Klon 16B12 derived from mouse, Hiss Diagnostics, Freiburg, Germany) were used for the IP. Precipitation was performed in 1 ml crude extract of approximately 10 mg/ml total protein and 50 µl protein G-agarose (Roche, Mannheim, Germany). Western blot detection was done with anti-GFP antibodies (Anti-GFP N-terminal, derived from rabbit, Product G 1544, Sigma–Aldrich, Munich, Germany).

4.4. The MTOC protein ApsB is associated with peroxisomes

It was shown, in a previous thesis of our laboratory (Suelmann, 1999), that ApsB interacts surprisingly with the Woronin body protein HexA. This interaction was the reason for the discovery of a peroxisomal targeting sequence type 2 (PTS2) in the N-terminal region of ApsB open reading frame. It was also shown that ApsB co-localizes partially with HexA and with another peroxisomal protein (AcuE). Those results led to the conclusion that ApsB co-localizes to a subclass of peroxisomes (Veith, 2006).

ApsB and HexA localized in different ways at septa. To deterime if ApsB and HexA are forming different structures at septa, deconvolution and laser-scanning spinning disc-microscopy were used. ApsB appeared as two spots in the centre of the septal pore **(Figure IV. 38, A)**, whereas HexA localized on each side of the pore **(Figure IV. 38, B)**. Time-course experiments revealed that the ApsB spot co-localized with the constricting ring during septation.
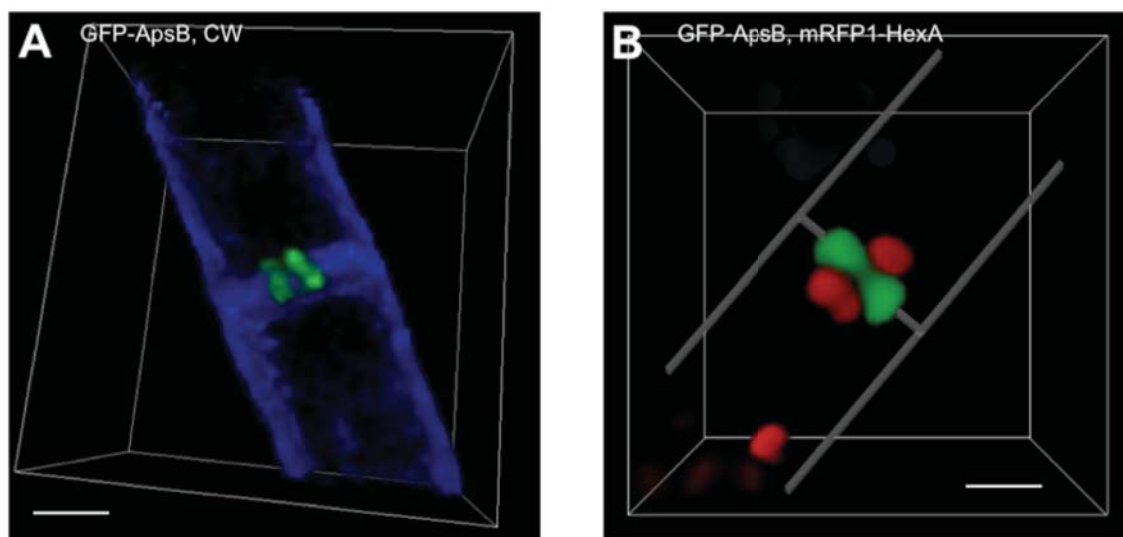
Figure IV. 38. Comparison between ApsB and HexA localization at septa. (A) GFP-ApsB appeared as two spots in the centre of the septal pore. The cell wall was stained with Calcofluor white M2R (fluorescent brightener 28 (F3543), Sigma Aldrich, Germany) 1:1000 dilution for 5 min. 3D view using Zeiss AxioImager Z1 with AxioVision software (V4.5). **(B)** Double staining of ApsB and HexA. GFP-ApsB appeared as two spots in the centre of the septal pore whereas HexA localized on each side of the pore (3 spots in the image). The cell wall is indicated with a line. 3D view using Zeiss Cell Observer® SD confocal microscope with AxioVision software (V4.5). Strains are SEa3 (A) and SDV73 (B). Scale bars 1 μm.

4.5. The PTS2 motif of ApsB is important for its function

A point mutation in the PTS2 motif of ApsB caused the same defects as an *apsB* deletion, a non-sporulating phenotype and a reduced number of MTs. Therefore it was assumed that PTS2 of ApsB is important for its function at septa (Veith, 2006).

To test if the function of the PTS2 mutated ApsB can be restored by adding a PTS1 targeting sequence (SRL) at the C-terminus of ApsB, the PTS2 mutated ApsB with the PTS1 signal fused to the C-terminal part of the protein (GFP-ApsB_PTS2^{mut}_SRL) expressed from the *alcA* promoter was transformed into strain AJC1.7 (*apsB10*) and into an *apsB*-deletion strain (SRS24). To create the latter plasmid, a PTS1 targeting sequence (SRL) was added to the C-terminus of ApsB by amplifying the full-length mutated gene *apsB*$^{3.2}$_*PTS2*^{mut} in pDV43 using the primers apsB_Asc_fwd and SRL_PTS1_PacI_rev, PTS1 sequence tagacggga was added just before the stop codon in the reverse primer. The PCR product was cloned between *Asc*I and *Pac*I restriction sites in the vector pMCB17apx and confirmed via sequencing, giving the plasmid pNZ16, which was transformed into the *apsB10* strain AJC1.7 generating strain SNZ34 (*apsB10, alcA(p)::GFP::apsB_PTS2*^{mut}_*SRL*). Ectopic integration of the construct and the presence of the mutated endogenous *apsB* locus were confirmed by PCR, Southern blot and sequencing of the PCR products. Likewise,

transformation of the *apsB* construct was done with pNZ16 into the *apsB*-deletion strain (SRS24), generating SNZ94 with the same rescue phenotype as in the case of AJC1.7
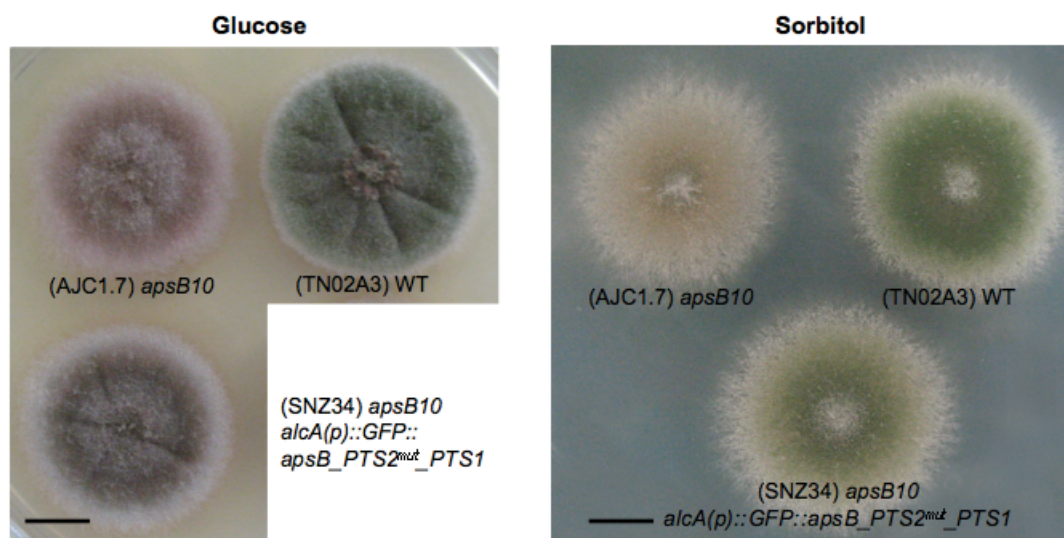

Figure IV. 39. The peroxisomal target sequence of ApsB is important for complementation of the oligosporogenic phenotype of *apsB* mutants. Transformation of an *apsB10* mutant strain with a mutated *apsB* version in which a PTS1 sequence was added at the C-terminus. WT (TN02A3), *apsB* mutant strain (AJC1.7, *apsB10*) and the transformed strain (SNZ34) were grown on glucose and under de-repressing conditions on sorbitol. Scale bars 1 cm.

The *apsB10* mutation converts codon 83 into a stop codon and thus the mutant is lacking most of the 1052 amino acid long ApsB protein. The transformed plasmids were integrated ectopically.

Transformants of both strains (SNZ34 and SNZ94) appeared with the brown *apsB*-like phenotype under repressing conditions (glucose), and a wild-type like, spore producing phenotype under de-repressing conditions (sorbitol). These results suggest that the ApsB-PTS1 protein was able to complement the oligosporogenic phenotype **(Figure IV. 39)**.

The number of MTs in the rescued strains was also similar to the wild-type, MTs were observed after immunostaining using anti MT antibodies (DM1A) and FITC labeled secondary antibodies **(Figure IV. 40)**. Those results suggest a novel function for peroxisomes in septal microtubule organization in *A. nidulans*.
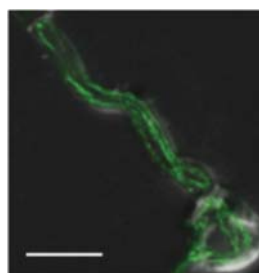
Figure IV. 40. Immunostaining of MTs with DM1A and Tyrosine-tubulin antibodies in SNZ94. Scale bar 5 μm.

4.6. On the role of peroxisomes

To further test if peroxisomes are involved in septal MTOC formation, the effect of a *pexC* mutation on ApsB and HexA localization and function was studied. PexC is the *A. nidulans* homologue of *S. cerevisiae* Pex3, which is essential for peroxisome membrane formation (Hynes *et al.*, 2008). The *pexC* mutant strain was always cultured in the presence of 2-5 mg/ml glufosinat as selection marker for the disruption construct. In the absence of the dominant marker, the disruption was very unstable. Whereas mRFP1-HexA localization was lost in strain SNZ103, GFP-ApsB was still observed at SPBs and septal MTOCs **(Figure IV. 41)**.
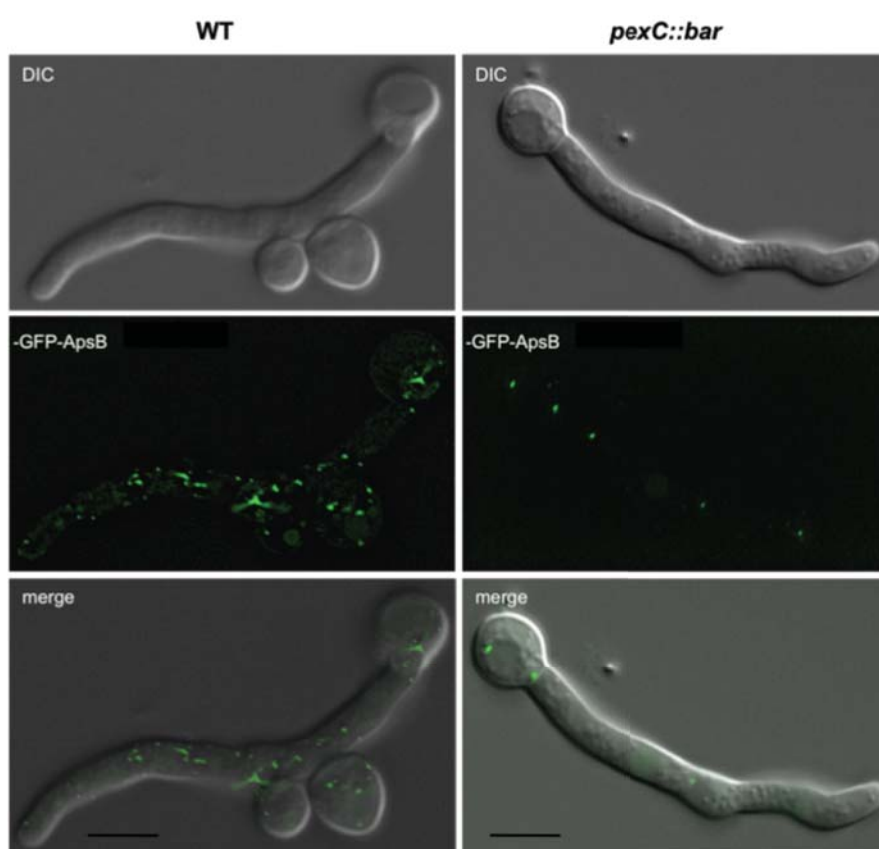
Figure IV. 41. ApsB localization in a *pexC* mutant strain. Z-stack images with deconvolution for GFP-ApsB in WT (SEa3) and in the *pexC* mutant strain (SNZ103). The arrow points to the ApsB signal at a septum. Scale bars 5 μm.

The number of cytoplasmic spots was drastically reduced. These results suggest that ApsB localization is affected by the lost of normal peroxisomal network. However, *pexC* mutant strains displayed a pleiotropic phenotype and are not easily comparable with wild-type with regards to hyphal morphology and asexual development.

5.   Characterization of a putative tubulin tyrosine ligase (*ttl)* gene

Tubulins and microtubules are subjected to several post-translational modifications of which the reversible detyrosination/tyrosination of the carboxy-terminal end of most alpha-tubulins has been extensively analyzed. This modification cycle involves a specific carboxypeptidase and the activity of the tubulin-tyrosine ligase (Ttl) (Erck *et al.*, 2000). Tubulin-tyrosine ligase (Ttl) catalyses the ATP-dependent post-translational addition of a tyrosine to the carboxy terminal end of detyrosinated alpha-tubulin. The true physiological function of Ttl has so far not been established. In normal cells, the tyrosinated form of tubulin predominates. However, in breast cancer cells, the detyrosinated form mostly predominates, with a correlation to tumour aggressiveness (Mialhe *et al.*, 2001). In summary Ttl functions in protein modification processes and has a tubulin-tyrosine ligase activity. In order to study the function of Ttl protein in *A. nidulans,* Broad Institute gene database (http://www.broadinstitute.org/) was searched and one homolog (*ttlA*) was found. The *ttlA* gene (AN4967) is located on chromosome III. The TtlA protein sequence was analyzed with the SMART program (http://smart.embl-heidelberg.de) and besides the tubulin tyrosine ligase domain between amino acid position 375 and 738, a SurE- like structural domain between amino acid position 1 and 213 was identified **(Figure IV. 42, A and B)**.

The SurE domain with the 3-layer alpha/beta/alpha topology is found in the stationary phase survival protein SurE, a metal ion-dependent phosphatase found in eubacteria, archaea and eukaryotes. In *E. coli*, SurE also has activity as a nucleotidase and exopolyphosphatase, and may be involved in stress response (Iwasaki & Miki, 2007). *E. coli* cells with mutations in the *surE* gene survive poorly in stationary phase. The structure of SurE homologues have been determined from *Thermotoga maritime* and the archaea *Pyrobaculum aerophilum* (Lee *et al.*, 2001; Mura *et al.*, 2003; Zhang *et al.*, 2001). The *T. maritima* SurE homologue has phosphatase activity that is inhibited by vanadate or tungstate, both of which bind adjacent to the divalent metal ion. This domain is found in acid phosphatases, 5'-nucleotidases, 3'-nucleotidases, and exopolyphosphatases and it has a hydrolase activity. In *A. nidulans* the function of the SurE domain in TtlA is not yet known **(Figure IV. 42, A and B)**.

A   TtlA

B

```
ATG CAT ATT CTT gtgggtcagaattattaatcttctttgtctcaggttaacagttttgttacgtag GTG GTG AAC GAC GAC GGC CCT CCG TCG AAC GAA
 M   H   I   L                                                                V   V   N   D   D   G   P   P   S   N   E

TCC TCT CCG TAT GTC CAT TCG TTC GTC CAC ACA CTA CAG TCT GCT GGG CAC ACC GTC TCA GTA GTC CTT CCT CAT CAG CAG CGA TCA
 S   S   P   Y   V   H   S   F   V   H   T   L   Q   S   A   G   H   T   V   S   V   V   L   P   H   Q   Q   R   S

TGG ATT GGT AAA GCC CAT CTT ATT GGC GCT GTC AAA CCA ACC TAT TTC CGG CCC GGA ACG CTG CAC AAA GAT GAT GGC ACA ACG
 W   I   G   K   A   H   L   I   G   A   A   V   K   P   T   Y   F   R   P   G   T   L   H   K   D   D   G   T   T

CAC GAG TAC CCG CGC GGC GAC AAC GAC CCA GAC GGC GAC GAG TGG ATT CTT ATA AAC TCA ACC CCC GCC AGT TGC GTG CAG ATT GGT
 H   E   Y   P   R   G   D   N   D   P   D   G   D   E   W   I   L   I   N   S   T   P   A   S   C   V   Q   I   G

CTC TAT CAC TAT TTC CAG GAC CGT GGG CCC GTT GAC CTC GTG GTA TCC GGA CCC AAT TAT GGC CGC AAT ACC ACG GCA CTT TTC GCT
 L   Y   H   Y   F   Q   D   R   G   P   V   D   L   V   V   S   G   P   N   Y   G   R   N   T   T   A   L   F   A

ATG TCG AGC GGG ACA ATC GGC GCT GCA ATG GAG GGC GCC GCA TGT GGA AAA CGC TCG ATT GCC CTC TCG TAT GCC TTC AGC TCG CGC
 M   S   S   G   T   I   G   A   A   M   E   G   A   A   C   G   K   R   S   I   A   L   S   Y   A   F   S   S   R

AAT CAT GAC CCT GTC ATC ATC GCG GAG GCG TCT CGG CAT TCA GTA CGG GTT ATT GAG TAC CTC GCG AAA AAC TGG GAT GAG GGT GTT
 N   H   D   P   V   I   I   A   E   A   S   R   H   S   V   R   V   I   E   Y   L   A   K   N   W   D   E   G   V

GAT TTG TAC AGC GTG AAT GTG CCG CTG GAA CCT GGT GTG AGC GAA AGC AAA GTA ATG TAT ACT GAG ATG CTC GAT AAT CGG TGG TCA
 D   L   Y   S   V   N   V   P   L   E   P   G   V   S   E   S   K   V   M   Y   T   E   M   L   D   N   R   W   S

TCC GGG AGT TGC TTT GAC GCT GTT GAT GCC GAG GTA CCG GTA GAA AAC CCA GAG CAG CGA GAA CAG ACC CTG CGG GAT CAG GAG GAG
 S   G   S   C   F   D   A   V   D   A   E   V   P   V   E   N   P   E   Q   R   E   Q   T   L   R   D   Q   E   E

AAG CTG GAA GAA GAT CCC ACT GCG AAC CCT AAT GCT AAG TCT GGA AGG AAA TCG CGG ATT GCC CAT AAG CAT TTT ATT TGG GCA CCA
 K   L   E   E   D   P   T   A   N   P   N   A   K   S   G   R   K   S   R   I   A   H   K   H   F   I   W   A   P

AAG TTT ACT GAC GTC TAT CGG AGT GTG GAG GAA AGT GCG CCT GGG AAT GAC GGC TGG ACT GTC AAG GAG GGA ATG ACG AG gtatgtc
 K   F   T   D   V   Y   R   S   V   E   E   S   A   P   G   N   D   G   W   T   V   K   E   G   M   T   S

aacaccacgccagtttcgccgagtatcttctaactagaaatag   T GTT ACT CCA TTA AAG GCT AAT TTC ATG CAT ACG CCC GGT ATC AAA GGG GAG
                                                V   T   P   L   K   A   N   F   M   H   T   P   G   I   K   G   E

ATT AAG CT gtgagtggattcggcgagcagttcctgtttagacgactgtttaaagcataaatcttgcgctttctgttatctatcaagcgatgctatgttctatttgtggatac
 I   K   L

acggtctgatagtgctatatcgcgtag   A TCG GAT AAT GAG GAG CCC GCC TTC TAT TCC ATA GTG GAT TGT GAC GAT CCC TAC GTC CAA GAA
                                S   D   N   E   E   P   A   F   Y   S   I   V   D   C   D   D   P   Y   V   Q   E

TTG GTC GAG CAA GCA CTC CGA TTT AGT ATG GGA TCC CGT TGC CGG TCT GTA TCC TCT ATA TCA GAG CTT CCC TCC CGG TCC ACT CCA
 L   V   E   Q   A   L   R   F   S   M   G   S   R   C   R   S   V   S   S   I   S   E   L   P   S   R   S   T   P

GTT TTC CAG TAC CGC GAA TAC GAA CGT TTG GAT TTC GAG CAC GCC ATG ACG AAC CCG ACA ACG TCC CTG ATA AAC GCC TAC ATC ATC
 V   F   Q   Y   R   E   Y   E   R   L   D   F   E   H   A   M   T   N   P   T   T   S   L   I   N   A   Y   I   I

CGC AAA GCT CTA ATT CGA AAA CAC TAC CTC GCT AAC ACC GTC TCA AAC TGG GTG ACC AAG CAC CCA GAA AGC GTG TTG GCG AAG CAC
 R   K   A   L   I   R   K   H   Y   L   A   N   T   V   S   N   W   V   T   K   H   P   E   S   V   L   A   K   H

GTC AAG GTC TCA GTG GAC TTT GAA CTC GAC TAT GCT GAA TTC CTT GAC GAC GCT CTA CTT GGA GCT TAC GAA CTT CGC GAA TGC TTT
 V   K   V   S   V   D   F   E   L   D   Y   A   E   F   L   D   D   A   L   L   E   A   Y   E   L   R   E   C   F

GAG GAG AAC GAA TCC AGA CCG GAC TCA GAG AAG GTA TGG TGG ATT CTT AAA CCG GGG ATG AGT GAT CGC GGA CAG GGG ATT CGG CTG
 E   E   N   E   S   R   P   D   S   E   K   V   W   W   I   L   K   P   G   M   S   D   R   G   Q   G   I   R   L

TTC AAC AGC GAA GAC CAG CTC CGT GAG ATA TTC GAG GAG TGG GAG CCT GAT TCT GAA GAT GAA GAA GAG GAC GAA TGC GGG GAG GAC
 F   N   S   E   D   Q   L   R   E   I   F   E   E   W   E   P   D   S   E   D   E   E   E   D   E   C   G   E   D

GAT GGC AAC GAC GAG ACA GAC AAG GCT CCC ACT AGC GGT GTG GTA ACA TCC CAG CTC CGC CAT TTC ATC GCC CAA CCC TAC ATC GAC
 D   G   N   D   E   T   D   K   A   A   T   S   G   V   V   T   S   Q   L   R   H   F   I   A   Q   P   Y   I   D

CCG CCT CTC CTT CTC CCC TCT CTC AAC AAC CGC AAA TTC CAC ATA AGA ACC TAC GTC CTC GCG ACA GGC TCT CTG AAG GTG TAC GTC
 P   P   L   L   L   P   S   L   N   N   R   K   F   H   I   R   T   Y   V   L   A   T   G   S   L   K   V   Y   V

TTT AAG GAG ATG CTC GCC CTC TTC GCA TCG AAG CCT TAC GTC TCC CCT ACC TCG CAG AAC AAT GAG ACC GAA GAC TCA ATC GCC GAC
 F   K   E   M   L   A   L   F   A   S   K   P   Y   V   S   P   T   S   Q   N   N   E   T   E   D   S   I   A   D

CTA ACC CGC CAC CTA ACC AAC ACT TGC TTT CAA GAC AAA TTC CTG CCA GAG TCT GAA ACC GTC CGC CGC TTC TGG TGT CTC CCC TCC
 L   T   R   H   L   T   N   T   C   F   Q   D   K   S   L   P   E   S   E   T   V   R   R   F   W   C   L   P   S

ATC CCG CCT CCA AAT ACA CAT CTA ACC GCC ACC TGG AAA GAA GAT ATT TAC GAG CAA ATC TGC GCC GTC ACA GGC GAG CTT TTC ACC
 I   P   P   P   N   T   H   L   T   A   T   W   K   E   D   I   Y   E   Q   I   C   A   V   T   G   E   L   F   T

GCT GCG GCG CGC GGC ATG ATG ATC CAT TTC CAG ACG ATG CCG AAT GCG TTT GAG GTC TTT GGA GTG GAC TTT TTG GTC GAT GAC ACG
 A   A   A   R   G   M   M   I   H   F   Q   T   M   P   N   A   F   E   V   F   G   V   D   F   L   V   D   D   T

GGC AAT GTG TGG TTG TTG GAA GTC AAT GCT TTC CCG GAT TTT GGA CAG ACT GGT GAG GAG CTC AGG GAT GTT GTT GTG GGC GGT TTA
 G   N   V   W   L   L   E   V   N   A   F   P   D   F   G   Q   T   G   E   E   L   R   D   V   V   V   G   G   L

TTC AAA GGT GTG ATT GGT GTG GCT AAG GGG TTC TTT GGT GAG GAG GGT AAG ACG GAA GAG AAT GGG ATG AGG CTG GTT GCG GAG
 F   K   G   V   I   G   V   A   V   K   G   F   F   G   E   E   G   K   T   E   E   N   G   M   R   L   V   A   E

CTG GAT CTT GGG AGG AAG AAT TGA
 L   D   L   G   R   K   N   *
```

Figure IV. 42. Analysis of the A. *nidulans* **ttlA gene. (A)** Domain prediction for the TtlA protein. The TtlA (757 amino acids) protein sequence was analyzed with the SMART program (http://smart.embl-heidelberg.de) and besides the Ttl domain, a SurE domain was identified. **(B)** The *ttlA* open reading frame has 2274 bp and three predicted introns (lower-case letters) were identified. The Ttl domain (labelled in gray) between amino acid position 375 to 738, the SurE domain (labelled in yellow) between amino acid position 1 to 213.

5.1. Deletion of *ttlA*

The *ttlA* open reading frame has been deleted in the wild-type strain TN02A3 with *pyroA* as selection marker. The flanking regions of *ttlA* were amplified by PCR using genomic DNA and the primers TTL-LB-fwd and TTL-LB-*Sfi*I-rev for the upstream region of *ttlA* and TTL-RB-*Sfi*I-fwd with TTL-RB-rev for the downstream region. In a three-fragment ligation, the *pyroA*-gene obtained from plasmid pNZ12 was ligated between the two *ttlA*-flanking regions, resulting in vector pNZ53. The deletion cassette was amplified with the primers TTL-LB-fwd and TTL-RB-rev, and the resulting PCR product was transformed into the pyro-auxotrophic *A. nidulans* strain TN02A3, and the deletion event was confirmed with Southern blot **(Figure IV. 43)**.
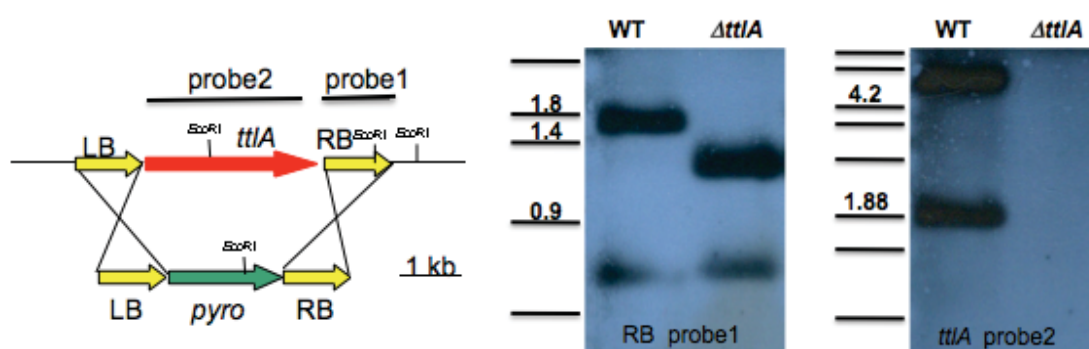
Figure IV. 43. Deletion of *ttlA*. Scheme of the deletion procedure and corresponding Southern blot. DNA was digested with *Eco*RI and the Southern blot was done using a RB-probe (probe1) and a *ttlA*-probe (probe2) as indicated.

One of the strains (SNZ75) was used for further analysis and the construction of *ttlA*-deletion strains in other genetic backgrounds. Colonies of this strain grew similar to the wild-type **(Figure IV. 44)**.
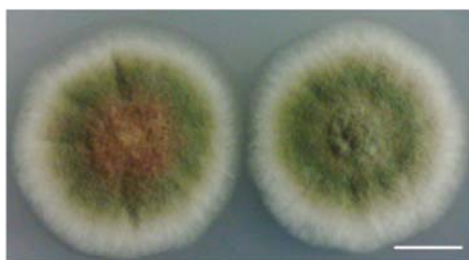
Figure IV. 44. Phenotype of the *ttlA* deletion strain. Growth of the strains TN02A3 (WT, left) and SNZ75 (*ΔttlA*, right), for 3 days at 37°C, on minimal medium glucose with supplements. Scale bars 1 cm.

Distribution of nuclei, visualized with DAPI **(Figure IV. 45, A),** or the organization of the microtubule cytoskeleton visualized by immunostaining with an alpha tubulin antibody (DM1A) and an anti-tubulin tyrosine antibody (clone TUB-1A2) **(Figure IV. 45, B)**, were similar to a wild-type strain. Immunostaining using anti-tubulin

tyrosine antibody (TUB-1A2) alone **(Figure IV. 45, C)**, results in much less signal and more punctuated MTs than in the case of using both antibodies together, suggesting some differences in the alpha tubulin tyrosination cycle.
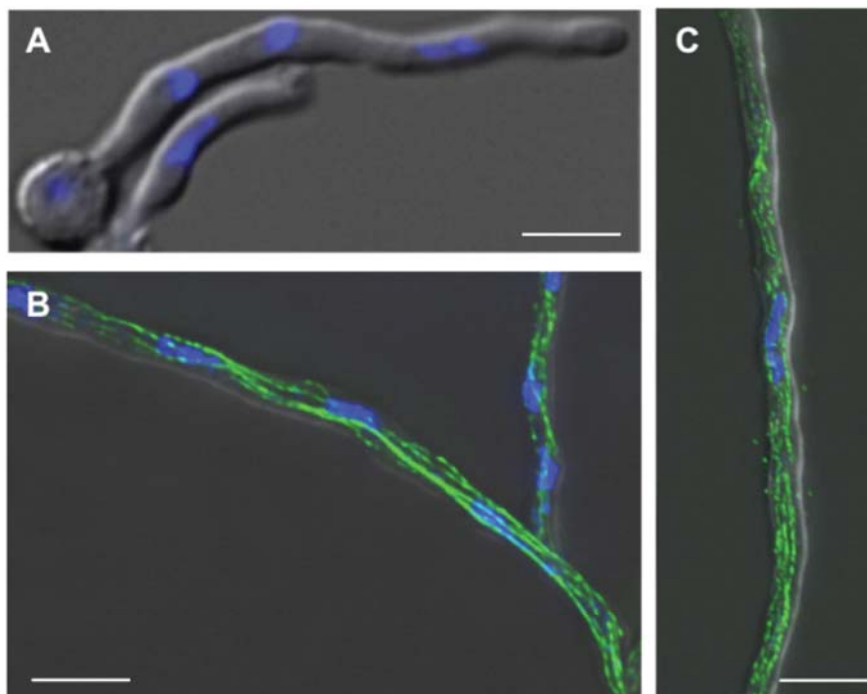
Figure IV. 45. Observation of nuclei and microtubules in a *ttlA*-deletion strain. DAPI staining **(A)** and immunostaining with anti alpha-tubulin antibodies **(B, C)** were used for the visualization. Strain is SNZ75, anti alpha tubulin TUB-1A2 and DM1A were used in **(B)**, only TUB-1A2 was used in **(C)**. Scale bars 5 μm.

Because the TtlA enzyme is supposed to change the equilibrium between tyrosinated and detyrosinated MTs, it was interesting to detect the amount of the two alpha tubulin species in *A. nidulans* wild-type and Δ*ttlA* (strain SNZ75) using the two antibodies described above: DM1A for all alpha tubulin and TUB-1A2 for the tyrosinated form. The same concentration of proteins was loaded onto SDS PAGE and western blot was done. Surprisingly, both strains showed a similar band intensity with DM1A antibodies and no specific band was detected in the case of TUB-1A2 antibodies **(Figure IV. 46)**.
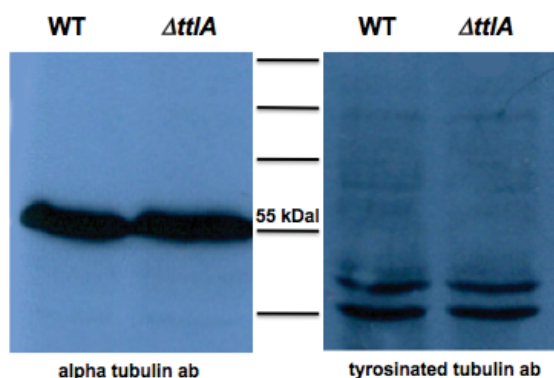
Figure IV. 46. Comparison of tyrosinated- and detyrosinated-alpha-tubulin amounts in a *ttlA*-deletion strain. Western blot of a *ttlA*-deletion strain and the WT strain (TN02A3) with anti alpha tubulin antibodies DM1A (left) and with anti tyrosinated alpha tubulin antibodies TUB-1A2 (right)

Next, GFP-UncA^{rigor} was used as a marker for detyrosinated MTs in the *ttl*A-deletion strain. The UncA^{rigor} construct pNZ15 was transformed into the *ttl*A-mutant strain resulting in sNZ91. GFP-UncA^{rigor} still localized to one distinct MT bundle spanning the entire hyphal compartment, and not to all MTs as it was expect if the deletion of *ttl*A caused a shift towards detyrosinated MTs **(Figure IV. 47)**.
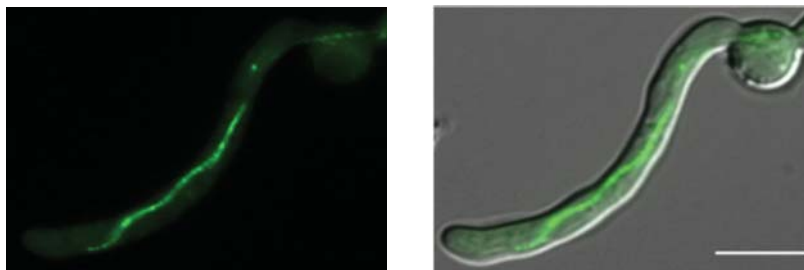
Figure IV. 47. GFP-UncA^{rigor} localization in a *ttl*A-deletion strain. UncA^{rigor} decorates one MT bundle. Strain SNZ91. Scale bar 5 μm.

5.2. TtlA localizes to MTs

The TtlA protein was visualized by fusion with a fluorescent protein (GFP or mRFP1 in the vector pNZ56 and pNZ57, respectively). To create an N-terminal GFP fusion construct of TtlA, a 2.5-kb full-length fragment of *ttl*A (starting from ATG) was amplified from genomic DNA, with the primers TTL_*Asc*I_ATG_fwd1 and TTL_*Pac*I_stop_rev1. The *Asc*I-*Pac*I fragment was subcloned into the corresponding sites of pNZ57, yielding pCS7-NZ, where mRFP1-TtlA was under the control of the *alc*A-promoter. To create an N-terminal GFP fusion construct of TtlA, the 1.3-kb TtlA *Asc*I-*Bam*HI fragment from pCS7-NZ was substituted by TlgA from pNZ56, yielding pCS8-NZ, where GFP-TtlA was also under the control of *alc*A(p). Both GFP and mRFP1 plasmids were transformed ectopically into the wild-type strain TN02A3, resulting in SCS7-NZ85 and SCS8-NZ86 respectively. Under de-repressing conditions, using glycerol medium, TtlA was observed in the cytoplasm and hardly along MTs **(Figure IV. 48; movie IV. 12)**.
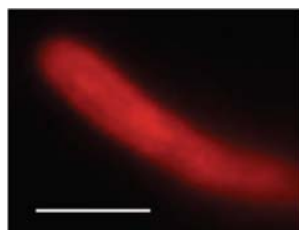
Figure IV. 48. Localization of mRFP1-TtlA. TtlA localizes to the cytoplasm and to microtubules. Some decorated microtubules are hardly to see near the tip (see movie IV. 12). Strain SCS8-NZ86. Scale bar 5 μm.

In order to test if TtlA over expression is accompanied with elevated level of tyrosinated alpha-tubulin, Western blot measurement of the amount of tyrosinated- and detyrosinated-alpha-tubulin was done, this time the mRFP1-TtlA over expressed strain was compared with the *ttl*A mutant strain. Identical concentrations of total extract were loaded into SDS PAGE and different antibodies were used: DM1A for all alpha tubulin forms, TUB-1A2 for detyrosinated alpha tubulin and OBT1660 for the detyrosinated form of alpha tubulin. No differences between the two strains were detectable.

6.   Identification of factors that determine the stability of microtubules in *A. nidulans*

One fascinating aspect of detyrosinated MTs is their increased stability. The modified C-terminal end is apparently only the consequence and not the cause for the stability. Hence, the open question is how the increased stability is achieved. It has been shown that microtubule-associated proteins are able to stabilize MTs (Kondo *et al.*, 1994). However, they are not able to discriminate between different MTs in one cell. If a certain MAP is expressed in a specific cell type, all MTs are rendered more stable. A differential increase of the stability has been explained with a different MT plus end cap. However, the mechanism remained elusive (Infante *et al.*, 2000).

To investigate this question, the effect of several MT plus end associated proteins has been studied, among them ClipA (Efimov *et al.*, 2006), AlpA (Enke *et al.*, 2007) and KipA (Konzack *et al.*, 2005).

6.1. AlpA

One possible candidate to influence the stability of MTs is AlpA. It is a homologue of the *Xenopus* XMAP215 protein, which has been shown recently to act as MT polymerase (Brouhard *et al.*, 2008). *A. nidulans* deletion of *alpA* caused a reduction of the number of cytoplasmic MTs and altered MT dynamics (Enke *et al.*, 2007). Those defects give the hyphae of *alpA*-deletion strains a curved phenotype, which resembles that of a (kinesin-7) *kipA*-deletion strain. Therefore it was interesting to find out whether the lack of both genes would result in a similar or a different phenotype compared to the single mutations. The double mutant showed a more severe phenotype than the individual mutations. Hyphae appeared even more curly and similar to the *alpA* mutant with more branches in older

hyphae. Colonies were much smaller than the colonies of the parent strains, indicating an additive effect of ΔkipA and ΔalpA **(Figure IV. 49, A)**.
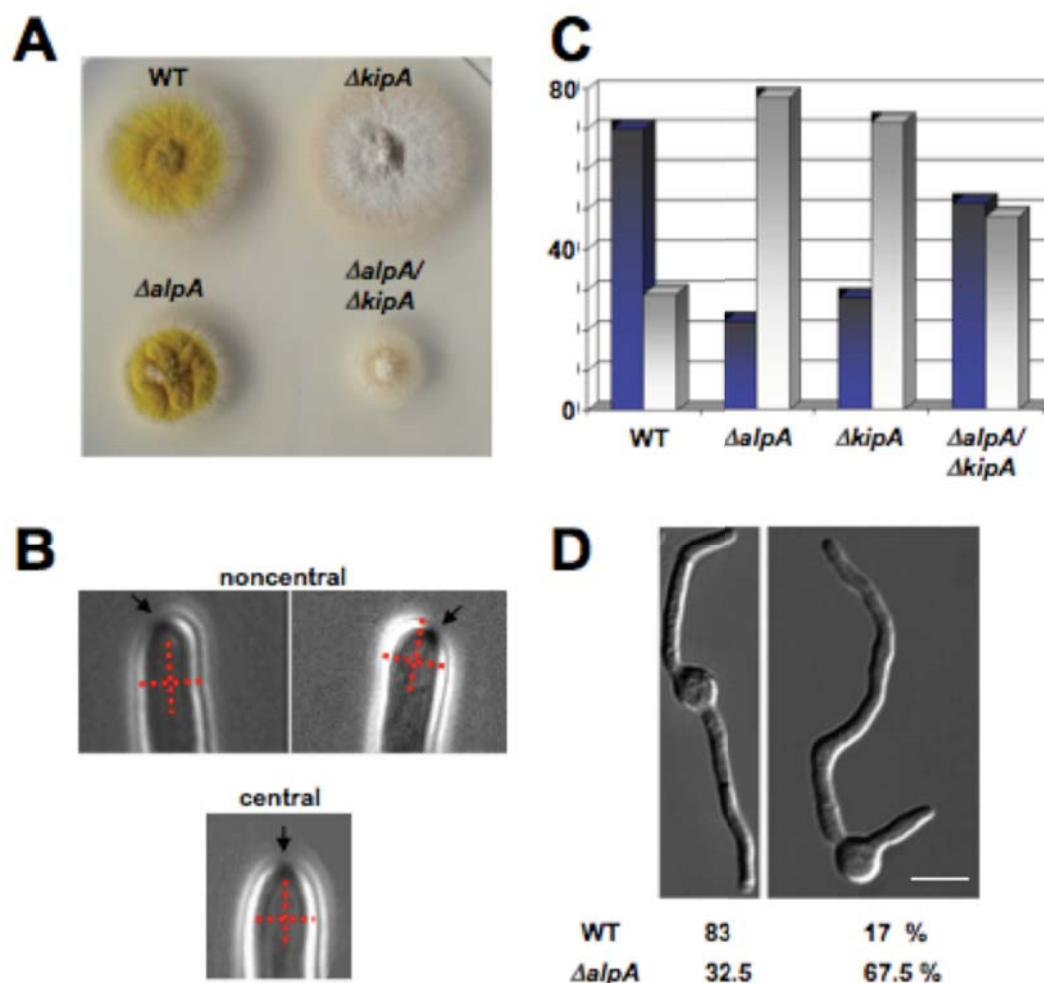
Figure IV. 49. Localization of the Spitzenkörper in hyphae of *alp*A-deletion strain and germination pattern. The Spitzenkörper was observed in growing hyphae. **(A)** Colonies of wild-type (RMS011), the ΔalpA (SDV83), the ΔkipA (SSK44), and the ΔalpA/ΔkipA (SAD1c) strain on an agar plate after three days of growth at 37°C. **(B)** Representative hpyhae with a Spitzenkörper in the centre of the cell or noncentral. To indicate the position of the organelle, a cross is introduced into the hypha. **(C)** Quantification of the location of the Spitzenkörper in the strains listed in (A). Dark blue columns represent hyphae with the Spitzenkörper in the centre and grey columns the ones where the Spitzenkörper was noncentral. Between 50 and 64 hyphae were analyzed for each strain. **(D)** Quantification of the germination pattern of conidiospores as displayed in the pictures. Wild-type (RMS011)(n= 200); *alpA* mutant (SDV83)(n= 268). Scale bar 5 μm.

Because growth direction of hyphae depends on the localization of the Spitzenkörper in the apex, the position of this organelle was analyzed in wild-type and compared to the one in the *alpA*-, the *kipA*-, and the *alpA, kipA* double-deletion strains. Whereas in wild-type the Spitzenkörper was found in the centre of the hyphae in 70 % and non-central in 30 % of the cases (n = 50), in the *alpA*-deletion strain only 22 % showed the central position and 78 % the non-central one (n = 50). In comparison, in the *kipA*-deletion strain the percentages were 28 % (central) and 72 % (non-central) (n= 50) and in the *alpA, kipA*-double deletion strain 52 % (central) and 48 % (non-central) (n = 64) **(Figure IV. 49, B and C)**.

It was surprising that the number of central and non-central positioning of the Spitzenkörper was almost even in the double mutant strain. In addition, it was noticed that in 18% of the cases two Spitzenkörper were observed in the hyphal tip. In comparison this number was only 5 % in wild-type, 10 % in the *alpA* and 5 % in the *kipA* mutant. If there were two Spitzenkörper in the apex, they were counted as one event of noncentral organelles in the quantification in **(Figure. IV. 49, C)**. In order to test whether AlpA might play a role in the initiation of polarized growth, the germination pattern of conidiospores was analyzed **(Figure IV. 49, D)**. Wild-type conidiospores produce a second germ tube after the first germ tube has reached a certain length and this second hypha emerges from a place opposite to the first hypha. In contrast, the *alpA*-deletion strain produced the second germ tube normally in angles smaller than 180° from the first hypha **(Figure IV. 49, D)**. This germination pattern resembled the one from the *kipA*-mutant strain.

To test the hypothesis that the AlpA activity is involved in the stabilization and the subsequent detyrosination process, the GFP-UncA^{rigor} protein was used as a labeling marker for stabilized MTs. As mentioned before $\Delta alpA$ strain shows a reduced number of cytoplasmic MTs and altered MT dynamics. This strain was crossed with the GFP-UncA^{rigor} strain (SNZ14), giving sNZ101, and the subcellular localization was studied. The *alp*A-deletion strain showed one stable MT bundle stained with GFP-UncA^{rigor} **(Figure IV. 50)**. Indicating that the stablilization of the detyrosinated bundle does not depend on AlpA activity, or that another protein substitutes AlpA and its function.
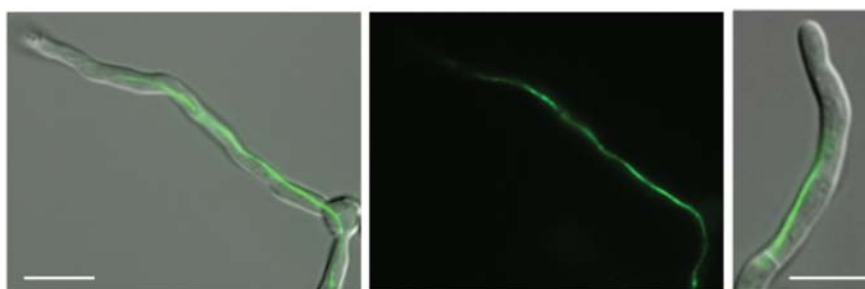
Figure IV. 50. Localization of the GFP-UncA^{rigor} in the *alp*A-mutant strain. One MT bundle decorated with the GFP. Strain SNZ101. Scale bars 5 μm.

6.2. TeaA

If AlpA influences the stability, it is important to know how the AlpA activity is controlled. One possibility is that this is achieved through the interaction with other proteins. One suggested candidate is the *A. nidulans* cell end marker protein TeaA (Takeshita *et al.*, 2008). TeaA

localizes at the tip of hyphae and at MT plus ends. The tip localization depends on the MT cytoskeleton and vice versa MT dynamics is regulated by TeaA. In the *teaA*-deletion mutant, some MTs did not converge at tips and other MTs failed to stop growing after reaching the tips and bent. This mutant strain was a good candidate for labeling MTs with GFP-UncA^{rigor}. After crossing the *teaA*-mutant strain with the GFP-UncA^{rigor}, strain sNZ89 was created, in which the rigor kinesin still localized to one MT bundle. In many hyphae the bundle splits near the tip **(Figure IV. 51)**, which indicates that the UncA bundle may loose the direction toward the tip of hyphae in the absence of TeaA.

Figure IV. 51. Localization of the GFP-UncA^{rigor} in the *tea*A mutant strain. One MT bundle decorated with the GFP-UncA^{rigor} signal. Strain is sNZ89. Scale bar 5 μm.

6.3. ClipA

Several proteins have been identified to regulate the MT plus-end dynamics referred to +TIPs in eukaryotic cells. In *A. nidulans*, one of the +TIPs, ClipA corresponding to CLIP-170, localizes to MT plus ends and promotes microtubule growth and their catastrophe after they reach the hyphal tip. The *clipA*-deletion strain shows in addition alterations in microtubule dynamics (Efimov *et al.*, 2006). Furthermore in mammalian fibroblasts cytoplasmic linker protein CLIP-170 localizes to the ends of tyrosinated microtubules but not to the ends of detyrosinated microtubules (Peris *et al.*, 2006).

In order to test if ClipA localizes also to the plus-ends of tyrosinated MTs in *A. nidulans*, UncA^{rigor} was used as a marker for detyrosinated MTs and transformed GFP-ClipA strain with the full-length UncA^{rigor} fused to mRFP1 (plasmid pCoS19) resulting in strain sNZ97. Unfortunately this strain shows many UncA^{rigor}–decorated-MT-bundles because of the ectopic integration of the full-length UncA plasmid, which results in high protein expression level of UncA thus labeling of UncA^{rigor} to many MTs. ClipA was co-localizing with all MT plus ends and surprisingly, some continuous decoration of MTs with GFP-ClipA was observed **(Figure IV. 52)**. Those observations suggest a role of UncA in ClipA transportation **(Figure IV. 54)**.
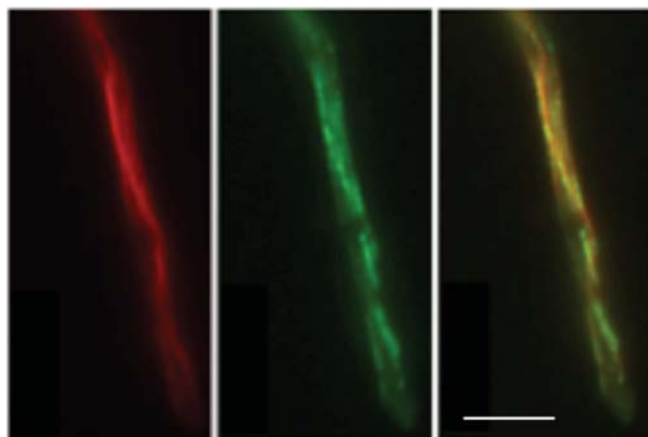
Figure IV. 52. Co-localization pattern of GFP-ClipA and the over expressed mRFP1-UncA^{rigor} in sNZ97. Scale bar 5 μm.

6.4. NudA

Because UncA^{rigor} spots are not completely immobile and to further analyze if another motor protein helps UncA^{rigor} to move, the co-localization pattern of UncA with the minus end directed motor protein dynein was observed. Strain LZ12 in which *A. nidulans* Dynein heavy chain was fused to GFP (GFP-NudA, kindly provided from X. Xiang, (Zhuang *et al.*, 2007)) was transformed with mRFP1-UncA^{rigor} (pNZ9) resulting in sNZ87. Many UncA spots were co-localizing with NudA GFP signals suggesting that the remaining motility in the UncA^{rigor} strain depends on dynein and that UncA and dynein counteract on vesicles to transport them to opposite directions **(Figure IV. 53)**.
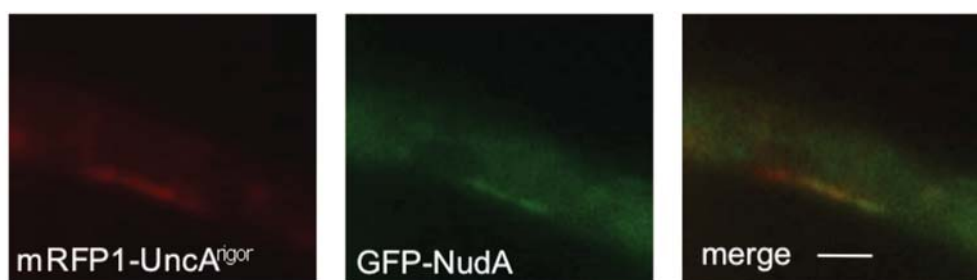
Figure IV. 53. Co-localization of GFP-NudA and mRFP1-UncA^{rigor} in sNZ87. Scale bar 1 μm.

Another candidate which moves in plus-end direction and can help UncA^{rigor} to keep moving is the kinesin-3 family member UncB. Next UncB will be characterized in detail, and the interaction with UncA will be studied.

7.   Localization of UncB in *A. nidulans*

The truncated Kinesin-3 related motor protein UncB was visualized by fusion with a fluorescent protein (GFP or mRFP1 in the vector pMCB17apx). To create an N-terminal GFP fusion construct of UncB, a 1.6-kb N-terminal fragment of *uncB* (starting from ATG) was amplified from genomic DNA, with the primers UncB_ATG2_*Asc*I_fwd and UncB_ATG2_*Pac*I_rev. The *Asc*I-*Pac*I fragment was sub-cloned into the corresponding sites of pCMB17apx, yielding pNZ2, where GFP-UncB was under the control of the *alcA*-promoter. To create an N-terminal mRFP1 fusion construct of UncB, the GFP *Kpn*I-*Asc*I fragment from pNZ2 was substituted by mRFP1 from pDM8, yielding pNZ10.

After homologous integration of the construct at the *uncB* locus, the 1.6-kb fragment becomes duplicated and the full-length *uncB*-open reading frame is fused to GFP and is under the control of the *alcA* promoter. The *GFP-uncB* strain (SNZ1), in which plasmid pNZ2 is homologously integrated, grew as the *uncB*-deletion strain similar to the wild-type strain **(Figure IV. 15)**.
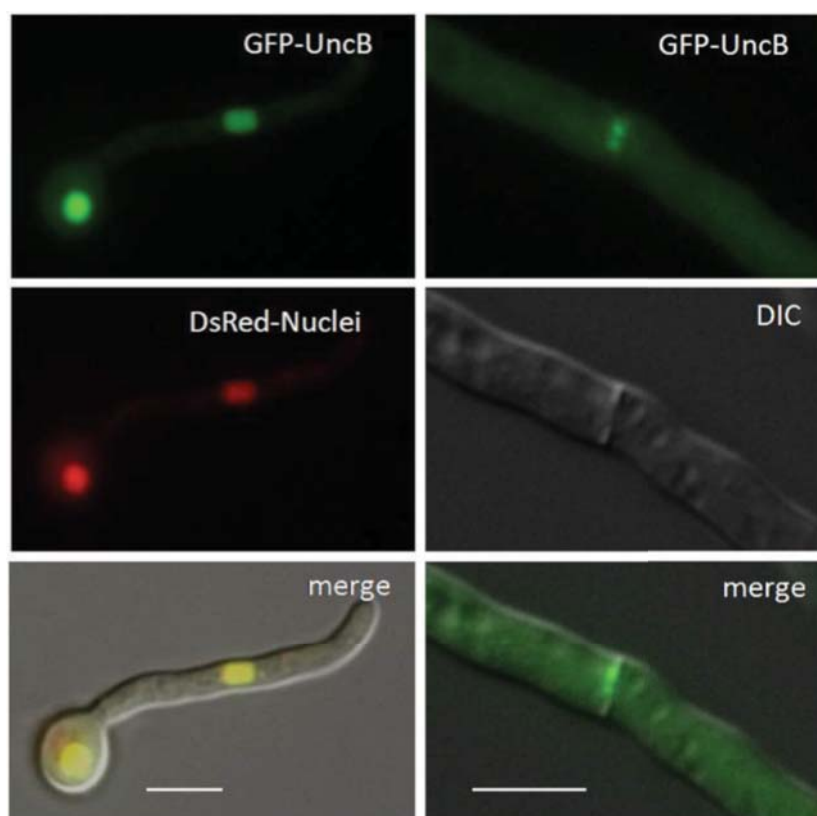
Figure IV. 54. Sub-cellular localization of GFP-UncB. (Left) Localization in nuclei, up: GFP-UncB, middle: DsRed-*stuA*, down: overlay. (Right) GFP-UncB at septa. Strain sNZ-SI39 (left) and sNZ1 (right). Scale bars 5 µm.

The GFP-UncB strain (SNZ1) showed the GFP signal in the nuclei and at septa, nuclei was visualized with DsRed-StuA in strain sNZ-SI39 **(Figure IV. 54)**. Few stained MTs were rarely visible **(Figure IV. 57, left)**.
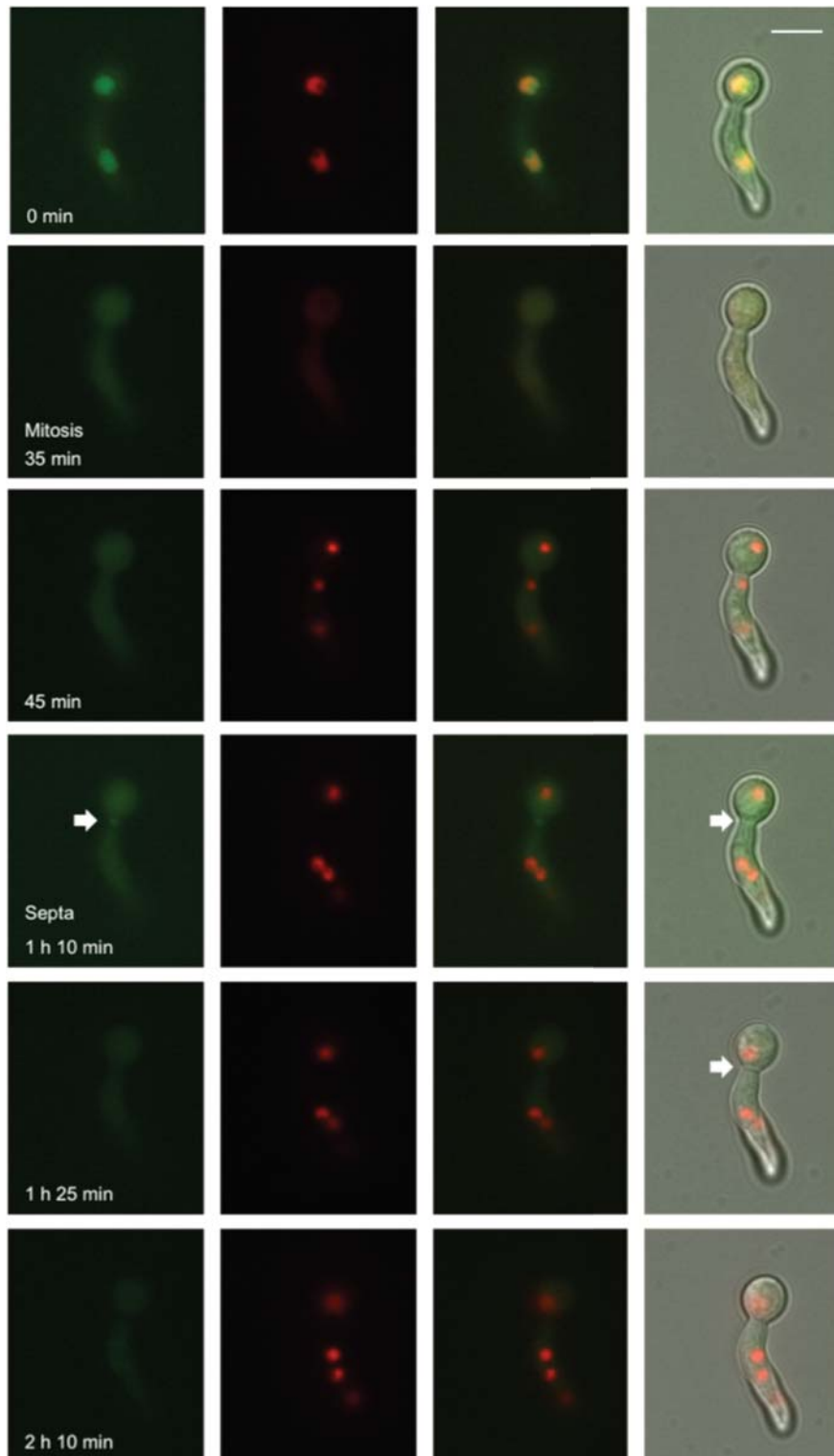
Figure IV. 55. Localization of UncB depends on the cell cycle. Mitosis and septum formation (arrows) times are mentioned. For more details, see text above. Strain sNZ-SI39. : GFP-UncB and DsRed-*stuA*. Scale bar 5 μm.

Time-resolved analysis revealed that those localization patterns depend on the cell cycle, the nuclei co-localization happened during G1 phase, whereas during mitosis the UncB fusion

protein dispersed into the cytoplasm. After mitosis UncB appeared again at septa during forming septa, and then disappeared until the G1 phase occurred again **(Figure IV. 55 and IV. 56, movie IV. 13)**. Between mitosis and forming septa, UncB was temporarily localized into the daughter nuclei **(Figure IV. 56, left)**.
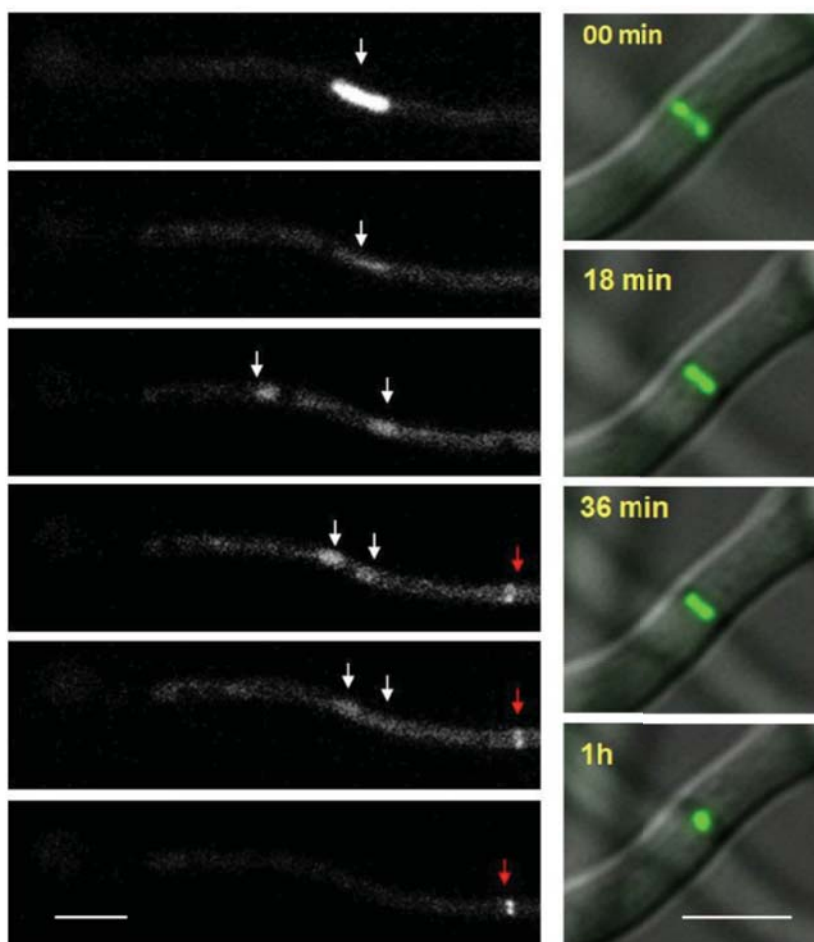
Figure IV. 56. Localization of UncB depends on the cell cycle. (Left) Localization of UncB to the nucleus and at septa after mitosis. (Right) Time-lapse of the formation of a septum. GFP-UncB was associated to the constricting ring. Strain SNZ1. Scale bars 5 μm.

In the case of strain SNZ5 in which pNZ2 was homologously and ectopically integrated and thus the fusion protein over-expressed, a very intense signal was seen along the MTs **(Figure IV. 57, right)**, and some mitotic spindles were also seen.
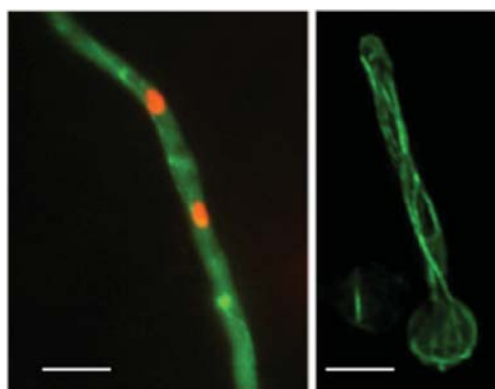
Figure IV. 57. Subcellular localization of GFP-UncB. GFP-UncB localized also to MTs. Most of the protein however, localized to the cytoplasm. (Left) Homologous integration, sNZ1. (Right) ectopic integration, sNZ5. Scale bars 5 μm.

To further analyze the UncB microtubular localization, co-transformation was done with a mRFP1-labelled kinesin-8 (KipB), which localizes on the astral, mitotic and cytoplasmic microtubules (Rischitor *et al.*, 2004). Indeed both GFP-UncB and mRFP1-KipB co-localized to all MTs **(Figure IV. 58)**.
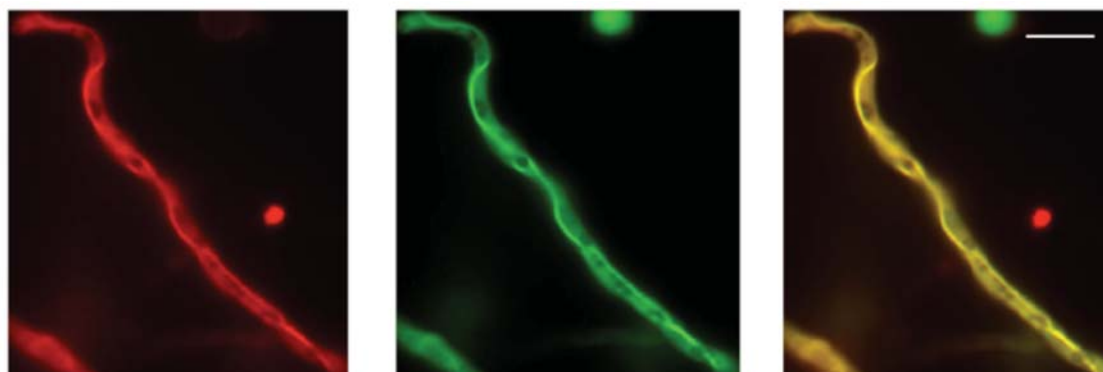
Figure IV. 58. Fluorescence image of over expressed GFP-UncB in *TN02A3* strain co-transformed with a mRFP1-labelled kinesin (KipB). (left) mRFP1-KipB. (middle) GFP-UncB. (right) merged picture. The strain SNZ10 was used. Scale bar 5 μm.

To exclude the possibility that the observed localizations were due to moderate over-expression (glycerol as carbon source) of the GFP-UncB fusion protein, the *alcA* promoter was replaced with a 1.23-kb DNA fragment derived from the putative *uncB* promoter. The putative promoter was amplified from genomic DNA with the primers UncB_nat(P)_*Avr*II_fwd and UncB_nat(P)_*BsiW*I_rev, digested with AvrII and *BsiW*I, and the two fragments were ligated with *Avr*II-*BsiW*I–digested pNZ2, yielding pNZ-SI38. This construct was transformed into TN02A3. One strain with a homologous integration event at the *uncB* locus was selected for further analysis (SNZ58). The GFP signal was very week in this strain, the septal localization was easy to detect, but nuclei localization was hardly detectable but still existing there, which confirm the latter localization results **(Figure IV. 59)**.
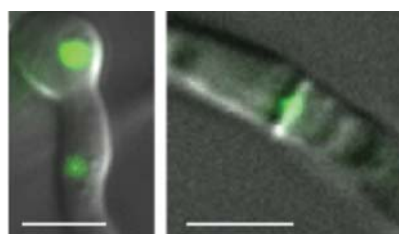
Figure IV. 59. GFP-UncB expressed under the natural promoter. UncB still localized to septa (right) and to nuclei (left). Strain sNZ58. Scale bars 5 μm.

In order to know if UncB uses its own motor to reach the different localization places, a rigor variant of UncB was generated with changed glycine residue 217 to glutamate and changed threonine residue 214 to proline using QuikChange XL site-directed mutagenesis Kit (Stratagene, Heidelberg, Germany). The used oligonucleotides were

UncB_Rigor_P-Loop_fwd and UncB_Rigor_P-Loop_rev and the plasmid pNZ-SI48 was the template for this amplification to yield the plasmid pNZ75. The wild-type TN02A3 and the *uncB*-deletion strain sNZ15 were transformed and searched for transformants in which pNZ75 was homologously (SNZ78) or ectopically (sNZ-SI38) integrated. In the case of homologous integration, the UncB motor accumulated in the nucleus also in daughter nuclei, localization at septa was rarely observed. The cell cycle localization dependency was also observed with time-lapse analysis, suggesting that another motor protein helps UncB to keep moving. The ectopic integration was much more surprising because bundles of MTs were observed **(Figure IV. 60)**.
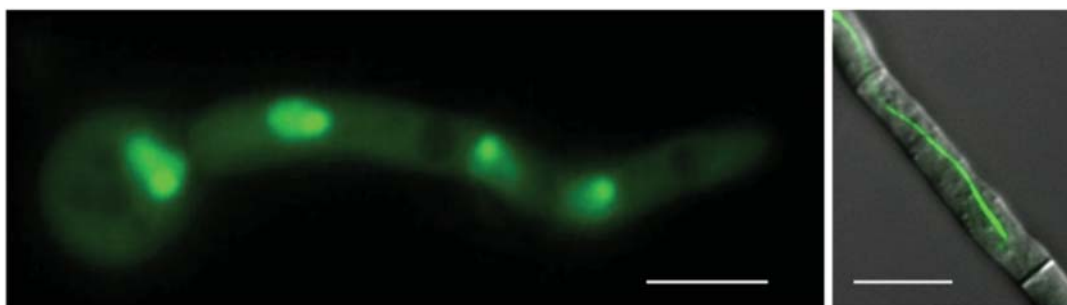
Figure IV. 60. Localization of UncB^{rigor}. (Left) the homologous integration strain shows high accumulation in nuclei. (Right) in the ectopically integration strain UncB decorates MT bundles. Strains sNZ78 (left) and sNZ-SI38 (right). Scale bars 5 μm.

One open question was if those MT bundles share the same MTs of UncA^{rigor}-decorated bundle. To further analyze this question, and because UncB in the over-expressed case labeled all MTs. The GFP-UncA^{rigor} strain was transformed with mRFP1-UncB and an UncB over expressing strain was found (sNZ18). In this strain UncB was decorating almost all MTs and indeed one of those bundles was the UncA^{rigor} MT bundle **(Figure IV. 61)**.
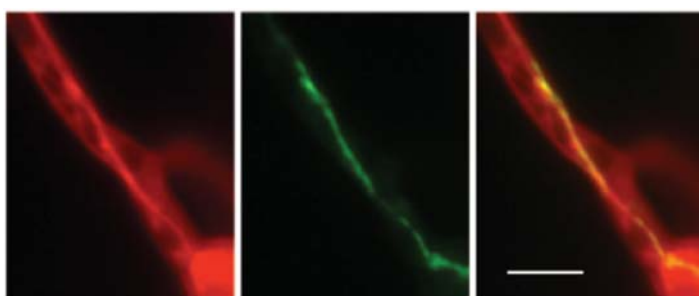
Figure IV. 61. Co-localization pattern of UncB and UncA^{rigor}. mRFP1-UncB, GFP-UncArigor and merge images show co-localization between both protein. Notice that mRFP1-UncB decorates many microtubules whereas UncA decorates just one bundle. Strain sNZ18. Scale bar 5 μm.

This result led us to further study the interaction between UncA^{rigor} and UncB using the BiFC system where both proteins were fused to the YFP N- or C-terminal halves, respectively. Indeed the interaction signals were decorating few MT bundles in sNZ64 and sNZ65 **(Figure IV. 62)**.
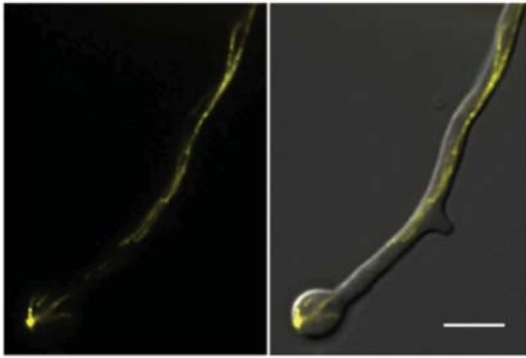
Figure IV. 62. BiFC interaction of UncB and UncA^{rigor}. BiFC assay analysis for UncB and UncA^{rigor} shows interaction along MT bundles in strain sNZ64. Scale bar 5 μm.

Those interactions are very important to decipher the role of UncB in *A. nidulans*. Further experiments are required to proof those interactions and to characterize the role of UncB and UncA and their interplay more precisely. One approach will be the identification of UncA-interacting proteins and the associated vesicles. Other open questions concern the functions of the modified microtubules and the responsible enzymes (TTL and TTCP) still have to be solved.

V.   Discussion

1.   UncA and Dynein transport vesicles into opposite directions

In this work it was shown that UncA is required for vesicle movement in *A. nidulans* and found that their transportation preferably occurs along a subpopulation of microtubules. Vesicle movement was dependent on the motor activity of UncA and occurred in both directions in the cell. This bidirectional movement and the accumulation of vesicles in the tip compartment of a dynein and a conventional kinesin mutant, is comparable to the situation in *U. maydis*, and can be explained if UncA and dynein transport vesicles in opposite directions, UncA towards the plus and dynein towards the minus end of microtubules (Wedlich-Söldner *et al.*, 2002b). The lack of one motor causes an imbalance of the forces and an asymmetric accumulation of the vesicles. However, first it was surprising that the vesicles only accumulated in the dynein mutant and not in the *uncA*-deletion strain. According to the above model one would have expected that the vesicles accumulate in the rear of the hyphae in *uncA*-mutation strain. To explain this, it has to be considered that in the tip compartment almost all microtubules are oriented with their plus ends towards the growing tip. In regions behind the first nucleus, however, the orientation is mixed and thus a single motor can transport cargoes antero- and retrograde (Konzack et al., 2005). This mixed orientation of microtubule polarities is due to overlapping microtubules emanating from neighbouring nuclei and in addition, from septa (Veith et al., 2005) **(Figure V. 01)**. The effect of the deletion of conventional kinesin may be secondary, because KinA is required for dynein localization at the microtubule plus end (Zhang *et al.*, 2003). Thus the observed accumulation of vesicles in the tip is likely due to the lack of dynein in the tip region.

The question concerning the nature of the transported vesicles was also addressed. It has already been shown that kin3 in *U. maydis* supports early endosomes motility, the kin3 deletion strain displayed about 33% reduced endosomal motility when the t-SNARE marker Yup1 was used as an endosomal marker (Wedlich-Söldner *et al.*, 2002b). In an earlier study, Wedlich-Söldner *et al.* showed that Yup1 links exo- and endocytosis in the phytopathogenic fungus *U. maydis* because in *yup1ts* cells, endocytosis was impaired and accumulation of Yup1-carrying endosomes at cell poles was abolished. These results suggested that a membrane recycling process via early endosomes supports polar growth in *U. maydis* (Wedlich-Söldner *et al.*, 2000). The membrane-selective fluorescent vital dye FM4-64 was used to visualize membrane internalization (Peñalva, 2005), and the syntaxin-like t-SNARE

protein TlgB (*S. cerevisiae* Tlg2) as an endosomal marker, which was used before in the filamentous fungus *A. oryzae* for endosome labelling (Kuratsu *et al.*, 2007). Both markers were not able to stain all UncA cargo vesicles, indicating that UncA is not only associated with endosomes. Identifying the different cargos of UncA is a crucial step in understanding the function of this motor.

Some answers could be revealed from the relation between endo- and exocytosis and polar growth. It was already shown that an early endosomal compartment involving bidirectionally moving membranes riding on MTs is intimately associated with hyphal polarized growth (Abenza *et al.*, 2009), confirming the apical recycling model suggested by Upadghyay & Shaw, 2008, which suggests a critical role for actin patch-mediated endocytosis to maintain polarized growth at the apex (Upadhyay & Shaw, 2008). The endocytic internalization machinery localizes preferentially to the hyphal subapical ring, which suggests that tight spatial coupling of apical secretion and subapical compensatory endocytosis underlies hyphal growth (Araujo-Bazan *et al.*, 2008; Taheri-Talesh *et al.*, 2008). Indeed, the same model has been proposed in eukaryotic cells as protein transport through the exocytic and endocytic pathways occurs via vesicle trafficking between successive membrane-bounded compartments, to demonstrate a spatially regulated SNARE interaction within the same membrane (Valkonen *et al.*, 2007). Furthermore, Jaiswal *et al.*, 2009, propose a model in which exocytosis of post-golgi vesicles is regulated by components of the endocytic machinery (Higuchi *et al.*, 2009; Jaiswal *et al.*, 2009). In summary, in filamentous fungi, endocytic recycling at the subapical region is closely associated with apical growth and exocytosis at the tip apical region. Those researches may help to understand the role of UncA movement and allow further analyzation for outstanding discoveries.
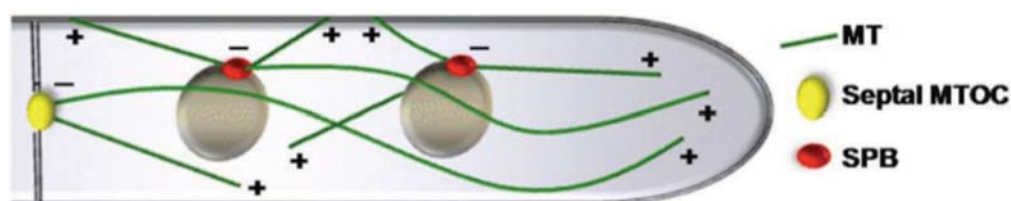
Figure V. 01. The mixed polarity of MTs indicated with + and – in the tip compartement of
***A. nidulans* hyphae.**

2.   UncA moves along a subpopulation of microtubules

One most surprising results of this work was the finding that UncA moved preferentially along one microtubule. This was in contrast to other kinesins (Kinesin-1 and Kinesin-7), which do not prefer any specific microtubule. These findings suggest the existence of modified microtubules in *A. nidulans*, which may also be the case in other filamentous fungi.

2.1. Microtubule modification

Biochemical analyses of tubulins of higher eukaryotes revealed that MTs are not only composed of alpha and beta tubulin but that multiple tubulin modifications exist. In most eukaryotes the C-terminus of alpha tubulin is characterized by two glutamate residues followed by an aromatic amino acid such as tyrosine in mammals **(Table V. 01)** and phenylalanine in *S. cerevisiae.* The tyrosine residue is cyclically removed by a carboxypeptidase (TTCP), and re-added to the chain by tubulin-tyrosine ligase (TTL). An equilibrium between the two modifying enzymes determines the status of the microtubule (Westermann & Weber, 2003) **(Figure V. 02)**.

α-tubulin Protein		C-terminal Sequence
Porc	(commercial antibody against tyrosinated MTs)	SYEDEDEGEEY
Human	Type 1A	EGEGEEEGEEY
A. nidulans	TubA	SLEEEGEEVEY
	TubB	SLDMEGEEAEY
N. crassa	TubA	DYNDVDVDAEY
	TubB	SMEGEDVEAEY
S. macrospora		SMEGEEVEAEY
M. grisea	1.	LGDEEGIEAEY
	2.	SFEPEEGDAEY
T. harzianum		SLDNEEMEAEY
U. maydis		SVDVGEEDLEY

Table V. 01. Comparison of the C-terminal amino acid sequences of alpha tubulins from six different fungi with Porc and Human alpha tubulin C-terminal sequences. Identical amino acids in porc and *A. nidulans* are highlighted. The region used from the human protein for the production of the antibody specific for tyrosinated or detyrosinated MTs is boxed.

Already in 1975 Arce *et al.* reported the post-translational incorporation of L-tyrosine into alpha-tubulin, suggesting the presence of tyrosinated and detyrosinated forms, which could not be explained at a molecular level at the time (Arce *et al.*, 1975). Other modifications are acetylation, polyglutamylation, polyglycylation or phosphorylation (Westermann & Weber, 2003). In general, not much is known about the modifying enzymes nor about the biological

functions of these modifications, although polyglutamylation has been implicated in cilium functioning and polycystic kidney disease (Liu *et al.*, 2002; Pathak *et al.*, 2007). Recently, it was also shown that tubulin glutamylation regulates ciliary motility by altering inner dynein arm activity (Suryavanshi *et al.*, 2010), and the suppression of tubulin-tyrosine ligase, resulting in an accumulation of detyrosinated tubulin, which favors tumor growth in animal models and human cancers, suggesting that TTL activity may play a role in tumor cell regulation and making microtubule modification a possible marker for cancer detection (Mialhe *et al.*, 2001). Recently, it was shown in TTL knock-out mice, that tubulin tyrosination is important for MT and actin organization, and the regulation of small GTPases activity in the growth cone of growing neuronal cells (Marcos *et al.*, 2009). In addition Creppe *et al.* (Creppe *et al.*, 2009) provide surprising evidence suggesting that the acetylation of α-tubulin by the histone acetyltransferase elongator controls the migration and differentiation of cortical neurons.

Some modifications were already detected in primitive eukaryotes such as *G. lamblia*, suggesting that they arose early during eukaryotic evolution (Weber *et al.*, 1997). In fungi, only detyrosinated MTs have been described so far in *S. cerevisiae* (the terminal amino acid is phenylalanine and not tyrosine) (Badin-Larcon *et al.*, 2004).
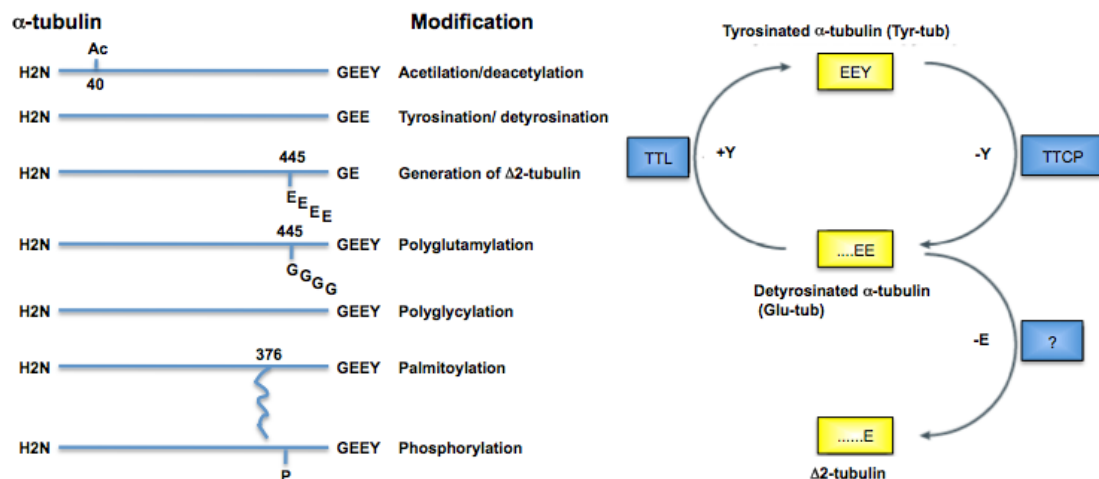
Figure V. 02. Overview of the various tubulin modifications and the tyrosination cycle of α-tubulin. The carboxy-terminal tyrosine of α-tubulin can be removed by the tubulin tyrosine carboxypeptidase (TTCP) to generate Glu-tubulin (Glu-tub). In an ATP-dependent reaction, the carboxy-terminal tyrosine (Tyr-tub) can be restored through the enzymatic activity of tubulin tyrosine ligase (TTL). Glu-tubulin can lose the penultimate glutamate residue through the activity of an unknown peptidase to generate Δ2-tubulin, which cannot function as a substrate for TTL and is therefore removed from the cycle. . Ac, acetate; E, glutamic acid; G, glycine; P, phosphate; TTCP, tubulin tyrosine carboxypeptidase; TTL, tubulin tyrosine ligase; Y, tyrosine.

This work provides results that support the existence of detyrosinated microtubules in *A. nidulans*, but no evidence was found for acetylated or polyglutamylated microtubules. To

our knowledge this is the first report of the existence of microtubule subpopulations in filamentous fungi.

2.2. Specificity of kinesins for modified MTs

The question of microtubule modifications and their roles *in vivo* raises the question about the specificity of the different motors. Motors thus are not only specific for their cargoes but apparently also for their tracks.

Kinesin motors contain both the ATPase and MT binding activity (Kuznetsov *et al.*, 1989; Scholey *et al.*, 1989). The first studied example for kinesin-MT interaction was conventional kinesin (Kinesin-1), which uses two identical motor domains to move along the microtubule, taking about 100 steps per run each of about 8 nm in size, and hydrolyzing one ATP molecule per step (Hackney, 1994; Hackney, 1995; Hua *et al.*, 1997; Schnitzer & Block, 1997). Initially, various types of models had been proposed to describe the Kin-1 processive and nonprocessive types of motion, the most popular being the "Hand over Hand" model (Asbury *et al.*, 2003; Kaseda *et al.*, 2003; Yildiz *et al.*, 2004). This model requires a tight coordination of ATP hydrolysis, microtubule binding, and force generation within the two kinesin heavy chains. The nucleotide state regulates the affinity of the motor for the filament, allowing kinesins to switch between a strong MT-binding state (ATP-free and nucleotide-free state) and a weak binding state (ADP state). The neck linker and the neck coiled-coil play important roles for the communication between the nucleotide and microtubule binding sites of both molecules (Thorn *et al.*, 2000).

The KIF1A (kinesin-3) microtubule complex has been studied in various nucleotide states, providing insights into the structural dynamics of KIF1A and kinesins in general (Kikkawa *et al.*, 2000; Kikkawa *et al.*, 2001; Kikkawa & Hirokawa, 2006; Kikkawa, 2008; Nitta *et al.*, 2004; Nitta *et al.*, 2008). Unc104 (kinesin-3) was found to bind microtubules with five-fold weaker affinity and two-fold higher stoichiometry compared to conventional kinesin. Unc104 and conventional kinesin binding affinities are primarily dependent on positively charged residues in the Unc104 K-loop and conventional kinesin neck coiled-coil. The kinesin-3 K-loop is an ATP-independent MT-binding site which contains multiple lysine residues, that are positively charged and can electrostatically interact with the negatively charged tails of the tubulin subunits (E-hook) (Okada & Hirokawa, 2000). Removal of these residues affects Unc104 and conventional kinesin binding affinity, but much less in the case of conventional kinesin (Al-Bassam *et al.*, 2007). The K-loop increases the affinity to the native MT so drastically that monomeric Kif1A motors could be observed to diffuse in one dimension along the MT in a pseudo-processive manner (Okada & Hirokawa, 1999; Okada & Hirokawa, 2000). This diffusion is abolished by either removing the highly positively charged

K-loop-insertion in the motor, or by removal of the E-hook (Nitta *et al.*, 2004; Okada & Hirokawa, 2000). In the meantime, increasing evidence emerged that biased diffusion is not the only type of motion, and probably not the most important one for KIF1A function (Al-Bassam *et al.*, 2003; Rashid *et al.*, 2005; Shimizu *et al.*, 2005; Tomishige *et al.*, 2002). Under different conditions KIF1A can dimerize by coiled-coil formation of the neck linker or stalk domains. Hence, the controlled induction of dimerization between KIF1A chains seems to be another way of regulating motor activity besides the K-loop and the tubulin E-hook interactions.

The E-hook, is the major site of differences between tubulin iso-forms (Sullivan & Cleveland, 1986), and subject of the post-translational modifications (Westermann & Weber, 2003), resulting in a change of the C-terminal charge of tubulin, thus affecting kinesin-microtubule interactions. There is increasing evidence that different modified microtubules play distinct roles in eukaryotic cells (Westermann & Weber, 2003). Ikegami *et al.* showed indirect evidence that Kif1A in mice binds preferentially to polyglutamylated microtubules. A model was proposed to argue the mechanism as to why the distribution of KIF1 (kinesin-3) is affected by loss of tubulin polyglutamylation, whereas distributions of Kinesin-2 and Kinesin-1 appear unaffected (Ikegami *et al.*, 2007). The model is based on the long and positively charged K-loop in kinesin-3 which can interact strongly with the highly negatively charged polyglutamate side chain of tubulin (Okada & Hirokawa, 2000). This ionic force may be required to maintain the interaction between monomeric forms of kinesin-3 and microtubules *in vivo*. Thus, loss of tubulin polyglutamylation would impair kinesin-3-microtubule interaction, when kinesin-3 is in the weak-binding state. In contrast, kinesin-1 can maintain attachment to microtubules by one motor-head, while the other head glides over the tubulin surface. Consequently, movement of kinesins other than kinesin-3 may be relatively insensitive to the loss of tubulin polyglutamylation (Ikegami *et al.*, 2007).

The finding that UncA is associated with modified microtubules is the second example for the specificity of kinesin-3 for certain microtubules, and surprisingly the specificity appears not to be evolutionarily conserved. Given that the mice motor binds to polyglutamylated and the fungal one to presumably detyrosinated microtubules. Another example for microtubule specificity was shown recently for conventional kinesin in neurites, where it binds preferentially to acetylated microtubules. Purified acetylated microtubules stimulated the kinesin activity (Reed *et al.*, 2006). Furthermore, Dunn et al. found that kinesin-1 Kif5c binds preferentially to detyrosinated microtubules (Dunn *et al.*, 2007), they show slower sliding of Kinesin-1 along detyrosinated MTs, indicating that detyrosination causes a slower stepping/ATP-turnover rate. This observation is consistent with a model in which detyrosination of MTs shifts the steady-state binding equilibrium of kinesin-1 heads towards strong binding by reducing the detachment rate of the weak binding kinesin. ADP

intermediate. This will decrease the probability of detachment following a step, giving rise, therefore, to longer processive runs. Detyrosination would then result in a slower motor that made longer processive runs, and increase the steady-state occupancy on MTs. An analogy might be that detyrosination gives the motor 'magnetic boots', attaching it more to the track, but making stepping more difficult. This might also result in a slower but more consistent and sustained delivery of kinesin-1 cargo to specific intracellular sites. In support of this idea, it has been shown previously that complete cleavage of the 'E-hook' reduced the velocity of a fungal kinesin-1 (Lakamper & Meyhofer, 2006; Skiniotis *et al.*, 2004), and shifted the normally weak binding kinesin (ADP state) towards strong binding (Thorn *et al.*, 2000). Both detyrosination and E-hook cleavage could produce their effects. In both cases they show that these are stable microtubules. Similar results presented by Cai *et al.* (Cai *et al.*, 2009) showed how the individual Kinesin-1 motor moves preferentially on a subset of acetylated and detyrosinated microtubules in COS cells, those microtubules were identified as the stable microtubules. In contrast, individual Kinesin-2 and Kinesin-3 motors do not select subsets of microtubules.

Microtubule modifications appear to act as traffic signs for certain microtubule-dependent motor proteins. However, the exact cellular function is largely enigmatic, and whether detyrosination has any effect on the UncA motor activity or the other way around remains to be shown. Further experiments in *A. nidulans* and other eukaryotes are required to better understand the biological importance of microtubule modifications and their interactions with molecular motors.

2.3. Microtubules, cellular shape and organelle distribution

Since a long time, biologists have been tried to answer the question about how cells establish and maintain an asymmetrical distribution of organelles. Microtubules play a fundamental role in these processes, because the disruption of MTs by MT antagonists results in the disruption of the normal distribution of mitochondria (Ball & Singer, 1982), endoplasmic reticulum (ER) (Ball & Singer, 1982), lysosomes and endosomes (Matteoni & Kreis, 1987), Golgi (Thyberg & Moskalewski, 1985), and vimentin intermediate filaments (Blose & Chacko, 1976). MTs have been shown to be dynamic structures in proliferating cells in culture (Saxton *et al.*, 1984; Schulze & Kirschner, 1986). This raises the question of how such dynamic structures as MTs can contribute to cellular organization, which would appear to require at least some structural stability. Kirschner and Mitchison hypothesized that MT dynamics may allow MTs to efficiently search the 3-dimensional space of the cell and, in response to environmental cues, dynamic MTs may become locally stabilized (Kirschner & Mitchison, 1986). Indeed, in polarized and differentiating cells, a subset of MTs is much more

stable than other dynamic MTs, and, consistent with a role for MTs in organizing cellular organelles, the stable MTs are usually oriented in the axis of polarization or differentiation (Bulinski & Gundersen, 1991).

One interesting question is how cells distinguish stabilized MTs from dynamic MTs. One clue to this question was that when MTs are stabilized *in vivo*, the tubulin comprising the MTs is modified by one or more post-translational modifications (Bulinski & Gundersen, 1991). The formation of this specialized array of microtubules in specific locations in cells undergoing morphogenesis suggests that it plays an important role in generating cellular asymmetries. A general mechanism for how cells establish internal organization can be summarized in three points (Gundersen *et al.*, 2004) **(Figure V. 03)**:

1) Dynamic microtubules are locally stabilized

2) Stable microtubules are post-translationally modified

3) Modified microtubules interact with other cellular organelles.
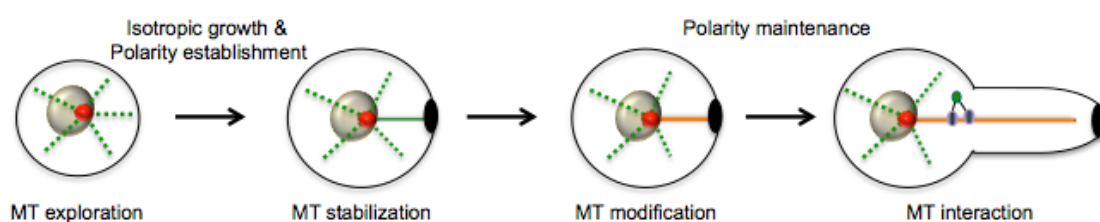
Figure V. 03. Diagram illustrating the function of tubulin modification in cell polarization. This model shows that on extracellular or intracellular stimulation, MTs become selectively stabilized and subsequently modified. Modified MTs are preferentially utilized in different interaction such as the kinesin-MT interaction.

Indeed modified microtubules were found to be more stable, nevertheless the modification was not the cause, but the consequence for the increased stability (Gundersen *et al.*, 1984; Gundersen *et al.*, 1987; Schulze *et al.*, 1987). Likewise, Veith *et al.* observed that some microtubules are not depolymerised as most microtubules are during mitosis of fast growing hyphae of *A. nidulans* (Veith et al., 2005). Indeed, here the GFP-UncA^{rigor} labelled microtubule was found intact in the cytoplasm during nuclear division **(Figure V. 04)**. This could be the reason for the evolution of the preference of the kin-3 motor in *A. nidulans.* If we assume that transportation of endosomes is important during all stages of the cell cycle, it would explain, why the organism would have an advantage if the motor transporting them would preferentially bind to the one remaining stable during mitosis. Because vesicle movement is important for fast polarized growth, the stability of microtubules may be important for the maintenance of hyphal extension during mitosis (Riquelme et al., 2003).

The stability of modified MTs makes them good candidates to support organelle distribution also in interphase. Thus the UncA^{rigor}-MT spans through all hyphal compartments

and connects nuclei with septa. Some nuclei were pulled along this bundle and displayed a pear-like shape, suggesting that the UncA^{rigor} MT might be responsible for nuclear positioning and organelle transportation. Likewise in *S. cerevisiae*, the change to Glu-MTs (alpha-tubulin lacks the terminal phenylalanine) caused a suppression of nuclear oscillations. This phenotype was observed along with a decreased association of the +Tip, CLIP-170 ortholog, Bik1 (Badin-Larcon *et al.*, 2004). Those two examples from fungi support the model for the important role of modified MTs in cell organization and shape maintenance.
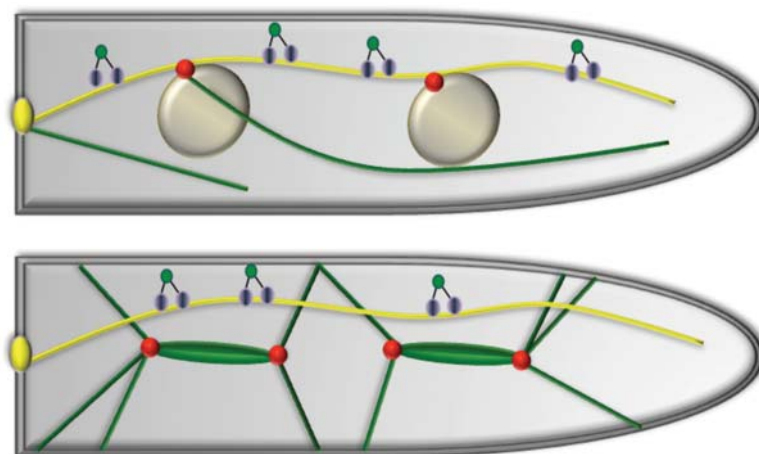
Figure V. 04. Proposed model for the arrangement of tyrosinated and detyrosinated microtubules and its interaction with kinesin-3 during mitosis and during interphase in *A. nidulans*.

It was clear that the stable modified MTs are formed from the nuclear spindle-pole bodies and from septal MTOCs, which we have described in *A. nidulans* (Veith *et al.*, 2005). The further characterization of sMTOC in *A. nidulans* was a second important part of my thesis.

3.   Septal MTOCs in *A. nidulans*

In order to have a clearer picture of MTOC distribution in *A. nidulans,* the interaction of the MTOC protein ApsB with gamma-tubulin was examined. Interactions were detected at spindle pole bodies, at septa, at the tip of growing hyphae and in spot-like structures in the cytoplasm. This is the first evidence for the presence of gamma-tubulin at septa and in the tip region. We had evidence before that MTOCs exist at septa, but the nature of these MTOCs remained elusive (Veith *et al.*, 2005). Our new results show that at least two other proteins associated with nuclear MTOCs exist in septal MTOCs, GcpC (GCP3 or SPC98) and the crucial gamma-tubulin. These findings are in agreement with the recent localization of GcpC (Xiong & Oakley, 2009). However, it is still unclear if sMTOCs share more or all proteins with nuclear MTOCs or whether specific proteins exist only at one or the other place. The biggest

unsolved question is still the anchorage of sMTOCs. Structurally the nuclear MTOC of *S. cerevisiae* has been studied the best and recently similar results were obtained in *Ashbya gossypii* (Jaspersen & Winey, 2004). It is likely that the situation is similar in *A. nidulans* and that nuclear MTOCs are embedded into the nuclear envelope. However, structural information about sMTOCs is still missing. Fluorescent microscopy indicated that the MTOC appears as two dots inside the septal rim. The structure is clearly different from Woronin bodies at septa. Sometimes the two ApsB dots appeared to be connected through a third small dot. This has been described before in *S. pombe* for the equatorial MTOCs (EMTOCs), which are also characterized by the ApsB homologous protein, mto1 (formerly named mod20 or mbo1) (Heitz *et al.*, 2001; Sawin *et al.*, 2004). In this yeast species MTs are generated from nuclear MTOCs, from EMTOC and interphase (iMTOC) microtubule organizing centres (Heitz *et al.*, 2001; Samejima *et al.*, 2005). The importance of non-nuclear associated MTOCs was nicely demonstrated in enucleate cells (Carazo-Salas & Nurse, 2006).

The data in this work suggest that the sMTOC is embedded into the septal membrane and contains the same essential γ-tubulin ring complex proteins as the SPB do. However, further analyses with higher resolution microscopy, such as transmission electron microscopy, are required to reveal the exact structure and function.

The ApsB-gamma-tubulin interaction was also identified in the tip of growing hyphae. This is the first account of gamma-tubulin in the tip. In comparison, in the chytridiomycete *Allomyces macrogynus* gamma-tubulin has been identified as a component of the Spitzenkörper (McDaniel & Roberson, 1998). Further evidence that gamma-tubulin may be functional in the tip comes from our observation that some MTs emenate from the tip and grow into the cytoplasm (Konzack *et al.*, 2005). We speculated at the time that either MTs, which did not stop growth after reaching the tip or MT fragments close to the tip could be the origin for the polymerization. However, the new results in this study point to the possibility that MTOCs exist in the apical region of the hyphae.

Several lines of evidence show that the spot-like appearance of ApsB and the ApsB-gamma-tubulin interaction is due to peroxisomal localization: Co-localization with AcuE and HexA, and the drastic reduction of the number of cytoplasmic spots in a *pexC* mutant. One very strong argument is the importance of the PTS2 sequence and the rescue of the PTS2 mutation by adding a PTS1 sequence to the C-terminus. The non-functionality of ApsB with a mutated PTS2 sequence could still be explained by the fact that this region appears to be evolutionarily conserved from yeast to human (Sawin *et al.*, 2004), but the rescue of the mutation by the addition of the PTS1 sequence speaks clearly against this possibility. We envisage three possible explanations for the role of the peroxisomal localization:

- Peroxisomes as hosts for sMTOCs.

- Peroxisomes catalyze a reaction, which is required for MTOC function at the septum and is ApsB-dependent.
- Peroxisomes as transport vehicles for sMTOC associated proteins.

3.1. On the role of peroxisomes

Peroxisomes are ubiquitous organelles of eukaryotes, which are surrounded by a single membrane (Heiland & Erdmann, 2005; Schrader & Fahimi, 2008). They serve a variety of functions, depending on the species, cell type and environmental or developmental conditions. In mammals, peroxisomes are involved in a number of catabolic and anabolic pathways, most importantly, the peroxide metabolism, the β-oxidation of long-chain fatty acids, and the biosynthesis of ether phospholipids (Kovacs *et al.*, 2003; Wanders & Waterham, 2006). The vital importance of the organelle in human is evident by the existence of a number of severely and often lethal disorders when the biogenesis of the organelle is impaired (Wanders, 2004). In plants peroxisomes are involved in photorespiration and typically contain the glyoxylate cycle as in protozoa and yeast (Hayashi & Nishimura, 2003).

Given the complexity of peroxisomal functions, it is obvious that a large number of proteins are targeted to these organelles. Peroxisomal membrane and matrix proteins are synthesized on free ribosomes in the cytosol and are imported post-translationally into pre-existing organelles (Heiland & Erdmann, 2005). The apparatus of protein import is clearly distinct from the import machinery of other organelles, because it translocates folded and even oligomeric proteins and there is evidence that they are descending from the ER (Gabaldón *et al.*, 2006). A large number of peroxisomal proteins employ a tripeptide sequence at their C-terminus, PTS1 (S/A/C-K/R/H-L/M) (Gould *et al.*, 1989). A second class of proteins uses a sequence close to their N-terminus, which is less conserved, consists of R/K-L/I/V-X_5-H/Q-L/A and is called PTS2 (Swinkels *et al.*, 1991). In both cases complex protein machineries are employed and some of the components appear to be used in PTS1- and PTS2-dependent protein translocation (Heiland & Erdmann, 2005).

A very distinct class of peroxisomes is represented by the fungal Woronin body. This structure is named after a Russian mycologist, who reported the characteristics of a distinct type of organelle in the fungus *Ascobolus pulcherrimus* (Buller, 1931; Woronin, 1864). Woronin bodies have been described in more than 50 species of ascomycota and deuteromycota, but are absent in single cell yeasts such as *S. cerevisiae* and *S. pombe*. Thus their function appears to be important for the filamentous life style. In *Neurospora crassa* they appear as hexagonal bodies in the cell and upon cell damage plug the septal pores after a few seconds (Jedd & Chua, 2000). This sealing mechanism is very important in syncytial organisms to prevent loss of the entire cytoplasm and hence death of the entire

mycelium after damage of one hypha (Maruyama *et al.*, 2005). Their exact composition, however, remained obscure for many decades until G. Jedd and N. H. Chua purified the organelle from *N. crassa* and identified the main constituent as a single protein, named Hex1 (Jedd & Chua, 2000; Yuan *et al.*, 2003). The protein forms hexagonal crystals and the existence of a PTS1 peroxisomal targeting sequence at the C-terminus of the protein indicated that the Woronin bodies represent specialized peroxisomes. Hex1 displays some sequence similarity to *eIF5*, and it is thought that Hex1 derived in evolution from *eIF5* by gene duplication and subsequent modification of the function (Yuan *et al.*, 2003). Another example for a peroxisome-associated function is the Pro40 protein in *Sordaria macrospora* (Engh *et al.*, 2007). This protein is implicated in the regulation of sexual development.

The results in this work suggested a transportation function of peroxisomes of the MTOC protein ApsB toward sMTOC. This is further reinforced by the observation of fast moving *mto1* (ApsB) spots in *S. pombe* (Sawin *et al.*, 2004). These structures may represent peroxisomes. However, many open questions remain to be solved, e.g. how the proteins are recruited from the peroxisomes to the sMTOCs. Against an important role of peroxisomes in sMTOC assembly speaks the observation that septal localization of ApsB and sMTOC function in mutants with defects in PTS1 or PTS2 peroxisomal protein import or in *pexC* mutants with lacking peroxisomes appeared similar to the situation in wild-type (results not shown). However, the *pexC* mutant strain displays pleiotropic phenotypes and the possibility of a piggy bag import mechanism might mask the possible effects of PTS1 or PTS2 defects (Hynes *et al.*, 2008).

The results in this study suggest that ApsB defines a new class of peroxisomes, which is - besides the Woronin bodies - the second example for peroxisomes as organelles with a function beyond metabolic pathways (Schrader & Fahimi, 2008).

VI. Materials and Methods

1.   Chemicals, equipments and kits

Chemicals were purchased from Roche (Mannheim), Merck (Darmstadt), Sigma (Taufkirchen), Roth (Karlsruhe), BIOMOL (Hamburg), AppliChem (Darmstadt), Difco (Augsburg), Gibco (Karlsruhe) und Stratagene (Amsterdam, Netherlands), otherwise the origin will be written in the text.

Restriction enzymes and other DNA-modifying enzymes were obtained from Amersham (Freiburg), New England Biolabs (NEB, Frankfurt) and MBI-Fermentas (St. Leon-Rot) or Invitrogen (NV Leek, The Netherlands). Enzymes for PCR were supplied from Takara (Clontech, Madison USA), Roche Diagnostics (Mannheim), New England Biolabs and MBI-Fermentas.

Nitrocellulose membranes (Hybond-N) for Southern blots were from Amersham and Pall Gelman Laboratories (Dreieich), filter paper (Miracloth) from Calbiochem (Heidelberg) and the Blocking-Reagent from Roche. As protein standard the Roti-Mark® Prestained from Roth was used. The Protran Nitrocellulose transfer membrane from Schleicher & Schuell (Whatman, Dassel) was applied for protein transfer. Developer and fixer were from Kodak-GmbH (Stuttgart). Autoradiographic films were obtained from Fuji (New RX, Fuji, Japan). Skim-milk was obtained from Roth and Bovine Serum Albumin (BSA) from Roth. For DNA-isolation from agarose gels Agarose Low Melt 3 from AppliChem was used in some cases. Agar for the media was purchased from Roth. DNA- and RNA-marker was provided by MBI-Fermentas (St. Leon-Rot).

DAPI mix and propidium iodide mix were from Molecular Probes (Vectashield Mounting Medium, H-1200 and H-1300 respectively, Burlingame, USA). Hoechst 33342 (H-3570) and FM4-64 (N-(3-triethylammoniumpropyl)-4-(6-(4-(diethylamino)phenyl)-hexatrienyl)) pyridinium dibromide) (T3166) were also obtained from Molecular Probes (Oregon, USA), Calcofluor white M2R or fluorescent brightener 28 (F3543) and Congo Red (860956), Cytochalasin A (C-6637), Benomyl (Paclitaxel T7191), Avidin (A9275), Brefeldin A (B7651), Sodium butyrate (303410), 2-(N-morpholine)-ethane sulfonic acid-sodium hydroxide (MES-NaOH) and Glufosinate-ammonium PESTANAL (BASTA) (45520) were purchased from Sigma-Aldrich.

Table VI. 01. Equipment used in this study

Equipment	Type	Manufacturer
Autoclave	Systec 3850 ELV Systec VE-75	Systec GmbH, Wettenberg Systec GmbH, Wettenberg
Centrifuge with rotors	Beckman J2-21 centrifuge Eppendorf centrifuge 5403 Eppendorf centrifuge 5415 R Eppendorf centrifuge 5424 Heraeus Biofuge 13 Kontron ultracentrifuge TGA-65 Sorvall RC 6+ centrifuge Universal 320 R	Beckman Coulter, Krefeld Eppendorf, Hamburg Eppendorf, Hamburg Eppendorf, Hamburg Kendro, Langenselbold Kontron, Zürich, Switzerland Thermo Scientific, Germany Hettich Zentrifuge, Germany
digital camera	PowerShot A630	Canon, China
Electroporation apparatus	Gene Pulser II, Pulse Controller	Bio-Rad, Munick
Electrotransfer apparatus	Mini-Trans-blot Mini-PROTEAN Tetra Cell	Bio-Rad, Munick Bio-Rad, Munick
Gelscanner	SnapScan1236υ	Agfa, Cologne
Heat block	Thermomixer 5436	Eppendorf
Hybridization oven	Personal HybTM H-B-1000 Hybridizer	Stratagene, Heidelberg UVP Laboratory products
Microscope	- Axio Imager. Z1. - Cell Observer-SD, confocal spinning disk microscope - Eclips E200 - SPD5 confocal microscope - Zeiss Axiophot.	Zeiss, Germany Zeiss, Germany Nikon Japan Leica, Germany Zeiss, Germany
Mini Gel migration Trough	Mupid-2 Mupid-EXU	Cosmobio Co. Eurogentec, Germany
PCR machine	Personal Cycler Primus 25 Primus 96 Rapid Cycler TRIOThermoblock	Biometra, Göttingen PeQLab, Erlangen PeQLab, Erlangen Idaho Technology, USA Biometra, Göttingen
Power supply apparatus	Power Pac 3000	Bio-Rad, Munick
Shaker/ incubation	Heraeus-Brutschrank Baureihe 6000 HT Infors Kleinschüttler KM-2	Kendro, Langenselbold Infors AG, Switzerland Edmund Bühler GmbH Tübingen
UV-cross Linker	UV Stratalinker 2400	Stratagene, Heidelberg
UV/Visible spectrophotometer	Ultrospec 3100 *pro* Nano drop ND-1000	Amersham Pharmacia Biotech, Freiburg PeQLab, Erlangen

Table VI. 02. Kits used in this study

Kit	Manufacturer
DIG DNA PCR labelling Kit	Roche, Mannheim
DNeasy Plant Kit	Qiagen, Hilden
Gateway®, LR clonase'™ Enzyme Mix	Invitrogen, Karlsruhe
Matchmacker'™ Two-Hybrid Library Construction & Screening Kit	Clontech, Madison
Nucleobond® AX	Macherey-Nagel, Düren
Peqgold® Agarose	PeQLab, Erlangen
QIAquick®Gel extraction Kit	Qiagen, Hilden
RNeasy Mini Kit	Qiagen, Hilden
Wizard DNA PCR-Preps-DNA-Purification-System	Promega, Mannheim

2.   Organisms and plasmids

The following *Aspergillus nidulans* **(Table VI. 03)** and *Escherichia coli* strains **(Table VI. 04)** were used in this study. All *A. nidulans* strains are carrying the *veA*1 mutation.

Table VI. 03. *A. nidulans* strains used in this study

Strain	Genotype	Source
AJC1.5	*biA1; apsB6*	(Clutterbuck, 1969)
AJC1.7	*biA1; apsB10*	(Clutterbuck, 1969)
AnKin26	*pyrG89; ΔargB::trpCΔB; pyroA4; ΔkinA::pyrG*	(Requena *et al.*, 2001)
BUY14	Nonsense mutation in *pex7* ortholog (PTS2), *acuJ-lacZ* fusion at *argB* locus *pabaA1; biA1; pexG14*	(Hynes *et al.*, 2008)
FGSC4	Glasgow Wild-type (VeA+)	FGSC, Kansas, USA
FGSC26	*biA1; veA1*	FGSC, Kansas, USA
GFP-ClipA	*pyrG89; wA3; pyroA4; alcA(p)::GFP::clipA::pyr4*	(Efimov *et al.*, 2006)
GR5	*pyrG89*; *wA3; pyroA4*	(Waring *et al.*, 1989)
LZ12	*pyrG89; pyroA4; ΔnkuA::argB; nudA(p)::GFP::nudA*	(Zhuang *et al.*, 2007)
PEX3KOB2	No peroxisomes, *amdS-lacZ* fusion at *amdS* locus *pabaA1; biA1; ΔnkuA::argB; pexC::bar*	(Hynes *et al.*, 2008)

PEX A9	PTS1+PTS2 peroxisomes, *acuJ-lacZ* fusion at *argB* locus *pexA9, pabaA1, yA2, biA1*	(Hynes *et al.*, 2008)
PEX F23	PTS1+PTS2 peroxisomes, *acuJ-lacZ* fusion at *argB* locus *pabaA1, biA1, yA2; pexF23::pyr4*	(Hynes *et al.*, 2008)
PEX M15	PTS1+PTS2 peroxisomes, *acuJ-lacZ* fusion at *argB* locus *pabaA1, biA1, yA2; pexM15*	(Hynes *et al.*, 2008)
RMS011	*pabaA1, yA2; ΔargB::trpCΔB; trpC801*	(Stringer *et al.*, 1991)
SAS6	*pyrG89, pabaA1; wA3*	A. Singh, Marburg
SCE05	*pyroA4; ΔargB::trpCΔB; alcA(p)::GFP::alpA*	(Enke *et al.*, 2007)
SCS13	TN02A3 transformed with pAT3 *pyrG89; pyroA4; argB2; ΔnkuA::argB; ΔalpA::pyr4*	(Enke *et al.*, 2007)
SCS1-NZ79	SNZ14 transformed with pCS3-NZ *alcA(p)::GFP::uncA^{rigor} ; alcA(p)::mRFP1::kinA$^{1.3}$*	This study
SCS2-NZ80	TN02A3 transformed with pCS3-NZ *pyrG89; alcA(p)::mRFP1::kinA$^{1.3}$*	This study
SCS3-NZ81	TN02A3 transformed with pCS2-NZ *pyrG89; alcA(p)::GFP::kinA$^{1.3}$*	This study
SCS4-NZ82	SNZ14 transformed with pCS5-NZ *alcA(p)::GFP::uncA^{rigor} ; alcA(p)::mRFP1::kinA^{rigor}*	This study
SCS5-NZ83	TN02A3 transformed with pCS5-NZ *pyrG89; alcA(p)::mRFP1::kinA^{rigor}*	This study
SCS6-NZ84	TN02A3 transformed with pCS4-NZ *pyrG89; alcA(p)::GFP::kinA^{rigor}*	This study
SCS7-NZ85	TN02A3 transformed with pCS8-NZ *pyrG89; alcA(p)::GFP::ttlA$^{1.3}$*	This study
SCS8-NZ86	TN02A3 transformed with pCS7-NZ *pyrG89; alcA(p)::mRFP1::ttlA$^{2.5}$*	This study
SDV83	*pyrG89, pabaA1, yA2; alpA::pyr4*	(Enke *et al.*, 2007)
SEa3	*wA3; pyroA4; alcA(p)::GFP::apsB*	V. P. Efimov, USA
SJW02	*wA3; pyroA4; ΔargB::trpCΔB; alcA(p)::GFP::tubA*	J. Warmboldt, Marburg
SJW100	*gpd(p)::DsRed::stuA(NLS);pyroA4; wA3; alcA(p)::GFP::tubA*	J. Warmboldt, Marburg
SNR1	*yA2; argB::trpCΔB; pyroA4; ΔkinA::pyr4*	(Requena *et al.*, 2001)
SNT30	*pyrG89; ΔargB::trpCΔB, ΔteaA::argB*	(Takeshita *et al.*, 2008)
SNT65	*teaA(p)::mRFP1::TeaA; alcA(p)::GFP::tubA*	(Takeshita *et al.*, 2008)
SNZ1	TN02A3 transformed with pNZ2, homologous integration *alcA(p)::GFP::uncB; pyroA4, ΔnkuA::argB*	This study
SNZ2	TN02A3 transformed with pAS3, homologous integration *alcA(p)::GFP::uncA; pyroA4, ΔnkuA::argB*	This study
SNZ3	TN02A3 transformed with pNZ5 *ΔuncB::pyr4; pyroA4, ΔnkuA::argB*	This study

SNZ4	SNZ2 transformed with pJH19 and pTN1 *alcA(p)::DsRed::stuA; alcA(p)::GFP::uncA, ΔnkuA::argB*	This study
SNZ5	TN02A3 transformed with pNZ2 (over expression) *alcA(p)::GFP:: uncB$^{79\text{-}1.68}$; pyroA4, ΔnkuA::argB*	This study
SNZ6	TN02A3 transformed with pNZ10, over expression *alcA(p)::mRFP1::uncB$^{79\text{-}1.68}$; pyroA4, ΔnkuA::argB*	This study
SNZ7	TN02A3 transformed with pNZ10, homologous integration *alcA(p)::mRFP1:: uncB$^{79\text{-}1.68}$; pyroA4, ΔnkuA::argB*	This study
SNZ8	TN02A3 transformed with pNZ9, homologous integration *alcA(p)::mRFP1::uncA$^{0.9}$; pyroA4, ΔnkuA::argB*	This study
SNZ9	TN02A3 transformed with pNZ13 *pyG89; ΔuncA::pyroA, ΔnkuA::argB*	This study
SNZ10	SNZ5 transformed with pPND1 and pTN1 *alcA(p)::GFP::uncB; alcA(p)::mRFP1::kipB; ΔnkuA::argB*	This study
SNZ11	GR5 transformed with pDV22 and pDV50 *wA3; pyroA4; alcA(p)::YFP^{N}::apsB$^{3.2}$; alcA(p)::YFP^{C}::mipA$^{1.8}$*	This study
SNZ12	SNZ9 transformed with pNZ2 *alcA(p)::GFP::uncB; ΔuncA::pyroA*	This study
SNZ13	TN02A3 transformed with pNZ16 *pyroA4; alcA(p)::GFP::apsB_PTS2^{mut}_SRL*	This study
SNZ14	TN02A3 transformed with pNZ15 *alcA(p)::GFP::uncA^{rigor} ; pyroA4*	This study
SNZ15	SNZ3 crossed with RMS011, Nr1-2 with *nkuA* deletion *pabaA1; yA2; ΔuncB::pyr4*	This study
SNZ16	TN02A3 transformed with pNZ17 *pyroA4; alcA(p)::GFP:: mipA$^{1.8}$*	This study
SNZ17	SNZ8 crossed with GFP Actin binding protein strain *alcA(p)::mRFP1::uncA; abpA::GFP*	This study
SNZ18	SNZ14 transformed with pNZ10 and pTN1, over expression *alcA(p)::mRFP1::uncB; alcA(p)::GFP::uncA^{rigor}*	This study
SNZ19	SNZ14 transformed with pSK700 and pTN1 *alcA(p)::GFP::uncA^{rigor}; alcA(p)::mRFP1::citrat syntase* (just N-terminal sequence with the mitochondrial import sequence)	This study
SNZ20	SNZ9 transformed with pRS54 and pNRSTE1 *ΔuncA::pyroA; alcA(p)::GFP::citrat syntase* (just N-terminal sequence with the mitochondrial import sequence)	This study
SNZ21	SNZ9 transformed with pJH19 and pNZ2, over expression *gpd(p)::DsRed::stuA(NLS); alcA(p)::GFP::uncB; ΔuncA::pyroA*	This study
SNZ22	SNZ16 transformed with pJH19 and pTN1 *gpd(p)::DsRed::stuA(NLS); alcA(p)::GFP:: mipA$^{1.8}$*	This study
SNZ25	SNZ15 transformed with pJH19 and pCK17 *gpd(p)::DsRed::stuA(NLS); ΔuncB::pyr4*	This study
SNZ26	SNZ8 crossed with SJW100 *alcA(p)::mRFP1::uncA; pyroA4; alcA(p)::GFP::tubA*	This study

SNZ27	SNZ9 crossed with RMS011 *pabaA1, yA2; ΔuncA::pyroA*	This study
SNZ29	SNZ9 crossed with SNZ15 *ΔuncB::pyr4; ΔuncA::pyroA*	This study
SNZ31	AJC1.5 transformed with pNZ15 *alcA(p)::GFP::uncA^{rigor} ; apsB6*	This study
SNZ32	GR5 transformed with pNZ16, homologous integration *pyroA4; alcA(p)::GFP::apsB_PTS2^{mut}_SRL*	This study
SNZ33	AJC1.7 transformed with pNZ17 *apsB10; alcA(p)::GFP::mipA^{1.8}*	This study
SNZ34	AJC1.7 transformed with pNZ16 *apsB10; alcA(p)::GFP::apsB_PTS2^{mut}_SRL*	This study
SNZ35	GR5 transformed with pNZ17, homologous integration *pyroA4; alcA(p)::GFP:: mipA ^{1.8}*	This study
SNZ36	SNZ9 crossed with AnKin26 *ΔuncA::pyroA; ΔkinA::pyrG*	This study
SNZ37	SNZ16 transformed with pNZS23 and pTN1 *apsB::3xHA; alcA(p)::GFP:: mipA ^{1.8}*	This study
SNZ43	SNZ-SI 40 crossed with SNT65 *ΔuncA::pyroA; teaA(p)::mRFP1::TeaA; alcA(p)::GFP::tubA*	This study
SNZ44	SJW100 crossed with PEX3KOB2 *biA1; pexC::bar; alcA(p)::GFP::tubA*	This study
SNZ45	SJW100 crossed with BUY14 *biA1; alcA(p)::GFP::tubA; pexG14*	This study
SNZ46	SJW100 crossed with PEXM15 *biA1; pexM15; alcA(p)::GFP::tubA*	This study
SNZ47	SJW100 crossed with PEXA9 *pexA9, biA1; alcA(p)::GFP::tubA*	This study
SNZ48	SJW100 crossed with PEXF23 *biA1; pexF23::pyr4; alcA(p)::GFP::tubA*	This study
SNZ50	SJW100 crossed with SNZ15 *yA2; alcA(p)::GFP::tubA*	This study
SNZ51	SNZ29 crossed with RMSO11 *pabaA1, ΔuncB::pyr4; ΔargB::trpCΔB; ΔuncA::pyroA*	This study
SNZ52	SNZ29 crossed with RMSO11 *ΔuncB::pyr4; ΔargB::trpCΔB; ΔuncA::pyroA*	This study
SNZ53	SNZ29 crossed with RMSO11 *pabaA1, ΔuncB::pyr4; ΔuncA::pyroA*	This study
SNZ54	TN02A3 transformed with pNZS20 *alcA(p)::mRFP1::uncA^{rigor}, pyroA4*	This study
SNZ55	SNZ14 crossed with SJW100 *alcA(p)::GFP::uncA^{rigor}, pyroA4; alcA(p)::GFP::tubA*	This study
SNZ56	SNZ1 crossed with SJW100 *alcA(p)::GFP::uncB; pyroA4; alcA(p)::GFP::tubA*	This study

SNZ58	TN02A3 transformed with pSINZ 38 *uncB(p)::GFP::uncB; pyroA4*	This study
SNZ59	TN02A3 transformed with pNZ-SI37 *pyroA4; apsB(p)::GFP::apsB*	This study
SNZ60	TN02A3 transformed with pNZ-SI37 and pNZ-SI36 *pyroA4; apsB(p)::GFP::apsB; mipA(p)::GFP:: mipA*	This study
SNZ61	TN02A3 transformed with pNZ-SI36 *pyroA4; mipA(p)::GFP:: mipA*	This study
SNZ62	SJW100 crossed with SNZ15 *ΔuncB::pyr4; alcA(p)::GFP::tubA*	This study
SNZ63	SNZ9 crossed with XX60 *ΔuncA::pyroA; ΔnudA::pyrG*	This study
SNZ64	TN02A3 transformed with pNZ-SI41 and pNZ-SI44 *alcA(p)::YFP^C::uncB; alcA(p)::YFP^N::uncA^{rigor}*	This study
SNZ65	TN02A3 transformed with pNZ-SI41 and pDV23 *alcA(p)::YFP^C::apsB; alcA(p)::YFP^N::uncA^{rigor}*	This study
SNZ66	SNZ9 crossed with RMS011 *yA2; ΔargB::trpCΔB; ΔuncA::pyroA*	This study
SNZ67	TN02A3 transformed with pNZ-SI 45 *apsB(p)::3xHA::apsB$^{3.2}$; pyroA4*	This study
SNZ68	TN02A3 transformed with pNZ58 *pyrG89; alcA(p)::GFP::tlgB*	This study
SNZ69	SNZ14 transformed with pNZ59 *alcA(p)::GFP::uncA^{rigor}; alcA(p)::mRFP1::tlgB*	This study
SNZ70	SNZ27 transformed with pNZ58 *yA2; ΔuncA::pyroA; alcA(p)::mRFP1::tlgB*	This study
SNZ71	SNR1 crossed with SNZ68 *ΔkinA::pyr4; alcA(p)::GFP::tlgB*	This study
SNZ72	SNZ51 crossed with SRS29 *ΔuncB::pyr4; ΔuncA::pyroA; gpd(p)::GFP::citrat syntase* (just N-terminal sequence with the mitochondrial import sequence)	This study
SNZ73	SNZ51 crossed with SNT65 *ΔuncB::pyr4; teaA(p)::mRFP1::TeaA; ΔuncA::pyroA*	This study
SNZ74	TN02A3 transformed with PNZ-SI49 *uncA(p)::GFP::uncA$^{0.9}$; pyroA4*	This study
SNZ75	TN02A3 transformed with pNZ53 *pyG89; ΔttlA::pyroA; ΔnkuA::argB*	This study
SNZ76	SNZ14 transformed with pPND1 and pTN1 *alcA(p)::mRFP1::kipB; alcA(p)::GFP::uncA^{rigor}*	This study
SNZ77	TN02A3 transformed with pNZ64, homologous integration *pyrG89; alcA(p)::GFP:: tubA$^{3.1}$*	This study
SNZ78	SNZ15 transformed with pNZ75 *yA2; ΔuncB::pyr4; alcA(p)::GFP::uncB^{rigor}*	This study

SNZ87	LZ12 transformed with pNZ9 *alcA(p)::mRFP1::uncA$^{0.9}$; nudA(p)::GFP::nudA*	This study
SNZ88	SNZ2 transformed with pNZ59 *alcA(p)::GFP::uncA; alcA(p)::mRFP1::tlgB*	This study
SNZ89	SNZ14 crossed with SNT30 *ΔteaA::argB; alcA(p)::GFP::uncA^{rigor}*	This study
SNZ90	SNZ14 crossed with SNT30 *ΔteaA::argB; alcA(p)::GFP::uncA*	This study
SNZ91	SNZ75 transformed with pNZ15 *ΔttlA::pyroA; ΔnkuA::argB; alcA(p)::GFP:: uncA^{rigor}*	This study
SNZ92	SNZ75 transformed with pNZ15 *ΔttlA::pyroA; ΔnkuA::argB; alcA(p)::GFP:: uncA*	This study
SNZ93	TN02A3 transformed with pNZ72 *alcA(p)::GFP:: tubB$^{1.9}$, pyroA4; ΔnkuA::argB*	This study
SNZ94	SRS24 transformed with pNZ16 *gpd(p)::GFP::stuA(NLS), pabaA1; biA1; ΔapsB::argB; trpC801;* *alcA(p)::GFP::apsB_PTS2^{mut}_SRL*	This study
SNZ95	AJC1.7 crossed with SNZ-SH80 *alpB(p)::alpB::GFP; apsB10*	This study
SNZ96	TN02A3 transformed with pNZ74 *alcA(p)::GFP::alpC^{alp4}; pyrG89*	This study
SNZ97	GFP-ClipA strain transformed with pCoS19 *pyrG89; uncA(p)::mRFP1::uncA^{rigor}; alcA(p)::GFP::clipA*	This study
SNZ98	GFP-ClipA strain transformed with pNZ67 *pyroA4; alcA(p)::GFP::clipA; alcA(p)::mRFP1:: tubA$^{3.1}$*	This study
SNZ99	TN02A3 transformed with pNZ67 *pyroA4; alcA(p)::mRFP1:: tubA$^{3.1}$*	This study
SNZ100	SNZ14 crossed with XX60 *alcA(p)::GFP::uncA^{rigor}; ΔnudA::pyrG*	This study
SNZ101	SNZ14 crossed with SDV83 *alcA(p)::GFP::uncA^{rigor}; ΔalpA::pyr4*	This study
SNZ102	TN02A3 transformed with pNZ73 *alcA(p)::GFP:: tubB$^{3.2}$; pyroA4; ΔnkuA::argB*	This study
SNZ103	MH11296 cotransformed with pDV21, pDV39 and pTN1 *alcA(p)::mRFP1::hexA; alcA(p)::GFP::apsB; Δpex3::bar*	This study
SNZ104	SNZ75 transformed with pNZ68 *ΔttlA::pyroA; ΔnkuA::argB; alcA(p)::mRFP1:: tubA^{Y}*	This study
SNZ105	TN02A3 transformed with pNZ82 *pyrG89; alcA(p)::3xHA::uncA*	This study
SNZ106	TN02A3 transformed with pNZ81 *pyrG89; alcA(p)::3xHA::uncB*	This study
SNZ107	TN02A3 transformed with pNZ-SI45 *pyroA4; apsB(p)::3xHA::apsB*	This study

SNZ108	TN02A3 transformed with pNZ84 and pNZ85 *uncB(p)::YFP^C::uncB; uncB(p)::YFP^N::uncB*	This study
SNZ109	sNZ54 transformed with pNZ64 *alcA(p)::mRFP1::uncA^{rigor}; alcA(p)::GFP:: tubA$^{3.1}$*	This study
SNZ110	TN02A3 transformed with pNZ78, homology strain *uncA(p)::GFP::uncA^{rigor}; pyroA4*	This study
SNZ-SH80	SO451 transformed with AlpB::GFP fusion PCR *alpB(p)::alpB::GFP; pyroA4; ΔnkuA::argB*	This study
SNZ-SI38	TN02A3 transformed with pSI-NZ32 *alcA(p)::GFP::uncB$^{1.6}$; pyroA4*	This study
SNZ-SI39	SNZ1 transformed with pJH19 *gpd(p)::DsRed::stuA(NLS); alcA(p)::GFP::uncB*	This study
SNZ-SI40	SNZ9 crossed with RMS011 *pabaA1, yA2; ΔuncA::pyroA*	This study
SNZ-SI41	SNZ-SI 40 crossed with SJW100 *ΔuncA::pyroA; alcA(p)::GFP::tubA*	This study
SNZ-SI42	TN02A3 transformed with pSI-N4 *pyroA4; alcA(p)::3xHA::apsB*	This study
SO451	*pyrG89; wA3; argB2; pyroA4; ΔnkuA::argB*	FGSC, USA
SRF200	*pyrG89; ΔargB::trpCΔB; pyroA4*	(Karos & Fischer, 1999)
SRS24	*gpd(p)::GFP::stuA(NLS), pabaA1; ΔapsB::argB; trpC801*	(Suelmann, 1999)
SRS27	*gpd(p)::GFP::stuA(NLS), pyrG89; ΔargB::trpCΔB; pyroA4*	(Suelmann, 1999)
SRS29	*SRF200 transformed with pRS54 and pDC1* *pyrG89; pyroA4; gpd(p)::GFP::citrat syntase* (just N-terminal sequence with the mitochondrial import sequence)	(Suelmann & Fischer, 2000)
SSK13	*pabaA1*; *wA3, ΔkipA::pyr4*	(Konzack *et al.*, 2005)
SSK44	*pabaA1*; *wA3, ΔkipA::pyr4; ΔargB::trpCΔB*	(Konzack *et al.*, 2005)
SSK92	*alcA(p)::GFP::kipA; pyroA4*	(Konzack *et al.*, 2005)
SSK114	*pyrG89; wA3, alcA(p)::GFP::kipA^{rigor}; pyroA4*	(Konzack *et al.*, 2005)
TALX207-10	*yA1; pyroA4; areA102; gpd(p)::GFP::acuE*	(Hynes *et al.,* 2008)
TN02A3	*pyrG89; argB2; pyroA4, ΔnkuA::argB*	(Nayak *et al.*, 2006)
XX60	*pyrG89; ΔnudA::pyrG*	(Xiang *et al.*, 1995)

Table VI. 04. *E. coli* **strains used in this study**

E. coli strain	Genotype	Source
BL21	F' *omp*T, *hsd*SB, (*r*B-*m*B-) *gal, dcm, rne*131	Invitrogen
DH5α	F' φ80, *lac*Z(M15 Δ(*lac*ZYA-*arg*F), U169, *rec*A1, *end*A1, *hsd*R17, (rk-, mk+) *pho*A, *sup*E44, λ– , *thi*-1, *gyr*A96, *rel*A1	Invitrogen
Top10	F' mcrA Δ(*mrr-hsd*RMS-*mcr*BC), φ80, *lac*Z ΔM15 Δ*lac*X74, nupG, *rec*A1, *ara*Δ139 Δ(*ara-leu*) 7679, galE15 galK16 rpsL(Str^R) endA1 λ$^-$	Invitrogen
Top10F'	F'[lacQ, Tn10 TetR)] mcrA, Δ(*mrr-hsd*RMS-*mcr*BC), φ80, *lac*Z ΔM15 Δ*lac*X74, *deo*R, nupG, *rec*A1, *ara*D139 Δ(*ara-leu*) 7679, *gal*U, *gal*K, *rpsl* (Str^R) *end*A1, λ –	Invitrogen
XL1 blue	*rec*A1, *end*A1, *gyr*A96, *thi*-1, *hsd*R17, *sup*E44, *rel*A1, *lac* [F'proAB *lac*I Q ZΔM15: Tn10 (TetR)]	Stratagene

Table VI. 05. Plasmids used in this study

Plasmid	Construction	Source
pAS3	0.9-kb *uncA* as *Asc*I-*Pac*I fragment in pMCB17apx alcA(p)::GFP::uncA$^{0.9}$, pyr4	This study
pCK17	*pabaA* ORF with promotor & terminator in pCR2.1-TOPO	Kastner C.
pCK28	*nsdD* in pDV7, *pyr4* replaced with *pyroA* alcA(p)::YFP^N:: nsdD; pyroA	Kastner C.
pCoS19	alcA(p)::mRFP1::uncA^{cDNA,rigor}, pyroA	(Seidel, 2009)
pCR2.1-TOPO	Cloning vector	Invitrogen
pCS1	*N. crassa pyr4* selectable marker as *Not*I fragment in pUMA208	(Enke *et al.*, 2007)
pCS1-NZ	1.3-kb *kinA* as *Asc*I-*Pac*I fragment in pCR2.1-TOPO	This study
pCS2-NZ	TlgA in pNZ56 replaced with *kinA* from pCS1-NZ alcA(p)::GFP::kinA$^{1.3}$, pyroA	This study
pCS3-NZ	TlgA in pNZ57 replaced with *kinA* from pCS1-NZ alcA(p)::mRFP1::kinA$^{1.3}$, pyroA	This study
pCS4-NZ	pCS2-NZ mutagenesis to introduce the G97E mutation in the p-loop of KinA alcA(p)::GFP::kinA^{rigor}, pyroA	This study
pCS5-NZ	GFP in pCS4-NZ replacedvc<< with mRFP1 alcA(p)::mRFP1::kinA^{rigor}, pyroA	This study
pCS7-NZ	TlgA in pNZ57 replaced with 2.5-kb TtlA ORF with stop codon alcA(p)::mRFP1::ttlA$^{2.5}$, pyroA	This study
pCS8-NZ	1.3-kb TtlA as *Asc*I- *Bam*HI fragment in pNZ56 alcA(p)::GFP::ttlA$^{1.3}$, pyroA	This study
pDC1	*argB* from *A. nidulans*	(Aramayo *et al.*, 1989)

pDM8	GFP replaced mRFP1 in pMCB17apx *alcA(p)::mRFP1::apsB*[1.5]*, pyr4*	(Veith *et al.*, 2005)
pDV23	*apsB* of pDV8 replaced with full-length *apsB*[3.2] *alcA(p)::YFP*[C]*::apsB*[3.2]*, pyr4*	(Veith, 2006)
pDV49	*apsB* of pDV7 replaced with full-length *gtubulin*[1.8] *alcA(p)::YFP*[N]*::mipA*[1.8]*, pyr4*	(Veith, 2006)
pDV50	*apsB* of pDV8 replaced with full-length *gtubulin*[1.8] *alcA(p)::YFP*[C]*::mipA*[1.8]*, pyr4*	(Veith, 2006)
pENTR[MT]/D-Topo	Cloning vector	Invitrogen
pJH19	*gpd(p)::stuA(NLS)::DsRed* , *argB*	(Toews *et al.*, 2004)
pMCB17apx	*alcA(p)::GFP*, for N-terminal fusion of GFP to proteins of interest; contains *N. crassa pyr4*	(Efimov *et al.*, 2006)
pMT-3xHA	Gateway cloning vector	(Toews *et al.*, 2004)
pNRSTE1	1.9-kb *pyr4* in pCR2.1-TOPO	(Requena *et al.*, 2001)
pNZ2	1.6-kb *uncB fragment* (second ATG) in pMCB17apx, *AscI*-*PacI* *alcA(p)::GFP::uncB*[1.6]*, pyr4*	This study
pNZ5	*uncB*-deletion construct: 1-kb UncB flanking regions ligated with *pyr4* from pCS1 in pCR2.1-TOPO *uncB-LB::pyr4::uncB-RB*	This study
pNZ8	*uncA*-deletion construct: 1-kb UncA flanking regions ligated with *pyr4* from pCS1 in pCR2.1-TOPO *uncA-LB::pyr4::uncA-RB*	This study
pNZ9	GFP in pAS3 replaced with mRFP1 *alcA(p)::mRFP1::uncA*[0.9]*, pyr4*	This study
pNZ10	GFP in pNZ2 replaced with mRFP1 *alcA(p)::mRFP1::uncB*[1.6]*, pyr4*	This study
pNZ11	1.7-kb *pyroA* fragment from pTN1, *NotI* sites in pCR2.1-TOPO	This study
pNZ12	*pyr4* in pCS1 replaced with *pyroA* fragment from pNZ11	This study
pNZ13	*uncA*-deletion construct: *pyr4* in pNZ8 replaced with *pyroA* from pNZ12 *uncA-LB::pyroA::uncA-RB*	This study
pNZ14	*uncB*-deletion construct: *pyr4* in pNZ5 replaced with *pyroA* from pNZ12 *uncB-LB::pyroA::uncB-RB*	This study
pNZ15	pAS3 mutagenesis to introduce the G116E mutation in the p-loop of UncA, (UncA[rigor]) *alcA(p)::GFP::uncA*[rigor]*, pyr4*	This study
pNZ16	PTS1 (SRL) before the stop codon of *apsBPTS2*[mut] in pDV43 *alcA(p)::GFP::apsB_PTS2*[mut]*_SRL; pyr4*	This study
pNZ17	pMCB17-apx containing 1.8-kb *mipA* ORF, *AscI*-*PacI* sites *alcA(p)::GFP::mipA*[1.8]*, pyr4*	This study
pNZ21	*apsB*[3.2] without stop codon in pENTR[MT]/D-Topo	This study

pNZ53	*ttlA*-deletion construct: 1-kb TtlA flanking regions ligated with *pyroA* from pNZ12 in pCR2.1-TOPO *ttlA-LB::pyroA::ttlA-RB*	This study
pNZ56	TlgA ORF AscI-PacI fragment in pCMB17apx, *pyr4* replaced with *pyroA* *alcA(p)::GFP::tlgA, pyroA*	This study
pNZ57	GFP in pNZ56 replaced with mRFP1 *alcA(p)::mRFP1::tlgA, pyroA*	This study
pNZ58	TlgB ORF fragment in pNZ56 *alcA(p)::GFP::tlgB, pyroA*	This study
pNZ59	GFP in pNZ58 replaced with mRFP1 *alcA(p)::mRFP1::tlgB, pyroA*	This study
pNZ61	0.45-kb TlgB fragment between *AscI-PacI* from pNZ57 *alcA(p)::mRFP1::tlgB$^{0.45}$, pyroA*	This study
pNZ62	1-kb *tubA(p)*, *Pfo*I restriction sites in pCR2.1-TOPO	This study
pNZ63	3.1-kb *tubA* (ORF with terminator) fragment in pCR2.1-TOPO	This study
pNZ64	TlgA from pNZ56 replaced with *tubA$^{3.1}$* from pNZ63 *alcA(p)::GFP::tubA$^{3.1}$, pyroA*	This study
pNZ65	pNZ64 point mutation to introduce a stop codon in place of the C-terminal tyrosine of *tubA*, (Glu-tubulin) *alcA(p)::GFP::tubA^{Y}, pyroA*	This study
pNZ66	pNZ64 two point mutation to introduce 2 stop codons in place of the C-terminal glutamic acid (E) and tyrosine (Y) of *tubA*, (Δ2-tubulin) *alcA(p)::GFP::tubA^{E-Y}, pyroA*	This study
pNZ67	*tubA$^{3.1}$* from pNZ63 in place of *apsB$^{1.5}$* from pDM8 *alcA(p)::mRFP1::tubA$^{3.1}$, pyr4*	This study
pNZ68	*tubA^{Y}* from pNZ65 in place of *uncA^{rigor}* from pNZS20 *alcA(p)::mRFP1::tubA^{Y}, pyr4*	This study
pNZ69	1-kb *tubA(p)* from pNZ62 in pfoI restriction sites of pNZ15	This study
pNZ72	1.9-kb *tubB* ORF as *AscI-PacI* fragment in pMCB17apx *alcA(p)::GFP::tubB$^{1.9}$, pyr4*	This study
pNZ73	3.2-kb *tubB* (ORF with terminator) fragment between *AscI-PacI* in pMCB17Apx *alcA(p)::GFP::tubB$^{3.2}$, pyr4*	This study
pNZ74	2.5-kb AlpC^{alp4} AscI-PacI in place of TlgA in pNZ56 *alcA(p)::GFP::alpC, pyroA*	This study
pNZ75	pNZ-SI48 mutagenesis to introduce the T214P and G217E mutations in the p-loop of UncB, (*uncB^{2,cDNA,rigor}*) *alcA(p)::GFP::uncB^{2,cDNA,rigor}, pyr4*	This study
pNZ76	Dendra UncB 1558 *alcA(p)::dendra::uncB$^{1.6}$, pyr4*	This study
pNZ77	Dendra UncB Rigor 1816 *alcA(p)::dendra::uncB$^{1.6, rigor}$, pyr4*	This study
pNZ78	*uncA* replaced with 0.9-kb *uncA^{rigor}* in pNZ-SI49 *uncA(p)::GFP::uncA^{rigor}, pyr4*	This study

pNZ79	*alcA(p)::mRFP1::uncA^{rigor}, pyroA*	This study
pNZ80	UncA full-length cDNA in pQE32	This study
pNZ81	*pyroA* in place of pyr4, *uncB* in place of *apsB* in pSI-N4 *alcA(p)::3xHA::uncB, pyroA*	This study
pNZ82	*uncA* in place of *uncB* in pNZ81 *alcA(p)::3xHA::uncA, pyroA*	This study
pNZ83	*uncA*(p) in place of *alcA(p)* in pNZ-SI40 *uncA(p)::YFP^{C}::uncA, pyr4*	This study
pNZ84	*uncB*(p) in place of *alcA(p)* in pNZ-SI43 *uncB(p)::YFP^{N}::uncB, pyroA*	This study
pNZ85	*uncB*(p) in place of *alcA(p)* in pNZ-SI44 *uncB(p)::YFP^{C}::uncB, pyr4*	This study
pNZD19	0.31-kb UncB fragment between *Asc*I-*Pac*I from pMCB17apx *alcA(p)::GFP::uncB$^{0.31}$, pyr4*	This study
pNZS20	GFP in pNZ15 replaced with mRFP1 *alcA(p)::mRFP1::uncA^{rigor}, pyr4*	This study
pNZS23	*apsB$^{3.2}$* from pNZ21 cloned into pMT-3xHA *alcA(p)::apsB$^{3.2}$::3xHA, argB*	This study
pNZ-SI36	*alcA(p)* of pNZ17 replaced with 1.16-kb *mipA(p)*, *Eco*RI-*Bsiw*I *γtubulin(p)::GFP::mipA$^{1.8}$, pyr4*	This study
pNZ-SI37	*alcA(p)* of pDV21 replaced with 1.33-kb *apsB(p)*, *Avr*II-*Kpn*I *apsB(p)::GFP::apsB$^{3.2}$, pyr4*	This study
pNZ-SI38	*alcA(p)* of pNZ2 replaced with 1.23-kb *uncB(p)*, *Avr*II-*Bsiw*I *uncB(p)::GFP::uncB$^{1.6}$, pyr4*	This study
pNZ-SI39	*nsdD* of pCK28 replaced with *uncA* from pAS3, *Asc*I-*Pac*I *alcA(p)::YFP^{N}::uncA, pyroA*	This study
pNZ-SI40	*mipA$^{1.8}$* of pDV50 replaced with 0.9-kb *uncA* from pAS3 *alcA(p)::YFP^{C}::uncA, pyr4*	This study
pNZ-SI41	*nsdD* of pCK28 replaced with 0.9-kb *uncA^{rigor}* from pNZS20 *alcA(p)::YFP^{N}::uncA^{rigor}, pyroA*	This study
pNZ-SI42	*mipA$^{1.8}$* of pDV50 replaced with 0.9-kb *uncA^{rigor}* from pNZS20 *alcA(p)::YFP^{C}::uncA^{rigor}, pyr4*	This study
pNZ-SI43	*nsdD* of pCK28 replaced with 1.6-kb *uncB* from pNZ2, *Asc*I/*Pac*I *alcA(p)::YFP^{N}::uncB, pyroA*	This study
pNZ-SI44	*mipA$^{1.8}$* of pDV50 replaced with 1.6-kb *uncB* from pNZ2 *alcA(p)::YFP^{C}::uncB, pyr4*	This study
pNZ-SI45	*alcA(p)* from pSI-N4 replaced with apsB(p) from pNZ-SI37, *Kpn*I-*Avr*II *apsB(p)::3xHA::apsB$^{3.2}$, pyr4*	This study
pNZ-SI47	2-kb *uncB* cDNA from pSI-NZ31 as *Asc*I-*Pac*I fragment in pCR2.1-TOPO	This study
pNZ-SI48	2-kb *uncB* cDNA from pNZ-SI47 in pMCB17apx *alcA(p)::GFP::uncB^{2,cDNA}, pyr4*	This study

pNZ-SI49	*alcA(p)* of pAS3 replaced with 1.5-kb *uncA(p)*, *Kpn*I-*Eco*RI *uncA(p)::GFP::uncA*[0.9]; *pyr4*	This study
pNZ-SI50	1.3-kb UncA C-terminal without PH domain in pDV2 (Gateway Vector) *uncA*[no PH]*::GFP*	This study
pNZ-SI70	UncA full-length cDNA, *Asc*I-*Pac*I, in pCR2.1-TOPO	This study
pNZ-SI71	UncA full-length cDNA from pNZ-SI70 in pNZ57 *alcA(p)::mRFP1::uncA*[cDNA], *pyroA*	This study
pPND1	GFP replaced with mRFP1 in pPR38 *alcA(p)::mRFP1::kipB*[1.2], *pyr4*	(Rischitor *et al.* 2004)
pRS54	*gpd(p)::citrate synthase (N)::sGFP* in pBluescript KS- (just N-terminal sequence with the mitochondrial import sequence)	(Suelmann & Fischer, 2000)
pSI-N4	pSM14 containing full-length *apsB* of 3.2-kb between *Asc*I and *Pac*I restriction sites. *alcA(p)::3xHA::apsB*[3.2], *pyr4*	This study
pSI-N5	UncA full-length cDNA, *Xma*I-BglII, in pCR2.1-TOPO	This study
pSI-NZ30	As pSI-N5 but the clone is in opposite direction	This study
pSI-NZ31	2-kb cDNA UncB, starts at the second ATG and includes a I60V mutation, as *Xma*I fragment in pCR2.1-TOPO	This study
pSI-NZ32	pNZ2 mutagenesis to introduce the the T214P and G217E mutations in the p-loop of UncB, (*uncB*[1.6,rigor]) *alcA(p)::GFP::uncB*[1.6,rigor], *pyr4*	This study
pSI-NZ51	1.7-kb UncA C-terminal without stop codon in pDV2 (Gateway GFP) *uncA*[no stop]*::GFP*	This study
pSI-NZ52	1.7-Kb UncA C-terminal in pMT-sGFP (Gateway Vector) *uncA*[no stop]*::sGFP*	This study
pSK700	sGFP in pRS54 replaces with DsRed *gpd(p)::citrate synthase (N)::DsRed* in pBluescript KS-	(Toews *et al.*, 2004)
pSM14	*GFP* of pMCB17apx replaced with *3xHA* between *Kpn*I and *Asc*I restriction sites	(Purschwitz *et al.*, 2009)
PTN1	*pyroA* from *A. fumigatus*	(Nayak *et al.*, 2006)

3.   Microbiological and genetic methods

3.1.   Cultivation, growth and storage of *E. coli* and *A. nidulans* strains

Media for *E. coli* were prepared as described (Sambrook & Russel, 1999), **(Table VI. 06)** and appropriately supplemented with antibiotics and necessary reagents in each experiment, **(Table VI. 07)**. Ingredients were added to ddH₂O, poured into bottles with loosen caps and autoclaved 20 min at 121°C. For solid media, 15 g agar per liter was added.

Glasware and porcelain was sterilized in the heat sterilizer for 3 h at 180°C. Heat-sensitive solutions such as antibiotics, amino acids and vitamins were filter-sterilized with 0.22 µm pore filter membrane (Schleicher und Schüll, Dassel), and added to the media after autoclaving. Minimal and complete media for *A. nidulans* growth were prepared according to the protocols (Pontecorvo *et al.*, 1953) **(Table VI. 08)**. The supplemented vitamins, amino acids and nucleotides for auxotrophic *A. nidulans* strains were listed in **(Table VI. 09)**.

Table VI. 06. Media for *E. coli*

Medium	Ingredients (1liter)
Luria-Bertani (LB)	10 g Trypton; 10 g Yeast extract; 5 g NaCl, pH 7.5
SOC	20 g Trypton; 5 g Yeast extract; 0.58 g NaCl; 0.185 g KCl; 2.03 g $MgCl_2$ x 7 H_2O; 2.46 g $MgSO_4$ x 7 H_2O; 3.6 g Glukose

Table VI. 07. Antibiotics and supplements for *E. coli* media

Substance	Stock solutions/Storage		End concentration
Ampicillin (Amp)	50 mg/ml in ethanol	/ -20°C	100 µg/ml
Kanamycin (Kan)	10 mg/ml in water	/ -20°C	50 µg/ml
Streptomycin	10 mg/ml in water	/ -20°C	50 µg/ml
Tetracycline	5 mg/ml in ethanol	/ -20°C	25 µg/ml
X-Gal	25 mg/ml in DMF	/ -20°C	40 µg/ml - 25 µl/plate
IPTG	24 mg/ml in water	/ -20°C	8 µg/ml - 40 µl/plate

Table VI. 08. Media and stock solutions for *A. nidulans*

Media or Stock	Preparation (per liter)
Minimal medium (MM)	50 ml Salt stock solution; 1 ml Trace elements stock solution; 20 g Glucose; adjust to pH 6.5 using 10 N NaOH. For protoplast transformation add 0.6 M KCl as osmoprotective substance
Complete medium (CM)	MM with 2 g Peptone; 1 g Yeast extract; 1 g Casamino acids; 1 ml Vitamin stock solution; 1 ml Trace elements stock solution; adjust to pH 6.5 using 10 N NaOH
20 x Salt stock solution	120 g $NaNO_3$; 10.4 g KCl; 10.4 g $MgSO_4$ x 7 H_2O; 30.4 g KH_2PO_4
1000 x Trace elements stock solution	22 g $ZnSO_4$ x 7 H_2O; 11 g H_3BO_3; 5 g $MnCl_2$ x 4 H_2O; 5 g $FeSO_4$ x 7 H_2O; 1.6 g $CoCl_2$ x 5 H_2O; 1.6 g $CuSO_4$ x 5 H_2O; 1.1 g $(NH_4)_6Mo_7O_{24}$ x 4 H_2O; 50 g Na_4 EDTA; adjust to pH 6.5-6.8 using KOH
1000 x Vitamin stock solution	0.1 g D-Biotin; 0.1 g Pyrodoxin-HCl; 0.1 g Thiamin-HCl; 0.1 g Riboflavin; 0.1 g p-Aminobenzoic acid; 0.1 g Nicotinic acid

Table VI. 09. Vitamins, amino acids and medium components

Component	Stock Concentration	Volume or weight per liter
Biotin	0.05 %	1 ml
Nicotinamid	0.5 %	1 ml
Pyridoxin-HCl	0.1 %	1 ml
p-Aminobenzoic acid (PABA)	0.1 %	1 ml
Riboflavin	0.25 %	1 ml
Arginin	-	1.2g
Uracil	-	1 g
Uridin	-	1.2g
Methionin	1 %	3 ml

For storage of *E. coli* strains, freshly grown bacterial suspension was adjusted to 15% end concentration of sterile glycerol and frozen at -80°C. The *A. nidulans* strains were grown on minimal or complete medium plates. Spores were suspended in 15-20% sterile glycerol and stored at -80°C. Bacterial cell culture density was determined via absorption measurement with 600 nm (ΔOD_{600}) in a spectrophotometer (Pharmacia LKB-UltraspecIII).

3.2. Genetic methods in *A. nidulans*

The strains used for crossing were inoculated side by side onto CM plates plus appropriate marker for 2 days, until the mycelium of both strains fused at the borders. Small agar square blocks were cut from these fused edges and transferred to MM plates, where just the growth of a heterokaryon is possible. Plates were sealed with adhesive tape and incubated 10-14 days at 37°C or 30°C in a humid chamber, to elevate the partial pressure of CO_2 and activate sexual development. The fruiting bodies (cleistothecia) developed after this time were isolated with help of a sterile inoculating needle, rolled until completely cleaned from Hülle-cells on the surface of an agar plate, and smashed in an Eppendorf tube with 0.5 ml sterile ddH$_2$0. An aliquot of the ascospore suspension was inoculated onto CM agar plates. After 2-3 days incubation, the grown colonies were transferred onto MM plates with different appropriate markers, to test for the missing auxotrophic marker. If more strains were analyzed, they were inoculated onto raster plates, which contained 20 colonies (Sievers *et al.*, 1997).

Table VI. 10. Markers for *A. nidulans*

Marker	Function	Chromosome	Reference
argB2	Arginine auxotrophy (ornithine carbamoyltransferase)	III	(Upshall *et al.*, 1986)
bar	Glufosinate resistance	-	(Nayak *et al.*, 2006)
biA1	Biotin auxotrophy	I	FGSC
pabaA1	Para aminobenzoic acid auxotrophy	I	FGSC
ptrA	Pyrithiamine resistance	-	(Goda *et al.*, 2005)
pyroA4	Pyridoxine auxotrophy	IV	FGSC
pyrG89	Uracil auxotrophy (orotidine-5´-phosphate decarboxylase)	I	(Balance *et al.*, 1983)
trpC801	Tryptophan auxotrophy (phosphoribosylanthranilat isomerase)	VIII	(Yelton *et al.*, 1984)
veA1	Conidia production in the dark	VIII	FGSC
wA3	White spores (polyketide synthase)	II	(Mayorga & Timberlake, 1990)
yA2	Yellow spores (laccase)	I	(Aramayo *et al.*, 1989)

4.   Molecular biological methods

4.1. DNA manipulations

4.1.1. Plasmid DNA preparation from *E. coli* cells

Isolation of plasmid DNA was done with an alkali-lysis method as described (Sambrook & Russel, 1999). For small volumes of DNA (miniprep), 2.5 ml of overnight liquid culture were centrifuged 1 min at 13000 rpm, the pellet resuspended in 200 µl Tris-EDTA Buffer, then 200 µl of Alkali-lysis buffer added and gently mixed, followed by addition of 200 µl neutralization buffer **(Table VI. 11)**. After 10 min centrifugation, plasmid DNA-containing supernatant was precipitated with 0.7 vol. isopropanol, followed by 70% ethanol washing. The dried pellet was resuspended in TE buffer. For large DNA volumes (midiprep), plasmid DNA from 50 ml *E. coli* overnight liquid culture were extracted using a Macherey-Nagel Nucleobond® Plasmid DNA Purification Kit, according to the manufacturer's protocols. Plasmid DNA concentration was determined via comparison between the intensity of ethidium bromide DNA bands on

agarose gels and the intensity of defined standards or the concentrations were calculated using NanoDrop (ND-1000, PeQLab, Erlangen).

Table VI. 11. Solutions used for plasmid extraction (miniprep)

Tris-EDTA buffer	5 ml 1M Tris-HCl (pH 7.5); 2 ml 0.5M EDTA (pH 8.0); 10 mg RNAse in 100 ml
Alkali-lysis buffer	0.2 M NaOH; 1% SDS
Neutralization buffer	1.5 M Potassium Acetate, pH 4.8
TE buffer	10 mM Tris-HCl; 1 mM EDTA; pH 8.0

4.1.2. Genomic DNA preparation from *A. nidulans*

Preparation of *A. nidulans* genomic DNA was done like in (Timberlake & Marshall, 1989), by inoculation in a 9 cm Ø plastic Petri dish of around 20 ml fresh liquid complete media with spore suspension from a colony grown on an agar plate, followed by incubation for 12 -15 h at 32°C. Then, the mycelium was harvested with a spatula, pressed briefly until dry between paper towels, and frozen in liquid nitrogen. The frozen mycelium was grounded in liquid nitrogen or kept at -80°C until isolation. *A. nidulans* genomic DNA was extracted by mixing with extraction buffer (50 mM EDTA / 0.2% SDS), incubated for 1 h 30 min at 68°C and centrifuged at 13000 rpm for 5 min, after that 8 M Potassium Acetat pH 4.2 was added to the supernatant and centrifuged again at 13000 rpm for 5 min. Finally the DNA was precipitated with the same volume isopropanol, washed twice with 70% ethanol and air dried. The dried pellet was resuspended in TE buffer. 5 µl extracted DNA was checked in a 1% agarose gel. For genomic DNA isolation and purification the DNeasy Plant Mini Kit was used.

4.1.3. Digestion of DNA with restriction endonucleases

DNA samples (200 ng-1 µg) were digested with restriction endonucleases using corresponding reaction buffers. Generally, digestions were prepared in 20-50 µl total volume, with 0.5-1 µl restriction enzyme (5-100 U/µl) and incubated at 37°C from 1 h to overnight. In other cases, enzyme, DNA, buffer volumes and reaction times varied depending on the specific requirements. For enzyme inactivation, the sample was incubated at 68°C for 10 min. *A. nidulans* genomic DNA was generally digested overnight. In the case of multiple digestion, the restriction digest was carried out first in the buffer with low salt concentration or the buffer compatible to both enzymes.

4.1.4. Dephosphorylation of digested DNA

After the digestion with restriction enzymes, the vector was dephosphorylated by Shrimp alkaline phosphatase (SAP) to remove the phosphate group at 5'-end, which prevented self-ligation of the vector. 0.1 unit / µM 5'-end with buffer was added to the sample. The mix was incubated 45 min at 37°C. If two enzymes with incompatible termini were used, the dephosphorylation process was omitted.

4.1.5. DNA precipitation

Contamination by small nucleic acid fragments, proteins and salt can be reduced to acceptable level by precipitating the DNA. In order to do this, 2.5 volume of ethanol and 1/10 volume 3.0 M NaAc (pH 5.2) were added to the DNA solution. The sample was mixed, kept at -80ºC for 15 min and centrifuged for 10 min at 13.000 rpm. The supernatant was discarded and the pellet was washed with 70% ethanol, followed by centrifugation at 13.000 rpm for 5-10 min. The pellet of purified DNA was dried completely in a speed vacuum or at 37°C for 10-20 min, and then dissolved in sterile ddH$_2$O or TE buffer.

4.2. Gel electrophoresis, DNA isolation and ligation

4.2.1. DNA agarose gel electrophoresis

The separation and identification of DNA fragments was done by running them by 50-100 V through 1% agarose gels (Sambrook & Russel, 1999), which were prepared by melting agarose into 0.5x TAE buffer and pouring it into gel chambers. DNA samples were mixed with 1/10 10x DNA Loading buffer. As standard DNA marker an *Eco*130I-cut λ DNA (MBI Fermentas, St. Leon-Rot) and other markers were used, and gels were run for 30 min - 4 h in gel chambers with 0.5x TAE buffer **(Table VI. 12)**. Then, the gel was stained for 15-30 min in 0.5 x TAE buffer with ethidium bromide (1 µg/µl). The DNA bands were visualized in the gel at 302 nm UV light. Photos were taken using a camera (INTAS, Goettingen) connected to a video printer.

Table VI. 12. Solutions used for DNA agarose gel electrophoresis

Solution	Composition
50 x TAE buffer (pH 8.0)	40 mM Tris-Acetate; 1 mM EDTA; pH 8.0
10 x Loading buffer	15% Ficoll 400; 5 mM EDTA (pH 8.0); 1% SDS; 1.5 M Bromphenol blue

For isolation of DNA fragments, 0.8%-1% low melting agarose gel was often used. The low melting gel separated by gel electrophoresis at 50 V was stained in 0.5-1 x TAE buffer with ethidium bromide. The appropriate DNA bands were cut out under UV light. The DNA purification was carried out according to the protocol of WizardTM PCR Preps DNA Purification System (Promega, Madison, WI, USA). Alternatively, the DNA from normal agarose gels was isolated with the QIAEX II Gel Extraction System (Qiagen, Hilden) or with Freeze and squeeze method, in which the agarose band was frozen for 10 min at -20°C, and than melted gently with the fingers, DNA drops were collected inside new sterile Eppis.

4.2.2. DNA ligation

DNA ligation was performed using T4 ligase (M0202S, NEB, Frankfurt) overnight at 16°C or Fast LinkTM System (Biozym, Hessisch Oldendorf) in a volume of 10-20 µl. Around 50 ng vector was used in one ligation. The ratio of vector to insert was 1: 3 respectively for cohesive end ligation.

4.3. Polymerase chain reaction (PCR) and cloning of PCR products

4.3.1. Polymerase chain reaction

Polymerase chain reaction (PCR) was performed with Taq (Qbiogene, Heidelberg), Expand (Roche, Mannheim) or Pfu (Promega, Madison, WI, USA) polymerases according to manufacturer protocols. Oligonucleotides synthesis was made by MWG Biotech (Ebersberg) or from Biomers (Ulm), and the concentration used for a PCR reaction was 0.4 pM/µl. As DNA template plasmid or cosmid DNA (0.2-10 ng) and genomic DNA (10-20 ng) were used. The PCR reactions were carried out in a capillary Rapid Cycler (Idaho Technology, Idaho Falls, ID, USA) or in a Personal Cycler (Biometra, Göttingen). The polymerization duration and annealing temperatures varied dependent on each application. PCR programs were generally used with 35-30 cycles, at a denaturation temperature of 95°C, and a polymerization temperature of 72°C. In the case of oligonucleotides containing restriction sites, the PCR reaction was first carried out for 4-5 cycles at a lower annealing temperature then the melting temperature of the primers. For used primers see **(Table VI. 13)**.

Standard PCR reaction

> 2.5 µl 10x PCR buffer + 50 mM MgCl$_2$
>
> 2.5 µl 10x BSA
>
> 2.5 µl 2.5 mM dNTP
>
> 2 µl each 5 picomole Primer fwd and rev
>
> 1 µl DNA template (10- 30 ng)
>
> 0.5 µl Taq DNA polymerase
>
> filled up to 25 µl with autoclaved dd H$_2$O

Table VI. 13. Primers used for PCR in this study

Restriction sites are *italic*, start and stop codons are underlined.

uncA amplification	
UncA_*Asc*I_fwd1	5´-G*GGCGCGCC*CGGC<u>ATG</u>GCGCCAGGAGGTGGTGGAAAC-3'
UncA_*Pac*I_rev1	5´-C*TTAATTAA*ACCTAGCACCGGTGGCTCCAGTCGAGTTC-3' Amplifying a 0.929-kb fragment
UncA_full_*Pac*I_rev	5´-C*TTAATTAA*<u>TCA</u>TCTCCCGGACCTGTTGGTCG-3'
UncA_4480_no_PH_*Pac*I_rev	5´-C*TTAATTAA*TCTCCCGGACCTGTTGGTCG-3'
UncA_3172_pENTR_fwd	5´-CACCCAGTTGTTTGTACCAGGCATCTCTG-3'

uncB amplification	
UncB_ATG2_*Asc*I_fwd	5'-G*GGCGCGCC*CGGC<u>ATG</u>GCGCTGGACCCTCGC-3'
UncB_ATG2_*Pac*I_rev	5'-C*TTAATTAA*CCATCTTGTTCTCCTCCATGAGC-3' Amplifying a 1.6-kb fragment, starting at the second ATG of *uncB*
UncB_full_*Pac*I_rev	5'-C*TTAATTAA*<u>TCA</u>GTTCCCCAAGATGTCCCC-3'
UncB_full_*Xma*I_fwd	5'-G*CCCGGG*<u>ATG</u>GCGCTGGACCCTCGC-3'
UncB_full_*Xma*I_rev	5'-G*CCCGGG*<u>TCA</u>GTTCCCCAAGATGTCCC-3'

ttlA amplification	
TTL_*Asc*I_ATG_fwd	5'-G*GGCGCGCC*CGGC<u>ATG</u>CATATTCTTGTGG-3'
TTL_*Pac*I_Stop_rev	5'-C*TTAATTAA*<u>TCA</u>ATTCTTCCTCCCAAGATCCAGC-3'

tlgA^{tlg1} amplification	
Tlg1_*nidulans*_*Asc*I_fwd	5'-G*GGCGCGCC*CGGC<u>ATG</u>TTCGGGGAAGTTTC-3'
Tlg1_*nidulans*_*Pac*I_rev	5'-C*TTAATTAA*CCCGCCCACGCAAGAAGGCC-3'

tlgB^{tlg2} amplification	
Tlg2_nidulans_*Asc*I_fwd	5'-G*GGCGCGCC*CGGC<u>ATG</u>TGGCGGGACCG-3'
Tlg2_*nidulans*_*Pac*I_rev	5'-C*TTAATTAA*<u>CTA</u>CGGGGCAACGATGCGGCC-3'

| **TlgB_mitte_*Pac*I_rev** | 5'-C*TTAATTAA*TTCATCTCCGCTACTCACCCCCCC-3' |

alpB^alp6 amplification (fusion PCR)

Alp6_mitte_fwd	5´-GGGAGGACAAATACAAACTCG-3'
Alp6_linker_rev	5´-ctccagcgcctgcaccagctccTTGCTCAGTCGAATCCTTCTTTTC-3'
Alp6_RB_link_fwd	5´-atcagtgcctcctctcagacagTAGCATACATGCAGTACATTTCTCG-3'
Alp6_RB_rev	5´-ACCGTCATGGCAGAAACGAAG-3'
Alp6_Nprimer_rev	5´-TTATCACCTGCTGGTTCTGAG-3'
Alp6_Nprimer_fwd	5´-CCAGTCTCGAGACCTCAATTG-3'

alpC^alp4 amplification

| **Alp4_ATG_*Asc*I_fwd** | 5´-G*GGCGCGCC*CGGCCAC<u>ATG</u>AACCCGCCACG-3' |
| **Alp4_full_*Pac*I_rev** | 5´-C*TTAATTAA*CCCAATCCGCGCAGGGTCG-3' |

tubA amplification

| **New_A tub_*Asc*I_fwd** | 5'-G*GGCGCGCC*CGGC<u>ATG</u>AGAGAAGTCATTAG-3' |
| **A tub_1.4 *Xma*I_*Pac*I_rev** | 5'-*TTAATTAA*GGGCCCCGGGGCTGGCTGC-3' |

tubB amplification

AN7570_TUBA2_*Asc*I_fwd	5'-*GGCGCGCC*CGGC<u>ATG</u>CGAGGCGAG-3'
AN7570_TUBA2_*Pac*I_rev	5'-C*TTAATTAA*<u>TTA</u>GTACTCGGCTTCTTCGCC-3'
AN7570_TUBA2_1.4_*Pac*I_rev	5'-C*TTAATTAA*TACAAATCTCCTGTCCCTTCGATTC-3'

mipA (γ-tubulin) amplification

| **Gamma_tub_*Asc*I_fwd** | 5'-C*GGCGCGCC*CGGG<u>ATG</u>CCTAGGTATACCCTC-3' |
| **Gamma_tub_*Pac*I_rev** | 5'-C*TTAATTAA*<u>TTA</u>TACTCCAACTTCATCCTTTCC-3' |

apsB amplification

apsB_*Asc*I_fwd	5´-TTTG*GGCGCGCC*CGGC<u>ATG</u>ACTCTAAAAGAGCAAAGTAGTACG-3'
SRL_PTSl_rev	5´-CC*TTAATTAA*<u>TCA</u>tagacgggaAACTTCGATATC-3'
For adding the PTS1 motif to *apsB*, SRL sequence is in lower case letter	
ApsB_fwd_Entry_Vector	5'-CACCATGACTCTAAAAGAGCAAAGTAG-3'
ApsB_full_rev_no_Stop	5'-AACTTCGATATCAACTGTGATGCC-3'

pyroA amplification

| **A.F.pyro_*Not*I_fwd** | 5'-*GCGGCCGC*GTAAGGTCAGTTCG-3' |
| **A.F.pyro_*Not*I_rev** | 5'-*GCGGCCGC*AATGCACAGAACACC-3' |

GFP amplification

GFP_F1_effi	5'-CTCGAGGTCGACGGTATCG-3'
GFP_R1_effi	5'-CAGGTCGACTCTAGAGGATCC-3'
GFP_Innen_Primer	5'-CCATTACCTGTCCACACAATCTGCC-3'
GFP_rev_primer	5'-CATGCCATGTGTAATCCCAGCAGC-3'

mRFP1 amplification

| mRFPI_Efi_fwd | 5'-GTCATCAAGGAGTTCATGCGCTTC-3' |
| mRFPI_Efi_rev | 5'-TCGTACTGTTCCACGATGGTGTAG-3' |

Detection of mutants and homologous integrations

Pyr4-3'_raus	5'-CTCGAGGACGAGCCGC-3'
Pyr4-5'_raus	5'AGGAAGCAGTCGAGAGC-3'
Raus_pyro_3'	5'-GGCCAAGAGAGGATGGTAATTGC-3'
Raus_pyro_5'	5'-CGTCAGGAACAGCTGGAAACGCC-3'
Raus_LB_UncA _fwd	5'-CGTCTGCTTAGACATTCCTTCCCC-3'
Raus_RB_UncA_rev	5'-CAGAGAATGCAAGGTCGCTTTGCC-3'
Raus_LB_UncB_fwd	5'-GTTTCTCAACGCTGGGATCAAGCG-3'
Raus_RB_UncB_rev	5'-GTCTTTGCTTGTGCTTCTGGGACC-3'
TTL_Raus_LB_fwd	5'-GATATTTGTGTCCGCCCTCGC-3'
TTL_Raus_RB_rev	5'-TCAAACGGACATAGCAGACATCGTCACC-3'
UncA_Innen_rev	5'-GTTAATGTCGGCAGGTGATATCGCG-3'
UncB_Innen_rev	5'-AGATCCGGCTCTGTTTCTGCCTCC-3'

Gene borders amplification, deletion cassettes

UncA_LB_fwd	5'-CGTCGATGGAAGGCATATACTACTCGC-3'
UncA_LB_*Sfi*I_rev	5'-C*GGCCATCTAGGCC*GACAACAAATTGC-3'
UncA_RB_*Sfi*I_fwd	5'-C*GGCCTGAGTGGCC*TCTATGTCTTCG-3'
UncA_RB_rev	5'-CATCCACGTCCCCATAACTAATACCACC-3'
UncB_LB_fwd	5'-GGAAGTACACCTGCATGCTAATATCATCAG-3'
UncB_LB_*Sfi*I_rev	5'-C*GGCCATCTAGGCC*GCGGTGAAGTATAG-3'
UncB_RB_*Sfi*I_fwd	5'-C*GGCCTGAGTGGCC*TGTTATGCGACGATG-3'
UncB_RB_rev	5'-GACGAGCAAGGGACGTGCCCTTCGGTG-3'
TTL_LB_fwd	5'-AATCGGGTCTGATCTCGTCCCAAGCGTACG-3'
TTL_LB_*Sfi*I_rev	5'-C*GGCCATCTAGGCC*TAGAAACACCATTCACG-3'
TTL_RB_*Sfi*I_fwd	5'-C*GGCCTGAGTGGCC*TAATCTCGAATATAGT-3'
TTL_RB_rev	5'-CGAGCCGATATTCGCTATGTACCTTGATAT-3'

Native promotor amplification	
UncA_nat (p)_*Eco*RI_fwd	5'-G*GAATTC*TCATCACCTACTGGAGGCGCGC-3'
UncA_nat (p)_*Kpn*I_rev	5'-C*GGTACC*TTTGGCCTATAGCCCATACACC-3'
γ tub_nat (p)_*Eco*RI_fwd	5'-G*GAATTC*CATACCCAGCATAAATTCGG-3'
γ tub_nat (p)_*Bsi*WI_rev	5'-C*CGTACG*CTTTCTTGCTTGCCTTAAG-3'
UncB_nat (p)_*Avr*II_fwd	5'-G*CCTAGG*TTATATCGGGAACTGTCACC-3'
UncB_nat (p)_BsiWI_rev	5'-C*CGTACG*ACAGAAGGTCGGTGTACC-3'
apsB_nat (p)_*Avr*II_fwd	5'-G*CCTAGG*CAAGCCGCAACTCCC-3'
apsB_nat (p)_*Kpn*I_rev	5'-C*GGTACC*GGATCTGCCACTGCG-3'
*Pfo*I_TubA (p)_fwd	5'-CCGCTG*TCCCGGA*CAGAGGTTTTCAAGAG-3'
*Pfo*I_TubA (p)_rev	5'-*TCCGGGA*CTTGTCTAGGTGGGTGGTGAGGG-3'

4.3.2. Cloning of PCR fragments

For the cloning of PCR products, restriction enzyme sites were added to both primers, or TA cloning was used. For TA cloning, the PCR products amplified with Expand (Roche, Mannheim) or other proof reading polymerases (e.g. Pfu, Promega, Madison, WI, USA) were incubated with Taq polymerase and then cloned into pCR2.1 TOPO (Invitrogen, NV Leek, The Netherlands).

4.3.3. Site directed mutagenesis

The P-loop sequences of *uncA* (pAS3)*, uncB* (pNZ2 and pNZSI48) and *kinA* (pCS2-NZ) were mutated using the maintained plasmids as a template **(Table VI. 05)** and the QuikChange XL site directed mutagenesis kit of Stratagene giving pNZ15, pSI-NZ32, pNZ75 and pCS4-NZ respectively. The same method was used to generate stop codons in place of tyrosine or two stop codons in place of tyrosine and glutamic acid at the C-terminal part of *tubA* using the plasmid pNZ64 (Tyr-tubulin) as a template to give pNZ65 (Glu-tubulin) and pNZ66 (Δ2-tubulin) respectively. Successful mutagenesis was confirmed by commercial sequencing (MWG Biotech, Ebersberg).

Table VI. 14. Primers used for this method:

UncA_P-Loop_Gly_fwd	5'-GGTCAGACCGGTTCG<u>GAG</u>AAGTCTTACTCG-3'
KinA_Rigor_P-loop_fwd	5'-CGGTCAAACCGGTGCA<u>GAG</u>AAGTCGTATAC-3'
UncB_Rigor_P-loop_fwd	5'-CGGTCAA<u>CCA</u>GGTTCT<u>GAG</u>AAGAGTTATAC-3'
Tyrosine_mut_TubA_fwd	5'-GGAGGGTGAGGAAGTTGAG<u>TAG</u>TAAGTGTAATGC-3'
E-Y_mut_3 Stop_TubA_fwd	5'-GGAGGGTGAGGAAGTT<u>TAGTAG</u>TAAGTGTAATGC-3'

And the corresponding reverse primers, nucleotides corresponding to the mutated amino acids are underlined

4.3.4. PCR from *A. nidulans* spores

Extraction of DNA of filamentous fungi for PCR analysis is usually time consuming and generally expensive, especially when it is done in order to check a great number of transformants for different mutations. To avoid this, conidia of *A. nidulans* were used directly for PCR analysis, without isolation of DNA. The PCR assay was performed with conidia obtained from freshly grown colonies on agar plates, at 37°C or 30°C for 2 days. The spores were harvested by gently scraping the colony surface with a sterile wire and transferred to the lid of an Eppendorf cup filled with 100 µl sterile ddH$_2$O. Collection of medium by this harvest was avoided, since agar may inhibit the PCR reaction. The samples were vigorously vortexed and the appropriate spore concentration was adjusted in a reaction tube (10^4-10^6 spores per reaction), followed by freezing them for 10-15 min at -80°C. The mix was added proportionally to the samples and they were generally subjected to the following PCR conditions: denaturation at 95°C for 5 min, 30 cycles of 95°C for 18 sec, appropriate annealing temperature and time, 72°C for 1-2 min, followed by 72°C for 5-10 min.

4.3.5. DNA sequencing

DNA sequencing was done by commercial sequencing (MWG Biotech, Ebersberg).

4.4. Transformation

4.4.1. Transformation of *E. coli*

The transformation of electrocompentent *E. coli* cells was done as described (Ausubel *et al.*, 2001). After dialysis of the ligation reaction product, 5 µl ligation solution and 50 µl *E. coli* electrocompetent cells were mixed and filled into a transformation glas cuvette (PEQLAB, Erlangen). The plasmids were transformed by electroporation with an electro shock of 2.5 kV for 5 ms (Gene-Pulser, Bio-Rad) into cells of the electrocompetent *E. coli* strain XL1-Blue (Stratagene, La Jolla, USA). Alternatively, chemically competent cells of the *E. coli* strain TOP10 F' (Invitrogen, Leek, Netherlands) were used according to the distributor's protocols.

4.4.2. Transformation of *A. nidulans*

Standard procedures of *Aspergillus* protoplast transformation were used (Yelton *et al.*, 1984). Spores were harvested from freshly grown plates (~109 conidia), inoculated in 500 ml volume minimal medium with appropriate suppplements, and shaken at 30°C in a water bath

for 12-16 h until the spores had germinated. The culture was filtered through sterile Miracloth followed by washing with Wash solution. The washed mycelium was collected on ice in a sterile 100 ml Erlenmeyer flask with 5 ml of Osmotic medium. After addition of GlucanX (Novozyme, 180 mg/ml sterile water) and 5 min incubation on ice, BSA (10 mg/0.5 ml sterile ddH$_2$O) was added into the flask. Subsequently, the digestion mixture was incubated at 30°C 70 rpm for 1-2 h until enough protoplasts were released. Then, after transfer in a 30 ml Corex tube, 10 ml of Trapping buffer was slowly added, followed by a centrifugation at 5000 rpm for 15 min using a HB-6 rotor. The obtained protoplast band was transferred into a new sterile tube, followed by washing with STC and centrifugation at 7000 rpm for 10 min. The protoplast pellet was gently resuspended in 100-300 µl STC for following transformation (for the solutions used, see **Table VI. 15**). 100 µl of protoplasts in STC and 100 µl DNA (10 µg DNA filled up to 100 µl STC) were mixed and incubated for 25 min at room temperature in a sterile falcon tube. Then, 2 ml PEG was added and the tube was rolled until the mixture was homogeneous, followed by 20 min incubation at room temperature. Finally, 8 ml STC was added and the entire mixture was spread onto osmotically stabilized medium (MM + 0.6 M KCl) with appropriate selection markers. The plates were incubated at 37°C until colonies were visible after 3- 4 days.

Table VI. 15. Solutions used for *A. nidulans* transformation

Solution	Composition
Mycelium wash solution	0.6 M MgSO$_4$
Osmotic medium	1.2 M MgSO$_4$, 10 mM Na$_3$PO$_4$ buffer, pH 5.8
Trapping buffer	0.6 M sorbitol, 0.1 M Tris-HCl, pH 7.0
STC	1.2 M sorbitol, 10 mM CaCl$_2$, 10 mM Tris-HCl, pH 7.5
PEG	60% PEG 4000, 10 mM CaCl$_2$, 10 mM Tris-HCl, pH 7.5

4.5. DNA-DNA hybridization (Southern blot analysis)

DNA-DNA hybridization was performed using DIG labelled DNA-PCR probes, amplified using the PCR DIG Probe Synthesis Kit from Roche (Mannheim), according to the distributor's protocols. The genomic DNA sample was digested overnight with the appropriate restriction enzyme. Next day DNA sample and positive control were separated at 50 V for 3-4 h through 1.2% long agarose gel electrophoresis, until the Bromphenole blue band was weakly visible in the lower third of the gel. Afterwards, the gel was stained with ethidium bromide and the marker bands were marked by making little holes with a 1µl pipet tip, than the gel was

washed for 10 min in depurination solution and denaturated through 2 times 15 min incubation in denaturation solution. After rinsing briefly in water, the gel was equilibrated by 2 times 15 min washing with neutralization solution and afterwards 10 min equilibration with 20x SSC.

After equilibration, the DNA bands were transferred overnight at RT by capillary forces to a neutral nitrocellulose membrane (Pall Gelman Laboratories, Dreieich). The transfer was setted up (bottom to top) as followed: A bridge of whatman paper (presoaked in 20x SSC and making contact to 20x SSC reservoirs at both ends), Gel (upside down), membrane (presoaked in 20x SSC), 3 layers of whatman paper (presoaked in 20X SSC), several layers of tissue and a glas plate. After blotting the membrane was cross-linked with UV radiation (254 nm, 1.200×10^2 µJ for each side). The membrane was then prehybridized in hybridization solution for 1h at 68°C and then further hybridized for 12 h with the probe at 68°C (Yoshida *et al.*), followed by stringent washing. The first washing step consisted of 2 washing times with 2x washing solution for 5 min at RT, respectively. In the second step the membrane was washed 2 times for 15 min at 68°C in 0.5x washing solution, respectively. After 5 min at RT in washing buffer, the membrane was incubated for 1h at RT in blocking buffer followed by 30 min incubation with 2 µl anti-DIG-Antibody-AP (Roche; 11 093 274 910) in 20 ml new blocking buffer. Free antibodies were washed away 2 times for 15 min in Washing buffer at RT. Finally the membrane was equilibrated in AP-buffer for 5 min at RT and transferred to a plastic film with AP-Substrate distributed evenly above (5 µl CDPStar, Roche in 500 µl AP-buffer). Detection was accomplished by means of autoradiography using films from Kodak (Rochester, NY, USA) or Fuji (New RX, Fuji, Japan). If the membrane was reused, stripping was carried out in stripping buffer, two times for 15 min at 37°C, followed by equilibration for 5 min in 2x SSC. The stripping result was checked by autoradiography (for the solutions used, see **Table VI. 16**).

Table VI. 16. Solutions used for Southern blot

Solution	Composition
Hybridization solution	5x SSC; 0.02% SDS; 1% Blocking Reagent (Roche); 0.1% N-Laurylsarcosin
Depurination solution	0.25 M HCl
Denaturation solution	0.5 M NaOH; 1.5 M NaCl
Neutralization solution	1.5 M NaCl; 0.25 M Tris-HCl, pH 7.5
20 x SSC	3 M NaCl; 0.3 M NaCitrat, pH 7.0
2 x Washing solution	2x SSC; 0.1% SDS
0.5 x Washing solution	0.5 x SSC; 0.1% SDS

Washing buffer	100 mM Maleic acid; 150 mM NaCl; 0.3 % Tween20
Blocking buffer	100 mM Maleic acid, 150 mM NaCl; 1 % Blocking Reagent
AP-buffer	0.1 M Tris-HCl, pH 9.5; 0.1 M NaCl; 50 mM MgCl2
Stripping buffer	0.2 M NaOH; 0.1% SDS

4.5.1. Construction of a cDNA library

A cDNA library was constructed using isolated total RNA as template (see 4.6.1), and the Matchmacker[TM] Two-Hybrid Library Construction & Screening Kit from Clontech according to the distributor's protocols.

4.6. RNA manipulations

4.6.1. Isolation of total RNA from *A. nidulans*

For the isolation of total RNA, 500 ml CM liquid culture inoculated with spore suspension from one plate was shaken at 200 rpm for 14 h at 37°C. The overnight grown mycelium was harvested, dried between paper towels, frozen in liquid nitrogen and grounded in a mortar. RNA extraction from grounded mycelium powder was carried out with TRIZOL (Gibco or Invitrogen) according to manufacturer protocol. The RNA was finally dissolved in 40-50 μl sterile DEPC H_2O with 0.5 U/μl RNase inhibitor (Promega, Mannheim). The RNA concentration was measured in a photometer (Pharmacia LKB, UltraspecIII). The RNA samples were diluted to 1 μg/μl with DEPC H_2O containing RNase inhibitor. The samples were kept at -80°C.

5.   Biochemical methods

5.1. Isolation of protein from *A. nidulans*

For protein extraction, spores were incubated overnight in liquid media (with 2% threonin for *alcA(p)* induction) shaking at 200 rpm at 37°C. The grown mycelium was filtered, dried and grounded in liquid nitrogen as for genomic DNA extraction. Then, the obtained powder was resuspended in the same amount of protein extraction buffer (20 mM TrisCl pH 8.0; 0-0.2 % Triton X-100; 150 mM NaCl, 10 μl Protease Inhibitor Cocktail, Sigma, Taufkirchen). The

slurry was centrifuged at 13.000 rpm at 4°C for 10 min and the total protein concentration of the supernatant was measured according to Bradford (Bradford, 1976). After centrifugation, the supernatant was stored at -80°C or aliquots selected for analysis were heated at 95°C for 5 min together with 4x SDS-gel loading buffer (240 mM Tris/HCl, pH 6.8; 8 % SDS; 40 % Glycerol; 12 % DTT; 0.004 % Bromophenol blue) prior to loading.

5.2. Determination of protein concentration (Bradford Assay)

Protein concentration was determined according to Bradford (Bradford, 1976) using the Roti®-Quant Reagent from Roth (Karlsruhe). This measurement is based upon Coomassie® Brilliant Blue G-250 dye-binding assay. Acryl-cuvettes (Sarstedt, Nümbrecht) were used for the determination of the protein concentration. 200 μl Roti®-Quant Reagent were added to samples (1 μl protein extraction buffer/ 0.8 ml ddH$_2$O), same was done with the standard protein (bovine serum albumin, BSA), afterwards they were gently mixed. After 5 min, the absorbance was measured in the photometer (Pharmacia LKB, UltrospecIII) at 595 nm. The standard curve was established with BSA (bovine serum albumin).

5.3. SDS Polyacrylamide Gel electrophoresis (SDS-PAGE)

For immunodetection of proteins Western blotting was performed. The SDS-PAGE gel consisted of a resolving gel overlaid by a stacking gel. The resolving gel was casted between the glass plates using Bio-Rad Mini Protean II equipment and overlaid with a thin layer of ddH$_2$O. After gel polymerization, the water was removed and the gel chamber was filled up with stacking gel. Protein samples were diluted to appropriate concentrations using 4x SDS gel-loading buffer, heated at 95°C for 5 min and loaded onto the gel. Electrophoresis took place at room temperature, first at 50 V until the sample moved out from the wells and then 100-120 V until tracking dye reached the bottom of separating gel (for the solutions used, see **Table VI. 17**).

Table VI. 17. Solutions used for SDS-PAGE

Solution	Composition
1x SDS gel electrophoresis buffer	3 g Tris-base; 18.8 g Glycine; 10 ml 10% SDS-solution in 1 liter of ddH$_2$O
5% Stacking Gel	0.83 ml 30% Acrylamid-Mix; 0.63 ml 1 M Tris pH 6.8; 0.05 ml 10% SDS; 0.1ml 10% APS; 0.006 ml TEMED; 4.6 ml ddH$_2$O.

8% Resolving Gel	2.7 ml 30% Acrylamid-Mix; 2.5 ml 1.5 M Tris pH 8.8; 0.1 ml 10% SDS ; 0.1 ml 10% APS; 0.006 ml TEMED; 4.6 ml ddH$_2$O.
4x SDS gel-loading buffer	200 mM Tris-HCl pH 6.8; 400 mM DTT; 8% SDS; 0.4% Bromophenolblue; 40% Glycerol

5.4. Western blotting and immunodetection

After electrophoresis, proteins were transferred from the gel to a Protran nitrocellulose transfer membrane (Whatman; Dassel). Electroblotting was performed in a "sandwich" assembly in Transfer buffer from 3 h to overnight at 30 mA at 4°C using Mini Trans-Blot® transfer gel apparatus (Bio-Rad, Munick). After transference, the membrane was stained for 5 min in Ponceau S solution, and then washed with water until the protein bands were distinctly visible. The membrane was incubated in blocking solution for 1 h at RT, then the hybridization with the first antibody diluted in blocking solution was done for 1-2 h at RT or overnight at 4°C. Afterwards, the membrane was washed 4 x 5 min in TBS-T, incubated for 1 h at RT with the peroxidase conjugated secondary antibody diluted with TBS-T and followed by 4 x 5 min washing in TBS-T (for the solutions and antibodies used, see **Table VI.18**). The detection was done with Luminol Solution as substrate for the horse raddish peroxidase (HRP). If the membrane was reused, stripping was carried out in stripping buffer, two times for 15 min at 50°C, followed by 2x washing for 5 min in washing buffer.

Table VI. 18. Solutions used for Western blot

Solution	Composition
10 x Transfer buffer	30.3 g Tris; 144 g Glycine in 1 liter of ddH$_2$O
Protein Transfer buffer	100 ml 10x Transfer buffer, 200 ml Methanol, 700 ml ddH$_2$O
Ponceau-S	0.1% Ponceau-S in 1% Acetic acid
10 x TBS	24.2 g Tris, 80 g NaCl in 1 liter of ddH$_2$O, pH 7.6
1 x TBS-T	1 x TBS, 0.1% Tween 20 (100%)
Blocking solution	TBS-T with 5% Skim milk
Primary antibody	Monoclonal antibody HA-11, clone 16B12, produced in mouse (MMS-101R, Hiss Diagnostics), dilution 1:1.000 in Blocking solution
	Anti-GFP, N-terminal, antibody produced in rabbit (G1544, Sigma, Steinheim), dilution 1:4.000 in Blocking solution
	Monoclonal anti–γ-tubulin clone GTU-88 produced in mouse (T-6557, Sigma, Steinheim), dilution 1:500 in Blocking solution
	Anti-γ-tubulin antibodies developed in Rabbit (T-3559, Sigma, Steinheim), dilution 1:500 in Blocking solution

Secondary antibody	Anti mouse IgG (Fab specific)-peroxidase conjugate antibody developed in goat (A2304, Sigma, Steinheim), dilution 1:10.000 in TBS-T
	Anti rabbit IgG (whole molecule) peroxidase conjugate Antibody (A0545, Sigma, Steinheim), dilution 1:4.000 in 1 x TBS-T
Luminol solution	1 ml solution A (50 mg Luminol in 200 ml 0.1 M Tris-HCl pH 8.6) 0.1 ml solution B (11 mg p-Hydroxycoumarin acid in 10 ml DMSO) 0.3 µl 35 % H_2O_2
Stripping buffer	1 X TBS; 2 % SDS; 0.1 M beta-Mercaptoethanol

5.5. Co-Immunoprecipitation

For immunoprecipitation a volume of 1 ml protein extract (about 1 mg/ml) was adjusted to 300 mM NaCl with 5 M NaCl and incubated with the appropriate monoclonal first antibodies, Monoclonal antibody HA-11 clone 16B12 produced in mouse (MMS-101R, Hiss Diagnostics) dilution 1:200, or Anti-GFP N-terminal antibody produced in rabbit (G1544, Sigma, Steinheim), dilution 1:800. After 1h incubation at 4°C, 50 µl Protein-G-Agarose (Roche, Mannheim, Germany) were added and incubated for additional 3h. Agarose beads were pelleted by centrifugation in an Eppendorf Centrifuge at 15.000 rpm at 4°C for 30s and washed three times with 1ml protein extraction buffer (paragraph 5.1, page 112). CoIP pellet was resuspended with 4 x SDS gel-loading buffer and denaturated for 5 min at 95°C. Protein extracts and CoIP pellets were loaded on a SDS-PAGE gel. For Western blotting antibodies raised against GFP, HA or γ-tubulin were used **(Table VI. 18)**.

6. Microscopic methods

6.1. Light and fluorescence microscopy

Light and fluorescence images were taken with the Zeiss Microscope "AxioImager Z1" (Carl Zeiss, Jena, Germany) Software: AxioVision V4.5, using a Planapochromatic 63x or 100x oil immersion objective lens, and the Zeiss AxioCam MRM camera. As UV lamp was used the HBO103 mercury arc lamp (Osram). Dynamic processes in the hyphae were quantified using the same software analyzing series of single pictures.

Alternatively the "Axiophot" Zeiss microscope was used, with a Planapochromatic 63x or 100x oil immersion objective lens and a CCD camera from Hamamatsu (Orca ER II (Software: Wasabi 1.4)) with optional RGB Modus. As UV lamp was used the Osram HBO50 mercury arc lamp (Osram). Time-lapse series were obtained with an automated Wasabi

program that acquires series of images with pause time, exposure time, and different exposures in each sequence. Image and video processing was done with Photoshop 6.0 (Adobe) and freeware programs such as ImageJ and VirtualDub (for filter setting see **Table VI. 19**).

Table VI. 19. Fluorescence microscopy filters

Fluorescent dye	Excitation filter Band-pass filter (BP) nm	Beam splitter (BS) nm	Barrier filter Long pass filter (LP) nm
sGFP FITC	450 – 490	510	520
YFP	D 510/20	530 DCLP	D 560/40
DsRed	546	580	590
DAPI Hoechst 33342	365	395	397

6.2. Preparation of microscopy samples

For live-cell imaging of germlings and young hyphae, cells were grown on coverslips in 0.5 ml of MM 2% glycerol (de-repression of the *alcA* promoter, moderate induction) or MM 2% glucose (repression of the *alcA* promoter). Cells were incubated at room temperature for 1–2 days. For pictures of young hyphae of each strain, the spores were inoculated on microscope slides coated with MM 2% glucose 0.8% agarose and grown at 30°C for 1 d. Images were captured at room temperature (200 msec. exposure time).

For timelapse studies, cells were incubated in glass bottom dishes (World Precision Instruments, Berlin) in 2 ml of MM glycerol or MM glucose medium. Incubation was at 30°C for 15 h or at RT for 24 h and images were captured at RT. In the case of DAPI staining for visualization of nuclei, strains were grown for 8 h at 37°C on coverslips with 500 µl appropriate medium, incubated with methanol and aceton (1/1) for 30 sec followed by 5 min incubation with 25µl mounting media with Vectashield DAPI (Vector Laboratories Inc., Burlingame CA).

6.3. Confocal Laser-Scanning Microscopy (CLSM)

Confocal images were taken with the TCS SP5 from Leica, and with the Cell Observer-SD confocal spinning disk microscope from Zeiss, using a planapochromatic 63x or 100x oil immersion objective lens. The Argon laser 65 mW (457 nm, 476 nm, 488 nm, 514 nm) was

used for GFP excitation, and the HeNe 1.2 mW (543 nm) laser for for DsRed excitation. Samples were prepared as described in 6.2.

6.4. Software used in this study

Microscopy:

Wasabi Software V 1.2 from Hamamatsu for Orca ERII camera

Zeiss AxioVison V4.5

Leica TCS SP5 Software packet

Image and Video manipulation

VectorNTI (Invitrogen):	Tree analysis (AlignX)
NCBI:	Blast analysis BlastP, BlastN
Adobe Photoshop CS:	brightness and contrast
ImageJ :	Video converting (avi)
virtual dub V 1.6:	Video manipulation
TMPGEnc (pegasys):	Video converting and manipulation (mpg, avi, mov)
RAD VideoTools:	mov to avi

6.5. Legends to the movies

Movie IV. 01.

GFP-UncA movement in a hyphal compartment of *A. nidulans*.

Movie IV. 02.

mRFP1-UncA movement along a GFP stained microtubule.

Movie IV. 03.

A. nidulans (TN02A3) treated with FM4-64.

Movie IV. 04- IV. 08.

FM4-64 vesicle movement in different mutant strains as indicated.

Movie IV. 09.

Depolymerization of a stable MT bundle toward septal MTOC in a mitotic cell of the GFP-α-tubulin strain sNZ77.

Movie IV. 10.

GFP-UncA movement in mitotic cells. Mitotic nuclei were observed with DsRed-StuA. Strain sNZ4.

Movie IV. 11.

depolymerization pattern of GFP-UncA^{rigor}-MT-bundle. Strain sNZ14.

Movie IV. 12.

Localization of mRFP1-TtlA to the cytoplasm and to microtubules. Strain SCS8-NZ86.

Movie IV. 13.

Localization of GFP-UncB to the nucleus and at septa depends on the cell cycle. Strain SNZ1.

7.   Bimolecular Fluorescence Complementation Assay (BiFC)

The bimolecular-fluorescence-complementation assay (BiFC) is another technique to analyze protein-protein interactions (Meng *et al.*, 2005). In the BiFC assay, a fluorescent protein like YFP is split into two halves, and those halves are fused to one of the two proteins of interest. If the two respective proteins interact, the two YFP halves are brought into close contact upon which the fluorescent ability is restored. This assay can be used in the organism one is working with, and the fluorescent signals are comfortable since no fixation is needed. Furthermore, the signals are observable *in vivo* and most importantly one can directly determine the location of interaction. The system in *A. nidulans* was recently established (Blumenstein *et al.*, 2005).

8.   Immunostaining

10^3 Spores/ml were inoculated with 0.5 ml MM on sterile coverslips for 12-24 h at RT. Cells were fixed for 30 min with formaldehyde, washed 2 times with PBS and digested for 1 h using digestion solution. Then the cells were washed again with PBS for 3 times and incubated for 10 min at -20°C with methanol. Afterwards samples were washed again for 2 times with PBS, and blocked for 15 min at RT with blocking solution, before overnight incubation at 4°C with first antibodies diluted in blocking solution. Next, cells were washed 4 times with TBS-T and incubated for 1 h at RT with second antibodies diluted in TBS-T (for antibodies see **Table VI. 21**). After washing for 4 times with TBS-T, coverslips were mounted on microscope slides with 25 μl mounting media with DAPI (Vector Laboratories Inc., Burlingame CA), sealed with nail polisher and stored at 4°C overnight in the dark before doing the microscopy (for solutions see **Table VI. 20**).

Table VI. 20. Solutions used for immunostaining

Solution	Composition
100ml Fixative solution	50 ml 200 mM PIPES pH6.7; 10 ml 500 mM EGTA pH8.5; 1 ml 1 M MgSO4; 10 ml DMSO; 21.6 ml 37% Formaldehyde
1x Phosphate buffered saline (PBS)	8 g NaCl; 0.2 g KCl; 1.44 g Na_2HPO_4; 0.24 g KH2PO4 in 1 liter of ddH_2O, pH 7.4
Digestion solution	50 mM sodium citrate pH 5.8 with 50% albumin with the next 4 enzymes (albumin could be aliquoted and frozen at -20°C): -Driselase 10.88-21.8 mg/ml, (D9515) Sigma Aldrich -Zymolyase (5U/μl) 1-2 μl/ml, (E1004) Zymo Research California -GlucaneX 80-160 mg/ml, (Glucanex 200G) Lamothe-Abiet France -β-D Glucanase 4-8 mg/ml, (0439-1) Interspex Products Inc., San Mateo, USA. (Stock solution 100 mg/ml in 100 mM sodium citrate pH 4.5, heated at 55°C for 5 min, than incubated on ice 30 min to reduce protease activity)
10 x TBS	24.2 g Tris; 80 g NaCl in 1 liter of ddH_2O, pH 7.6
1x TBS-T	TBS, 0.1% Tween 20 (100%)
Blocking solution	TBS-T with 5% Skim milk
Mounting media	0.1 M Tris-HCl pH 8; 50% Glycerol; 1 mg/ml phenylendiamine; optional DAPI (depend on the amount of material, range 0.1-1 μg/ml). Or use the commercial mounting media with DAPI from VECTASHIELD (H-1200, Burlingame, CA)
Methanol	

Table VI. 21. Antibodies used for immunostaining

Primary Antibodies

Anti-γ-tubulin antibodies developed in rabbit (T-3559, Sigma-Aldrich).

Monoclonal anti–γ-tubulin clone GTU-88 produced in mouse (T-6557, Sigma-Aldrich)
Immunogen is a synthetic γ-tubulin peptide (AA 38-53), conjugate to KLH. The antibody recognize an epitope located within the N-terminal region of γ-tubulin.

Anti-GFP, N-terminal, antibody produced in rabbit (G1544, Sigma-Aldrich)
Peptide corresponding to amino acids 3-17 of the Green Fluorescent protein (GFP) from jellyfish *Aequorea Victoria*, conjugated to maleimide-activated KLH through an N-terminal added cysteine residue as immunogen.

Monoclonal antibody HA-11, clone 16B12, produced in mouse (MMS-101R, Hiss iagnostics)
It is raised against the twelve AA peptide CYPYDVPDYASL. It recognizes the influenza hemagglutinin epitope (YPYDVPDYA).

Monoclonal anti-α-tubulin clone DM1A, produced in mouse (T-9026, Sigma-Aldrich)
Purified chick brain tubulin was used as the immunogen.

Monoclonal anti-tubulin, acetylated, antibody, clone 6-11B-1, produced in mouse (T6793, Sigma-Aldrich)
The immunogen was acetylated tubulin from the outer arm of *Strongylocentrotus purpuratus* (sea urchin). The antibody recognizes an epitope located on the α3 isoform of *Chlamydomonas* axonemal α-tubulin, within four residues of Lys-40 when this amino acid is acetylated.

Monoclonal anti-tubulin tyrosine, antibody, clone TUB-1A2, produced in mouse (T9028, Sigma-Aldrich)
The epitope was the C-terminal 10 amino acids with an added Tryosine SYEDEDEGEE(Y).This antibody was prepared according to the protocol in EMBO J. 1987 Sep;6(9):2597-606. The peptide sequence was derived from porcine brain.

Monoclonal anti-tubulin, polyglutamylated, antibody, clone B3, produced in mouse (T9822, Sigma-Aldrich)
Immunogen is a purified *Lytechinus pictus* (sea urchin) sperm axonemal proteins. The epitope recognized by the antibody is localized in the C-terminal region of α- and β-tubulins (the glutamylated motif at amino acid 445-457 of α-tubulin.

Polyclonal anti human tubulin (detyrosinated, Glu-Tubulin), produced in rabbit (OBT1660, AbD serotec) (detyrosinated, Glu-Tubulin)
The Immunogen is a synthetic peptide corresponding to the C-terminal portion of de-tyrosinated tubulin. It recognizes specifically the de-tyrosinated form of the tubulin alpha chain (Glu tubulin).

Secondary Antibodies

Anti mouse IgG (Fab specific)-FITC, antibody produced in goat using purified mouse IgG Fab fragment as the immunogen (F4018, Sigma-Aldrich)

Anti mouse TgG (whole molecule)-FITC, produced in goat using purified mouse IgG as immunogen, affinity Isolated antibody (F0257, Sigma-Aldrich)

Polyclonal Cy^{TM}3-conjugated affinipure goat anti mouse IgG (H+L), (115-165-062, Dianova)

Cy^{TM}3-conjugated affinipure goat anti-rabbit IgG (H+L), (111-165-045, Dianova)

9. Calcofluor white (CFW) and Congo red (CR) assay

The assay was done as described (Ram & Klis, 2006). Calcofluor white (CFW) fluorescent brightener (F-3543, Sigma) and Congo red (CR) (860956, Sigma) was added to the fungal growth medium. The free di-acid form of CFW (fluorescent brightener F-3543) does not directly dissolve in water. A 1% (wt/vol) stock solution was prepared by dissolving CFW in 0.5% (wt/vol) KOH and 83% (vol/vol) glycerol. CR was in the di-

Figure 30. The chemical structures of CFW (a) and CR (b)

sodium form, which is readily dissolved in water. Solutions were prepared fresh at the day of the experiment with protection from light by wrapping the containers in aluminium foil. The CM medium was buffered to pH 5.5–7.0 to prevent acidification, and therefore protonation and precipitation of CFW and CR. Buffering the medium was done with 50 mM phthalate-NaOH (pH 6.0). Solutions were added to the cooled agar CM medium (60°C- 70°C). The

plates were stored overnight in the dark at room temperature (15°C- 25°C), to be used the next day. Storing the plates for longer time period is not preferable.

A. nidulans spores from a wild-type and different deletion strains (*ΔuncA*, *ΔkinB*, *ΔuncA* and *ΔkinB* double deletion strain) were prepared as a 10-fold dilution series ($5x10^0$-$5x10^4$) and spotted in 10 μl volumes on plates containing CFW or CR and on a control plate. The plates were incubated in the dark at 30°C for 3 days. Sensitivity to CFW and CR is determined by comparing the extent of colony formation between parental and mutant strains on the control plate and the plates containing CFW or CR.

10. Glucoamylase secretion in *A. nidulans* in solid state- and submerged-fermentation

The protocol was done as described (te Biesebeke *et al.*, 2005). *A. nidulans* spores from a wild-type and different *uncA*-deletion strain were cultivated in liquid and solid minimal media **(Table VI. 08)** with 2% starch as a sole carbon source. Starch liquid medium was prepared by shaking 4 g soluble starch in 100 ml H_2O in shake flasks in a rotary shaker at room temperature for 5 min at 250 rpm. The suspension was poured through Miracloth, where 2 g of starch (dry weight) remained in the filter resulting in 2% starch liquid medium (SLM), which was sterilised for 15 min at 120°C. Surface growth on starch solid medium (SSM) was performed on 1% agar plates of 2% starch liquid medium. Submerged cultivations were performed with 25 ml SLM inoculated with 10^6 spores/ml and incubated in shake flasks at 30°C in a rotary shaker at 250 rpm. Solid state cultivation was performed after inoculation of nitrocellulose (NC) membranes (3 mm pore size) placed on the agar plates of 2% SSM (25 ml), with $2.5×10^7$ spores (10^6 spores/ml 2% SSM) followed by an incubation at 30°C. Liquid and membrane biomass transfer cultivations were performed as described by (te Biesebeke *et al.*, 2005). After production of biomass in starch medium (17 h in 2% SLM and 48 h in 2% SSM) samples were transfered to fresh starch medium (2% SLM and 2% SSM, respectively). Samples taken at time points 0, 2, 6, 8, 10 and 12 h in the case of membrane biomass transfer cultivation, and 0, 0.5, 1, 6, 8 and 24 h in the case of liquid transfer cultivation, were used for glucose determination. The wet weight biomass of *A. nidulans* grown in 2% SLM was determined after filtering the biomass through Miracloth. The wet weight biomass of *A. nidulans* grown on 2% SSM was determined after weighting the biomass grown on the filter. The extracellular growth medium (1 ml) of *A. nidulans* grown in 2% SLM was boiled for 5 min and used for determination of glucose concentrations. Extracts of the growth medium of *A. nidulans* grown on 2% SSM were obtained after removing the membrane with biomass and freezing the 2% SSM at -20°C. Subsequently, the 2% SSM was thawed and, after addition of

10 ml ddH$_2$O, vortexed for 2 min, centrifuged for 5 min at 3.500 rpm, boiled for 5 min and used for determination of glucose concentrations. Glucose concentration was analysed enzymatically using the glucose oxidase method (GOD), in which 0.1 ml sample with 2 ml GOD-reaction-solution (6 mmol KI; 1.5 mmol Na$_2$WO$_4$ and about 10 U GOD in 100 ml phosphate buffer, pH 7) were mixed, after 30 min the extinction was measured in a spectro-photometer (Pharmacia LKB, UltrospecIII) at 366 nm. To obtain the glucose concentration, the extinction was compared to a standard curve made by measuring extinctions of a glucose standard solution (1.11 mmol/l) with different dilutions (0.2; 0.4; 0.6 and 0.8 mmol/l).

In the case of solid state fermentation, SSM was covered with Gram's Iodine (0.33 g iodine; 0.66 g potassium iodine; 100 ml H$_2$O), which stains the remaining starch in the media. Halos surrounding the different strains were compared to estimate the amount of glucoamylase secretion.

VII. Literature

Abenza, J. F., Pantazopoulou, A., Rodriguez, J. M., Galindo, A. & Penalva, M. A. (2009). Long-distance movement of Aspergillus nidulans early endosomes on microtubule tracks. *Traffic* 10, 57-75.

Adio, S. & Woehlke, G. (2009). Properties of the kinesin-3 NcKin3 motor domain and implications for neck function. *FEBS J* 276, 3641-3655.

Akhmanova, A. & Hoogenraad, C. C. (2005). Microtubule plus-end-tracking proteins: mechanisms and functions. *Curr. Opin. Cell Biol.* 17, 47-54.

Al-Bassam, J., Cui, Y., Klopfenstein, D., Carragher, B. O., Vale, R. D. & Milligan, R. A. (2003). Distinct conformations of the kinesin Unc104 neck regulate a monomer to dimer motor transition. *J Cell Biol* 163, 743-753.

Al-Bassam, J., van Breugel, M., Harrison, S. C. & Hyman, A. (2006). Stu2p binds tubulin and undergoes an open-to-closed conformational change. *J. Cell Biol.* 172, 1009-1022.

Al-Bassam, J., Roger, B., Halpain, S. & Milligan, R. A. (2007). Analysis of the weak interactions of ADP-Unc104 and ADP-kinesin with microtubules and their inhibition by MAP2c. *Cell Motil Cytoskeleton* 64, 377-389.

Aldaz, H., Rice, L. M., Stearns, T. & Agard, D. A. (2005). Insights into microtubule nucleation from the crystal structure of human gamma-tubulin. *Nature* 435, 523-527.

Allan, V. (1996). Motor proteins: a dynamic duo. *Curr Biol* 6, 630-633.

Aramayo, R., Adams, T. H. & Timberlake, W. E. (1989). A large cluster of highly expressed genes is dispensable for growth and development in *Aspergillus nidulans*. *Genetics* 122, 65-71.

Araujo-Bazan, L., Penalva, M. A. & Espeso, E. A. (2008). Preferential localization of the endocytic internalization machinery to hyphal tips underlies polarization of the actin cytoskeleton in Aspergillus nidulans. *Mol Microbiol* 67, 891-905.

Arce, C. A., Rodriguez, J. A., Barra, H. S. & Caputo, R. (1975). Incorporation of L-tyrosine, L-phenylalanine and L-3,4dihydroxyphenylalanine as single units into rat brain tubulin. *Eur. J. Biochem.* 59, 145-149.

Asai, D. J. & Koonce, M. P. (2001). The dynein heavy chain: structure, mechanics and evolution. *Trends Cell Biol.* 11, 196-202.

Asbury, C. L., Fehr, A. N. & Block, S. M. (2003). Kinesin moves by an asymmetric hand-over-hand mechanism. *Science* 302, 2130-2134.

Ausubel, F., Brent, R., Kingston, R. E., Moore, D. D., Seidman, J. G., Smith, J. A. & Struhl, K. (2001). *Short protocols in molecular biology*: John Wiley & Sons, Inc.

Baas, P. W., Pienkowski, T. P., Cimbalnik, K. A., Toyama, K., Bakalis, S., Ahmad, F. J. & Kosik, K. S. (1994). Tau confers drug stability but not cold stability to microtubules in living cells. *J. Cell Sci.* 107, 135-143.

Baas, P. W. & Qiang, L. (2005). Neuronal microtubules: when the MAP is the roadblock. *Trends Cell Biol.* 15, 183-187.

Badin-Larcon, A. C., Boscheron, C., Soleilhac, J. M. & other authors (2004). Suppression of nuclear oscillations in *Saccharomyces cerevisiae* expressing Glu tubulin. *PNAS* 101, 5577-5582.

Balance, D. J., Buxton, F. P. & Turner, G. (1983). Transformation of *Aspergillus nidulans* by the orotidine-5'-phosphate decarboxylase gene. *Biochem. Biophys. Res. Comm.* 112, 284-289.

Ball, E. H. & Singer, S. J. (1982). Mitochondria are associated with microtubules and not with intermediate filaments in cultured fibroblasts. *Proc Natl Acad Sci U S A* 79, 123-126.

Banuett, F., Quintanilla, R. H., Jr. & Reynaga-Pena, C. G. (2008). The machinery for cell polarity, cell morphogenesis, and the cytoskeleton in the Basidiomycete fungus Ustilago maydis-a survey of the genome sequence. *Fungal Genet Biol* 45 Suppl 1, S3-S14.

Beinhauer, J. D., Hagan, I. M., Hegemann, J. H. & Fleig, U. (1997). Mal3, the fission yeast homologue of the human APC-interacting protein EB-1 is required for microtubule integrity and the maintenance of cell form. *J. Cell Biol.* 139, 717-728.

Bloom, G. & Endow, S. (1995). Motor proteins kinesin. *Protein Profile* 1, 1112–1138.

Bloom, K. (2001). Nuclear migration: cortical anchors for cytoplasmic dynein. *Curr. Biol.* 11, R326-329.

Blose, S. H. & Chacko, S. (1976). Rings of intermediate (100 A) filament bundles in the perinuclear region of vascular endothelial cells. Their mobilization by colcemid and mitosis. *J Cell Biol* 70, 459-466.

Blumenstein, A., Vienken, K., Tasler, R., Purschwitz, J., Veith, D., Frankenberg-Dinkel, N. & Fischer, R. (2005). The *Aspergillus nidulans* phytochrome FphA represses sexual development in red light. *Curr. Biol.* 15, 1833-1838.

Bobola, N., Jansen, R. P., Shin, T. H. & Nasmyth, K. (1996). Asymmetric accumulation of Ash1p in postanaphase nuclei depends on a myosin and restricts yeast mating-type switching to mother cells. *Cell* 84, 699-709.

Bowman, A. B., Patel-King, R. S., Benashski, S. E., McCaffery, J. M., Goldstein, L. S. & King, S. M. (1999). Drosophila roadblock and Chlamydomonas LC7: a conserved family of dynein-associated proteins involved in axonal transport, flagellar motility, and mitosis. *J Cell Biol* 146, 165-180.

Bradford, M. M. (1976). A rapid and sensitive method for the quantitation of microgram quantities of protein utilizing the principle of protein dye binding. *Anal Biochem* 72, 248-254.

Brazer, S. C., Williams, H. P., Chappell, T. G. & Cande, W. Z. (2000). A fission yeast kinesin affects Golgi membrane recycling. *Yeast* 16, 149-166.

Brouhard, G. J., Stear, J. H., Noetzel, T. L., Al-Bassam, J., Kinoshita, K., Harrison, S. C., Howard, J. & Hyman, A. A. (2008). XMAP215 is a processive microtubule polymerase. *Cell* 132, 79-88.

Browning, H., Hayles, J., Mata, J., Aveline, L., Nurse, P., and McIntosh, J.R. (2000). Tea2p is a kinesin-like protein required to generate polarized growth in fission yeast. *J Cell Biol* 151, 15–27.

Browning, H., Hackney, D.D., and Nurse, P. (2003). Targeted movement of cell end factors in fission yeast. *Nat Cell Biol* 5, 812–818.

Brunner, D. & Nurse, P. (2000). CLIP170-like tip1p spatially organizes microtubular dynamics in fission yeast. *Cell* 102, 695-704.

Bulinski, J. C. & Gundersen, G. G. (1991). Stabilization of post-translational modification of microtubules during cellular morphogenesis. *Bioessays* 13, 285-293.

Buller, A. H. R. (1931). *Researches on fungi*. New York: Hafner Publishing Co.

Busch, K. E. & Brunner, D. (2004). The microtubule plus end-tracking proteins mal3p and tip1p cooperate for cell-end targeting of interphase microtubules. *Curr. Biol.* 14, 548-559.

Busch, K.E., Hayles, J., Nurse, P., and Brunner, D. (2004). Tea2p kinesin is involved in spatial microtubule organization by transporting tip1p on microtubules. *Dev Cell* 16: 831–843.

Cai, D., McEwen, D. P., Martens, J. R., Meyhofer, E. & Verhey, K. J. (2009). Single molecule imaging reveals differences in microtubule track selection between Kinesin motors. *PLoS Biol* 7, e1000216.

Carazo-Salas, R. E. & Nurse, P. (2006). Self-organization of interphase microtubule arrays in fission yeast. *Nat Cell Biol* 8, 1102-1107.

Carey, M., Kakidani, H., Leatherwood, J., Mostashari, F. & Ptashne, M. (1989). An amino-terminal fragment of Gal4 binds DNA as a dimer. *J Mol. Biol.* 209, 423-432.

Carvalho, P., Gupta, M.L.J., Hoyt, M.A., and Pellman, D. (2004). Cell cycle control of kinesin-mediated transport of Bik1 (CLIP-170) regulates microtubule stability and dynein activation. *Dev Cell* 6, 815–829.

Cassimeris, L. & Spittle, C. (2001). Regulation of microtubule-associated proteins. *Int Rev Cytol* 210, 163-226.

Chain, P. S., Grafham, D. V., Fulton, R. S. & other authors (2009). Genomics. Genome project standards in a new era of sequencing. *Science* 326, 236-237.

Chang, F. (2001). Establishment of a cellular axis in fission yeast. *Trends Genet* 17, 273-278.

Clutterbuck, A. J. (1969). A mutational analysis of conidial development in *Aspergillus nidulans*. *Genetics* 63, 317-327.

Creppe, C., Malinouskaya, L., Volvert, M. L. & other authors (2009). Elongator controls the migration and differentiation of cortical neurons through acetylation of alpha-tubulin. *Cell* 136, 551-564.

Damveld, R. A., vanKuyk, P. A., Arentshorst, M., Klis, F. M., van den Hondel, C. A. & Ram, A. F. (2005). Expression of agsA, one of five 1,3-alpha-D-glucan synthase-encoding genes in Aspergillus niger, is induced in response to cell wall stress. *Fungal Genet Biol* 42, 165-177.

Desai, A. & Mitchison, T. J. (1997). Microtubule polymerization dynamics. *Annu. Rev. Cell Dev. Biol.* 13, 83-117.

Dorner, C., Ciossek, T., Muller, S., Moller, P. H., Ullrich, A. & Lammers, R. (1998). Characterization of KIF1C, a new kinesin-like protein involved in vesicle transport from the Golgi apparatus to the endoplasmic reticulum. *J Biol Chem* 273, 20267-20275.

Doshi, P., Bossie, C. A., Doonan, J. H., May, G. S. & Morris, N. R. (1991). Two α-tubulin genes of *Aspergillus nidulans* encode divergent proteins. *Mol. Genet. Genomics* 225, 129-141.

Dunn, S., Morrison, E. E., Liverpool, T. B., Molina-Paris, C., Cross, R. A., Alonso, M. C. & Peckham, M. (2007). Differential trafficking of Kif5c on tyrosinated and detryosinated microtubules in live cells. *J. Cell Sci.* 121, 1085-1095.

Durocher, D., Taylor, I. A., Sarbassova, D., Haire, L. F., Westcott, S. L., Jackson, S. P., Smerdon, S. J. & Yaffe, M. B. (2000). The molecular basis of FHA domain:phosphopeptide binding specificity and implications for phospho-dependent signaling mechanisms. *Mol Cell* 6, 1169-1182.

Durocher, D. & Jackson, S. P. (2002). The FHA domain. *FEBS Lett* 513, 58-66.

Eckley, D. M., Gill, S. R., Melkonian, K. A., Bingham, J. B., Goodson, H. V., Heuser, J. E. & Schroer, T. A. (1999). Analysis of dynactin subcomplexes reveals a novel actin-related protein associated with the arp1 minifilament pointed end. *J Cell Biol* 147, 307-320.

Efimov, V., Zhang, J. & Xiang, X. (2006). CLIP-170 homologue and NUDE play overlapping roles in NUDF localization in *Aspergillus nidulans*. *Mol Biol Cell* 17, 2021-2034.

Engh, I., Würtz, C., Witzel-Schlömp, K., Zhang, H. Y., Hoff, B., Nowrousian, M., Rottensteiner, H. & Kück, U. (2007). The WW domain protein PRO40 is required for fungal fertility and associates with Woronin Bodies. *Eukaryot. Cell* 6, 831-843.

Enke, C., Zekert, N., Veith, D., Schaaf, C., Konzack, S. & Fischer, R. (2007). *Aspergillus nidulans* Dis1/XMAP215 protein AlpA localizes to spindle pole bodies and microtubule plus ends and contributes to growth directionality. *Eukaryot. Cell* 6, 555-562.

Erck, C., Frank, R. & Wehland, J. (2000). Tubulin-tyrosine ligase, a long-lasting enigma. *Neurochem Res* 25, 5-10.

Erickson, H. P. & Stoffler, D. (1996). Protofilaments and rings, two conformations of the tubulin family conserved from bacterial FtsZ to alpha/beta and gamma tubulin. *J Cell Biol* 135, 5-8.

Fink, G., Schuchardt, I., Colombelli, J., Stelzer, E. & Steinberg, G. (2006). Dynein-mediated pulling forces drive rapid mitotic spindle elongation in Ustilago maydis. *EMBO J* 25, 4897-4908.

Fischer, R., Zekert, N. & Takeshita, N. (2008). Polarized growth in fungi - interplay between the cytosekelton, positional markers and membrane domains. *Mol. Microbiol.* 68, 813-826.

Fuchs, F. & Westermann, B. (2005). Role of Unc104/KIF1-related motor proteins in mitochondrial transport in *Neurospora crassa*. *Mol Biol Cell* 16, 153-161.

Gabaldón, T., Snel, B., van Zimmeren, F., Hemrika, W., Tabak, H. & Hyunen, M. A. (2006). Origin and evolution of the peroxisomal proteome. *Biol Direct* 1, 1-14.

Galagan, J. E., Calvo, S. E., Cuomo, C. & other authors (2005). Sequencing of *Aspergillus nidulans* and comparative analysis with *A. fumigatus* and *A. oryzae*. *Nature* 438, 1105-1115.

Gard, D. L. & Kirschner, M. W. (1987). A microtubule-associated protein from Xenopus eggs that specifically promotes assembly at the plus-end. *J. Cell Biol.* 105, 2203-2215.

Gierz, G. & Bartnicki-Garcia, S. (2001). A three-dimensional model of fungal morphogenesis based on the vesicle supply center concept. *J Theor Biol* 208, 151-164.

Gill, S. R., Schroer, T. A., Szilak, I., Steuer, E. R. & Sheetz, M. P. (1991). Dynactin, a conserved, ubiquitously expressed component of an activator of vesicle motility mediated by cytoplasmic dynein. *J. Cell Biol.* 115, 1639-1650.

Goda, H., Nagase, T., Tanoue, S. & other authors (2005). Nuclear translocation of the heterotrimeric CCAAT binding factor of Aspergillus oryzae is dependent on two redundant localising signals in a single subunit. *Arch Microbiol* 184, 93-100.

Gordon, C. L., Archer, D. B., Jeenes, D. J., Doonan, J. H., Wells, B., Trinci, A. P. & Robson, G. D. (2000a). A glucoamylase::GFP gene fusion to study protein secretion by individual hyphae of Aspergillus niger. *J Microbiol Methods* 42, 39-48.

Gordon, C. L., Khalaj, V., Ram, A. F. & other authors (2000b). Glucoamylase::green fluorescent protein fusions to monitor protein secretion in Aspergillus niger. *Microbiology* 146 (Pt 2), 415-426.

Gould, S. J., Keller, G. A., Hosken, N., Wilkinson, J. & Subramani, S. (1989). A conserved gripeptide sorts prtoeins to peroxisomes. *J. Cell Biol.* 108, 1657-1664.

Gundersen, G. G., Kalnoski, M. H. & Bulinski, J. C. (1984). Distinct populations of microtubules: Tyrosinated and nontyrosinated alpha tubulin are distributed differently *in vivo*. *Cell* 38, 779-789.

Gundersen, G. G., Khwaja, S. & Bulinski, J. C. (1987). Postpolymerization detyrosination of alpha-tubulin: A mechanism for subcellular differentiation of microtubules. *J. Cell Biol.* 105, 251-264.

Gundersen, G. G., Gomes, E. R. & Wen, Y. (2004). Cortical control of microtubule stability and polarization. *Curr Opin Cell Biol* 16, 106-112.

Gurunathan, S., Marash, M., Weinberger, A. & Gerst, J. E. (2002). t-SNARE phosphorylation regulates endocytosis in yeast. *Mol Biol Cell* 13, 1594-1607.

Hackney, D. D. (1994). The rate-limiting step in microtubule-stimulated ATP hydrolysis by dimeric kinesin head domains occurs while bound to the microtubule. *J Biol Chem* 269, 16508-16511.

Hackney, D. D. (1995). Highly processive microtubule-stimulated ATP hydrolysis by dimeric kinesin head domains. *Nature* 377, 448-50

Hall, D. H. & Hedgecock, E. M. (1991). Kinesin-related gene *unc-104* is required for axonal transport of synaptic vesicles in *C. elegans*. *Cell* 65, 837-847.

Hammond, J. W., Cai, D., Blasius, T. L., Li, Z., Jiang, Y., Jih, G. T., Meyhofer, E. & Verhey, K. J. (2009). Mammalian kinesin-3 motors are dimeric *in vivo* and move by processive motility upon relase of autoinhibition. *PLOS Biol* 7, 650-663.

Han, G., Liu, B., Zhang, J., Zuo, W., Morris, N. R. & Xiang, X. (2001). The Aspergillus cytoplasmic dynein heavy chain and NUDF localize to microtubule ends and affect microtubule dynamics. *Curr. Biol.* 11, 19-24.

Hasson, T. & Mooseker, M. S. (1995). Molecular motors, membrane movements and physiology: emerging roles for myosins. *Curr Opin Cell Biol* 7, 587-594.

Hawkins, T., Mirigian, M., Selcuk Yasar, M. & Ross, J. L. (2009). Mechanics of microtubules. *J Biomech* 43, 23-30.

Hayashi, M. & Nishimura, M. (2003). Entering a new era of research on plant peroxisomes. *Curr Opin Plant Biol* 6, 577-582.

Heald, R. & Nogales, E. (2002). Microtubule dynamics. *J Cell Sci* 115, 3-4.

Heiland, I. & Erdmann, R. (2005). Biogenesis of peroxisomes. *FEBS J* 272, 2362-2372.

Heitz, M. J., Petersen, J., Valovin, S. & Hagan, I. M. (2001). MTOC formation during mitotic exit in fission yeast. *J Cell Sci* 114, 4521-4532.

Hestermann, A. & Graf, R. (2004). The XMAP215-family protein DdCP224 is required for cortical interactions of microtubules. *BMC Cell Biol* 5, 24.

Higuchi, Y., Arioka, M. & Kitamoto, K. (2009). Endocytic recycling at the tip region in the filamentous fungus Aspergillus oryzae. *Commun Integr Biol* 2, 327-328.

Hirokawa, N. (1998). Kinesin and dynein superfamily proteins and the mechanism of organelle transport. *Science* 279, 519-526.

Hirokawa, N., Noda, Y., Tanaka, Y. & Niwa, S. (2009). Kinesin superfamily motor proteins and intracellular transport. *Nat Rev Mol Cell Biol* 10, 682-696.

Hirose, K. & Amos, L. A. (2007). High-resolution structural analysis of the kinesin-microtubule complex by electron cryo-microscopy. *Methods Mol Biol* 392, 213-230.

Hoepfner, D., Brachat, A. & Philippsen, P. (2000). Time-lapse video microscopy analysis reveals astral microtubule detachment in the yeast spindle pole mutant *cnm67*[v]. *Mol. Biol. Cell* 11, 1197-1211.

Holthuis, J. C., Nichols, B. J., Dhruvakumar, S. & Pelham, H. R. (1998). Two syntaxin homologues in the TGN/endosomal system of yeast. *EMBO J* 17, 113-126.

Holzbaur, E. L. & Vallee, R. B. (1994). DYNEINS: molecular structure and cellular function. *Annu Rev Cell Biol* 10, 339-372.

Horio, T., Uzawa, S., Jung, M. K., Oakley, B. R., Tanaka, K. & Yanagida, M. (1991). The fission yeast γ-tubulin is essential for mitosis and is localized at microtubule organizing centers. *J. Cell Sci.* 99, 693-700.

Hua, W., Young, E. C., Fleming, M. L. & Gelles, J. (1997). Coupling of kinesin steps to ATP hydrolysis. *Nature* 388, 390-393.

Hwang, E., Kusch, J., Barral, Y., and Huffaker, T.C. (2003). Spindle orientation in *Saccharomyces cerevisiae* depends on the transport of microtubule ends along polarized actin cables. *J Cell Biol* 161, 483-488.

Hyman, A. A., Middleton, K., Centola, M., Mitchison, T. J. & Carbon, J. (1992). Microtubule-motor activity of a yeast centromere-binding protein complex. *Nature* 359, 533-536.

Hynes, M. J., Murray, S. L., Khew, G. S. & Davis, M. A. (2008). Genetic analysis of the role of peroxisomes in the utilization of acetate and fatty acids in *Aspergillus nidulans*. *Genetics* 178, 1355-1369.

Ikegami, K., Heier, R. L., Raruishi, M. & other authors (2007). Loss of α-tubulin polyglutamylation in ROSA22 mice is assocated with abnormal targeting of KIF1A and modulated synaptic function. *PNAS* 104, 3213-3218.

Infante, A. S., Stein, M. S., Zhai, Y., Borisy, G. G. & Gundersen, G. G. (2000). Detyrosinated (Glu) microtubules are stabilized by an ATP-sensitive plus-end cap. *J. Cell Sci.* 113, 3907-3919.

Iwasaki, W. & Miki, K. (2007). Crystal structure of the stationary phase survival protein SurE with metal ion and AMP. *J Mol Biol* 371, 123-136.

Jaiswal, J. K., Rivera, V. M. & Simon, S. M. (2009). Exocytosis of post-Golgi vesicles is regulated by components of the endocytic machinery. *Cell* 137, 1308-1319.

Jaspersen, S. L. & Winey, M. (2004). The budding yeast spindle pole body: structure, duplication, and function. *Annu Rev Cell Dev Biol* 20, 1-28.

Jedd, G. & Chua, N.-H. (2000). A new self-assembled peroxisomal vesicle required for efficient resealing of the plasma membrane. *Nat. Cell Biol.* 2, 226-231.

Joshi, H. C., Palacios, M. J., McNamara, L. & Cleveland, D. W. (1992). Gamma-tubulin is a centrosomal protein required for cell cycle-dependent microtubule nucleation. *Nature* 356, 80-83.

Karcher, R. L., Deacon, S. W. & Gelfand, V. I. (2002). Motor-cargo interactions: the key to transport specificity. *Trends Cell Biol* 12, 21-27.

Karki, S. & Holzbaur, E. L. (1995). Affinity chromatography demonstrates a direct binding between cytoplasmic dynein and the dynactin complex. *J Biol Chem* 270, 28806-28811.

Karos, M. & Fischer, R. (1999). Molecular characterization of HymA, an evolutionarily highly conserved and highly expressed protein of *Aspergillus nidulans*. *Mol. Genet. Genomics* 260, 510-521.

Kaseda, K., Higuchi, H. & Hirose, K. (2003). Alternate fast and slow stepping of a heterodimeric kinesin molecule. *Nat Cell Biol* 5, 1079-1082.

Keating, T. J. & Borisy, G. G. (1999). Centrosomal and non-centrosomal microtubules. *Biol Cell* 91, 321-329.

Kikkawa, M., Okada, Y. & Hirokawa, N. (2000). 15 A resolution model of the monomeric kinesin motor, KIF1A. *Cell* 100, 241-252.

Kikkawa, M., Sablin, E. P., Okada, Y., Yajima, H., Fletterick, R. J. & Hirokawa, N. (2001). Switch-based mechanism of kinesin motors. *Nature* 411, 439-445.

Kikkawa, M. & Hirokawa, N. (2006). High-resolution cryo-EM maps show the nucleotide binding pocket of KIF1A in open and closed conformations. *EMBO J* 25, 4187-4194.

Kikkawa, M. (2008). The role of microtubules in processive kinesin movement. *Trends Cell Biol* 18, 128-135.

Kilmartin, J. V. (1994). Genetic and biochemical approaches to spindle function and chromosome segregation in eukaryotic microorganisms. *Curr. Opin. Cell Biol.* 6, 50-54.

Kim, S. V. & Flavell R. A. (2008). Myosin I: From yeast to human. *Cell Mol. Life Sci.* 56, 2128-2137.

King, S. M., Barbarese, E., Dillman, J. F., 3rd, Benashski, S. E., Do, K. T., Patel-King, R. S. & Pfister, K. K. (1998). Cytoplasmic dynein contains a family of differentially expressed light chains. *Biochemistry* 37, 15033-15041.

King, S. M. (2000). The dynein microtubule motor. *Biochim. Biophys. Acta* 1496, 60-75.

King, S. M. & Schroer, T. A. (2000). Dynactin increases the processivity of the cytoplasmic dynein motor. *Nat. Cell Biol.* 2, 20-24.

Kinoshita, K., Habermann, B. & Hyman, A. A. (2002). XMAP215: a key component of the dynamic microtubule cytoskeleton. *Trends Cell Biol.* 12, 267-273.

Kirk, K. E. & Morris, N. R. (1991). The *tubB* α-tubulin gene is essential for sexual development in *Aspergillus nidulans*. *Genes Dev.* 5, 2014-2023.

Kirk, K. E. & Morris, N. R. (1993). Either α-tubulin isogene product is sufficient for microtubule function during all stages of growth and differentiation in *Aspergillus nidulans*. *Mol. Cell. Biol.* 13, 4465-4476.

Kirschner, M. W. & Mitchison, T. (1986). Microtubule dynamics. *Nature* 324, 621.

Klopfenstein, D. R., Tomishige, M., Stuurman, N. & Vale, R. D. (2002). Role of phosphatidylinositol(4,5)bisphosphate organisation in membrane transport by the Unc104 kinesin motor. *Cell* 109, 347-358.

Kondo, S., Sato-Yoshitake, R., Noda, Y., Aizawa, H., Nakata, T., Matsuura, Y. & Hirokawa, N. (1994). KIF3A is a new microtubule-based anterograde motor in the nerve axon. *J. Cell Biol.* 125, 1095-1107.

Konzack, S., Rischitor, P., Enke, C. & Fischer, R. (2005). The role of the kinesin motor KipA in microtubule organization and polarized growth of *Aspergillus nidulans*. *Mol. Biol. Cell* 16, 497-506.

Kovacs, W. J., Krisans, S., Hogenboom, S., Wanders, R. J. & Waterham, H. R. (2003). Cholesterol biosynthesis and regulation: role of peroxisomes. *Adv Exp Med Biol* 544, 315-327.

Kumar, S., Lee, I. H. & Plamann, M. (2000). Cytoplasmic dynein ATPase activity is regulated by dynactin-dependent phosphorylation. *J. Biol. Chem.* 275, 31798-31804.

Kuratsu, M., Taura, A., Shoji, J.-Y., Kikuchi, S., Arioka, M. & Kitamoto, K. (2007). Systematic analysis of SNARE localization in the filamentous fungus *Aspergillus oryzae*. *Fungal Genet. Biol.* 44, 1310-1323.

Kuznetsov, S. A., Vaisberg, Y. A., Rothwell, S. W., Murphy, D. B. & Gelfand, V. I. (1989). Isolation of a 45-kDa fragment from the kinesin heavy chain with enhanced ATPase and microtubule-binding activities. *J Biol Chem* 264, 589-595.

Lakamper, S. & Meyhofer, E. (2006). Back on track - on the role of the microtubule for kinesin motility and cellular function. *J Muscle Res Cell Motil* 27, 161-171.

Lang, C., Grava, S., Finlayson, M., Trimble, R., Philippsen, P. & Jaspersen, S. L. (2010a). Structural mutants of the spindle pole body cause distinct alterations of cytoplasmic microtubules and nuclear dynamics in multinucleated hyphae. *Mol Biol Cell* Epub.

Lang, C., Grava, S., van den Hoorn, T., Trimble, R., Philippsen, P. & Jaspersen, S. L. (2010b). Mobility, microtubule nucleation and structure of microtubule-organizing centers in multinucleated hyphae of *Ashbya gossypii*. *Mol Biol Cell* 21, 18-28.

Lawrence, C. J., Dawe, R. K., Christie, K. R. & other authors (2004). A standardized kinesin nomenclature. *J Cell Biol* 167, 19-22.

Lee, J., Shin, H., Choi, J. & other authors (2004). An intramolecular interaction between the FHA domain and a coiled coil negatively regulates the kinesin motor KIF1A. *EMBO J* 23, 1506-1515.

Lee, J. Y., Kwak, J. E., Moon, J., Eom, S. H., Liong, E. C., Pedelacq, J. D., Berendzen, J. & Suh, S. W. (2001). Crystal structure and functional analysis of the SurE protein identify a novel phosphatase family. *Nat Struct Biol* 8, 789-794.

Lehmler, C., Steinberg, G., Snetselaar, K. M., Schliwa, M., Kahmann, R. & Bölker, M. (1997). Identification of a motor protein required for filamentous growth in *Ustilago maydis*. *EMBO* 16, 3464-3473.

Lenz, J. H., Schuchardt, I., Straube, A. & Steinberg, G. (2006). A dynein loading zone for retrograde endosome motility at microtubule plus-ends. *EMBO J* 25, 2275-2286.

Levin, D. E. (2005). Cell wall integrity signaling in Saccharomyces cerevisiae. *Microbiol Mol Biol Rev* 69, 262-291.

Liang, A., Ruiz, F., Heckmann, K., Klotz, C., Tollon, Y., Beisson, J. & Wrigth, M. (1996). Gamma-tubulin is permanently associated with basal bodies in ciliates. *Eur J Cell Biol* 70, 331-338.

Liu, S., Lu, W., Obara, T., Kuida, S., Lehoczky, J., Dewar, K., Drummond, I. A. & Beier, D. R. (2002). A defect in anovel Nek-family kinase causes cystic kidney disease in the mouse and in zebrafish. *Development* 129, 5839-5846.

Macara, I. G. & Mili, S. (2008). Polarity and differential inheritance- universal attributes of life?. *Cell* 135, 801-812.

Maekawa, H., Usui, T., Knop, M. & Schiebel, E. (2003). Yeast Cdk1 translocates to the plus end of cytoplasmic microtubules to regulate but cortex interactions. *EMBO* 22, 438-449.

Maekawa, H. & Schiebel, E. (2004). Cdk1-Clb4 controls the interaction of astral microtubule plus ends with subdomains of the daughter cell cortex. *Genes Dev.* 18, 1709-1724.

Marcos, S., Moreau, J., Backer, S., Job, D., Andrieux, A. & Bloch-Gallego, E. (2009). Tubulin tyrosination is required for the proper organization and pathfinding of the growth cone. *PLoS One* 4, e5405.

Martin, M. A., Osmani, S. A. & Oakley, B. R. (1997). The role of gamma-tubulin in mitotic spindle formation and cell cycle progression in *Aspergillus nidulans*. *J. Cell Sci.* 110, 623-633.

Maruyama, J., Juvvadi, P. R., Ishi, K. & Kitamoto, K. (2005). Three-dimensional image analysis of plugging at the septal pore by Woroinin body during hypotonic shock inducing

hyphal tip bursting in the filamentous fungus *Aspergillus oryzae*. *Biochem. Biophys. Res. Comm.* 331, 1081-1088.

Mata, J. & Nurse, P. (1997). *tea1* and the microtubular cytoskeleton are important for generating global spatial order within the fission yeast cell. *Cell* 89, 939-949.

Matteoni, R. & Kreis, T. E. (1987). Translocation and clustering of endosomes and lysosomes depends on microtubules. *J Cell Biol* 105, 1253-1265.

May, G. S., Gambino, J., Weatherbee, J. A. & Morris, N. R. (1985). Identification and functional analysis of beta-tubulin genes by site specific integrative transformation in *Aspergillus nidulans*. *J. Cell Biol.* 101, 712-719.

Mayorga, M. E. & Timberlake, W. E. (1990). Isolation and molecular characterization of the Aspergillus nidulans wA gene. *Genetics* 126, 73-79.

McDaniel, D. P. & Roberson, R. W. (1998). γ-tubulin is a component of the Spitzenkörper and centrosomes in hyphal-tip cells of *Allomyces macrogynus*. *Protoplasma* 203, 118-123.

Meng, J. J., Rojas, M., Bacon, W., Stickney, J. T. & Ip, W. (2005). Methods to study protein-protein interactions. *Methods Mol Biol* 289, 341-358.

Meurer-Grob, P., Kasparian, J. & Wade, R. H. (2001). Microtubule structure at improved resolution. *Biochemistry* 40, 8000-8008.

Mialhe, A., Lafanechère, L., Treilleux, I. & other authors (2001). Tubulin detyrosination is a frequent occurrence in breast cancers of poor prognosis. *Cancer Res* 61, 5024-5027.

Miki, H., Setou, M., Kaneshiro, K. & Hirokawa, N. (2001). All kinesin superfamily protein, KIF, genes in mouse and human. *Proc Natl Acad Sci U S A* 98, 7004-7011.

Mitchison, T. & Kirschner, M. (1984). Dynamic instability of microtubule growth. *Nature* 312, 237-242.

Mitchison, T. J. & Nurse, P. (1985). Growth in cell length in the fission yeast *Schizosaccharomyces pombe*. *J. Cell Sci.* 75, 357-376.

Montegi, F., Arai, R. & Mabuchi, I. (2001). Identification of two type V myosins in fission yeast, one of which functions in polarized cell growth and moves rapidly in the cell. *Mol. Biol. Cell* 12, 1367-1380.

Morris, N. R., Lai, M. H. & Oakley, C. E. (1979). Identification of a gene for α-tubulin in *Aspergillus nidulans*. *Cell* 16, 437-442.

Mulvihill, D. P., Edwards, S. R. & Hyams, J. S. (2006). A critical role for the type V myosin, Myo52, in septum deposition and cell fission during cytokinesis in *Schizosaccharomyces pombe*. *Cell Mot Cytoskel* 63, 149-161.

Mura, C., Katz, J. E., Clarke, S. G. & Eisenberg, D. (2003). Structure and function of an archaeal homolog of survival protein E (SurEalpha): an acid phosphatase with purine nucleotide specificity. *J Mol Biol* 326, 1559-1575.

Nakata, T. & Hirokawa, N. (1995). Point mutation of adenosine triphosphate-binding motif generated rigor kinesin that selectively blocks anterograde lysosome membrane transport. *J. Cell Biol.* 131, 1039-1053.

Nangaku, M., Sato-Yoshitake, R., Okada, Y., Noda, Y., Takemura, R., Yamazaki, H. & Hirokawa, N. (1994). KIF1B, a novel microtubule plus end-directed monomeric motor protein for transport of mitochondria. *Cell* 79, 1209-1220.

Nayak, T., Szewczyk, E., Oakley, C. E., Osmani, A., Ukil, L., Murray, S. L., Hynes, M. J., Osmani, S. A. & Oakley, B. R. (2006). A versatile and efficient gene-targeting system for Aspergillus nidulans. *Genetics* 172, 1557-1566.

Nelson, W. J. (2003). Adaptation of core mechanisms to generate cell polarity. *Nature* 422, 766-774.

Nitta, R., Kikkawa, M., Okada, Y. & Hirokawa, N. (2004). KIF1A alternately uses two loops to bind microtubules. *Science* 305, 678-683.

Nitta, R., Okada, Y. & Hirokawa, N. (2008). Structural model for strain-dependent microtubule activation of Mg-ADP release from kinesin. *Nat Struct Mol Biol* 15, 1067-1075.

Nogales, E., Wolf, S. G. & K.H., D. (1998). Structure of the αβ tubulin dimer by electron crystallography. *Nature* 391, 199-203.

Oakley, B. R., Oakley, C. E. & Rinehart, J. E. (1987). Conditionally lethal *tubA* α-tubulin mutations in *Aspergillus nidulans*. *Mol. Genet. Genomics* 208, 135-144.

Oakley, C.E. & Oakley, B.R. (1989). Identification of gamma-tubulin, a new member of the tubulin superfamily encoded by *mipA* gene of *Aspergillus nidulans*. *Nature* 338, 662-664.

Oakley, B. R., Oakley, C. E., Yoon, Y. & Jung, K. M. (1990). γ-Tubulin is a component of the spindle pole body in *Aspergillus nidulans*. *Cell* 61, 1289-1301.

Oakley, B. R. (1992). Gamma-tubulin: the microtubule organizer? *T Cell Biol. 2: 1-5*.

Oakley, B. R. (2004). Tubulins in *Aspergillus nidulans*. *Fungal Genet. Biol.* 41, 420-427.

Ohkura, H., Garcia, M. A. & Toda, T. (2001). Dis1/TOG universal microtubule adaptors - one MAP for all? *J. Cell Sci.* 114, 3805-3812.

Okada, Y., Yamazaki, H., Sekine-Aizawa, Y. & Hirokawa, N. (1995). The neuron-specific kinesin superfamily protein KIF1A is a unique monomeric motor for anterograde axonal transport of synaptic vesicle precursors. *Cell* 81, 769-780.

Okada, Y. & Hirokawa, N. (1999). A processive single-headed motor: Kinesin superfamily protein KIF1A. *Science* 283, 1152-1157.

Okada, Y. & Hirokawa, N. (2000). Mechanism of the single-headed processivity: diffusional anchoring between the K-loop of kinesin and the C terminus of tubulin. *PNAS* 97, 640-645.

Otsuka, A. J., Jeyaprakash, A., García-Añoveros, J., Tang, L. Z., Fisk, G., Hartshorne, T., Franco, R. & Born, T. (1991). The *C. elegans unc-104* gene encodes a putative kinesin heavy chain-like protein. *Neuron* 6, 113-122.

Pathak, N., Obara, T., Mangos, S., Liu, Y. & Drummond, I. A. (2007). The zebrafish fleer gene encodes an essential regulator of cilia tubulin polyglutamylation. *Mol Biol Cell* 18, 4353-4364.

Pel et al., H. J. (2007). Genome sequencing and analysis of the versatile cell factory *Aspergillus niger* CBS 513.88. *Nat Biotechnol* 25, 221-231.

Peñalva, M. A. (2005). Tracing the endocytic pathway of *Aspergillus nidulans* with FM4-64. *Fungal Genet. Biol.* 42, 963-975.

Peris, L., Thery, M., Faure, J. & other authors (2006). Tubulin tyrosination is a major factor affecting the recruitment of CAP-Gly proteins at microtubule plus ends. *J Cell Biol* 174, 839-849.

Pierce, D. W., Hom-Booher, N., Otsuka, A. J. & Vale, R. D. (1999). Single-molecule behavior of monomeric and heteromeric kinesins. *Biochemistry* 38, 5412-5421.

Pollard, T. D. (2009). Mechanics of cytokinesis in eukaryotes. *Curr. Opin. Cell Biol.* 22, 50-56.

Pollock, N., deHostos, E. L., Turck, C. W. & Vale, R. D. (1999). Reconstitution of membrane transport powered by a novel dimeric kinesin motor of the Unc104/KIF1A family purified from Dictyostelium. *J. Cell Biol.* 147, 493-506.

Pontecorvo, G., Roper, J. A., Hemmons, L. M., MacDonald, K. D. & Bufton, A. W. J. (1953). The genetics of *Aspergillus nidulans*. *Adv Genet* 5, 141-238.

Pringle, J. R., Bi, E., Harkins, H. A., Zahner, J. E., DeVirglio, C., Chant, J., Corrado, K. & Fares, H. (1995). Establishment of cell polarity in yeast. *Cold Spring Harb Symp Quant Biol*, 729-744.

Pruyne, D., Legesse-Miller, A., Gao, L., Dong, Y. & Bretscher, A. (2004). Mechanisms of polarized growth and organelle segregation in yeast. *Annu Rev Cell Dev Biol* 20, 559-591.

Purschwitz, J., Müller, S. & Fischer, R. (2009). Mapping the interaction sites of *Aspergillus nidulans* phytochrome FphA with the global regulator VeA and the white collar protein LreB. *Mol. Genet. Genomics* 281, 35-42.

Ram, A. F. & Klis, F. M. (2006). Identification of fungal cell wall mutants using susceptibility assays based on Calcofluor white and Congo red. *Nat Protoc* 1, 2253-2256.

Rashid, D. J., Bononi, J., Tripet, B. P., Hodges, R. S. & Pierce, D. W. (2005). Monomeric and dimeric states exhibited by the kinesin-related motor protein KIF1A. *J Pept Res* 65, 538-549.

Reed, N. A., Dawen, C., Blasius, T. L., Jih, G. T., Meyhofer, E., Gaertig, J. & Verhey, K. J. (2006). Microtubule acetylation promotes kinesin-1 binding and transport. *Curr. Biol.* 16.

Requena, N., Alberti-Segui, C., Winzenburg, E., Horn, C., Schliwa, M., Philippsen, P., Liese, R. & Fischer, R. (2001). Genetic evidence for a microtubule-destabilizing effect of conventional kinesin and analysis of its consequences for the control of nuclear distribution in Aspergillus nidulans. *Mol Microbiol* 42, 121-132.

Riquelme, M., Roberson, R. W., McDaniel, D. P. & Bartnicki-Garcia, S. (2002). The effects of *ropy-1* mutation on cytoplasmic organization and intracellular motility in mature hyphae of *Neurospora crassa*. *Fungal Genet. Biol.* 37, 171-179.

Riquelme, M., Fischer, R. & Bartnicki-Garcia, S. (2003). Apical growth and mitosis are independent processes in *Aspergillus nidulans*. *Protoplama* 222, 211-215.

Rischitor, P., Konzack, S. & Fischer, R. (2004). The Kip3-like kinesin KipB moves along microtubules and determines spindle position during synchronized mitoses in *Aspergillus nidulans* hyphae. *Eukaryot. Cell* 3, 632-645.

Rivera, S. B., Koch, S. J., Bauer, J. M., Edwards, J. M. & Bachand, G. D. (2007). Temperature dependent properties of a kinesin-3 motor protein from *Thermomyces lanuginosus*. *Fungal Genet. Biol.* 44, 1170-1179.

Sambrook, J. & Russel, D. W. (1999). *Molecular Cloning: A laboratory manual*. Cold Spring Harbor, New York: Cold Spring Harbor Laboratory Press.

Samejima, I., Laurenco, P. C. C., Snaith, H. A. & Sawin, K. E. (2005). Fission yeast mto2p regulates microtubule nucelation by the centrosomin-related protein mto1p. *Mol Biol Cell* 16, 3040-3051.

Sampson, K. & Heath, I. B. (2005). The dynamic behaviour of microtubules and their contributions to hyphal tip growth in *Aspergillus nidulans*. *Microbiology* 151, 1543-1555.

Sawin, K. E. & Nurse, P. (1998). Regulation of cell polarity by microtubules in fission yeast. *J Cell Biol* 142, 457-471.

Sawin, K. E., Lourenco, P. C. C. & Snaith, H. A. (2004). Microtubule nucleation at non-spindle pole body microtubule-organizing centers requires fission yeast centrosomin-related protein mod20p. *Curr. Biol.* 14, 763-775.

Sawin, K. E. & Tran, P. T. (2006). Cytoplasmic microtubule organization in fission yeast. *Yeast* 23, 1001-1014.

Saxton, W. M., Stemple, D. L., Leslie, R. J., Salmon, E. D., Zavortink, M. & McIntosh, J. R. (1984). Tubulin dynamics in cultured mammalian cells. *J Cell Biol* 99, 2175-2186.

Schafer, D. A., Gill, S. R., Cooper, J. A., Heuser, J. E. & Schroer, T. A. (1994). Ultrastructural analysis of the dynactin complex: An actin-related protein is a component of a filament that resembles F-actin. *J. Cell Biol.* 126, 403-412.

Schliwa, M. & Woehlke, G. (2003). Molecular motors. *Nature* 422, 759-765.

Schnitzer, M. J. & Block, S. M. (1997). Kinesin hydrolyses one ATP per 8-nm step. *Nature* 388, 386-390.

Schoch, C. L., Aist, J. R., Yoder, O. C. & Turgeon, B. G. (2003). A complete inventory of fungal kinesins in representative filamentous ascomycetes. *Fungal Genet. Biol.* 39, 1-15.

Scholey, J. M., Heuser, J., Yang, J. T. & Goldstein, L. S. (1989). Identification of globular mechanochemical heads of kinesin. *Nature* 338, 355-357.

Schrader, M. & Fahimi, H. D. (2008). The peroxisome: still a mysterious organelle. *Histochem Cell Biol* 129, 421-440.

Schroer, T. A. & Sheetz, M. P. (1991). Two activators of microtubule-based vesicle transport. *J Cell Biol.* 115, 1309-1318.

Schuchardt, I., Aßmann, D., Thines, E., Schuberth, C. & Steinberg, G. (2005). Myosin-V, kinesin-1, and kinesin-3 cooperate in hyphal growth of the fungus *Ustilago maydis*. *Mol. Biol. Cell* 16, 5191-5201.

Schulze, E. & Kirschner, M. (1986). Microtubule dynamics in interphase cells. *J Cell Biol.* 102, 1020-1031.

Schulze, E., Asai, D. J., Bulinski, J. C. & Kirschner, M. (1987). Posttranslational modification and microtubule stability. *J. Cell Biol.* 105, 2167-2177.

Schuyler, S. C. & Pellman, D. (2001). Search, capture and signal: games microtubules and centrosomes play. *J. Cell Sci.* 114, 247-255.

Seidel, C. (2009). Untersuchung des Kinesin-3 Motors UncA in *Aspergillus nidulans*. Diploma thesis. Karlsruhe, Karlsruhe Institute of Technolgy (KIT).

Seiler, S., Nargang, F. E., Steinberg, G. & Schliwa, M. (1997). Kinesin is essential for cell morphogenesis and polarized secretion in *Neurospora crassa*. *EMBO* 16, 3025-3034.

Seiler, S., Plamann, M. & Schliwa, M. (1999). Kinesin and dynein mutants provide novel insights into the roles of vesicle traffic during cell morphogenesis in *Neurospora*. *Curr. Biol.* 9, 779-785.

Shaw, B. D. & Momany, M. (2002). Aspergillus nidulans polarity mutant swoA is complemented by protein O-mannosyltransferase pmtA. *Fungal Genet Biol* 37, 263-270.

Sheeman, B., Carvalho, P., Sagot, I., Geiser, J., Kho, D., Hoyt, M. A. & Pellman, D. (2003). Determinants of *S. cerevisiae* dynein localization and activation: Implications for the mechanism of spindle positioning. *Curr. Biol.* 13, 364-372.

Sheir-Neiss, G., Nardi, R. V., Gealt, M. A. & Morris, N. R. (1976). Tubulin-like protein from *Aspergillus nidulans*. *Biochem. Biophys. Res. Comm.* 69, 285-290.

Sheir-Neiss, G., Lai, M. & Morris, N. R. (1978). Identification of a gene for β-tubulin in *Aspergillus nidulans*. *Cell* 15, 639-647.

Shepard, K. A., Gerber, A. P., Jambhekar, A., Takizawa, P. A., Brown, P. O., Herschlag, D., DeRisi, J. L. & Vale, R. D. (2003). Widespread cytoplasmic mRNA transport in yeast: identification of 22 bud-localized transcripts using DNA microarray analysis. *PNAS* 100, 11429-11434.

Shimizu, Y., Morii, H., Arisaka, F. & Tanokura, M. (2005). Stalk region of kinesin-related protein Unc104 has moderate ability to form coiled-coil dimer. *Biochem Biophys Res Commun* 337, 868-874.

Sievers, N., Krüger, M. & Fischer, R. (1997). Kreuzung von *Aspergillus nidulans*. *Biol Unserer Zeit* 6, 383-388.

Skiniotis, G., Cochran, J. C., Muller, J., Mandelkow, E., Gilbert, S. P. & Hoenger, A. (2004). Modulation of kinesin binding by the C-termini of tubulin. *EMBO J* 23, 989-999.

Snell, V. & Nurse, P. (1994). Genetic analysis of cell morphogenesis in fission yeast - a role for casein kinase II in the establishment of polarized growth. *EMBO* 13, 2066-2074.

Song, Y. H., Marx, A., Muller, J., Woehlke, G., Schliwa, M., Krebs, A., Hoenger, A. & Mandelkow, E. (2001). Structure of a fast kinesin: implications for ATPase mechanism and interactions with microtubules. *EMBO J* 20, 6213-6225.

Stearns, T., Evans, L. & Kirschner, M. W. (1991). Gamma-tubulin is a highly conserved component of the centrosome. *Cell* 65, 825-836.

Steinberg, G., Wedlich-Soldner, R., Brill, M. & Schulz, I. (2001). Microtubules in the fungal pathogen Ustilago maydis are highly dynamic and determine cell polarity. *J Cell Sci* 114, 609-622.

Steinberg, G. (2007). On the move: endosomes in fungal growth and pathogenicity. *Nat Rev Microbiol* 5, 309-316.

Straube, A., Brill, M., Oakley, B. R., Horio, T. & Steinberg, G. (2003). Microtubule organization requires cell cycle-dependent nucleation at dispersed cytoplasmic sites: polar and perinuclear microtubule organizing centers in the plant pathogen *Ustilago maydis*. *Mol. Biol. Cell* 14, 642-657.

Stringer, M. A., Dean, R. A., Sewall, T. C. & Timberlake, W. E. (1991). *Rodletless*, a new *Aspergillus* developmental mutant induced by directed gene inactivation. *Genes Dev.* 5, 1161-1171.

Suelmann, R. (1999). *In vivo* und molekulare Analyse der Zellkernwanderung und der Mitochondrienverteilung in *Aspergillus nidulans*. Dissertation. Marburg, University of Marburg.

Suelmann, R. & Fischer, R. (2000). Mitochondrial movement and morphology depend on an intact actin cytoskeleton in *Aspergillus nidulans*. *Cell Motil. Cytoskel.* 45, 42-50.

Sullivan, K. F. & Cleveland, D. W. (1986). Identification of conserved isotype-defining variable region sequences for four vertebrate beta tubulin polypeptide classes. *Proc Natl Acad Sci U S A* 83, 4327-4331.

Suryavanshi, S., Edde, B., Fox, L. A. & other authors (2010). Tubulin glutamylation regulates ciliary motility by altering inner dynein arm activity. *Curr Biol* 20, 435-440.

Swinkels, B. W., Gould, S. J., Bodnar, A. G., Rachubinski, R. A. & Subramani, S. (1991). A novel, cleavable peroxisomal targeting signal at the amino-terminus of the rat 3-ketoacyl-CoA thiolase. *EMBO J* 10, 3255-3262.

Taheri-Talesh, N., Horio, T., Araujo-Bazan, L., Dou, X., Espeso, E. A., Penalva, M. A., Osmani, S. A. & Oakley, B. R. (2008). The tip growth apparatus of Aspergillus nidulans. *Mol Biol Cell* 19, 1439-1449.

Takeshita, N., Higashitsuji, Y., Konzack, S. & Fischer, R. (2008). Apical sterol-rich membranes are essential for localizing cell end markers that determine growth directionality in the filamentous fungus *Aspergillus nidulans*. *Mol. Biol. Cell* 19, 339-351.

te Biesebeke, R., van Biezen, N., de Vos, W. M., van den Hondel, C. A. & Punt, P. J. (2005). Different control mechanisms regulate glucoamylase and protease gene transcription in Aspergillus oryzae in solid-state and submerged fermentation. *Appl Microbiol Biotechnol* 67, 75-82.

Thorn, K. S., Ubersax, J. A. & Vale, R. D. (2000). Engineering the processive run length of the kinesin motor. *J. Cell Biol.* 151, 1093-1100.

Thyberg, J. & Moskalewski, S. (1985). Microtubules and the organization of the Golgi complex. *Exp Cell Res* 159, 1-16.

Timberlake, W. E. & Marshall, M. A. (1989). Genetic engineering of filamentous fungi. *Science* 244, 1313-1317.

Toews, M. W., Warmbold, J., Konzack, S., Rischitor, P. E., Veith, D., Vienken, K., Vinuesa, C., Wei, H. & Fischer, R. (2004). Establishment of mRFP1 as fluorescent marker in *Aspergillus nidulans* and construction of expression vectors for high-throughput protein tagging using recombination in *Escherichia coli* (GATEWAY). *Curr. Genet.* 45, 383-389.

Tomishige, M., Klopfenstein, D. R. & Vale, R. D. (2002). Conversion of Unc104/KIF1A kinesin into a processive motor after dimerization. *Science* 297, 2263-2267.

Tran, P. T., Marsh, L., Doye, V., Inoue, S. & Chang, F. (2001). A mechanism for nuclear positioning in fission yeast based on microtubule pushing. *J. Cell Biol.* 153, 397-411.

Upadhyay, S. & Shaw, B. D. (2008). The role of actin, fimbrin and endocytosis in growth of hyphae in Aspergillus nidulans. *Mol Microbiol* 68, 690-705.

Upshall, A., Gilbert, T., Saari, G., O'Hara, P. J., Weglenski, P., Berse, B., Miller, K. & Timberlake, W. E. (1986). Molecular analysis of the argB gene of Aspergillus nidulans. *Mol Gen Genet* 204, 349-354.

Vale, R. D. & Milligan, R. A. (2000). The way things move: looking under the hood of molecular motor proteins. *Science* 288, 88-95.

Vale, R. D. (2003). The molecular motor toolbox for intracellular transport. *Cell* 112, 467-480.

Valkonen, M., Kalkman, E. R., Saloheimo, M., Penttila, M., Read, N. D. & Duncan, R. R. (2007). Spatially segregated SNARE protein interactions in living fungal cells. *J Biol Chem* 282, 22775-22785.

Veith, D., Scherr, N., Efimov, V. P. & Fischer, R. (2005). Role of the spindle-pole body protein ApsB and the cortex protein ApsA in microtubule organization and nuclear migration in *Aspergillus nidulans*. *J. Cell Sci.* 118, 3705-3716.

Veith, D. (2006). Die Funktion des Spindelpolkörper-Proteins ApsB bei der Mikrotubulus-Organisation und Zellkernwanderung in *Aspergillus nidulans*. Dissertation. Marburg/Lahn, University of Marburg.

Vinh, D. B., Kern, J. W., Hancock, W. O., Howard, J. & Davis, T. N. (2002). Reconstitution and characterization of budding yeast gamma-tubulin complex. *Mol Biol Cell* 13, 1144-1157.

Wanders, R. J. (2004). Metabolic and molecular basis of peroxisomal disorders: a review. *Am J Med Genet* 126A, 355-375.

Wanders, R. J. & Waterham, H. R. (2006). Biochemistry of Mammalian peroxisomes revisited. *Ann. Rev. Biochem.* 75, 295-332.

Waring, R. B., May, G. S. & Morris, N. R. (1989). Characterization of an inducible expression system in *Aspergillus nidulans* using *alcA* and tubulin coding genes. *Gene* 79, 119-130.

Weatherbee, J. A., May, G. S., Gambino, J. & Morris, N. R. (1985). Involvement of a particular species of beta-tubulin (beta 3) in conidial development in *Aspergillus nidulans*. *J. Cell Biol.* 101, 706-711.

Weber, I., Gruber, C. & Steinberg, G. (2003). A class-V myosin required for mating, hyphal growth, and pathogenicity in the dimorphic plant pathogen *Ustilago maydis*. *Plant Cell* 15, 2826-2842.

Weber, K., Schneider, A., Westermann, S., Muller, N. & Plessmann, U. (1997). Posttranslational modifications of a- and b-tubulin in Giardia lamblia an ancient eukaryote. *FEBS Lett* 419, 87-91.

Wedlich-Söldner, R., Bölker, M., Kahmann, R. & Steinberg, G. (2000). A putative endosomal t-SNARE links exo- and endocytosis in the phytopathogenic fungus *Ustilago maydis*. *EMBO J* 19, 1974-1986.

Wedlich-Söldner, R., Schulz, I., Straube, A. & Steinberg, G. (2002a). Dynein supports motility of endoplasmic reticulum in the fungus *Ustilago maydis*. *Mol. Biol. Cell* 13, 965-977.

Wedlich-Söldner, R., Straube, A., Friedrich, M. W. & Steinberg, G. (2002b). A balance of KIF1A-like kinesin and dynein organizes early endosomes in the fungus *Ustilago maydis*. *EMBO J* 21, 2946-2957.

Weil, C. F., Oakley, C. E. & Oakley, B. R. (1986). Isolation of *mip* (microtubule-interacting protein) mutations of *Aspergillus nidulans*. *Mol. Biol. Cell* 6, 2963-2968.

West, R. R., Malmstrom, T., Troxell, C. L. & McIntosh, J. R. (2001). Two related kinesins, *klp5*[+] and *klp6*[+], foster microtubule diassembly and are required for meiosis in fission yeast. *Mol. Biol. Cell* 12, 3919-3932.

West, R. R., Malmstrom, T. & McIntosh, J. R. (2002). Kinesins *klp5*[+] and *klp6*[+] are required for normal chromosome movement in mitosis. *J. Cell Sci.* 115, 931-940.

Westerholm-Parvinen, A., Vernos, I. & Serrano, L. (2000). Kinesin subfamily UNC104 contains a FHA domain: boundaries and physicochemical characterization. *FEBS Lett* 486, 285-290.

Westermann, S. & Weber, K. (2003). Post-translational modifications regulate microtubule function. *Nat Rev Mol Cell Biol* 4, 938-947.

Wickstead, B. & Gull, K. (2006). A "Holistic" kinesin phylogeny reveals new kinesin families and predicts protein functions. *Mol. Biol. Cell* 17, 1734-1743.

Win, T. Z., Gachet, Y., Mulvihill, D. P., May, K. M. & Hyams, J. S. (2001). Two type V myosins with non-overlapping functions in the fission yeast *Schizosaccharomyces pombe*: Myo52 is concerned with growth polarity and cytokinesis, Myo51 is a cmponent of the cytokinetic actin ring. *J. Cell Sci.* 114, 69-79.

Woo, M., Lee, K. & Song, K. (2003). MYO2 is not essential for viability, but is required for polarized growth and dimorphic switches in *Candida albicans*. *FEMS Microbiol Lett* 218, 195-202.

Woronin, M. (1864). Entwicklungsgeschichte der *Ascobolus pucherrimus* Cr. und einiger Pezizen. *Abh Senkenb Naturforsch* 5, 333-344.

Xiang, X., Roghi, C. & Morris, N. R. (1995). Characterization and localization of the cytoplasmic dynein heavy chain in *Aspergillus nidulans*. *PNAS* 92, 9890-9894.

Xiang, X. & Plamann, M. (2003). Cytoskeleton and motor proteins in filamentous fungi. *Curr Opin Microbiol* 66, 628-633.

Xiang, X. & Fischer, R. (2004). Nuclear migration and positioning in filamentous fungi. *Fungal Genet. Biol.* 41, 411-419.

Xiang, X. (2006). A +TIP for a smooth trip. *J. Cell Biol.* 172, 651-654.

Xiong, Y. & Oakley, B. R. (2009). *In vivo* analysis of the functions of gamma-tubulin-complex proteins. *J Cell Sci.* 122, 4218-4227.

Yamamoto, A. & Hiraoka, Y. (2003). Cytoplasmic dynein in fungi: insights from nuclear migration. *J. Cell Sci.* 116, 4501-4512.

Yelton, M. M., Hamer, J. E. & Timberlake, W. E. (1984). Transformation of *Aspergillus nidulans* by using a *trpC* plasmid. *PNAS* 81, 1470-1474.

Yildiz, A., Tomishige, M., Vale, R. D. & Selvin, P. R. (2004). Kinesin walks hand-over-hand. Science 303, 676-678.

Yin, H., Pruyne, D., Huffaker, T.C., and Bretscher, A. (2000). Myosin V orientates the mitotic spindle in yeast. *Nature* 406, 1013–1015.

Yuan, P., Jedd, G., Kumaran, D., Swaminathan, S., Shio, H., Hewitt, D., Chua, N.-H. & Swaminathan, K. (2003). A Hex-1 crystal lattice required for Woronin body function in *Neurospora crassa*. *Nature Struc Biol* 10, 264-270.

Zekert, N. & Fischer, R. (2009). The *Aspergillus nidulans* kinesin-3 UncA motor moves vesicles along a subpopulation of microtubules. *Mol. Biol. Cell* 20, 673-684.

Zhang, J., Li, S., Fischer, R. & Xiang, X. (2003). The accumulation of cytoplasmic dynein and dynactin at microtubule plus-ends is kinesin dependent in *Aspergillus nidulans*. *Mol. Biol. Cell* 14, 1479-1488.

Zhang, R. G., Skarina, T., Katz, J. E. & other authors (2001). Structure of Thermotoga maritima stationary phase survival protein SurE: a novel acid phosphatase. Structure 9, 1095-1106.

Zheng, Y., Bender, A. & Cerione, R. A. (1995). Interactions among proteins involved in bud-site selection and bud-site assembly in *Saccharomyces cerevisiae*. *J. Biol. Chem.* 270, 626-630.

Zhuang, L., Zhang, J. & Xiang, X. (2007). Point mutations in the stem region and the fourth AAA domain of cytoplasmic dynein heavy chain partially suppress the phenotype of

Nadine Zekert

Karlsruhe, den 24.10. 2011

Name: Nadine Zekert
Date of birth: 12. April 1980
Nationality: Syrian
Family status: married, one child

School education

- 1985 – 1992   Al-Manar private elementary school, Damascus, Syria
- 1992 – 1995   Al-Nour private comprehensive school, Damascus, Syria
- 1995 – 1998   Al-Nour private high school, Damascus, Syria

University Education

- 06/1998   Bachelor in Pharmacy and Pharmaceutical Chemistry, University of Damascus, Syria
- 09/2004   Diploma in Microbiology, Hematology and Immunology, University of Damascus, Syria
- 07/2006   Diploma in Molecular Biology, Dept. of Microbiology, Karlsruhe Institute of Technology (KIT), Karlsruhe, Germany 07/2006
- Since 09/2006 PhD thesis in Molecular Biology, Dept. of Microbiology, Karlsruhe Institute of Technology (KIT), Karlsruhe, Germany

Participations and contributions to conferences

- 03/2006   Annual Conference of the Association for General and Applied Microbiology VAAM, Jena, Germany. **Poster**
- 03/2007   24th Fungal Genetics Conference (FGSC), Asilomar, California, (USA). **Talk + two Posters**
- 03/2007   2nd meeting on fungi of Marburg and Karlsruhe, Austria, Kleinwalsertal. **Two talks**
- 12/2007   Meeting of the priority program "Lebensmittel und Gesundheit", Karlsruhe, Germany. **Talk + Poster**
- 03/2008   31st Annual Meeting of the German Society for cell Biology (DGZ), Marburg, Germany. **Poster**
- 04/2008   European Conference on Fungal Genetics (ECFG9), Edinburgh, UK. **Poster**
- 09/2008   10th Young Scientist Meeting "Biology of cell division", German Cancer Research Center, Heidelberg, Germany. **Talk + Poster**

- 03/2009   25th fungal genetics conference (FGSC), Asilomar, California, USA. **Talk + Poster**
- 09/2009   9th VAAM Symposium "Molecular Biology of Fungi", Münster, Germany. **Poster**
- 06/2010   EMBO Conference Series "Microtubules Structure, Regulation and Functions", Heidelberg, Germany. **Poster**
- 08/2010   International Mycology Conference (IMC9) "the biology of fungi", Edinburgh, UK. **Talk**
- 04/2011   Annual Conference of the Association for General and Applied Microbiology (VAAM), Karlsruhe, Germany. **Talk**

Publications

- **Enke, C.*, Zekert, N.*, Veith, D.*, Schaaf, C., Konzack, S. & Fischer, R. (2007).** *Aspergillus nidulans* Dis1/XMAP215 protein AlpA localizes to spindle pole bodies and microtubule plus ends and contributes to growth directionality. *Eukaryot Cell* **6**, 555-562.
  * equal contribution
- **Zekert, N. & Fischer, R. (2009).** The *Aspergillus nidulans* kinesin-3 UncA motor moves vesicles along a subpopulation of microtubules. *Mol Biol Cell* **20**, 673-684. **An InCytes from the MBC Selection, Journal Cover 15.01.09**.
- **Zekert, N.*, Veith, D.* & Fischer, R. (2010).** Interaction of the *Aspergillus nidulans* MTOC component ApsB with gamma-tubulin and evidence for a role of a subclass of peroxisomes in the formation of septal MTOCs. *Eukaryot Cell* **9**, 795-805.
  * equal contribution

  Review:
- **Fischer, R., Zekert, N. & Takeshita, N. (2008).** Polarized growth in fungi - interplay between the cytoskeleton, positional markers and membrane domains. *Mol Microbiol* **68**, 813-826.

Membership

- Association for General and Applied Microbiology   (VAAM)

Acknowledgement

First of all I am deeply indebted to my supervisor
"**Prof. Dr. Reinhard Fischer**"

for trusting me and giving me the chance to work on this project, for his tireless support with ideas and advices, for his patience and prompt help in my working and living in Karlsruhe. His encouragement and Knowledge improved my skills and prepared me for future challenges. I am so lucky to have a Doctor-Father like you!

Similarly foremost all my deep gratitude belongs to my parents
"**Edgar and Nouhad**"

who always guided me towards discovering new beginnings with the most love that can ever be. I am so thankful for your love, encouragement, teaching, support, friendship and trust. I thank God for having you and for having your genes in my genome!
Without you I would never be the person I am! I love you!

My gratitude belongs also to my sister and my brother
"Myriam and Bernar"

who are my supporter, care and love resource. Thanks for being always beside me.

My special thank to all my friends in Syria, specially
"**May Daoud, Rouba Kilzi and Aline Saradourian**"
for their endless love and support.

To **Onkel Gerhard and Onkel Bernhard together with Tante Anneliese und Renate**, for their love and care. For helping me with all my problems and accidents and for the joy they bring to my life. Thank you for being my German families!

Here I wish to express my special thank to all my former and present colleagues.
"**Sylvia Müller, Sabrina Hettinger, Constanze Seidel, Ramona Demir, Sonja Sand, Janina Purschwitz ;), Carolin Schaaf, Norio Takeshita, Kay Vienken, Daniel Veith, Christian Kastner, Elisabeth Poth, Saturnino Herrero de Vega, Friederike Bathe, Julio Rodriguez, Yuhei Higashitsuji, Debjani Saha, Tobias Schunck, Jan Siebenbrock, Tanja Sauerbrunn, Maren Hedtke, Daniel Mania, Claudia Kempf and Elke Wohlmann**" and to "**Nicole Helber and Michael Pacher**". Thank you for sharing scientific opinions and fruitful ideas, for technical help and for motivation and for making me laugh.

I wish to express my warm and sincere thank to
"**Prof. Dr. Jörg Kämper, Prof. Dr. Natalia Requena, their groups and for the Nadicom**"
Thank you for your kind help every time I needed!

I would like to thank the Syrian high-education ministry for its financial support and all my professors in my original Institute in Syria.

Special cordial thanks I address to my husband
"**Rawad Zodi**"
for his love, care and support. Thank you for being "with **Marc**" my joy of life

Finally I want to thank God for giving me such an amazing life!

Aspergillus nidulans Dis1/XMAP215 Protein AlpA Localizes to Spindle Pole Bodies and Microtubule Plus Ends and Contributes to Growth Directionality[▽][†]

Cathrin Enke,[1,2][‡] Nadine Zekert,[1][‡] Daniel Veith,[1,2][‡] Carolin Schaaf,[1] Sven Konzack,[1,2] and Reinhard Fischer[1,2]*

University of Karlsruhe, Applied Microbiology, Hertzstrasse 16, D-76187 Karlsruhe,[1] and Max Planck Institute for Terrestrial Microbiology, Karl-von-Frisch-Str., D-35043 Marburg,[2] Germany

The dynamics of cytoplasmic microtubules (MTs) is largely controlled by a protein complex at the MT plus end. In *Schizosaccharomyces pombe* and in filamentous fungi, MT plus end-associated proteins also determine growth directionality. We have characterized the Dis1/XMAP215 family protein AlpA from *Aspergillus nidulans* and show that it determines MT dynamics as well as hyphal morphology. Green fluorescent protein-tagged AlpA localized to MT-organizing centers (centrosomes) and to MT plus ends. The latter accumulation occurred independently of conventional kinesin or the Kip2-familiy kinesin KipA. *alpA* deletion strains were viable and only slightly temperature sensitive. Mitosis, nuclear migration, and nuclear positioning were not affected, but hyphae grew in curves rather than straight, which appeared to be an effect of reduced MT growth and dynamics.

Microtubules (MTs) are hollow tubes which are generated from microtubule-organizing centers, and they perform multiple structural and dynamic functions in a cell. Although comprising an important part of the cell skeleton, MTs are very dynamic structures, which assemble at one end α,β-tubulin dimers, stop growth after some time, undergo a catastrophe event, and subsequently shrink. This dynamic instability is regulated by a number of different MT-associated proteins (MAPs), one of which was discovered in *Xenopus* and named XMAP215 (5). Similar proteins, which are meanwhile classified in the Dis1/XMAP215 family, exist in eukaryotes from yeast to plants and humans (17). Common to all of them is their association with MTs and the presence of TOG domains and HEAT repeats, which are responsible for interactions with many different associated proteins. One MAP can interact through its TOG domains and HEAT repeats with several other MAPs. The proteins were classified into three different groups (17). Members of the first group have four TOG domains, including one to five HEAT repeats within each of them, and a conserved C terminus. Human ch-TOG belongs to the first group together with *Xenopus* XMAP215, *Drosophila* (Msps), *Dictyostelium* (DdCP224), and *Arabidopsis* (MOR1) (Fig. 1). The second group has only one known member from *Caenorhabditis elegans* (ZYG-9). Members of the third group have only two TOG domains with several HEAT repeats and, in comparison to group one members, do not have a conserved

C terminus. However, all of them harbor a coiled-coil region instead. XMAP215 proteins have a prominent MT-stabilizing function (12). Recently, it was shown nicely in *Saccharomyces cerevisiae* that the Dis1/XMAP215 protein Stu2 binds to tubulin heterodimers and associates to the MT plus end, where it appears to be responsible for the loading of α,β-tubulin dimers to the growing end (1). This activity may explain the Stu2 stabilization activity of MTs in living cells.

Besides the MT stabilization activity of Dis1/XMAP215 proteins, DdCP224, the *Dictyostelium discoideum* homologue, is involved in MT-cortex interactions. There is evidence that this contact is mediated by cortical dynein with which DdCP224 is able to physically interact (9).

In this paper, we have analyzed the function of the Dis1/XMAP215-like protein AlpA in *Aspergillus nidulans*. The protein localized at the spindle pole bodies (the fungal homologues of centromeres) and at MT plus ends. Interestingly, deletion of the gene was not lethal, although a drastic reduction of the MT array and MT dynamics was observed. Hyphae of an *alpA* deletion strain grew in curves, suggesting that AlpA is involved in the determination of growth directionality.

MATERIALS AND METHODS

Strains, plasmids, and culture conditions. Supplemented minimal and complete media for *A. nidulans* were prepared as described previously, and standard strain construction procedures were as described by Hill and Käfer (10). A list of *A. nidulans* strains used in this study is given in Table 1. Standard laboratory *Escherichia coli* strains (XL1-Blue) were used. Plasmids are listed in Table 2.

Light and fluorescence microscopy. For live-cell imaging, cells were grown in glass-bottom dishes (World Precision Instruments, Berlin, Germany) in 4 ml of minimal medium containing either 2% glycerol (or ethanol) or 2% glucose as a carbon source. Medium was supplemented with pyridoxine, *p*-aminobenzoic acid, biotin, arginine, uracil, or uridine depending on the auxotrophy of the strains. Cells were incubated at room temperature for 1 to 2 days, and images were captured using an Axiophot microscope (Zeiss, Jena, Germany), a Planapochromatic 63× or 100× oil immersion objective lens, and an HBO50 Hg lamp. Alternatively, a Zeiss AxioImager Z1 with the latest AxioVision software

FIG. 1. AlpA belongs to the third group of the Dis1/XMAP215 family. (A) Two TOG domains, eight HEAT repeats, and a coiled-coil region were identified, which are common to all class three members, including *S. pombe* Alp14 and Dis1, which is the Dis1/XMAP215 family-founding protein, and *S. cerevisiae* Stu2. Members of the first group include human ch-TOG, *Xenopus* XMAP215, *Drosophila melanogaster* Msps, *D. discoideum* DdCP224, and *Arabidopsis thaliana* MOR1. So far, there is only one known group two member, namely ZYG-9 of *Caenorhabditis elegans*. (B) Phylogenetic analysis of *S. pombe* Alp14 (Sp) homologues with *S. cerevisiae* (Sc), *A. nidulans* (An), *A. fumigatus* (Af), and *A. oryzae* (Ao). Accession numbers are indicated.

(v 4.5) was used. Fluorescence was observed using standard Zeiss filter combinations no. 09 (fluorescein isothiocyanate, green fluorescent protein [GFP]) and no. 15 (DsRed). Images were collected and analyzed with a Hamamatsu Orca ER II camera system and the Wasabi software (version 1.2) or Zeiss Axiocam and AxioVision software. Time-lapse series were obtained with an automated Wasabi program that acquires series of images with 2- or 5-s intervals, 0.1- or 0.75-s exposure time, and about 100 exposures in a sequence. Image and video processing were done with the Wasabi software from Hamamatsu, Adobe Photoshop, ImageJ (NIH, Bethesda, MD), and virtual dub (http://www.virtualdub.org).

To determine SPK position, strains were grown on a microscope slide for 24 h at room temperature in MM containing 17% gelatin, and images were captured using differential interference contrast microscopy.

Molecular Techniques. Standard DNA transformation procedures were used for *A. nidulans* (30) and *E. coli* (22). For PCR experiments, standard protocols were applied using a Biometra Personal Cycler (Biometra, Göttingen, Germany) for the reaction cycles. DNA sequencing was done commercially (MWG Biotech, Ebersberg, Germany). Total DNA was extracted from *A. nidulans* in the following way. Spores were inoculated in liquid minimal medium plus supplements and grown for 16 to 24 h at 37°C without shaking. Hyphal mats were harvested, dried with tissue paper, and ground in liquid nitrogen. The resulting powder was mixed with extraction buffer (50 mM EDTA, 0.2% sodium dodecyl sulfate) and incubated for 30 min to 2 h at 68°C in a water bath. Sodium dodecyl sulfate was removed from the suspension by addition of sodium acetate solution (8 M, pH

4.2) and centrifugation. From the supernatant, total DNA was precipitated with isopropanol, and the pellet was washed twice with 70% ethanol, air dried, resuspended in TE buffer, and stored at 4°C. Southern hybridizations were performed according to the DIG Application Manual for Filter Hybridization (Roche Applied Science, Technical Resources; Roche Diagnostics GmbH, Mannheim, Germany).

Deletion of *alpA* and construction of a Δ*alpA*/Δ*kipA* double mutant. The *alpA* flanking regions were amplified by PCR using genomic DNA and the primers *alpA*_LB_fwd (5′-TCAAGGGCAGAGAGGGATGCAATC-3′) and *alpA*_LB_rev_Sfi (5′-CGGCCATCTAGGCCTGCGGAAGGTGGCGATG-3′) for the upstream region of *alpA* and *alpA*_RB_fwd_Sfi (5′-CGGCCTGAGTGGCCTGTACGGTCAACTTTAGG-3′) and *alpA*_RB_rev (5′-GAGTTCGCTAAGCTCCTCAGTGCCATC-3′) for the downstream region and cloned into pCR2.1-TOPO to generate pAT1 and pAT2, respectively (the Sfi restriction sites are underlined in the primer sequences). In a three-fragment ligation, the *pyr4* gene from plasmid pCS1 was ligated between the two *alpA*-flanking regions, resulting in vector pAT3. The vector pAT3 was digested with restriction enzyme KpnI, and the linearized plasmid was transformed into the uracil/uridin-auxotrophic strain TNO2A3. Among six transformants, five displayed homologous integration of the deletion cassette at the *alpA* locus. As primers for the indicative PCR, we used oligonucleotides derived from the *pyr4* gene: *pyr4*-5′ (5′-GGTTGAGGAAGCAGTCGAGAGC-3′) and *pyr4*-3′ (5′-CTCGAGGACGAGCCGC-3′) and the *alpA* external primers *alpA*_5′-outside (5′-TACCCTAAGGTCACTACG-3′) and *alpA*_3′-outside (5′-AGATGGGTGTTCCTTACG-3′). Two of the Δ*alpA* strains (SCS13a and SCS13b) were also analyzed by Southern blotting (data not shown). In both strains, uracil/uridine prototrophy was linked to the *alpA* deletion, as shown by crossing them with uracil/uridin-auxotrophic *alpA* wild-type strains (data not shown).

To generate a Δ*alpA*/Δ*kipA* double mutant, we crossed the *kipA* deletion strain SSK44 with the deletion strain of *alpA* (SCS13). Heterokaryon formation was forced on MM, where none of the parent strains can grow alone. Progeny strains were screened by PCR and Southern blotting for the double deletion (data not shown).

Bioinformatics. Protein sequences were aligned using vector NTI software (Invitrogen), MegAlign, and ClustalW software (http://www.embl-heidelberg.de). TOG domains and heat repeats of AlpA were identified using "REP" from the ExPASy database.

RESULTS

Identification of a Dis1/XMAP215 family protein in *A. nidulans*. To characterize the role of the MT plus end complex for polarized growth, we searched the *A. nidulans* database with the *Schizosaccharomyces pombe* Alp14 protein sequence (4) (http://www.broad.mit.edu). The putative homologue AlpA (An5521.2) is a 96.4-kDa protein comprised of 891 amino acid residues. The open reading frame is disrupted by three short introns, 70 bp, 72 bp, and 72 bp in size. The intron-exon borders were confirmed by reverse transcription-PCR of small cDNAs, subsequent sequencing, and comparison with the sequence of genomic DNA. Protein analysis revealed eight HEAT repeats embedded in two TOG domains at the N terminus and a coiled-coil region at the C terminus (Fig. 1A). According to Ohkura et al. (17), MAPs of the Dis1/XMAP215 family are grouped into three classes (Fig. 1A). Sequence comparison of *A. nidulans* AlpA, which belongs to group three of the Dis1/TOG family, with related proteins from *S. pombe* showed a similarity of 30% to Alp14 and 23% to Dis1 (Fig. 1B). In contrast to *S. pombe*, where two proteins of this family exist, a protein with higher similarity to Dis1 was not found in *A. nidulans*. Sequence similarities of putative Alp14 homologues in *Aspergillus oryzae* (Ao_AlpA) and *Aspergillus fumigatus* (Af_AlpA) displayed similarities of 44.8% and 43.6% to Alp14 but of 84.2% and 84.5% to *A. nidulans* AlpA and 89.1% to each other. A Dis1 homologue was also not identified in the latter two *Aspergillus* species.

TABLE 1. *A. nidulans* strains used in this study

Strain	Genotype[a]	Source or reference
GR5	*pyrG89 wA3 pyroA4*	28
GFP-NudA	*pyrG89 wA2 pyroA4 ΔnudA::pyr4 alcA(p)::GFP::nudA::pyr4*	6
GFP-NudF	*pyrG89 wA2 pyroA4 ΔnudF::pyr4 alcA(p)::GFP::nudF::pyr4*	6
RMS011	*pabaA1 yA2 ΔargB::trpCΔB trpC801*	25
SCE01	SJW02 transformed with pCE05; *wA3 ΔargB::trpCΔB pyroA4 alcA(p)::alpA::mRFP1 alcA(p)::GFP::tubA*	This work
SCE05	SRF200 transformed with pCE08; *ΔargB::trpCΔB pyroA4 alcA(p)::GFP::alpA* (single homologous integration)	This work
SCE10	SRF200 transformed with pCE06; *pyrG89 ΔargB::trpCΔB pyroA4 alcA(p)::alpA::GFP*	This work
SCE12	SRF200 transformed with pCE06, pJW18, and pPND1; *alcA(p)::mRFP1::stuA alcA(p)::alpA::GFP alcA(p)::mRFP::kipB^rigor*	This work
SCE35	SSK44 transformed with pCE06; *pabaA1 wA3 ΔargB::trpCΔB ΔkipA::pyr4 alcA(p)::alpA::GFP* (single integration)	This work
SCS13a/b	TNO2A3 transformed with pAT3; *pyrG89 pyroA4 argB2 ΔnkuA::argB ΔalpA::pyr4*	This work
SDV69f	SNR1 transformed with pCE06; *ΔkinA::pyr4 pyroA4 alcA(p)::GFP::alpA* (single integration)	This work
SDV83b	SCS13 crossed with RMS011; *pabaA1 yA2 pyrG89 ΔalpA::pyr4*	This work
SDV86	SDV83b crossed with SJW02; *pabaA1 yA2 pyrG89 alcA(p)::GFP::tubA ΔalpA::pyr4*	This work
SDV87	SDV83b crossed with SSK92; *pabaA1, yA2, pyrG89; alcA(p)::GFP::kipA ΔalpA::pyr4*	This work
SDV96	TN02A3 transformed with pPND1 and pCE06; *alcA(p)::mRFP1::kipB^rigor alcA(p)::alpA::GFP*	This work
SDV100	SDV83 transformed with pGFP-NudA; *ΔalpA alcA(p)::GFP::nudA* (single integration)	This work
SDV101	SDV83 transformed with pGFP-NudF; *ΔalpA alcA(p)::GFP::nudF* (single integration)	This work
SDV102	SDV83 crossed to GFP-ClipA; *ΔalpA alcA(p)::GFP::clipA*	This work
SJW02	*wA3 pyroA4 alcA(p)::GFP::tubA ΔargB::trpCΔB*	J. Warmbold, Marburg, Germany
AnKin26	*pyrG89 yA2 ΔargB::trpCΔB ΔkinA::pyr4*	18
SRF200	*pyrG89 ΔargB::trpCΔB pyroA4*	11
SSK44	*pabaA1 wA3 ΔargB::trpCΔB ΔkipA::pyr4*	13
SSK92	*wA3 pyroA4 alcA(p)::GFP::kipA*	13
TNO2A3	*pyrG89 pyroA4 argB2 ΔnkuA::argB*	16
SNR1	*ΔargB::trpCΔB pyroA4 ΔkinA::pyr4*	18
ΔclipA	*pyrG89 wA3 ΔclipA::pyroA*	2
SAD1c	SSK44 crossed with SCS13; *wA3 pyroA4 ΔkipA::pyr4 ΔalpA::pyr4*	This work

[a] Only relevant genotypes are indicated. All strains carry the *veA1* mutation.

AlpA localizes to MT plus ends during mitosis and in interphase. To analyze the function of *alpA* in *A. nidulans*, we studied the subcellular localization of the protein. We fused the *alpA* gene at the 3′ or 5′ end with GFP (pCE06, pCE08) or mRFP1 (pCE05) and transformed it into strain TN02A3 (SDV96) or SJW02 (SCE01). MTs were labeled in green (GFP) or red (mRFP1). The *alpA* construct was expressed under the control of the *alcA* promoter, with glycerol as a carbon source. Glycerol leads to derepression of the promoter but not induction, unlike ethanol (3). The expression levels under these conditions are quite low, and the problem of mislocalization of fusion proteins is minimized. Several transformant strains were analyzed in vivo, and identical results were obtained. AlpA localization and behavior were identical in C- and N-terminally fused GFP constructs (SCE10, SCE05). In general, the AlpA-GFP and AlpA-mRFP1 signal intensities

TABLE 2. Plasmids used in this study

Plasmids	Construction[a]	Source or reference
pAT1	1,000 bp upstream of *alpA* ORF (= LB) cloned into pCR2.1	This work
pAT2	1,001 bp downstream of *alpA* ORF (= RB) cloned into pCR2.1	This work
pAT3	*alpA*-LB::*N. crassa pyr-4*::*alpA*-RB in pCS2.1	This work
pCE05	*alcA::alpA::mRFP1 argB*; gateway construct of pMT01	26; this work
pCE06	*alcA::alpA::GFP argB*; gateway construct of pMT-sGFP	26; this work
pCE08	*alcA(p)::GFP::alpA pyr4*; 1 kb of *alpA* with AscI und PacI inserted into pMCB17apx	27; this work
pCR2.1-TOPO	Cloning vector	Invitrogen
pCS1	*N. crassa pyr-4* selectable marker as NotI fragment in pUMA208	This work
pGFP-NudA	*alcA(p)::GFP::nudA::pyr4*	6
pGFP-NudF	*alcA(p)::GFP::nudF::pyr4*	6
pPND1	Rigor mutant of KipB for staining MTs, *alcA(p)::mRFP1::kipB^rigor*	21
pMCB17apx	pMCB17 version for fusion of GFP to N termini of proteins of interest	27
pJW18	Red nuclei, *alcA(p)::mRFP1::stuA*	J. Warmbold, Marburg, Germany

[a] ORF, open reading frame.
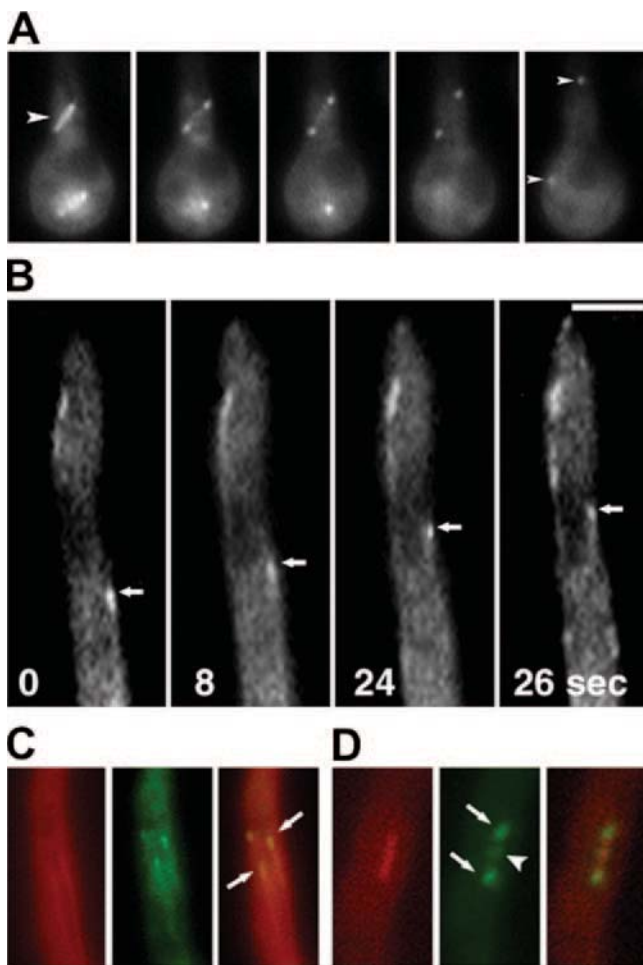
FIG. 2. AlpA localization during mitosis and in interphase. (A) During mitosis, GFP-AlpA was distributed along short spindles (arrowhead in the first frame). As the spindle elongated GFP-AlpA was redistributed to the spindle poles (arrowheads in the last frame). Frames are shown in 2-min intervals. The strain was SCE05. (B) GFP-AlpA movement can be seen as comet-like structures, indicating the association with the MT plus ends (see Movie S01 in the supplemental material) (C, D) MTs were visualized by decoration with a red-labeled kinesin rigor mutant protein (mRFP1-KipB^{rigor}) during interphase (C) and mitosis (D) (strain SDV96). The arrows point to a GFP-AlpA signal at MT plus ends (C) and to the spindle pole bodies (D). The arrow head in panel D points to the center of the spindle, where the protein could be associated with the kinetochores. Bars, 3 μm (A) and 2 μm (B to D).

were very low, which sometimes made a high-resolution analysis difficult. Figure 2A shows a mitotic spindle decorated with associated GFP-AlpA. During early mitosis, the complete spindle was covered with GFP-AlpA. As the spindle elongated, GFP-AlpA was distributed exclusively to the spindle poles (Fig. 2A). At some stage of mitosis, presumably the early metaphase, GFP-AlpA was detected in the middle of the spindle, suggesting association with the plus ends of the spindle MTs contacting the kinetochors (Fig. 2D). In interphase cells, GFP-AlpA localized to MTs as well, notably to the MT plus ends (Fig. 2B, C), and followed MT growth as comet-like structures (see Movie S01 in the supplemental material). This was similar to kinesin KipA, dynein heavy chain NudA, and NudF localization (29).

alpA deletion strains show defects in polarized growth. The *alpA* gene was deleted by homologous recombination where the *alpA* ORF was replaced by the *Neurospora crassa pyr4* gene. We used *A. nidulans* strain TNO2A3, which has a very high frequency of homologous integration (16). Homologous single integration was verified by Southern blot and PCR analysis in 3 of 7 tested strains (data not shown). Compared to the wild type, *alpA* deletion strains showed reduced colony size and compact growth, especially at higher temperatures (Fig. 3A). Although the conidiospore number was slightly reduced in *alpA* deletion strains, the morphology of conidiophores was indistinguishable from that of the wild type. Interestingly, and in contrast to the situation in *S. cerevisiae*, deletion strains were viable. This was surprising because we found only one Alp14 similar protein in the *A. nidulans* genome in comparison to two in *S. pombe*, where Dis1 can substitute for Alp14 (Fig. 1). Hyphae of the *alpA* deletion strain did not show any difference with regard to nuclear distribution or septation, but hyphal morphology was changed. While wild-type hyphae grow relatively straight, the *alpA* deletion strain produced curly or curved hyphae (Fig. 3B, C), which were similar to hyphae of a *kipA* deletion strain (13). In addition to the curved growth phenotype, we noticed an increased number of branches in older hyphae. To show that the observed phenotypes were due to the deletion event, we constructed a plasmid where about 1 kb of the 5′ end of the *alpA* gene was fused to GFP and under the control of the inducible *alcA* promoter. The construct was integrated at the *alpA* locus (confirmed by Southern blotting), resulting in a full-length, GFP-fused version under the control of the *alcA* promoter (strain SCE05). The strain was used in the localization experiments described above. Under repressing conditions (glucose), SCE05 showed the knockout-like curved growth (Fig. 3D), whereas under inducing conditions (ethanol), wild-type-like growth was restored (Fig. 3E). This result proved that the GFP-tagged protein version was fully functional.

The curved growth phenotype in the *alpA* mutant resembled that of a *kipA* deletion strain (13). Therefore, we asked whether the lack of both genes would result in a similar or a different phenotype than that of the single mutations. The double mutant showed a more severe phenotype than the individual mutations. Hyphae appeared even more curly and similar to the *alpA* mutant, with more branches in older hyphae. Colonies were much smaller than the colonies of the parent strains, indicating an additive effect of $\Delta kipA$ and $\Delta alpA$ (Fig. 4A).

Because the growth direction of hyphae depends on the localization of the Spitzenkörper in the apex, we analyzed the position of this organelle in the wild type and compared it to the one in the *alpA*, *kipA*, and *alpA kipA* double deletion strains. Whereas in the wild type, the Spitzenkörper was found in the center of the hyphae in 70% and noncentral in 30% of the cases (n = 50), in the *alpA* deletion strain, only 22% showed the central position and 78% the noncentral one (n = 50). In comparison, in the *kipA* deletion strain, the percentages were 28% (central) and 72% (noncentral) (n = 50), and in the *alpA kipA* double deletion strain, the percentages were 52% (central) and 48% (noncentral) (n = 64) (Fig. 4B, C). It was surprising that the number of central and noncentral positioning of the Spitzenkörper was almost even in the double mutant
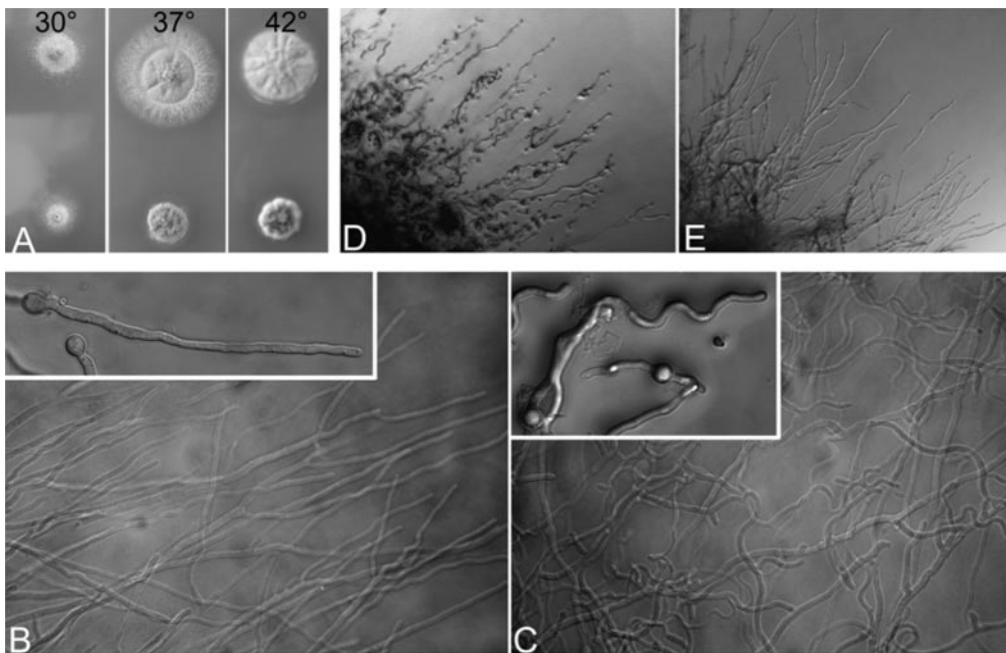
FIG. 3. Phenotype of an *alpA* deletion strain. (A) In comparison to a control strain (top, RMS011), the Δ*alpA* strain (bottom, SDV83b) grew slower and colonies were more compact. While wild-type hyphae grew straight (B), hyphae of the *alpA* deletion strain showed a curved growth phenotype (C). (D) In a strain having the only functional copy of *alpA* under the control of the inducible *alcA* promoter (SCE05), curved growth was observed under repressing conditions (glucose), but wild-type hyphal morphology was restored when grown under inducing conditions (ethanol) (E).

strain. In addition, we noticed that in 18% of the cases two Spitzenkörper were observed in the hyphal tip. In comparison, this number was only 5% in the wild type, 10% in the *alpA* mutant, and 5% in the *kipA* mutant. If there were two Spitzenkörper in the apex, we counted them as one event of non-central organelles in the quantification shown in Fig. 4A.

To test whether AlpA might play a role in the initiation of polarized growth, we analyzed the germination pattern of conidiospores (Fig. 4D). Wild-type conidiospores produce a second germ tube after the first germ tube has reached a certain length, and this second hypha emerges from a place opposite the first hypha. In contrast, the *alpA* deletion strain produced the second germ tube normally in angles smaller than 180° from the first hypha (Fig. 4D). This germination pattern resembled the one from the *kipA* mutant strain (13).

AlpA determines cytoplasmic MT dynamics. To further unravel the function of *alpA* in *A. nidulans*, we studied the effect of the *alpA* deletion on the MT cytoskeleton. MTs were visualized in the *alpA* deletion strain by GFP staining (6) (strain SDV86). Compared to he wild type (SJW02), the number of MTs was reduced in the Δ*alpA* strain. Basically, only one thick MT bundle (according to Veith et al. [27]), connecting adjacent nuclei, was visible, in addition to some shorter MTs emerging from the nuclear spindle pole bodies, while in the wild-type strain several single and bundled MTs were present (Fig. 5A, B). In addition, the normally highly dynamic MTs appeared more stable and less dynamic. Whereas wild-type MTs polymerize at a rate of 14 μm per min (6), the extension rate in the *alpA* mutant was only 6 μm per minute. It has to be noted that growth of MTs only occurred occasionally. Most MTs did not elongate nor shrink. After MTs have reached the

hyphal tip, they normally disassemble (MT catastrophe) within 20 s (see Movie S02 in the supplemental material) (13). In the Δ*alpA* background, fewer MTs reached the tip (4 in 5 min, compared to 20 in the wild type [36 hyphae analyzed]), and disassembly did not occur within minutes (see Movie S03 in the supplemental material). In addition, the number of emerging MTs in the mutant was reduced by 85% (25 hyphae analyzed). The mitotic spindle and mitosis itself were indistinguishable from that of the wild type (see Movie S04 in the supplemental material).

To analyze whether AlpA influences the stability of MTs, we tested the sensitivity of an *alpA* deletion strain (SDV83b) toward the microtubule-destabilizing agent benomyl. Whereas the wild type was able to produce colonies up to a concentration of 0.8 μg/ml, the *alpA* mutant was unable to grow at concentrations higher than 0.6 μg/ml (Fig. 6). This result suggests that AlpA stabilizes MTs in *A. nidulans*.

Interdependence of AlpA with other MT plus end-associated proteins. The fact that AlpA localized to the MT plus end in interphase cells raised the question of how it reaches the destination and whether this localization depends on the presence or activity of other MT plus end-associated proteins. To this end, we studied interactions between AlpA and the kinesins KinA and KipA, the dynein pathway components NudA and NudF, and the Clip170 homologue ClipA.

We analyzed AlpA MT plus end localization in Δ*kipA* and Δ*kinA* mutant backgrounds (strains SCE35 and SDV69f). The situation for GFP-AlpA in the Δ*kipA* and Δ*kinA* backgrounds was wild-type-like (not shown). Both KipA and KinA have been shown to be involved in MT plus end accumulation of ClipA and NudA, respectively (2, 31), but neither of those
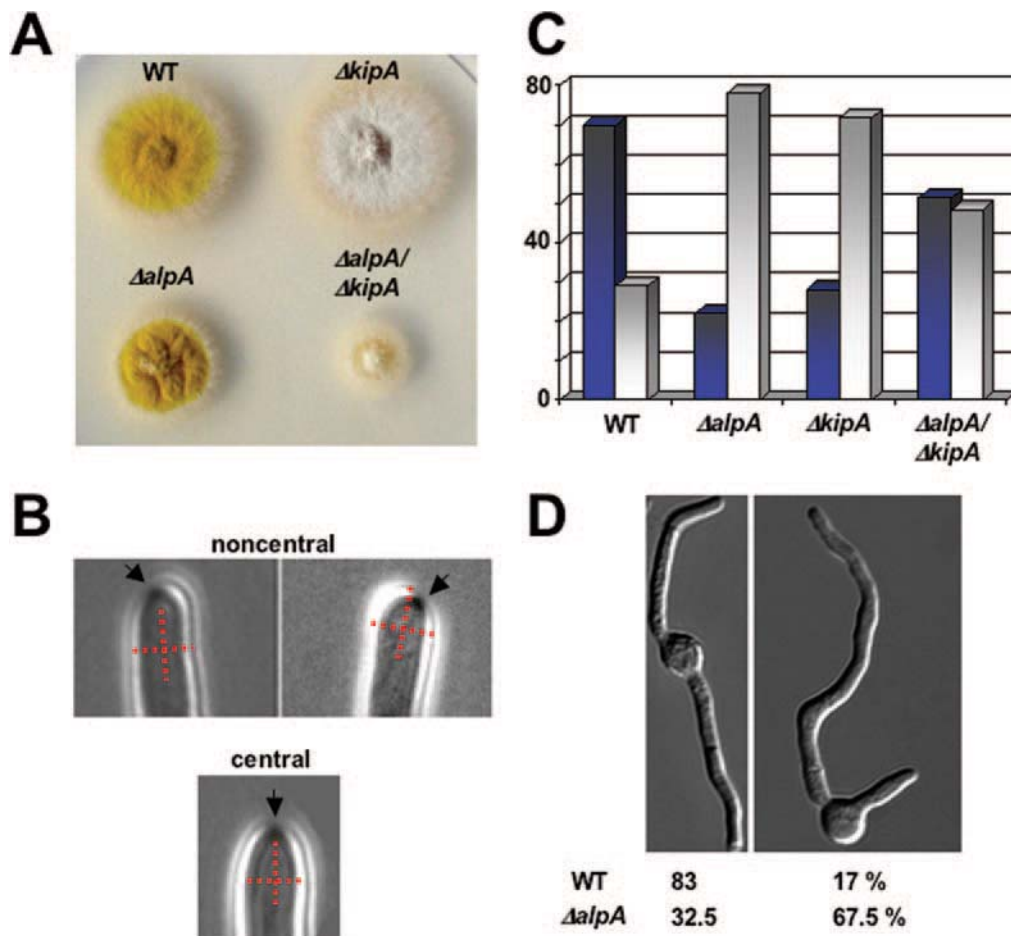
FIG. 4. Localization of the Spitzenkörper in hyphae and germination pattern. The Spitzenkörper was observed in growing hyphae as described previously (19). (A) Colonies of the wild-type (RMS011) (WT), ΔalpA (SDV83), ΔkipA (SSK44), and ΔalpA ΔkipA (SAD1c) strains on an agar plate after 3 days of growth at 37°C. (B) Representative hypha with a Spitzenkörper in the center of the cell or noncentral. To indicate the position of the organelle, we introduced a cross into the hypha. (C) Quantification of the location of the Spitzenkörper in the strains listed for panel A. Dark blue columns represent hyphae with the Spitzenkörper in the center and gray columns the ones where the Spitzenkörper was noncentral. Between 50 and 64 hyphae were analyzed for each strain. (D) Quantification of the germination pattern of conidiospores as displayed in the pictures. Wild type (RMS011), $n = 200$; alpA mutant (SDV83), $n = 268$.

two kinesins was responsible for AlpA plus end localization. These results are in agreement with recent findings in *S. cerevisiae*, where Al-Bassam et al. (1) showed for the AlpA homologue Stu2 that it localizes to MT plus ends independently of any motor protein. Localization was dependent on the second TOG domain of Stu2, whereas the first TOG domain promotes the addition of α,β-tubulin dimers to the growing MT end.

To analyze the role of AlpA at the MT plus end and in polarized growth, we sought to determine whether AlpA is required for the recruitment of other proteins, such as the kinesin-like protein KipA, ClipA, the dynein motor NudA, or one of its regulators (NudF) to this place. Therefore, we constructed *alpA* deletion strains in which KipA or ClipA were labeled with GFP. Normally, both proteins accumulate at the MT plus end and hitchhike with the growing MT end. The visible movement of the KipA- or ClipA-GFP spots were described as comets (see Movie S05 in the supplemental material) (2, 13). KipA movement in an *alpA* deletion strain was reduced, and GFP-KipA partly decorated cyto-

plasmic MTs behind the plus end instead of moving with the MT plus end (Fig. 5C, D; see also Movie 06 in the supplemental material). An accumulation of the GFP fusion protein was still visible at the MT plus end. Because MTs did not extend as fast as in the wild type (see above), KipA-GFP comets were not observed. Similar results were obtained for ClipA (our own results and L. Zhuang and X. Xiang [Bethesda, MD], personal communication), dynein (NudA), and its regulator NudF. In strains with fusion proteins of GFP-NudA and GFP-NudF in a Δ*alpA* background (strains SDV100 and SDV101), MTs were similarly GFP decorated (Fig. 5E, F). However, in comparison to KipA, longer stretches of MTs were decorated with either NudA or NudF. Further experiments should address the question of whether the slight differences in localization are of functional importance or due to, e.g., different protein amounts of NudA, NudF, and KipA. The fact that the localization of components of the dynein pathway appears to be affected in *alpA* mutants does not cause nuclear distribution defects (see above) suggests that even in the absence of AlpA sufficient

FIG. 6. Benomyl sensitivity of the wild-type (upper row of colonies) and *alpA* deletion (lower row) strains. Benomyl was added in concentrations from 0 to 0.8 μg/ml, and colonies were grown for 2 days at 37°C.

FIG. 5. *alpA* affects MTs and MT plus end-localized proteins. (A) Several MTs and bundles thereof stained with GFP are obvious in the wild type (SJW02). (B) The number and dynamics (see Movies S02 and S03 in the supplemental material) of MTs in an *alpA* deletion strain (SDV86) were reduced compared to the wild type. Arrowheads point to nuclei and arrows to spindle pole bodies. (C) While GFP-KipA localized to MT plus ends and moved as comets in the wild type (SSK92) (see Movie S05 in the supplemental material), (D) GFP-KipA decorated short fragments of MTs in the Δ*alpA* background (SDV87) (see Movie S06 in the supplemental material). Fragments of MTs were also GFP decorated in Δ*alpA* strains with GFP-NudA (E) and GFP-NudF (F) fusion proteins (strains SDV100 and SDV101). Arrows in panels D to F point to MT plus ends as determined by the growth at this end. Bars in panel B, 5 μm (A, C, and D), 6 μm (B), and 4 μm (E and F).

amounts of, e.g., dynein reach their normal place in the cell and serve the wild-type function.

DISCUSSION

In this paper, we characterized the Dis1/XMAP215 family protein AlpA from *A. nidulans* and found that it is associated with the MT plus end during mitosis and in interphase. AlpA plays a role in controlling MT dynamics and is important for the determination of growth polarity. Whereas the mechanism of MT stabilization was recently shown in *S. cerevisiae* (1), a role in polarized growth has not been described before. Polarized growth of filamentous fungi depends on the continuous delivery of secretory vesicles (7, 20). These vesicles provide new membranes and deliver, e.g., enzymes for cell wall biosynthesis. Because the vesicles are generated some distance away from the growing tip, they need to be transported long distances. It is assumed that MTs and conventional kinesin provide the basis for this long-distance transportation (18, 23). The first destination of the vesicles is an organelle close to the apex named the vesicle supply center or Spitzenkörper (8). The location of this organelle determines growth direction. For the last few micrometers between the Spitzenkörper and the cell membrane, fungi probably employ the actin cytoskeleton and its associated motors. According to this model, MTs contribute to polarized growth as tracks for the transportation of vesicles. Surprisingly, deletion of *alpA* seems not to affect long-distance vesicle transportation and accumulation of the vesicles in the Spitzenkörper significantly, despite the dramatic effects on MT organization. This result suggests that only few MTs are sufficient for efficient vesicle transportation. This is in agreement with observations that the growth rate of hyphae does not change during mitosis, although most of the cytoplasmic MTs are degraded during nuclear division (19). Another explanation for the observed growth in the *alpA* deletion strain could be the vesicle transport activity of the actin cytoskeleton. However, the fact that mutations in tubulin-encoding genes or in MT-dependent motor protein encoding-genes affect hyphal extension highly suggests an important role of MTs in polarized growth (18, 23). Although the Spitzenkörper was not obviously reduced in size in the *alpA* mutant, the position appears to be dependent on AlpA, as it was shown before for KipA (Fig. 5). An open question remains, however, why the number of centrally localized Spitzenkörpers increased again in the *alpA kipA* double mutant. Perhaps this is linked to the observation that the number of hyphae with two Spitzenkörpers in the apex was increased.

Results with *S. pombe* and *A. nidulans* suggest a second role for MTs in the determination of growth direction, and this feature is obviously affected in *alpA* deletion strains (13–15). According to the model of *S. pombe*, so called cell-end factors

are transported towards the MT plus end and hitchhike with the growing MTs towards the cell cortex. A cell end factor is, for instance, the membrane-associated protein Mod5, which was suggested to act as an anchor for Tea1 and Tea4. The latter protein in turn binds the formin For3, which catalyzes actin polymerization (15, 24). Although we were not able to identify a Mod5 homologue in *A. nidulans* or other aspergilli yet, the presence of the kinesin KipA (Tea2) and TeaA (Tea1) as well as a curved growth phenotype upon deletion of either of them (13) (results for TeaA are unpublished) suggests at least partial conservation of the mechanism. If this is the case and if deletion of *alpA* caused a phenotype similar to that of deletion of *kipA*, the question is how AlpA is involved in polarity determination. It was shown in *D. discoideum* that DdCpd224 interacts with cortical dynein and thereby could mediate the contact between MT plus ends and the cortex (9). In *A. nidulans*, the situation could be similar, and a missing cortical contact could lead to the curved hyphal growth. However, it has to be noted that dynein mutants of *A. nidulans* do not display the same hyphal growth phenotype. In addition, dynein-mediated MT-cortical interactions are required for nuclear migration and nuclear positioning (27). Both phenomena were not affected in *alpA* mutants. Therefore, it seems likely that the lack of AlpA drastically reduces MT dynamics and that this leads to a reduction of specific cell end marker delivery. One of the key challenges is therefore to identify such cell end marker proteins in filamentous fungi. The fact that the *alpA kipA* double mutant displayed a more severe phenotype with regard to hyphal extension in comparison to the strains with only one mutation suggests that the two genes also act in different pathways.

ACKNOWLEDGMENTS

REFERENCES

1. **Al-Bassam, J., M. van Breugel, S. C. Harrison, and A. Hyman.** 2006. Stu2p binds tubulin and undergoes an open-to-closed conformational change. J. Cell Biol. **172:**1009–1022.
2. **Efimov, V., J. Zhang, and X. Xiang.** 2006. CLIP-170 homologue and NUDE play overlapping roles in NUDF localization in *Aspergillus nidulans*. Mol. Biol. Cell **17:**2021–2034.
3. **Felenbok, B., M. Flipphi, and I. Nikolaev.** 2001. Ethanol catabolism in *Aspergillus nidulans*: a model system for studying gene regulation. Prog. Nucleic Acid Res. Mol. Biol. **69:**149–204.
4. **Galagan, J. E., S. E. Calvo, C. Cuomo, L.-J. Ma, J. R. Wortman, S. Batzoglou, S.-I. Lee, M. Baştürkmen, C. C. Spevak, J. Clutterbuck, V. Kapitonov, J. Jurka, C. Scazzocchio, M. Farman, J. Butler, S. Purcell, S. Harris, G. H. Braus, O. Draht, S. Busch, C. d'Enfert, C. Bouchier, G. H. Goldman, D. Bell-Pedersen, S. Griffiths-Jones, J. H. Doonan, J. Yu, K. Vienken, A. Pain, M. Freitag, E. U. Selker, D. B. Archer, M. A. Peñalva, B. R. Oakley, M. Momany, T. Tanaka, T. Kumagai, K. Asai, M. Machida, W. C. Nierman, D. W. Denning, M. Caddick, M. Hynes, M. Paoletti, R. Fischer, B. Miller, P. Dyer, M. S. Sachs, S. A. Osmani, and B. W. Birren.** 2005. Sequencing of *Aspergillus nidulans* and comparative analysis with *A. fumigatus* and *A. oryzae*. Nature **438:**1105–1115.
5. **Gard, D. L., and M. W. Kirschner.** 1987. A microtubule-associated protein from *Xenopus* eggs that specifically promotes assembly at the plus-end. J. Cell Biol. **105:**2203–2215.
6. **Han, G., B. Liu, J. Zhang, W. Zuo, N. R. Morris, and X. Xiang.** 2001. The *Aspergillus* cytoplasmic dynein heavy chain and NUDF localize to microtubule ends and affect microtubule dynamics. Curr. Biol. **11:**19–24.
7. **Harris, S. D., and M. Momany.** 2004. Polarity in filamentous fungi: moving beyond the yeast paradigm. Fungal Genet. Biol. **41:**391–400.
8. **Harris, S. D., N. D. Read, R. W. Roberson, B. Shaw, S. Seiler, M. Plamann, and M. Momany.** 2005. Polarisome meets Spitzenkörper: microscopy, genetics, and genomics converge. Eukaryot. Cell **4:**225–229.
9. **Hestermann, A., and R. Gräf.** 2004. The XMAP215-family protein DdCP224 is required for cortical interactions of microtubules. BMC Cell Biol. **5:**24–33.
10. **Hill, T. W., and E. Käfer.** 2001. Improved protocols for *Aspergillus* minimal medium: trace element and minimal medium salt stock solutions. Fungal Genet. Newsl. **48:**20–21.
11. **Karos, M., and R. Fischer.** 1999. Molecular characterization of HymA, an evolutionarily highly conserved and highly expressed protein of *Aspergillus nidulans*. Mol. Genet. Genomics **260:**510–521.
12. **Kinoshita, K., B. Habermann, and A. A. Hyman.** 2002. XMAP215: a key component of the dynamic microtubule cytoskeleton. Trends Cell Biol. **12:**267–273.
13. **Konzack, S., P. Rischitor, C. Enke, and R. Fischer.** 2005. The role of the kinesin motor KipA in microtubule organization and polarized growth of *Aspergillus nidulans*. Mol. Biol. Cell **16:**497–506.
14. **Martin, S. G., and F. Chang.** 2003. Cell polarity: a new mod(e) of anchoring. Curr. Biol. **13:**R711–730.
15. **Martin, S. G., W. H. McDonald, J. R. Yates III, and F. Chang.** 2005. Tea4p links microtubule plus ends with the formin For3p in the establishment of cell polarity. Dev. Cell **8:**479–491.
16. **Nayak, T., E. Szewczyk, C. E. Oakley, A. Osmani, L. Ukil, S. L. Murray, M. J. Hynes, S. A. Osmani, and B. R. Oakley.** 2006. A versatile and efficient gene targeting system for *Aspergillus nidulans*. Genetics **172:**1557–1566.
17. **Ohkura, H., M. A. Garcia, and T. Toda.** 2001. Dis1/TOG universal microtubule adaptors—one MAP for all? J. Cell Sci. **114:**3805–3812.
18. **Requena, N., C. Alberti-Segui, E. Winzenburg, C. Horn, M. Schliwa, P. Philippsen, R. Liese, and R. Fischer.** 2001. Genetic evidence for a microtubule-destabilizing effect of conventional kinesin and analysis of its consequences for the control of nuclear distribution in *Aspergillus nidulans*. Mol. Microbiol. **42:**121–132.
19. **Riquelme, M., R. Fischer, and S. Bartnicki-Garcia.** 2003. Apical growth and mitosis are independent processes in *Aspergillus nidulans*. Protoplasma **222:**211–215.
20. **Riquelme, M., C. G. Reynaga-Peña, G. Gierz, and S. Bartnicki-García.** 1998. What determines growth direction in fungal hyphae? Fungal Genet. Biol. **24:**101–109.
21. **Rischitor, P., S. Konzack, and R. Fischer.** 2004. The Kip3-like kinesin KipB moves along microtubules and determines spindle position during synchronized mitoses in *Aspergillus nidulans* hyphae. Eukaryot. Cell **3:**632–645.
22. **Sambrook, J., and D. W. Russel.** 1999. Molecular cloning: a laboratory manual, 3rd ed. Cold Spring Harbor Laboratory Press, Cold Spring Harbor, NY.
23. **Seiler, S., F. E. Nargang, G. Steinberg, and M. Schliwa.** 1997. Kinesin is essential for cell morphogenesis and polarized secretion in *Neurospora crassa*. EMBO J. **16:**3025–3034.
24. **Snaith, H. A., and K. E. Sawin.** 2003. Fission yeast mod5p regulates polarized growth through anchoring of tea1p at cell tips. Nature **423:**647–651.
25. **Stringer, M. A., R. A. Dean, T. C. Sewall, and W. E. Timberlake.** 1991. *Rodletless*, a new *Aspergillus* developmental mutant induced by directed gene inactivation. Genes Dev. **5:**1161–1171.
26. **Toews, M. W., J. Warmbold, S. Konzack, P. E. Rischitor, D. Veith, K. Vienken, C. Vinuesa, H. Wei, and R. Fischer.** 2004. Establishment of mRFP1 as fluorescent marker in *Aspergillus nidulans* and construction of expression vectors for high-throughput protein tagging using recombination in *Escherichia coli* (GATEWAY). Curr. Genet. **45:**383–389.
27. **Veith, D., N. Scherr, V. P. Efimov, and R. Fischer.** 2005. Role of the spindle-pole body protein ApsB and the cortex protein ApsA in microtubule organization and nuclear migration in *Aspergillus nidulans*. J. Cell Sci. **118:**3705–3716.
28. **Waring, R. B., G. S. May, and N. R. Morris.** 1989. Characterization of an inducible expression system in *Aspergillus nidulans* using *alcA* and tubulin coding genes. Gene **79:**119–130.
29. **Xiang, S., G. Han, D. A. Winkelmann, W. Zuo, and N. R. Morris.** 2000. Dynamics of cytoplasmic dynein in living cells and the effect of a mutation in the dynactin complex actin-related protein Arp1. Curr. Biol. **10:**603–606.
30. **Yelton, M. M., J. E. Hamer, and W. E. Timberlake.** 1984. Transformation of *Aspergillus nidulans* by using a *trpC* plasmid. Proc. Natl. Acad. Sci. USA **81:**1470–1474.
31. **Zhang, J., S. Li, R. Fischer, and X. Xiang.** 2003. The accumulation of cytoplasmic dynein and dynactin at microtubule plus-ends is kinesin dependent in *Aspergillus nidulans*. Mol. Biol. Cell **14:**1479–1488.

Micro**Review**

Polarized growth in fungi – interplay between the cytoskeleton, positional markers and membrane domains

Reinhard Fischer, Nadine Zekert and Norio Takeshita*

Department of Applied Microbiology, University of Karlsruhe, Hertzstrasse 16, D-76187 Karlsruhe, Germany.

Summary

One kind of the most extremely polarized cells in nature are the indefinitely growing hyphae of filamentous fungi. A continuous flow of secretion vesicles from the hyphal cell body to the growing hyphal tip is essential for cell wall and membrane extension. Because microtubules (MT) and actin, together with their corresponding motor proteins, are involved in the process, the arrangement of the cytoskeleton is a crucial step to establish and maintain polarity. In *Saccharomyces cerevisiae* and *Schizosaccharomyces pombe,* actin-mediated vesicle transportation is sufficient for polar cell extension, but in *S. pombe,* MTs are in addition required for the establishment of polarity. The MT cytoskeleton delivers the so-called cell-end marker proteins to the cell pole, which in turn polarize the actin cytoskeleton. Latest results suggest that this scenario may principally be conserved from *S. pombe* to filamentous fungi. In addition, in filamentous fungi, MTs could provide the tracks for long-distance vesicle movement. In this review, we will compare the interaction of the MT and the actin cytoskeleton and their relation to the cortex between yeasts and filamentous fungi. In addition, we will discuss the role of sterol-rich membrane domains in combination with cell-end marker proteins for polarity establishment.

Introduction

The establishment of polarity is a fundamental process in biology. Polarized growth is realized in fungi and is the

dominant growth form of filamentous fungi. In single-cell yeasts, such as in budding yeast *Saccharomyces cerevisiae* and in fission yeast *Schizosaccharomyces pombe*, polarized growth is restricted to certain times during the cell cycle, whereas in filamentous fungi, such as *Aspergillus nidulans* or *Neurospora crassa*, cell extension is a continuous and indefinite process (Snell and Nurse, 1994; Pringle *et al.*, 1995; Riquelme *et al.*, 2003). Filamentous fungi are widely distributed in nature and can cause severe problems as contaminants of food and feed as well as pathogens of plants and animals. Many laboratories are trying to obtain a detailed understanding of the process, because the molecular analysis of polarized growth may lead to the identification of targets for new antifungal drugs. A second important aspect is that filamentous fungi are widely used in biotechnology. It is assumed that heterologously produced hydrolytic enzymes are secreted through the same machinery as the enzymes required for polarized growth (Seiler *et al.*, 1997; Pel *et al.*, 2007). Here, the understanding of the molecular components might help to increase the production of secreted enzymes or open up new avenues for the production of heterologous proteins.

Polarized growth is studied by genetic, molecular biological, biochemical and cell biological methods. This research field has benefited more than others from the combination of the still ongoing improvement of the microscopic techniques and the development of fluorescent reporter proteins in recent years. Fantastic work has been performed in several laboratories leading to many breakthroughs in *S. pombe* and *S. cerevisiae,* and significant progress in understanding polarized growth in filamentous fungi.

Several overviews have recently summarized different aspects of polarized growth (Chang and Peter, 2003; Nelson, 2003; Xiang and Plamann, 2003; Harris and Momany, 2004; Harris *et al.*, 2005; Virag and Harris, 2006a; Fischer, 2007; Steinberg, 2007). In this review, we will focus mainly on the latest findings on the role of the cytoskeleton, and its dependence on and interaction with protein complexes at the growing cell cortex.

On the role of microtubules and the actin cytoskeleton in S. cerevisiae*,* S. pombe *and* A. nidulans

Microtubules (MTs) grow and shrink in a tread-milling manner if they are polymerized *in vitro*. In contrast, MTs are rather stable at the minus end *in vivo* and are dynamic mainly at the plus end, which exhibits alternating rounds of growth and shrinkage. In most higher eukaryotic cells, MTs distribute radially, and are nucleated from a perinuclear centrosome or MT-organizing centre (MTOC) with their plus ends facing the cell periphery (Keating and Borisy, 1999). In *S. cerevisiae*, the MTOC is localized in the nuclear envelope and named spindle pole body (SPB) (Jaspersen and Winey, 2004). Only few MTs are found in interphase cells and they are disassembled as the mitotic spindle is formed. *S. pombe* has both the SPB and perinuclear MTOCs (Sawin and Tran, 2006) and, in the filamentous fungus *A. nidulans* SPBs, cytoplasmic MTOCs and MTOCs associated with septa are responsible for the formation and maintenance of the MT array (Veith *et al.*, 2005). MTs are oriented along the long axis in the cigar-shaped cells of *S. pombe* as well as in the extremely elongated compartments of *A. nidulans* (Höög *et al.*, 2007). Understanding the regulation of MT formation and their dynamics is one of the main foci of recent research. Proteins called plus-end tracking proteins (+TIPs), because they associate and remain at growing MT plus ends, regulate MT dynamics and are very important for MT–cortex interactions (Akhmanova and Hoogenraad, 2005; Xiang, 2006). In *S. cerevisiae,* these interactions with the cell cortex play crucial roles in positioning of the mitotic spindle; in *S. pombe,* they signal polarity information to the cell cortex; and in *A. nidulans,* they are involved in both nuclear migration and polarity determination (Fig. 1 and Table 1) (Nelson, 2003).

Saccharomyces cerevisiae

In *S. cerevisiae*, cortical capture of astral MTs (MTs formed from the two SPBs during mitosis) establishes spindle polarity. During mitosis, Kar9 directs one SPB towards the bud by linking astral MTs to the actin cytoskeleton (Fig. 1). Kar9 initially localizes to the old SPB, and is transported by the kinesin Kip2 (kinesin-7) along astral MTs to the plus ends (Liakopoulos *et al.*, 2003; Maekawa *et al.*, 2003; Moore *et al.*, 2006). The asymmetric localization of Kar9 depends on its interaction with +TIPs, such as Bim1 and Bik1 (EB1 and CLIP-170 in higher eukaryotes respectively), and the cyclin-dependent kinase Cdc28 (Pearson and Bloom, 2004; Moore and Miller, 2007). Once the growing MTs reach the cortex, Kar9 interacts with class-V myosin Myo2, which in turn pulls Kar9 together with the attached MT along an actin cable towards the growing tip. This leads to proper spindle ori-
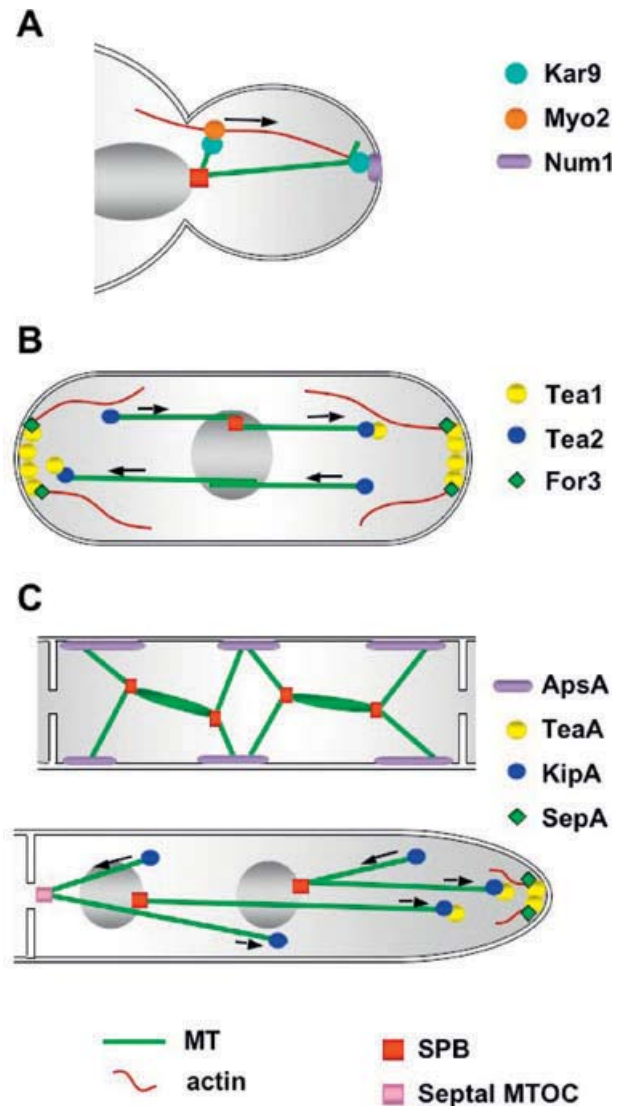
Fig. 1. Scheme of the MT and actin cytoskeleton in *S. cerevisiae*, *S. pombe* and *A. nidulans*.
A. In *S. cerevisiae*, actin cables capture MT plus ends and thereby regulate MT localization and shrinkage to orient the mitotic spindle.
B. On the other hand, interphase MTs in *S. pombe* determine actin cable localization through the deposition of the cell-end marker protein Tea1, which recruits formin.
C. In *A. nidulans*, early results suggest conservation of the *S. cerevisiae* machinery during mitosis (upper panel) and conservation of the *S. pombe* machinery for polarized growth (lower panel). See text for details.

entation from the mother cell to the bud (Yin *et al.*, 2000; Hwang *et al.*, 2003). For spindle elongation and movement into the bud, pulling forces mediated by astral MT sliding along the bud cortex are required. In this process, the cortical anchor protein Num1 captures the astral MT plus ends (Farkasovsky and Küntzel, 1995; 2001; Heil-Chapdelaine *et al.*, 2000) and cytoplasmic dynein, also accumulated at the MT plus ends, becomes activated

Table 1. Homologue proteins in three fungi.

	S. cerevisiae	*S. pombe*	*A. nidulans*
+TIPs			
CLIP-170	Bik1	Tip1	ClipA
EB1	Bim1	Mal3	AN2862.3
APC	Kar9	None	None
XMAP215	Stu2	Alp14	AlpA
Dynein (heavy chain)	Dyn1	Dhc1	NudA
Lis1	Pac1	?	NudF
Cortical anchor	Num1 (nuclear migration)[a]	Mcp5 (nuclear oxillation in meiosis)[a]	ApsA (nuclear distribution)[a]
Kinesin-7	Kip2 (nuclear migration defect)[b]	Tea2 (T-shape or bent cell)[b]	KipA (Curved hyphae)[b]
Cell-end marker	Kel1, Kel2 (cell fusion defects during mating)[b]	Tea1, Tea3 (T-shape or bent cell)[b]	TeaA (Zig-zag hyphae)[b]
Cortical receptor	?	Mod5 (T-shape or bent cell)[b]	TeaR (Curved hyphae)[b]
Formin	Bni1, Bnr1	For3, Fus1, Cdc12	SepA
Polarisome	Spa2	SPAC3G9.05	SpaA
	Bud6	Bud6	BudA
Cdc42	Cdc42	Cdc42	ModA
Rac1	None	None	RacA

a. Protein functions or **b.** mutant phenotypes are shown in branckets.

once it contacts the cortex. Kip2 kinesin transports Kar9, dynein and Bik1 to the MT plus end (Carvalho *et al.*, 2004). Bik1 and Pac1 (dynein activator LIS1 homologue) play roles in targeting and activation of dynein at MT plus ends (Lee and Oberle, 2003; Sheeman *et al.*, 2003). In summary, actin cables capture MT plus ends through the interaction of class-V myosin with Kar9, and thereby regulate MT localization and shrinkage to orient the mitotic spindle. MTs are not necessary for polarized growth of the emerging bud.

Schizosaccharomyces pombe

In *S. pombe*, the molecular function of astral MTs in spindle alignment and elongation remains unclear, and a functional counterpart of Kar9 has not yet been identified. Nevertheless, a Num1 homologue, Mcp5, exists and appears to perform similar functions as in *S. cerevisiae*, the contact between astral MTs and the cortex (Yamashita and Yamamoto, 2006). However, in contrast to *S. cerevisiae,* Mcp5 shows meiosis-specific expression and localizes at the cell cortex during meiosis. Deletion of the gene caused a lack of nuclear oscillations during the meiotic prophase. In contrast to *S. cerevisiae*, in *S. pombe*, interphase MTs have a function in signalling polarity information to the cell ends. MT plus ends normally keep elongating until they reach the cell ends, and then shrink. This intrinsic characteristic of MTs is used to transport and deliver the cell-end marker protein, Tea1 (tip elongation aberrant), to the cell ends (Mata and Nurse, 1997). Tea2 (kinesin-7) transports Tea1 to MT plus ends (Browning *et al.*, 2000; 2003). The proteins were indentified by screening for strains with bent and T-shaped cells (Snell and Nurse, 1994). Tea1 is crucial for the formation of a protein complex that organizes the actin cytoskeleton

(see blow). Secretion vesicles are then transported along the actin filaments to support cell growth.

The regulation of MT dynamics is essential for the signalling of polarity information. Two +TIPs, Tip1 (CLIP-170) and Mal3 (EB1), are important for suppressing MT catastrophe (the growth to shrinkage transitions) (Brunner and Nurse, 2000; Busch and Brunner, 2004). In Δ*tip1* cells, MTs initiate catastrophe anywhere the MT plus ends contact the cortex and, in Δ*mal3* cells, MTs undergo catastrophe even before they reach the cortex. As a result, these mutants have shorter MT bundles. The mutants with abnormal MTs show defects in polarized growth and exhibit bent or T-shaped cells. Tea2, which transports Tea1 to MT plus ends, also transports Tip1, and thus Δ*tea2* cells also exhibit same defects in MTs and polarized growth (Browning *et al.*, 2000; 2003; Busch *et al.*, 2004).

Aspergillus nidulans *and other filamentous fungi*

In *A. nidulans,* MTs are required for nuclear migration and positioning as in *S. cerevisiae*. An *apsA* mutant, lacking the *S. cerevisiae* Num1 homologue, exhibits a defect in nuclear distribution (Fischer and Timberlake, 1995; Suelmann *et al.*, 1998; Veith *et al.*, 2005). Although alignment of mitotic spindles is not required in syncytial fungal compartments, deletion of *apsA* leads to a lack of spindle oscillations. This indicates that mitotic spindles are held in place through contacts with astral MTs on each side of the spindle and the cortex. How and whether interphase nuclear distribution is regulated by MT–cortex interactions are still unclear. Because a Kar9 homologue cannot be detected in the genomes of Aspergilli, it is also not clear whether the actin cytoskeleton is involved in MT–cortical interactions.
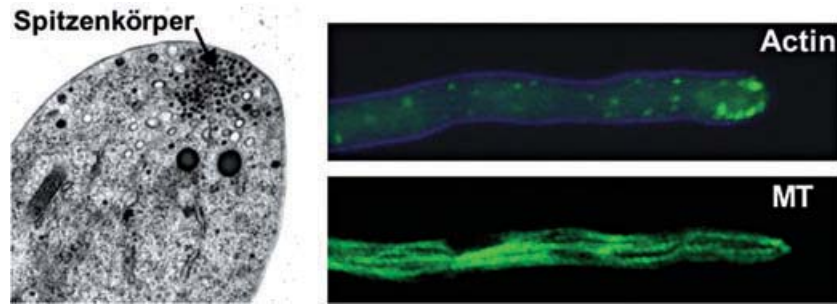
Fig. 2. The Spitzenkörper, the actin and the MT cytoskeleton in *A. nidulans*. left: transmission electron micrograph of a hyphal tip. The small vesicles accumulating in the Spitzenkörper (SPK) are visible. Actin (right, upper picture) and MTs (right, lower picture) visualized in a hyphal tip as GFP fusion proteins. The actin-GFP distribution shows only the presence of actin patches. Actin cables are only rarely visible in *A. nidulans* (Araujo-Bazan *et al.*, 2008; Taheri-Talesh *et al.*, 2008). The left picture was provided by B. Richardson (Athens, GA).

It was reported recently that interphase MTs also play a role in signalling polarity information to the hyphal tips in *A. nidulans*, as described in *S. pombe*. MTs in *A. nidulans* have mixed polarities in hyphal compartments, but the tip compartment contains two to eight MTs, most of which are oriented with their plus ends towards the tip and merge at one point (Fig. 2) (Konzack *et al.*, 2005; Sampson and Heath, 2005). Proteins such as Tea1 and Tea2 appear to be conserved in *A. nidulans* as TeaA (Tea1) and KipA (Tea2) respectively (Konzack *et al.*, 2005; Takeshita *et al.*,

2008). Although overall sequence similarity between Tea1 and TeaA is only 27%, the architecture of the two proteins is similar. KipA localizes to MT plus ends and regulates the position of TeaA at hyphal tips (Fig. 3) (see below). Knockout mutants in the respective genes show defects in maintenance of polarized growth and exhibit curved or zigzag-shaped hyphae.

The regulation of MT dynamics by +TIPs, ClipA (CLIP-170) and KipA is different in *A. nidulans* from that in *S. pombe*. In Δ*clipA* mutants, more MTs fail to undergo long-
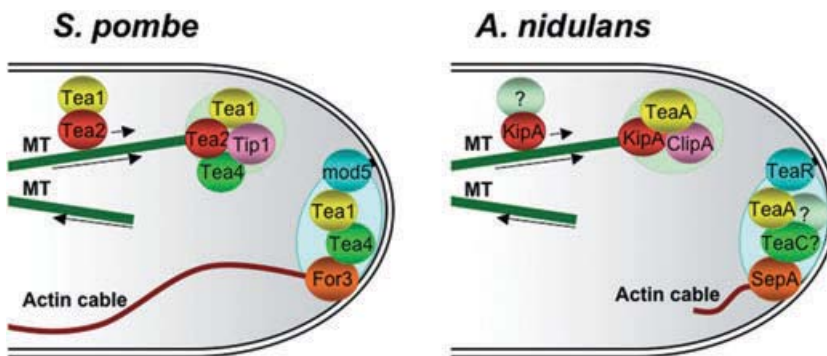
Fig. 3. Scheme of the transport of cell-end markers in *S. pombe* and *A. nidulans*, localization of the corresponding proteins as GFP or mRFP fusion proteins and phenotypes of the corresponding mutants, as indicated. Taken from Konzack *et al.* (2005) and Takeshita *et al.* (2008). For details see the text. TeaC is the homologue of Tea4. GFP-KipA spots moved towards the tip (time, left at 0 and right after 12 s). mRFP1-TeaA or GFP-TeaR produced under native promoter control localized to one point at the tip and along the tip membrane (upper panels). Differential interference contrast images of wild type, Δ*kipA*, Δ*teaA*, Δ*teaR* strains. Δ*kipA* and Δ*teaR* strains exhibited curved hyphae and Δ*teaA* strains exhibited zigzag hyphae (lower panels).
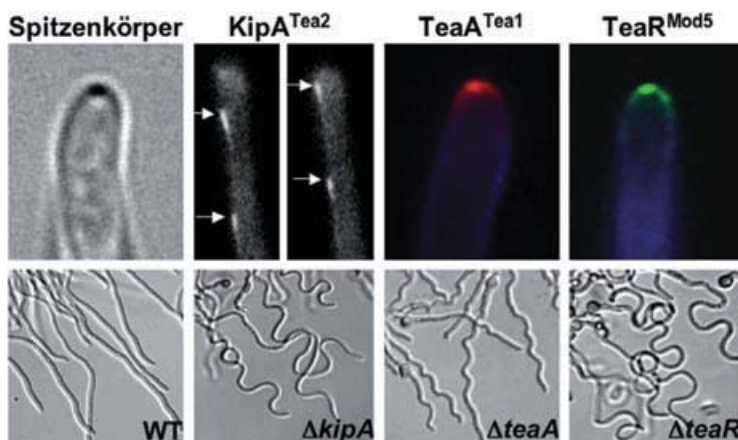
range growth towards the tip but MTs that reach the tips are less likely to undergo catastrophe (Efimov *et al.*, 2006). Moreover, in Δ*kipA* mutants, MTs elongate to the tips but do not merge in one point (Konzack *et al.*, 2005), whereas the *S. pombe tip1* (CLIP-170) or *tea2* mutants have shorter MTs. Whereas Tea2 is required for Tea1 and Tip1 transport in *S. pombe*, in *A. nidulans*, *kipA* deletion only partially affects MT plus-end localization of ClipA at an elevated temperature and KipA is not required for TeaA accumulation at the hyphal tip but is needed for correct TeaA positioning (Efimov *et al.*, 2006; Takeshita *et al.*, 2008). These differences remain unexplained so far.

A third role for MTs in *A. nidulans* and other filamentous fungi is probably an involvement in vesicle transport. Hyphal tip growth in filamentous fungi is a complex and regulated process, which involves the synthesis and plasticity of the cell wall, transport and extension of the membrane, diverse cytoplasmic movements, turgor pressure and certain ion gradients (Torralba *et al.*, 2001; Virag and Harris, 2006a). A structure named the Spitzenkörper localized in the apical dome of the hyphae is involved in polarized growth (Fig. 2) (Girbardt, 1957). It represents an accumulation of vesicles and determines growth direction of fungal hyphae (Grove and Bracker, 1970; Riquelme *et al.*, 1998). The exact structure and organization are still not completely understood. It is thought to act as vesicle supply centre (VSC) for growing tips. According to a model, vesicles are delivered to the Spitzenkörper via MT-dependent transportation and from the Spitzenkörper to the cortex via actin-dependent vesicle movement. Already, early ultrastructural studies with *Fusarium acuminatum* supported this model. Vesicles were observed closely associated with MTs and, after MT disassembly with the anti-MT agent benomyl, intracellular vesicle transport appeared to be inhibited (Howard and Aist, 1980; Howard, 1981). However, these experiments did not unambiguously show that MTs are required as tracks for vesicles, because the observations were done in fixed cells. In addition, anti-MT drugs not only disassemble cytoplasmic MTs but also inhibit mitosis. Thus, secondary effects could also occur and account for the observed changes in the appearance of the Spitzenkörper and growth inhibition. More direct evidence for the involvement of MTs in long-distance vesicle movement comes from the study of the role of MT-dependent kinesins. For instance, the deletion of conventional kinesin (kinesin-1) in *A. nidulans* or *N. crassa* reduced the growth rate significantly (Seiler *et al.*, 1997; Requena *et al.*, 2001). Especially in *N. crassa*, the kinesin-1 mutant showed defects in Spitzenkörper stability and protein secretion (Seiler *et al.*, 1997; 1999), suggesting a possible role in vesicle transportation similar to the role in neurons. Similarly, Unc104-like kinesins (kinesin-3) in *A. nidulans* and the dimorphic fungus *Ustilago maydis* also have roles in hyphal growth (Schu-

chardt *et al.*, 2005) (N. Zekert, pers. comm.). These kinesins are not essential for growth but are necessary for fast extension of hyphae. However, it should be noted that also the kinesin motors could cause secondary effects, which are responsible for the observed growth rate reduction. For instance, it was shown in *A. nidulans* that conventional kinesin is required for dynein targeting to growing MT plus ends (Zhang *et al.*, 2003). Another aspect is that MT dynamics could affect the position of other proteins and organelles by pushing the cytoplasmic matrix. Near the tip, most MTs are growing towards the cortex and could thereby generate a forward-directed cytoplasmic matrix flow (Sampson and Heath, 2005; Mouriño-Pérez *et al.*, 2006). Stronger evidence for the importance of secretion for polarized growth came recently from a study on exocytosis (Taheri-Talesh *et al.*, 2008). In this paper, the authors used GFP-tagged markers for exocytotic vesicles and studied the secretion in live cells. They showed that exocytotic vesicles accumulate in the Spitzenkörper, and are transported from there to the membrane. Recycling of the proteins occurs by endocytosis, which is localized in a zone a few micrometres behind the growing tip. Thus exocytosis and endocytosis are linked processes and are both required for tip extension. The importance of endocytosis for polarized growth was also shown by Araujo-Bazan *et al.* (2008).

Whereas actin-dependent vesicle secretion is necessary for growth in all fungi, the importance of MTs appears to be different. In *Candida albicans*, a fungus that can switch between budding and filamentous growth, as well as in the constitutively filamentously growing *Ashbya gossypii,* MTs are not necessary for filamentous growth (Alberti-Segui *et al.*, 2001; Rida *et al.*, 2006). The importance of the actin cytoskeleton in *S. cerevisiae*, *C. albicans* and *A. gossypii* may be also reflected in the fact that they have two to three formins, that actin cables are well established in the cell and that Cdc42, small GTPase and master regulator of actin organization are essential for polarity establishment (Wendland and Philippsen, 2001; Bassilana and Arkowitz, 2006). In contrast, the filamentous fungi *A. nidulans* and *N. crassa* have only one formin, actin cables are rarely observed (Torralba *et al.*, 1998; Virag and Griffith, 2004; Araujo-Bazan *et al.*, 2008; Taheri-Talesh *et al.*, 2008) and Cdc42 deletion does not show severe morphological phenotypes in *A. nidulans* (Virag *et al.*, 2007). The poorer actin cytoskeleton in filamentous fungi may suggest that the actin cytoskeleton is necessary but not sufficient for hyphal growth and that MTs are required in addition.

The role of molecular motors for polarized growth

Three classes of cytoskeleton-dependent motor proteins, kinesins, dynein and myosin, are involved in the transport

of proteins, vesicles and organelles. According to the latest nomenclature, kinesins are grouped into 14 families (kinesins 1–14) and one orphan family (Lawrence *et al.*, 2004). The number of kinesins in fungi ranges from six in *S. cerevisiae*, to nine in *S. pombe*, 10 or 11 in *N. crassa* and *A. nidulans* respectively (Schoch *et al.*, 2003; Rischitor *et al.*, 2004). In comparison, fungi contain a single cytoplasmic dynein (Yamamoto and Hiraoka, 2003). In yeasts, myosins of three families (myosins I, II and V) are conserved, and myosin V transports secretion vesicles to polarization sites.

Three kinesin families (1, 3 and 7) are involved in polarized growth in fungi. As outlined above, members of the kinesin-7 family (Kip2 in *S. cerevisiae*, Tea2 in *S. pombe,* KipA in *A. nidulans*) are used to deliver proteins to the MT plus ends. Kip2 transports Bik1 (CLIP-170), Kar9 (for spindle polarity) and dynein, while Tea2 transports Tip1 (CLIP-170) and Tea1 (for cell polarity). KipA is not essential for ClipA (CLIP-170) and TeaA transport, likewise, dynein accumulation at the MT plus end is independent of KipA but depends on the kinesin-1 family protein conventional kinesin (KinA) (Zhang *et al.*, 2003). Surprisingly, kinesin-7 family kinesins in *U. maydis* have no critical role in polarized growth (Schuchardt *et al.*, 2005).

Members of the kinesin-1 family (conventional kinesin) play important roles in filamentous growth, probably in the transportation of vesicles (Seiler *et al.*, 1997; Requena *et al.*, 2001). However, additional roles were reported, for example, defects on mitochondrial distribution were observed in kinesin-1 mutants of *N. crassa* and *Nectria haematococca,* and defective vacuolar distribution was found in the corresponding *U. maydis* mutant (Lehmler *et al.*, 1997; Steinberg *et al.*, 1998; Wu *et al.*, 1998; Steinberg, 2000). Members of the kinesin-1 family do not exist in *S. cerevisiae*, whereas in *S. pombe* such a kinesin functions in Golgi membrane recycling (Brazer *et al.*, 2000). Hence, it appears that kinesin-1 can bind to different cargoes and, thus, be involved in different cellular processes.

Other kinesins with a role in polarized growth are those of the kinesin-3 family. This motor does not exist in *S. pombe* or *S. cerevisiae* but in *U. maydis*, *N. crassa* and other filamentous fungi. In *U. maydis*, it is involved in endosome transport and necessary for hyphal growth (Wedlich-Söldner *et al.*, 2002a). In *A. nidulans*, one motor of this family is clearly involved in polarized growth but, as in *U. maydis*, double deletion of kinesin-1 and kinesin-3 is not lethal (Schuchardt *et al.*, 2005; N. Zekert, pers. comm.). In comparison, two related kinesin-3 motors in *N. crassa* act together on mitochondrial distribution (Fuchs and Westermann, 2005). Our understanding of vesicle and organelle transport towards the tip is still quite limited and it seems that different motors play different roles in different fungi.

Cytoplasmic dynein has various roles in nuclear migration and organelle transport in fungi (Yamamoto and Hiraoka, 2003; Xiang and Fischer, 2004). The role in nuclear migration has been best studied in *S. cerevisiae*. Dynein mediates the contact of astral MTs to the cortex and slides the MTs on the contact sites by moving along the MTs towards the minus end. Consequently, the nucleus moves to the bud neck and the opposing pulling forces along the cell axis contribute to spindle pole separation (Bloom, 2001; Yamamoto and Hiraoka, 2003). In filamentous fungi, dynein mediates organelle and vesicle transport (Xiang and Plamann, 2003). In *N. crassa*, dynein is involved in retrograde transport of vesicles and a dynein mutant showed defects in the organization and stability of the Spitzenkörper (Seiler *et al.*, 1999; Riquelme *et al.*, 2002). In *U. maydis*, it functions in endoplasic reticulum (ER) organization and endosome transport (Wedlich-Söldner *et al.*, 2002a, b). Moreover, dynein and its regulator accumulated at MT plus ends within the hyphal tips possibly ensure that endosomes reach the tips and contribute to tip growth by endocytic membrane recycling (Lenz *et al.*, 2006).

Myosin function is also studied well in *S. cerevisiae*. Actin cables are nucleated from the bud tip to the mother cell during bud growth and one myosin V, Myo2, transports vesicles and other organelles, such as the Golgi, mitochondria, vacuoles and peroxisomes (Pruyne *et al.*, 2004). Some mRNA molecules such as *ASH1* are transported by another myosin V, Myo4 (Bobola *et al.*, 1996; Shepard *et al.*, 2003). In *S. pombe*, a new daughter cell grows at the previous cell end in a monopolar manner, and then initiates growth at the previous cell division site in a bipolar manner. This phenomenon is named NETO (new end take-off) (Mitchison and Nurse, 1985). Actin cables grow towards the growing cell ends, only towards the old ends before NETO and towards both ends after NETO, and Myo52, a myosin V, is responsible for polarized secretion of vesicles along actin cables and hence membrane enlargement and secretion of cell wall-synthesizing enzymes (Montegi *et al.*, 2001; Win *et al.*, 2001; Mulvihill *et al.*, 2006). Although in filamentous fungi, the function of myosin V is largely unclear, these myosins are required for filamentous growth and pathogenicity in *U. maydis* and *C. albicans* (Weber *et al.*, 2003; Woo *et al.*, 2003; Schuchardt *et al.*, 2005).

If we accept the model of long-distance MT-dependent vesicle transportation and subsequent accumulation in an organelle called VSC or Spitzenkörper and actin-dependent short-distance transportation from the VSC towards the surface, one interesting yet open question is whether different motor proteins (kinesin, dynein and myosin) are always attached to the vesicles or whether they associate with the vesicles as required (Fig. 2).

*Cell-end markers and polarity determination*

In *S. cerevisiae*, the decision to initiate a new polarized growth site depends on intrinsic factors and is determined by the last budding site. In *S. pombe*, cell growth occurs first at the previous cell division site, and interphase MTs are used to establish the polarity site. In both yeasts, mutation analysis revealed some proteins that act as cortical landmarks. Once the polarity site is marked at the cell cortex, the landmarks regulate localization and activation of cascades of small GTPases (Cdc42 and other Rho-type GTPase) (Chang and Peter, 2003). In *S. cerevisiae*, activated Cdc42 regulates multiple downstream effectors and establishes cell polarity, organizes the actin cytoskeleton and the septin ring, and directs membrane traffic and the formation of membrane compartments (Pruyne and Bretscher, 2000; Park and Bi, 2007). In general, polarity site selection is not essential for polarized growth, but the polarity-establishing machinery is essential for cell polarity.

Interestingly, the initiation of polarized growth in *S. cerevisiae* depends on the genotype at the mating-type (MAT) locus. MAT a or α cells exhibit axial budding, which means that a new daughter bud emerges next to the previous one. On the other hand, diploid MAT a/α cells exhibit a bipolar budding pattern, where a new bud emerges from the opposite pole of the previous daughter (Kron and Gow, 1995). Bud3, Bud4 and Axl2/Bud10 are landmark proteins for the axial budding pattern, and Bud8, Bud9 and Rax2 for the bipolar budding pattern (Madden and Snyder, 1998). In the case of axial budding, the landmark proteins localize to a septin ring. Septins are GTPases, which assemble into a ring structure (septin ring) at the previous bud neck at the end of the cell cycle, and guide new bud formation next to the septin ring. In contrast, the mechanism of landmark protein localization for bipolar budding is not fully understood. Genetic analyses revealed that several other processes besides the septin ring and the timing of *BUD8* and *BUD9* gene expression are involved in the mechanism (Ni and Snyder, 2001; Schenkman *et al.*, 2002). In both cases, the landmarks recruit and activate the polarity-establishing machinery, the Cdc42 cascade, at the cell surface. The mediator Rsr1-Bud1 (Ras small GTPase) regulates the link between the landmarks and Cdc42. The landmarks activate Rsr1-Bud1 through the recruitment of its guanine nucleotide exchange factor (GEF) Bud5 (Bender, 1993). Activated Rsr1-Bud1 regulates Cdc42 activity through the recruitment of its GEF Cdc24. Once Cdc42 is activated at the proper site, multiple effectors, such as formins (Bni1, Bnr1), p21-activated kinases (Ste20 and Cla4) and GTPase activating protein (GAP) for the Rab-type GTPase Sec4 (Msb3 and Msb4), lead to the local assembly and orientation of the actin cytoskeleton and vesicle delivery for bud growth. The local Cdc42 activity is amplified in a self-sustaining positive feedback loop (Butty *et al.*, 2002; Wedlich-Söldner and Li, 2003).

In *S. pombe,* some of the bud site landmark proteins from *S. cerevisiae* are not conserved. However, other genes were identified by polarity mutant screening (T-shaped or bent cells). Among these were the above-mentioned *tea1* and *tea2* genes, and the novel landmark-encoding *mod5* gene (morphology defective). Mutants of these genes exhibit T-shaped or bent cells as a result of the mislocalization of the polarity site away from the centre of the cell end. Mod5 plays a very important role, because it anchors Tea1 at the cell pole (Fig. 3). Mod5 harbours a CAAX (cysteine, two aliphatic amino acids followed by any amino acid) prenylation motif at the C terminus. The cysteine is covalently prenylated, which anchors the protein in the membrane (Snaith and Sawin, 2003). Tea1 and Mod5, also named cell-end markers, accumulate interdependently at the growing cell ends and contribute to the spatial distribution of actin cables. At the cell ends, Tea1 interacts with a number of additional components, and a large protein complex is formed that includes the formin For3, which nucleates the actin cable assembly, and Bud6, an actin-binding protein (Feierbach *et al.*, 2004; Martin *et al.*, 2005). Bud6 in *S. cerevisiae* stimulates formin activity and Bud6 in *S. pombe* is required for proper For3 localization (Feierbach *et al.*, 2004; Moseley and Goode, 2005). After cell division, Tea1 is delivered to the new end by MTs, and For3 and Bud6 localize there after Tea1 is anchored. Therefore, Tea1 contributes to cell polarity and actin cable organization through the interaction with For3 and Bud6. Their interactions link the MT with the actin cytoskeleton in fission yeast. Transition from monopolar to bipolar growth (NETO) depends on the localization of For3 to the new end and, thus, *tea1* and *bud6* mutants display defects in NETO. Besides these components, Tea4, which links Tea1 and For3, and Tea3, a Tea1-related, Kelch repeat-containing protein, are also necessary for NETO (Arellano *et al.*, 2002; Martin *et al.*, 2005). Tea3 binds independently to Tea1 and Mod5, and is required for Tea1 anchorage specifically at non-growing cell ends (Snaith *et al.*, 2005). Although the contribution of Cdc42 on For3 localization in *S. pombe* is not well understood, relief of autoinhibition of For3 by Cdc42 and/or Bud6 is necessary for For3 localization (Martin *et al.*, 2007). Bud6 is also directly or indirectly recruited to the new end by Tea1 and Tea4 (Feierbach *et al.*, 2004). Whereas MTs and Tea1 play central roles in the decision of the growth site, they are not required for polarity establishment. This led to models that local self-activation and lateral inhibition are responsible for polarized growth (Castagnetti *et al.*, 2007).

S. cerevisiae-type landmarks are poorly or not conserved in *A. nidulans* and other filamentous fungi, leading
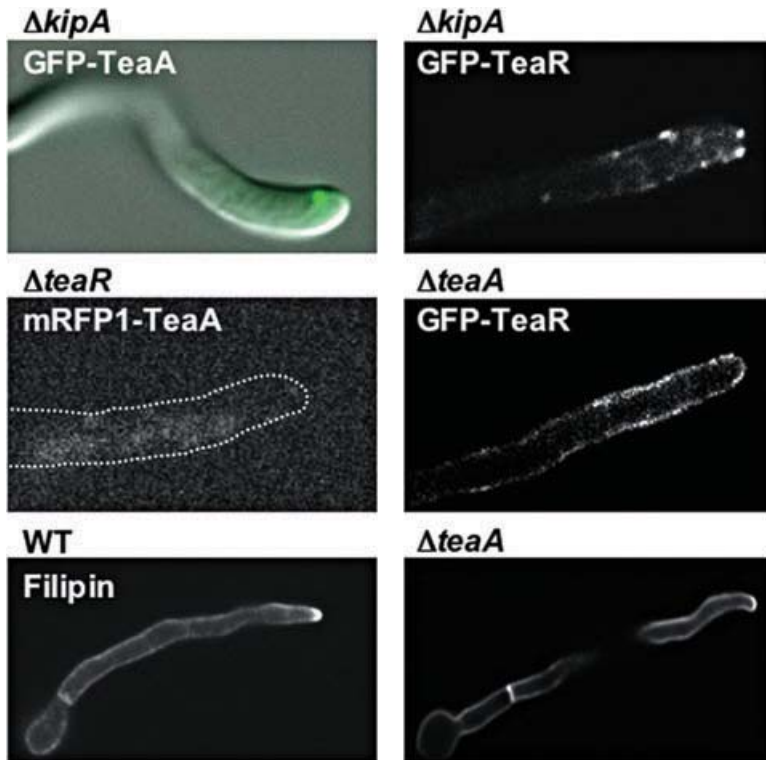
Fig. 4. Interdependence of the localization of cell-end markers and on the KipA motor protein in hyphae of *A. nidulans*. Taken from Takeshita *et al.* (2008). In the Δ*kipA* mutant, GFP1-TeaA still localized to one point at the hyphal tip but often moved away from the centre of the apex (left upper panel) and some GFP-TeaR signal localized at the membrane of the apex and others dispersed along the membrane away from the tip (right upper panel). In the Δ*teaR* mutant, mRFP1-TeaA was not observed at the tip (left middle panel). In the Δ*teaA* mutant, GFP-TeaR lost the preference for the hyphal tip and diffused all along the membrane (right middle panel). wild type (WT) (left lower panel) and the Δ*teaA* mutants (right lower panel) were stained with filipin. Filipin accumulated at the tip and at septa.

to speculations that novel mechanisms could be at work (Harris and Momany, 2004). However, the *S. pombe* cell-end marker Tea1 appears to be conserved in filamentous fungi (Takeshita *et al.*, 2008)(see above). Two Tea1 homologues exist in *S. cerevisiae* (Kel1 and Kel2), where they are involved in cell fusion during mating (Philips and Herskowitz, 1998). Despite the central role of Mod5 for polarized growth in *S. pombe*, a sequence homologue was not identified in *S. cerevisiae* or any filamentous fungus. In recent work, a protein that could act as a membrane anchor for TeaA was discovered in *A. nidulans* and named TeaR (Fig. 3) (Takeshita *et al.*, 2008). TeaR was identified by screening for proteins that harbour a C-terminal prenylation motif. TeaR shows low identity to Mod5 (15.4%) and is conserved in all filamentous fungi whose genomes have been analysed. Deletion of *teaR* produces meandering instead of straight hyphae. This curved hyphal phenotype resembles that of *kipA* mutants. In comparison, *teaA* mutant hyphae display a rather zigzag growth phenotype. Both TeaA and TeaR localize to one point at the tip and along the tip membrane. TeaA was shown to interact with TeaR by split YFP and yeast two-hybrid technology. The localization of both proteins is interdependent, as it is in *S. pombe.* TeaA colocalizes with the formin SepA at hyphal tips. These results suggest conservation of the *S. pombe* polarity site selection mechanism in *A. nidulans*, although the interaction of cell-end marker and formin is still unknown. Homologous protein of Tea4, which links Tea1

and For3 in *S. pombe*, exists in *A. nidulans*, known as TeaC, and its functional analysis is in progress (Higashitsuji *et al.*, unpubl. results). However, the role of KipA appears to be different from that of *S. pombe* Tea2. Whereas Tea2 transports Tea1 to the MT plus end, in *A. nidulans* TeaA still localized to tips in the *kipA*-deletion mutant. Interestingly, KipA is required for correct TeaA and TeaR positioning (Fig. 4). KipA might transport additional landmark and cell-end marker proteins. Although MTs had been demonstrated to be necessary for hyphal tip localization of TeaA (Takeshita *et al.*, 2008), meanwhile the localization of TeaA at MT plus ends was also revealed (Takeshita *et al.*, unpubl. results).

Besides their role in organizing the actin cytoskeleton, the cell-end marker proteins might play a role in organizing the MT cytoskeleton itself. In *A. nidulans*, MT plus ends are centred in the hyphal apex and merge in the TeaA protein spot at the tip (Takeshita *et al.*, 2008). This raises the question about the interaction of MT plus ends with the cell-end markers or landmark proteins. That the integrity of the MT plus-end protein complex is indeed required for cell polarity establishment, besides the transportation of potential cell-end marker proteins, comes from the observation that the lack of the Dis1/XMAP215 protein AlpA causes meandering hyphae in *A. nidulans*, just like the absence of the cell-end marker proteins (Enke *et al.*, 2007). XMAP215 is a processive MT polymerase (Brouhard *et al.*, 2008), and the conserved protein family

promotes MT growth. Indeed, *alpA* deletion in *A. nidulans* led to a reduced number of MTs and reduced dynamics (Enke *et al.*, 2007).

Cdc42, its regulators, and its downstream machinery, such as the polarisome, Arp2/3, and exocyst complex, are conserved from *S. cerevisiae* to *A. nidulans* (Harris and Momany, 2004; Virag and Harris, 2006a). The role of polarisome components in *A. nidulans,* BudA and SpaA, corresponding to *S. cerevisiae* Bud6 and Spa2, was analysed and SpaA was shown to be dispensable for Spitzenkörper organization (Virag and Harris, 2006b). It was also shown that a scaffold protein for the polarity-establishing machinery, BemA, corresponding to *S. cerevisiae* Bem1, is required for proper hyphal growth and formin SepA localization (Leeder and Turner, 2008). Surprisingly, whereas Cdc42 is essential in budding and fission yeast, it is not essential in *A. nidulans* and *U. maydis* (Mahlert *et al.* 2006; Virag *et al.*, 2007). In addition to Cdc42, another Rho GTPase, a Rac1 homologue, appears to function in hyphal growth of both fungi. The functional relationship of the Cdc42 and Rac1 homologues and the cell-end markers employed for actin cytoskeleton organization and hyphal polarity establishment is an important next question.

The role of the membrane – sterol-rich lipid microdomains

In both *S. pombe* and *A. nidulans,* Mod5 (TeaR) is necessary for Tea1 (TeaA) positioning, and *vice versa* (Fig. 4). Which other molecules or factors, besides MTs, guide the proteins to their destination? Mod5 and TeaR are assumed to localize to the membrane through their prenyl residue, because their prenylation motifs are essential for their localization and function (Snaith and Sawin, 2003; Takeshita *et al.*, 2008). Hence, the membrane environment could be important for their localization. Membranes are no longer considered as homogeneous, and sterols and sphingolipids can cluster into domains within mixtures with glycerophospholipids. These domains, termed lipid rafts, contribute to specific protein localization of, for example, GPI-anchored and lipid-associated proteins, at a specific site, and play important roles in cell signalling and cell polarity (Rajendra and Simons, 2005). In fungi, lipid rafts can be observed as clusters by staining with filipin, a sterol-binding dye (Alvarez *et al.*, 2007). These domains, termed sterol-rich membrane domains, are detected at polarized growth sites in several fungi, for example, in the tip of the mating projection in *S. cerevisiae* and *Cryptococcus neoformans,* the growing cell ends and the site of cytokinesis in *S. pombe,* and the hyphal tips and septa in *C. albicans* and *A. nidulans* (Bagnat and Simons, 2002; Nichols *et al.*, 2004; Wachtler and Balasubramanian, 2006). The sterol-

rich domains contribute to polarized growth in *C. albicans* (Martin and Konopka, 2004). In *A. nidulans,* another correlation of the sterol-rich domains and fomin SepA localization was revealed by analysing mutants such as *mesA*. The corresponding gene encodes a tip-localized membrane protein and its mutation enhances *sepA* defects (Pearson *et al.*, 2004). In addition, *barA* and *basA*, which encode a ceramide synthase and a sphingolipid C4-hydroxylase, respectively, were identified by screening for mutants resistant or sensitive to heat-stable antifungal factor. These three mutants exhibited depolarized filipin staining, mislocalized SepA and actin cables, and severe polarity growth defects (Pearson *et al.*, 2004; Li *et al.*, 2006; 2007).

Cell-end markers or sterol-rich microdomains – which is first

Intact sterol-rich domains are required for cell-end marker localization at the tips in *A. nidulans* (Takeshita *et al.*, 2008). Treatment with filipin causes mislocalization of TeaA and TeaR. However, the cell-end markers cannot be the only targets whose localization is regulated by the sterol-rich domains, because the disruption of the sterol-rich domains led to defects in polarity establishment that are not identical to the polarity mispositioning in the cell-end marker deletion mutants (Takeshita *et al.*, 2008). The *A. nidulans* mutants with depolarized sterol-rich domains have defects in the localization and activation of SepA, as they do not have actin cables (Pearson *et al.*, 2004; Li *et al.*, 2006). Sterol-rich domains could also be required for the localization of the Cdc42 cascade, or Cdc42 itself, which localizes to the plasma membrane through post-translational geranyl–geranyl modification. Whereas the sterol-rich domains are necessary for cell-end marker localization, the sterol-rich domains still localized to the hyphal tips in *teaA*- or *teaR*-deletion mutants (Fig. 4) (Takeshita *et al.*, 2008). These results suggest that the sterol-rich domains determine cell-end marker localization and not the other way around. If the known cell-end markers do not themselves organize the sterol-rich domains, the question that arises is how the sterol-rich domains are organized and positioned at polarized growth sites. In *S. pombe*, class I myosin is required for proper organization of the sterol-rich domains (Takeda and Chang, 2005), whereas Cdc15 is also required for its organization at cell division sites during cytokinesis (Takeda *et al.*, 2004). Septins, which colocalize with the sterol-rich domains at growth sites, are also speculated to have a role in the organization of the membrane domains (Douglas *et al.*, 2005). Interestingly, these proteins, class I myosin and septins, are members of the Cdc42 cascade. Indeed, a relationship between the Cdc42 pathway and sterol synthesis has recently been revealed. Ste20, p21-
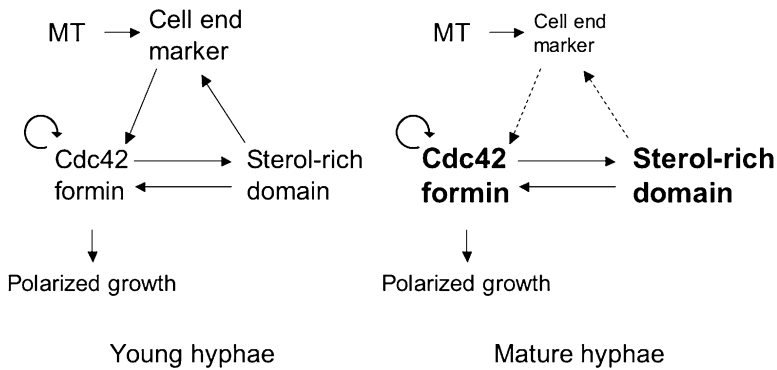
Fig. 5. Scheme of the interdependence of cell-end markers and lipid rafts. See text for details.

activated kinase and effector of Cdc42, interacts with proteins involved in sterol synthesis and regulates cell polarity (Tiedje *et al.*, 2007). Homologues of oxysterol-binding proteins, which regulate the synthesis and transport of sterols, function in Cdc42-dependent polarity establishment (Kozminski *et al.*, 2006). The Cdc42 cascade is thought to amplify the intensity by positive feedback loops (Wedlich-Söldner and Li, 2003). Sterol-rich domains might increase the local concentration of Cdc42 cascade proteins, and function in such a positive feedback loop. If this were true, cell-end markers, the Cdc42 cascade and sterol-rich domains were in a three-art interaction (Fig. 5). This means that cell-end markers regulate the positioning of the Cdc42 cascade by interaction with formin, that the Cdc42 cascade and sterol-rich domains function cooperatively and amplify the intensity, and that the sterol-rich domains support cell-end marker positioning. Evidence indicates that the sterol-rich domains act upstream of the cell-end markers. In addition, the sterol-rich domains are likely required for the localization of additional factors other than the cell-end markers. However, the following model is also possible. The sterol-rich domains recruit both the Cdc42 cascade and cell-end markers. In addition, MTs independently recruit cell-end markers, which also recruit the Cdc42/formin cascade. Cdc42/formin sets up a feedback loop with sterol-rich domains. These ideas could explain why in *A. nidulans* the defect in growth directionality in the cell-end marker mutants is most prominent in young hyphae. Whereas the position information of cell-end markers might be important for Cdc42 cascade localization in young hyphae, the Cdc42 cascade and the sterol-rich domains in mature hyphae could stabilize their localization interdependently, and polarized growth could be maintained without the position information of cell-end markers.

Conclusion

In the past decade, our knowledge about the molecular components involved in polarized growth in *S. cerevisiae*, *S. pombe* or *A. nidulans* and other fungi has improved

tremendously. Nevertheless, the comparison of the mechanism in different organisms shows that our picture of the process is still far from complete. Especially the advance of the understanding of the process in filamentous fungi should allow to identify new proteins determining polarized growth. The example of *kipA* deletion in *A. nidulans* shows that this motor protein apparently does not transport TeaA as in *S. pombe*, but other components, which are required for correct localization of TeaA and TeaR. It will be the challenge for future research to identify such targets and further unravel the mechanism of polarized growth in filamentous fungi.

Acknowledgements

References

Akhmanova, A., and Hoogenraad, C.C. (2005) Microtubule plus-end-tracking proteins: mechanisms and functions. *Curr Opin Cell Biol* **17:** 47–54.

Alberti-Segui, C., Dietrich, F., Altmann-Jöhl, R., Hoepfner, D., and Philippsen, P. (2001) Cytoplasmic dynein is required to oppose the force that moves nuclei towards the hyphal tip in the filamentous ascomycete *Ashbya gossypii*. *J Cell Sci* **114:** 975–986.

Alvarez, F.J., Douglas, L.M., and Konopka, J.B. (2007) Sterol-rich plasma membrane domains in fungi. *Eukaryot Cell* **6:** 755–763.

Araujo-Bazan, L., Penalva, M.A., and Espeso, E.A. (2008) Preferential localization of the endocytic internalization machinery to hyphal tips underlies polarization of the actin cytoskeleton in Aspergillus nidulans. *Mol Microbiol* **67:** 891–905.

Arellano, M., Niccoli, T., and Nurse, P. (2002) Tea3p is a cell end marker activating polarized growth in Schizosaccharomyces pombe. *Curr Biol* **12:** 751–756.

Brouhard, G.J., Stear, J.H., Noetzel, T.L., Al-Bassam, J., Kinoshita, K., Harrison, S.C. *et al.* (2008) XMAP215 is a processive microtubule polymerase. *Cell* **132:** 79–88.

Bagnat, M., and Simons, K. (2002) Cell surface polarization during yeast mating. *Proc Natl Acad Sci USA* **99:** 14183–14188.

Bassilana, M., and Arkowitz, R.A. (2006) Rac1 and Cdc42 have different roles in *Candida albicans* development. *Eukaryot Cell* **5:** 321–329.

Brazer, S.C., Williams, H.P., Shappeu, T.G., and Cande, W.Z. (2000) A fission yeast kinesin affects Golgi membrane recycling. *Yeast* **16:** 149–166.

Bender, A. (1993) Genetic evidence for the roles of the bud-site-selection genes BUD5 and BUD2 in control of the Rsr1p (Bud1p) GTPase in yeast. *Proc Natl Acad Sci USA* **90:** 9926–9929.

Bloom, K. (2001) Nuclear migration: cortical anchors for cytoplasmic dynein. *Curr Biol 11*: R326–R329.

Bobola, N., Jansen, R.P., Shin, T.H., and Nasmyth, K. (1996) Asymmetric accumulation of Ash1p in postanaphase nuclei depends on a myosin and restricts yeast mating-type switching to mother cells. *Cell* **84:** 699–709.

Browning, H., Hayles, J., Mata, J., Aveline, L., Nurse, P., and McIntosh, J.R. (2000) Tea2p is a kinesin-like protein required to generate polarized growth in fission yeast. *J Cell Biol* **151:** 15–27.

Browning, H., Hackney, D.D., and Nurse, P. (2003) Targeted movement of cell end factors in fission yeast. *Nat Cell Biol* **5:** 812–818.

Brunner, D., and Nurse, P. (2000) CLIP170-like tip1p spatially organizes microtubular dynamics in fission yeast. *Cell* **102:** 695–704.

Busch, K.E., and Brunner, D. (2004) The microtubule plus end-tracking proteins mal3p and tip1p cooperate for cell-end targeting of interphase microtubules. *Curr Biol* **14:** 548–559.

Busch, K.E., Hayles, J., Nurse, P., and Brunner, D. (2004) Tea2p kinesin is involved in spatial microtubule organization by transporting tip1p on microtubules. *Dev Cell* **16:** 831–843.

Butty, A.C., Perrinjaquet, N., PEtit, A., Jaquenoud, M., Segall, J.E., Hofmann, K., *et al.* (2002) A positive feedback loop stabilizes the guanine-nucleotide exchange factor Cdc24 at sites of polarization. *EMBO J* **21:** 1565–1576.

Carvalho, P., Gupta, M.L.J., Hoyt, M.A., and Pellman, D. (2004) Cell cycle control of kinesin-mediated transport of Bik1 (CLIP-170) regulates microtubule stability and dynein activation. *Dev Cell* **6:** 815–829.

Castagnetti, S., Novác, B., and Nurse, P. (2007) Microtubules offset growth site from the cell centre in fission yeast. *J Cell Sci* **120:** 2205–2213.

Chang, F., and Peter, M. (2003) Yeasts make their mark. *Nat Cell Biol* **5:** 294–299.

Douglas, L.M., Alvarez, F.J., McCreary, C., and Konopka, J.B. (2005) Septin function in yeast model systems and pathogenic fungi. *Eukaryot Cell* **4:** 1503–1512.

Efimov, V., Zhang, J., and Xiang, X. (2006) CLIP-170 homologue and NUDE play overlapping roles in NUDF localization in *Aspergillus nidulans*. *Mol Biol Cell* **17:** 2021–2034.

Enke, C., Zekert, N., Veith, D., Schaaf, C., Konzack, S., and Fischer, R. (2007) *Aspergillus nidulans* Dis1/XMAP215 protein AlpA localizes to spindle pole bodies and microtubule plus ends and contributes to growth directionality. *Eukaryot Cell* **6:** 555–562.

Farkasovsky, M., and Küntzel, H. (1995) Yeast Num1p associates with the mother cell cortex during S/G2 phase and affects microtubular functions. *J Cell Biol* **131:** 1003–1014.

Farkasovsky, M., and Küntzel, H. (2001) Cortical Num1p interacts with the dynein intermediate chain Pac11p and cytoplasmic microtubules. *J Cell Biol* **152:** 251–262.

Feierbach, G., Verde, F., and Chang, F. (2004) Regulation of a formin complex by the microtubule plus end protein tea1p. *J Cell Biol* **165:** 697–707.

Fischer, R. (2007) The role of the cytoskeleton in polarized growth of filamentous fungi. In *The Mycota* Vols VIII, VIII. Gow, N.A.R., and Howard, R.J. (eds). Heidelberg: Springer, pp. 121–135.

Fischer, R., and Timberlake, W.E. (1995) *Aspergillus nidulans apsA* (anucleate primary sterigmata) encodes a coiled-coil protein necessary for nuclear positioning and completion of asexual development. *J Cell Biol* **128:** 485–498.

Fuchs, F., and Westermann, B. (2005) Role of Unc104/KIF1-related motor proteins in mitochondrial transport in Neurospora crassa. *Mol Biol Cell* **16:** 153–161.

Girbardt, M. (1957) Der Spitzenkörper von *Polystictus versicolor*. *Planta* **50:** 47–59.

Grove, S.N., and Bracker, C.E. (1970) Protoplasmic organization of hyphal tips among fungi: vesicles and Spitzenkörper. *J Bacteriol* **104:** 989–1009.

Harris, S.D., and Momany, M. (2004) Polarity in filamentous fungi: moving beyond the yeast paradigm. *Fungal Genet Biol* **41:** 391–400.

Harris, S.D., Read, N.D., Roberson, R.W., Shaw, B., Seiler, S., Plamann, M., and Momany, M. (2005) Polarisome meets Spitzenkörper: microscopy, genetics, and genomics converge. *Eukaryot Cell* **4:** 225–229.

Heil-Chapdelaine, R.A., Oberle, J.R., and Cooper, J.A. (2000) The cortical protein Num1p is essential for dynein-dependent interactions of microtubules with the cortex. *J Cell Biol* **151:** 1337–1344.

Höög, J.L., Schwartz, C., Noon, A.T., O'Toole, E.T., Matronarde, D.N., McIntosh, J.R., and Antony, C. (2007) Organization of interphase microtubules in fission yeast analyzed by electron tomography. *Dev Cell* **12:** 349–361.

Howard, R.J. (1981) Ultrastructural analysis of hyphal tip cell growth in fungi: spitzenkörper, cytoskeleton and endomembranes after freeze-substitution. *J Cell Sci* **48:** 89–103.

Howard, R.J., and Aist, J.R. (1980) Cytoplasmic mirotubules and fungal morphogenesis: ultrastructural effects of methyl benzimidazole-2-ylcarbamate determined by freeze-substitution of hyphal tip cells. *J Cell Biol* **87:** 55–64.

Hwang, E., Kusch, J., Barral, Y., and Huffaker, T.C. (2003) Spindle orientation in *Saccharomyces cerevisiae* depends on the transport of microtubule ends along polarized actin cables. *J Cell Biol* **161:** 483–488.

Jaspersen, S.L., and Winey, M. (2004) The budding yeast spindle pole body: structure, duplication, and function. *Annu Rev Cell Dev Biol* **20:** 1–28.

Keating, T.J., and Borisy, G.G. (1999) Centrosomal and non-centrosomal microtubules. *Biol Cell* **91:** 321–329.

Konzack, S., Rischitor, P., Enke, C., and Fischer, R. (2005) The role of the kinesin motor KipA in microtubule organi-

zation and polarized growth of *Aspergillus nidulans*. *Mol Biol Cell* **16:** 497–506.

Kozminski, K.G., Alfaro, G., Dighe, S., and Beh, C.T. (2006) Homologues of oxysterol-binding proteins affect Cdc42p- and Rho1p-mediated cell polarization in *Saccharomyces* cerevisiae. *Traffic* **7:** 1224–1242.

Kron, S.J., and Gow, N.A. (1995) Budding yeast morphogenesis: signalling, cytoskeleton and cell cycle. *Curr Opin Cell Biol* **7:** 845–855.

Lawrence, C.J., Dawe, R.K., Christie, K.R., Cleveland, D.W., Dawson, S.C., Endow, S.A., *et al.* (2004) A standardized kinesin nomenclature. *J Cell Biol* **167:** 19–22.

Lee, W.L., Oberle, J.R., and Cooper, J.A. (2003) The role of the lissencephaly protein Pac1 during nuclear migration in budding yeast. *J Cell Biol* **160:** 355–364.

Leeder, A.C., and Turner, G. (2008) Characterisation of Aspergillus nidulans polarisome component BemA. *Fungal Genet Biol* (in press).

Lehmler, C., Steinberg, G., Snetselaar, K.M., Schliwa, M., Kahmann, R., and Bölker, M. (1997) Identification of a motor protein required for filamentous growth in *Ustilago maydis*. *EMBO J* **16:** 3464–3473.

Lenz, J.H., Schuchardt, I., Straube, A., and Steinberg, G. (2006) A dynein loading zone for retrograde endosome motility at microtubule plus-ends. *EMBO J* **25:** 2275–2286.

Li, S., Du L., Yuen, G., and Harris, S.D. (2006) Distinct ceramide synthases regulate polarized growth in the filamentous fungus *Aspergillus nidulans*. *Mol Biol Cell* **17:** 1218–1227.

Li, S., Bao, D., Yuen, G., Harris, S.D., and Calvo, A.M. (2007) basA regulates cell wall organization and asexual/sexual sporulation ratio in *Aspergillus nidulans*. *Genetics* **176:** 243–253.

Liakopoulos, D., Kusch, J., Grava, S., Vogel, J., and Barral, Y. (2003) Asymmetric loading of Kar9 onto spindle poles and microtubules ensures proper spindle alignment. *Cell* **112:** 561–574.

Madden, K., and Snyder, M. (1998) Cell polarity and morphogenesis in budding yeast. *Ann Rev Microbiol* **52:** 687–744.

Maekawa, H., Usui, T., Knop, M., and Schiebel, E. (2003) Yeast Cdk1 translocates to the plus end of cytoplasmic microtubules to regulate but cortex interactions. *EMBO J* **22:** 438–449.

Mahlert, M., Leveleki, L., Hlubek, A., Sandrock, B., and Bölker, M. (2006) Rac1 and Cdc42 regulate hyphal growth and cytokinesis in the dimorphic fungus *Ustilago maydis*. *Mol Microbiol* **59:** 567–578.

Martin, S.W., and Konopka, J.B. (2004) Lipid raft polarization contributes to hyphal growth in *Candida albicans*. *Eukaryot Cell* **3:** 675–684.

Martin, S.G., McDonald, W.H., Yates, J.R.R., and Chang, F. (2005) Tea4p links microtubule plus ends with the formin for3p in the establishment of cell polarity. *Dev Cell* **8:** 479–491.

Martin, S.G., Rincon, S.A., Basu, R., Perez, P., and Chang, F. (2007) Regulation of the formin for3p by cdc42p and bud6p. *Mol Biol Cell* **18:** 4155–4167.

Mata, J., and Nurse, P. (1997) tea1 and the microtubular cytoskeleton are important for generating global spatial order within the fission yeast cell. *Cell* **89:** 939–949.

Mitchison, T.J., and Nurse, P. (1985) Growth in cell length in the fission yeast Schizosaccharomyces pombe. *J Cell Sci* **75:** 357–376.

Montegi, F., Arai, R., and Mabuchi, I. (2001) Identification of two type V myosins in fission yeast, one of which functions in polarized cell growth and moves rapidly in the cell. *Mol Biol Cell* **12:** 1367–1380.

Moore, J.K., and Miller, R.K. (2007) The cyclin-dependent kinase Cdc28p regulates multiple aspects of Kar9p function in yeast. *Mol Biol Cell* **18:** 1187–1202.

Moore, J.K., D'Silva, S., and Miller, R.K. (2006) The CLIP-170 homologue Bik1p promotes the phosphorylation and asymmetric localiztion of Kar9p. *Mol Biol Cell* **17:** 178–191.

Moseley, J.B., and Goode, B.L. (2005) Differential activities and regulation of *Saccharomyces cerevisiae* formin proteins Bni1 and Bnr1 by Bud6. *J Biol Chem* **280:** 28023–28033.

Mouriño-Pérez, R.R., Roberson, R.W., and Bartnicki-Garcia, S. (2006) Microtubule dynamics and organization during hyphal growth and branching in *Neurospora crassa*. *Fungal Genet Biol* **43:** 389–400.

Mulvihill, D.P., Edwards, S.R., and Hyams, J.S. (2006) A critical role for the type V myosin, Myo52, in septum deposition and cell fission during cytokinesis in *Schizosaccharomyces pombe*. *Cell Mot Cytoskel* **63:** 149–161.

Nelson, W.J. (2003) Adaptation of core mechanisms to generate cell polarity. *Nature* **422:** 766–774.

Ni, L., and Snyder, M. (2001) A genomic study of the bipolar bud site selection pattern in *Saccharomyces cerevisiae*. *Mol Biol Cell* **12:** 2147–2170.

Nichols, C.B., Fraser, J.A., and Heitman, J. (2004) PAK kinases Ste20 and Pak1 govern cell polarity at different stages of mating in *Cryptococcus neoformans*. *Mol Biol Cell* **15:** 4476–4489.

Park, H.O., and Bi, E. (2007) Central roles of small GTPases in the development of cell polarity in yeast and beyond. *Microbiol Mol Biol Rev* **71:** 48–96.

Pearson, C.G., and Bloom, K. (2004) Dynamic microtubules lead the way for spindle positioning. *Nat Rev Mol Cell Biol* **5:** 481–492.

Pearson, C.L., Xu, K., Sharpless, K.E., and Harris, S.D. (2004) MesA, a novel fungal protein required for the stabilization of polarity axes in *Aspergillus nidulans*. *Mol Biol Cell* **15:** 3658–3672.

Pel, H.J., de Winde, J.H., Archer, D.B., Dyer, P.S., Hofmann, G., Schapp, P.J., *et al.* (2007) Genome sequencing and analysis of the versatile cell factory *Aspergillus niger* CBS 513.88. *Nat Biotechnol* **25:** 221–231.

Philips, J., and Herskowitz, I. (1998) Identification of Kel1p, a kelch-domain-containing protein invovled in cell fusion and morphology in *Saccharomyces cerevisiae*. *J Cell Biol* **143:** 375–389.

Pringle, J.R., Bi, E., Harkins, H.A., Zahner, J.E., DeVirglio, C., Chant, J., *et al.* (1995) Establishment of cell polarity in yeast. *Cold Spring Harb Symp Quant Biol* **60:** 729–744.

Pruyne, D., and Bretscher, A. (2000) Polarization of cell growth in yeast. *J Cell Sci* **113:** 1013–1015.

Pruyne, D., Legesse-Miller, A., Gao, L., Dong, Y., and Bretscher, A. (2004) Mechanisms of polarized growth and organelle segregation in yeast. *Annu Rev Cell Dev Biol* **20:** 559–591.

Rajendra, L., and Simons, K. (2005) Lipid rafts and membrane dynamics. *J Cell Sci* **118:** 1099–1102.

Requena, N., Alberti-Segui, C., Winzenburg, E., Horn, C., Schliwa, M., Philippsen, P., *et al.* (2001) Genetic evidence for a microtubule-destabilizing effect of conventional kinesin and analysis of its consequences for the control of nuclear distribution in *Aspergillus nidulans. Mol Microbiol* **42:** 121–132.

Rida, P.C., Nishikawa, A., Won, G.Y., and Dean, N. (2006) Yeast-to-hyphal transition triggers formin-dependent Golgi localization to the growing tip in *Candida albicans. Mol Biol Cell* **17:** 4364–4378.

Riquelme, M., Reynaga-Peña, C.G., Gierz, G., and Bartnicki-García, S. (1998) What determines growth direction in fungal hyphae? *Fungal Genet Biol* **24:** 101–109.

Riquelme, M., Roberson, R.W., McDaniel, D.P., and Bartnicki-Garcia, S. (2002) The effects of *ropy-1* mutation on cytoplasmic organization and intracellular motility in mature hyphae of *Neurospora crassa. Fungal Genet Biol* **37:** 171–179.

Riquelme, M., Fischer, R., and Bartnicki-Garcia, S. (2003) Apical growth and mitosis are independent processes in *Aspergillus nidulans. Protoplasma* **222:** 211–215.

Rischitor, P., Konzack, S., and Fischer, R. (2004) The Kip3-like kinesin KipB moves along microtubules and determines spindle position during synchronized mitoses in *Aspergillus nidulans* hyphae. *Eukaryot Cell* **3:** 632–645.

Sampson, K., and Heath, I.B. (2005) The dynamic behaviour of microtubules and their contributions to hyphal tip growth in *Aspergillus nidulans. Microbiology* **151:** 1543–1555.

Sawin, K.E., and Tran, P.T. (2006) Cytoplasmic microtubule organization in fission yeast. *Yeast* **23:** 1001–1014.

Schenkman, L.R., Caruso, C., Pagé, N., and Pringle, J.R. (2002) The role fo cell cycle-regulated expression in the localization of spatial landmark proteins in yeast. *J Cell Biol* **156:** 829–841.

Schoch, C.L., Aist, J.R., Yoder, O.C., and Turgeon, B.G. (2003) A complete inventory of fungal kinesins in representative filamentous ascomycetes. *Fungal Genet Biol* **39:** 1–15.

Schuchardt, I., Assmann, D., Thines, E., Schuberth, C., and Steinberg, G. (2005) Myosin-V, Kinesin-1, and Kinesin-3 cooperate in hyphal growth of the fungus *Ustilago maydis. Mol Biol Cell* **16:** 5191–5201.

Seiler, S., Nargang, F.E., Steinberg, G., and Schliwa, M. (1997) Kinesin is essential for cell morphogenesis and polarized secretion in *Neurospora crassa. EMBO J* **16:** 3025–3034.

Seiler, S., Plamann, M., and Schliwa, M. (1999) Kinesin and dynein mutants provide novel insights into the roles of vesicle traffic during cell morphogenesis in *Neurospora. Curr Biol* **9:** 779–785.

Sheeman, B., Carvalho, P., Sagot, I., Geiser, J., Kho, D., Hoyt, M.A., and Pellman, D. (2003) Determinants of S. cerevisiae dynein localization and activation: implications for the mechanism of spindle positioning. *Curr Biol* **13:** 364–372.

Shepard, K.A., Gerber, A.P., Jambhekar, A., Takizawa, P.A., Brown, P.O., Herschlag, D., *et al.* (2003) Widespread cytoplasmic mRNA transport in yeast: identification of 22 bud-localized transcripts using DNA microarray analysis. *Proc Natl Acad Sci USA* **100:** 11429–11434.

Snaith, H.A., and Sawin, K.E. (2003) Fission yeast mod5p regulates polarized growth through anchoring of tea1p at cell tips. *Nature* **423:** 647–651.

Snaith, H.A., Samejima, I., and Sawin, K.E. (2005) Multistep and multimode cortical anchoring of tea1p at cell tips in fission yeast. *EMBO J* **24:** 3690–3699.

Snell, V., and Nurse, P. (1994) Genetic analysis of cell morphogenesis in fission yeast – a role for casein kinase II in the establishment of polarized growth. *EMBO J* **13:** 2066–2074.

Steinberg, G. (2000) The cellular roles of molecular motors in fungi. *Trends Microbiol* **8:** 162–168.

Steinberg, G. (2007) Hyphal growth: a tale of motors, lipids, and *the Spitzenkörper. Eukaryot Cell 6*: 351.360.

Steinberg, G., Schliwa, M., Lehmler, C., Bölker, M., Kahmann, R., and McIntosh, J.R. (1998) Kinesin from the plant pathogenic fungus *Ustilago maydis* is involved in vacuole formation and cytoplasmic migration. *J Cell Sci* **111:** 2235–2246.

Suelmann, R., Sievers, N., Galetzka, D., Robertson, L., Timberlake, W.E., and Fischer, R. (1998) Increased nuclear traffic chaos in hyphae of apsB mutants of *Aspergillus nidulans*: molecular characterization of *apsB* and *in vivo* observation of nuclear behaviour. *Mol Microbiol* **30:** 831–842.

Taheri-Talesh, N., Horio, T., Araujo-Bazan, L., Dou, X., Espeso, E.A., Penalva, M.A., *et al.* (2008) The tip growth apparatus of *Aspergillus nidulans. Mol Biol Cell* (in press).

Takeda, T., Kawate, T., and Chang, F. (2004) Organization of a sterol-rich membrane domain by cdc15p during cytokinesis in fission yeast. *Nat Cell Biol* **6:** 1142–1144.

Takeda, T., and Chang, F. (2005) Role of fission yeast myosin I in organization of sterol-rich membrane domains. *Curr Biol* **15:** 1331–1336.

Takeshita, N., Higashitsuji, Y., Konzack, S., and Fischer, R. (2008) Apical sterol-rich membranes are essential for localizing cell end markers that determine growth directionality in the filamentous fungus *Aspergillus nidulans. Mol Biol Cell* **19:** 339–351.

Tiedje, C., Holland, D.G., Just, U., and Höfken, T. (2007) Proteins involved in sterol synthesis interact with Ste20 and regulate cell polarity. *J Cell Sci* **120:** 3613–3624.

Torralba, S., Raudaskoski, M., Pedregosa, A.M., and Laborda, F. (1998) Effect of cytochalasin A on apical growth, actin cytoskeleton organization and enzyme secretion in *Aspergillus nidulans. Microbiology* **144:** 45–53.

Torralba, S., Heath, I.B., and Ottensmeyer, F.P. (2001) Ca(2+) shuttling in vesicles during tip gorwth in *Neurospora crassa. Fungal Genet Biol* **33:** 181–193.

Veith, D., Scherr, N., Efimov, V.P., and Fischer, R. (2005) Role of the spindle-pole body protein ApsB and the cortex protein ApsA in microtubule organization and nuclear migration in *Aspergillus nidulans. J Cell Sci* **118:** 3705–3716.

Virag, A., and Griffith, A.J. (2004) A mutation in the Neurospora crassa actin gene results in multiple defects in tip growth and branching. *Fungal Genet Biol* **41:** 213–225.

Virag, A., and Harris, S.D. (2006a) The Spitzenkörper: a molecular perspective. *Mycol Res* **110:** 4–13.

Virag, A., and Harris, S.D. (2006b) Functional characterization of Aspergillus nidulans homologues of *Saccharomyces cerevisiae* Spa2 and Bud6. *Eukaryot Cell* **5:** 881–895.

Virag, A., Lee, M.P., Si, H., and Harris, S.D. (2007) Regulation of hyphal morphogenesis by *cdc42* and *rac1* homologues in *Aspergillus nidulans*. *Mol Microbiol* **66:** 1579–1596.

Wachtler, V., and Balasubramanian, M.K. (2006) Yeast lipid rafts? – An emerging view. *T Cell Biol* **16:** 1–4.

Weber, I., Gruber, C., and Steinberg, G. (2003) A class-V myosin required for mating, hyphal growth, and pathogenicity in the dimorphic plant pathogen *Ustilago maydis*. *Plant Cell* **15:** 2826–2842.

Wedlich-Söldner, R., and Li, R. (2003) Spontaneous cell polarization: undermining determinism. *Nat Cell Biol* **5:** 267–270.

Wedlich-Söldner, R., Straube, A., Friedrich, M.W., and Steinberg, G. (2002a) A balance of KIF1A-like kinesin and dynein organizes early endosomes in the fungus *Ustilago maydis*. *EMBO J* **21:** 2946–2957.

Wedlich-Söldner, R., Schulz, I., Straube, A., and Steinberg, G. (2002b) Dynein supports motility of endoplasmic reticulum in the fungus *Ustilago maydis*. *Mol Biol Cell* **13:** 965–977.

Wendland, J., and Philippsen, P. (2001) Cell polarity and hyphal morphogenesis are controlled by multiple Rho-Protein modules in the filamentous fungus *Ashbya gossypii*. *Genetics* **157:** 601–610.

Win, T.Z., Gachet, Y., Mulvihill, D.P., May, K.M., and Hyams, J.S. (2001) Two type V myosins with non-overlapping functions in the fission yeast *Schizosaccharomyces pombe*: Myo52 is concerned with growth polarity and cytokinesis, Myo51 is a cmponent of the cytokinetic actin ring. *J Cell Sci* **114:** 69–79.

Woo, M., Lee, K., and Song, K. (2003) MYO2 is not essential for viability, but is required for polarized growth and dimorphic switches in *Candida albicans*. *FEMS Microbiol Lett* **218:** 195–202.

Wu, Q., Sandrock, T.M., Turgeon, B.G., Yoder, O.C., Wirsel, S.G., and Aist, J.R. (1998) A fungal kinesin required for organelle motility, hyphal growth, and morphogenesis. *Mol Biol Chem* **9:** 89–101.

Xiang, X. (2006) A +TIP for a smooth trip. *J Cell Biol* **172:** 651–654.

Xiang, X., and Fischer, R. (2004) Nuclear migration and positioning in filamentous fungi. *Fungal Genet Biol* **41:** 411–419.

Xiang, X., and Plamann, M. (2003) Cytoskeleton and motor proteins in filamentous fungi. *Curr Opin Microbiol* **66:** 628–633.

Yamamoto, A., and Hiraoka, Y. (2003) Cytoplasmic dynein in fungi: insights from nuclear migration. *J Cell Sci* **116:** 4501–4512.

Yamashita, A., and Yamamoto, M. (2006) Fission yeast Num1p is a cortical factor anchoring dynein and is essential for the horse-tail nuclear movement during meiotic prophase. *Genetics* **173:** 1187–1196.

Yin, H., Pruyne, D., Huffaker, T.C., and Bretscher, A. (2000) Myosin V orientates the mitotic spindle in yeast. *Nature* **406:** 1013–1015.

Zhang, J., Li, S., Fischer, R., and Xiang, X. (2003) The accumulation of cytoplasmic dynein and dynactin at microtubule plus-ends is kinesin dependent in *Aspergillus nidulans*. *Mol Biol Cell* **14:** 1479–1488.

Molecular Biology of the Cell
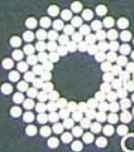
The *Aspergillus nidulans* Kinesin-3 UncA Motor Moves Vesicles along a Subpopulation of Microtubules

Nadine Zekert and Reinhard Fischer

University of Karlsruhe and Karlsruhe Institute of Technology, Institute of Applied Biosciences, Microbiology, D-76187 Karlsruhe, Germany

The extremely polarized growth form of filamentous fungi imposes a huge challenge on the cellular transport machinery, because proteins and lipids required for hyphal extension need to be continuously transported to the growing tip. Recently, it was shown that endocytosis is also important for hyphal growth. Here, we found that the *Aspergillus nidulans* kinesin-3 motor protein UncA transports vesicles and is required for fast hyphal extension. Most surprisingly, UncA-dependent vesicle movement occurred along a subpopulation of microtubules. Green fluorescent protein (GFP)-labeled UncA^{rigor} decorated a single microtubule, which remained intact during mitosis, whereas other cytoplasmic microtubules were depolymerized. Mitotic spindles were not labeled with GFP-UncA^{rigor} but reacted with a specific antibody against tyrosinated α-tubulin. Hence, UncA binds preferentially to detyrosinated microtubules. In contrast, kinesin-1 (conventional kinesin) and kinesin-7 (KipA) did not show a preference for certain microtubules. This is the first example for different microtubule subpopulations in filamentous fungi and the first example for the preference of a kinesin-3 motor for detyrosinated microtubules.

INTRODUCTION

The microtubule cytoskeleton in eukaryotic cells is essential for many dynamic processes. Among them are chromosome segregation, organelle movement, or the transportation of proteins, such as signaling complexes (Basu and Chang, 2007). These diverse functions are attributed not only to the inherent dynamic instability but also to the association with different molecular motor proteins, such as dynein and kinesin. Conventional kinesin is currently probably the best-studied molecular motor (Schliwa and Woehlke, 2003). ATP hydrolysis causes a small conformational change in a globular motor domain that is amplified and translated into movement with the aid of accessory structural motifs. Additional domains outside the motor unit are responsible for dimerization, regulation, and interactions with other molecules. The activity of conventional kinesin is required for exocytosis and thereby for fast fungal hyphal extension (Seiler *et al.*, 1997; Requena *et al.*, 2001).

Within the superfamily of kinesins, 17 families have been defined according to sequence similarities in the motor domain. One of these families is the Kif1/Unc-104 family, which has been renamed into the kinesin-3 family (Lawrence *et al.*, 2004; Wickstead and Gull, 2006). This plus-end–directed motor harbors the motor domain in the N terminus (N-type), a pleckstrin homology (PH) domain for the binding of membranous cargoes at the C terminus and a fork-head-associated (FHA) domain (Klopfenstein *et al.*, 2002). In contrast to the majority of dimeric kinesins, most Kin-3 kinesins are monomeric motors (Okada and Hirokawa, 1999,

2000), but a lysine-rich loop in KIF1A binds to the negatively charged C terminus of tubulin and compensates for the lack of a second heavy chain, allowing KIF1A to move processively like a dimeric motor (Okada and Hirokawa, 1999, 2000).

Unc-104 was first discovered in *Caenorhabditis elegans* shortly after the discovery of conventional kinesin (Otsuka *et al.*, 1991). Mutations in *unc-104* caused uncoordinated and slow movement of corresponding mutants. The motor is required for synaptic vesicle transport (Hall and Hedgecock, 1991). Later, the motor was also discovered in mouse due to sequence similarities of cDNAs from a library of murine brain (Okada *et al.*, 1995). The motor is associated with certain vesicles of the neuron, which transport synaptic vesicle proteins. The motor activity was measured in gliding assays and movement was measured at 1.2 μm/s, the fastest kinesin with anterograde movement at the time. It was observed that Kif1A apparently only binds to special vesicles and is only required for the anterograde transportation of certain synaptic proteins.

Although simple lower eukaryotes, e.g., *Saccharomyces cerevisiae*, serve as models for many cell biological phenomena, *S. cerevisiae* does not contain a member of the kinesin-3 family. However, this motor family was characterized in *Dictyostelium discoideum*, *Ustilago maydis*, *Neurospora crassa*, and *Thermomyces lanuginosus* (Pollock *et al.*, 1999; Rivera *et al.*, 2007). In *N. crassa*, one kinesin-3 motor, Kin2, is involved in mitochondrial distribution (Fuchs and Westermann, 2005). The kinesin-3 family contains also a unique fungal subgroup of "truncated" proteins, which do not have FHA and PH domains and may constitute a new subfamily (Schoch *et al.*, 2003). Although the structure of the protein is very different from other kinesin-3 family members, it is very interesting that in *N. crassa* Kin3 can rescue the lack of Kin2 (Fuchs and Westermann, 2005).

In *U. maydis*, a kinesin-3 motor is required for endosome movement (Schuchardt *et al.*, 2005; Steinberg, 2007). Deletion

Table 1. *A. nidulans* strains used in this study

Strain	Genotype	Source
TN02A3	*pyrG89; argB2, nkuA::argB; pyroA4*	Nayak *et al.* (2006)
GR5	*pyrG89; wA3; pyroA4*	Waring *et al.* (1989)
RMS011	*pabaA1, yA2; argB::trpCΔB*	Stringer *et al.* (1991)
SJW02	*wA3; pyroA4; argB::trpCΔB; alcA(p)::GFP::tubA,* (GFP-MTs)	Toews *et al.* (2004)
SJW100	SJW02 transformed with pJH19, *pyroA4* (GFP-MT, DsRed labeled nuclei)	Toews *et al.* (2004)
SSK114	*wA3; pyroA4; alcA(p)::GFP::kipA-rigor* (GFP-KipA^rigor)	Konzack *et al.* (2005)
SNR1	*yA2; argB::trpCΔB; pyroA4; ΔkinA::pyr4* (kinA deletion)	Requena *et al.* (2001)
AnKin26	*ΔkinA::pyrG, argB::trpCΔB; pyroA4*	Requena *et al.* (2001)
SNZ2	TN02A3 transformed with pAS3, *pyroA4* (GFP-UncA)	This study
SNZ3	TN02A3 transformed with pNZ5, *pyroA4* (uncB deletion)	This study
SNZ4	SNZ2 transformed with pJH19 (DsRed-stuA, GFP-UncA)	This study
SNZ8	TN02A3 transformed with pNZ9, *pyroA4* (mRFP1-UncA)	This study
SNZ9	TN02A3 transformed with pNZ13, *pyrG89* (uncA deletion)	This study
SNZ14	TN02A3 transformed with pNZ15, *pyroA4* (GFP-UncA^rigor)	This study
SNZ15	SNZ3 crossed with RMS011, *pabaA1* (uncB deletion)	This study
SNZ26	SNZ8 crossed with SJW100, *pyroA4* (GFP-MT, mRFP1-UncA)	This study
SNZ27	SNZ9 crossed with RMS011, *pabaA1* (uncA deletion)	This study
SNZ29	SNZ9 crossed with SNZ15 (uncA and uncB double deletion)	This study
SNZ36	SNZ9 crossed with AnKin26 (uncA and kinA double deletion)	This study
SNZ54	TN02A3 transformed with pNZS20, *pyroA4* (mRFP1-UncA^rigor)	This study
SCS4-NZ	SNZ14 transformed with pCS5-NZ (GFP-UncA^rigor, mRFP1-KinA^rigor)	This study
SCS5-NZ	TN02A3 transformed with pCS5-NZ, *pyrG89* (mRFP1-KinA^rigor)	This study
SNZ63	SNZ9 crossed with XX60 (uncA and nudA double deletion strain)	This study
SNZ69	SNZ14 transformed with pNZ59 (GFP-UncA^rigor, mRFP1-TlgB)	This study
XX60	*nudA deletion in GR5, nudA::pyrG*	Xiang *et al.* (1995)
SNZ74	TN02A3 transformed with PNZ-SI49, *pyroA4* (uncA(P)-GFP-uncA)	This study

All strains harbor the *veA1* mutation.

of *kin-3* reduces endosome motility to 33% and abolishes endosome clustering at the distal cell pole and at septa. It was proposed that dynein and Unc104 counteract on endosomes to arrange them at opposing cell poles (Wedlich-Söldner *et al.*, 2002). Schuchardt *et al.* (2005) also presented evidence that Kin3 is required for exocytosis, because acid phosphatase secretion was lowered to 50% in *kin-3* deletion strains.

In filamentous fungi it has been shown recently that not only exocytosis but also endocytosis is important for polarized growth (Araujo-Bazan *et al.*, 2008; Fischer *et al.*, 2008; Taheri-Talesh *et al.*, 2008; Upadhyay and Shaw, 2008). However, no information was available on how endosomes are transported in *A. nidulans* or other filamentous fungi. In this study, two members of the kinesin-3 family were identified in *A. nidulans* and one of these members, UncA, was studied in detail. We present evidence that UncA is associated with endosomes and other vesicles and transports them surprisingly, along a subpopulation of microtubules.

MATERIALS AND METHODS

Strains, Plasmids, and Culture Conditions

Supplemented minimal (MM) and complete media (CM) for *A. nidulans* and standard strain construction procedures are described by Hill and Käfer (2001). A list of *A. nidulans* strains used in this study is given in Table 1 and Supplemental Table 1. Standard laboratory *Escherichia coli* strains (XL-1 blue, Top 10) were used. Plasmids are listed in Table 2 and Supplemental Table 2.

Molecular Techniques

Standard DNA transformation procedures were used for *A. nidulans* (Yelton *et al.*, 1984) and *Escherichia coli* (Sambrook and Russel, 1999). For polymerase chain reaction (PCR) experiments, standard protocols were applied. DNA sequencing was done commercially (MWG Biotech, Ebersberg, Germany). Genomic DNA was extracted from *A. nidulans* with the DNeasy Plant Mini kit (QIAGEN, Hilden, Germany). DNA analyses (Southern hybridizations) were performed as described previously (Sambrook and Russel, 1999).

Deletion of uncA and uncB

The flanking regions of *uncA* were amplified by PCR using genomic DNA and the primers UncA-LB-fwd (5-CGTCGATGGAAGGCATATACTACTCGC-3) and UncA-LB-Sfi-rev (5-CGGCCATCTAGGCCGACAACAAATTGC-3) for the upstream region of *uncA* and UncA-RB-Sfi-fwd (5-CGGCCTGAGTGGCC-TCTATGTCTTCG-3) and UncA-RB-rev (5-CATCCACGTCCCCATAACTA-ATACCACC-3) for the downstream region. The fragments were cloned into pCR2.1-TOPO to generate pNZ7 and pNZ6, respectively. The SfiI restriction sites are underlined. In a three-fragment ligation, the *pyroA*-gene obtained from plasmid pNZ12 was ligated between the two *uncA*-flanking regions, resulting in vector pNZ13. The deletion cassette was amplified with the primers UncA-LB-fwd (5-CGTCGATGGAAGGCATATACTACTCGC-3) and UncA-RB-rev (5-CATCCACGTCCCCATAACTAATACCACC-3), and the resulting PCR product was transformed into the pyro-auxotrophic *A. nidulans* strain TN02A3.

The *uncB* flanking regions were amplified by PCR using genomic DNA and the primers uncB_LB_fwd (5-GGAAGTACACCTGCATGCTAATATCAT-CAG-3) and uncB_LB_Sfi_rev (5-CGGCCATCTAGGCCGCGGTGAAGTAT-AGAC-3) for the upstream region of *uncB* and uncB_RB_Sfi_fwd (5-CGGC-CTGAGTGGCCTGTTATGCGACGATG-3) and uncB_RB_rev (5-GACGAG-CAAGGGACGTGCCCTTCGGTG-3) for the downstream region and cloned into pCR2.1-TOPO, to generate pNZ3 and pNZ4, respectively. The restriction sites are underlined. The two *uncB*-flanking regions were ligated upstream and downstream of the *pyr4* marker in pCS1, generating pNZ5. This plasmid was cut with EcoRI and BglII, generating a fragment containing *pyr4* flanked by *uncB* sequences. This fragment was transformed into the uracil-auxotrophic strain TN02A3.

In each case, transformants were screened by PCR for the homologous integration event. Single integration of the construct was confirmed by Southern blotting (Supplemental Figure 1). One *uncA*- and one *uncB*-deletion strain were selected from the transformants and named SNZ9 and SNZ3, respectively. The coupling of the observed phenotypes with the gene-deletion events was confirmed by crosses and by down-regulation of the genes through the inducible *alcA* promoter (see below). A *uncA/uncB* double deletion strain was created by crossing the single *uncA* and *uncB* deletions generating SNZ29.

Tagging of Proteins with the Green Fluorescent Protein (GFP) and Monomeric Red Fluorescent Protein (mRFP) 1

To create an N-terminal GFP fusion construct of UncA, a 0.9-kb N-terminal fragment of *uncA* (starting from ATG) was amplified from genomic DNA,

Table 2. Plasmids used in this study

Plasmid	Construction	Source
pTN1	*pyroA* from *A. fumigatus*	Nayak *et al.* (2006)
pAS1	0.9-kb *uncA* fragment in pCR2.1-TOPO	This study
pAS3	0.9-kb *uncA* fragment in pCMB17apx	This study
pCR2.1-TOPO	Cloning vector	Invitrogen
pCS1	*N. crassa pyr-4* selectable marker as NotI fragment in pUMA208	Enke *et al.* (2007)
pCMB17apx	*alcA(p)::GFP*, for N-terminal fusion of GFP to proteins of interest; contains *N. crassa pyr4*	Efimov *et al.* (2006)
pDM8	GFP replaced mRFP1 in pCMB17apx	Veith *et al.* (2005)
pDC1	*argB* from *A. nidulans*	Aramayo *et al.* (1989)
pJH19	*gpd(p)::stuA(NLS)::DsRed* and *argB* as selectable marker	Toews *et al.* (2004)
pNZ1	1.6-kb *uncB* fragment with AscI and PacI sites in pCMB17apx	This study
pNZ3	1.0-kb 5-flanking region of *uncB* with SfiI site in pCR2.1-TOPO	This study
pNZ4	1.0-kb 3-flanking region of *uncB* with SfiI site in pCR2.1-TOPO	This study
pNZ5	*uncB*-deletion construct: flanking regions from pNZ3 and pNZ4 ligated with *pyr4* from pCS1	This study
pNZ6	1.0-kb 3-flanking region of *uncA* with SfiI site in pCR2.1-TOPO	This study
pNZ7	1.0-kb 5-flanking region of *uncA* with SfiI site in pCR2.1-TOPO	This study
pNZ8	*uncA*-deletion construct: flanking regions from pNZ6 and pNZ7 ligated with *pyr4* from pCS1	This study
pNZ9	GFP in pAS3 replaced with mRFP1	This study
pNZ11	1.7-kb *pyroA* fragment from pTN1 with NotI sites in pCR2.1-TOPO	This study
pNZ12	*pyr4* in pCS1 replaced with a 1.7-kb *pyroA* fragment from pNZ11	This study
pNZ13	*uncA*-deletion construct: *pyr4* in pNZ8 replaced with *pyroA* from pNZ12	This study
pNZ15	pAS3 mutagenesis to introduce the G116E mutation in the p-loop of UncA, (UncA[rigor])	This study
pNZS20	GFP in pNZ15 replaced with mRFP1	This study
pCS1-NZ	1.3-kb *kinA* fragment in pCR2.1-TOPO	This study
pCS2-NZ	1.3-kb *kinA* fragment in pCMB17apx, *pyr4* replaced with *pyroA*	This study
pCS3-NZ	1.3-kb *kinA* fragment in pDM6, *pyr4* replaced with *pyroA*	This study
pCS4-NZ	pCS2-NZ mutagenesis to introduce the G97E mutation in the p-loop of KinA, (KinA[rigor])	This study
pCS5-NZ	GFP in pCS4-NZ replaces with mRFP1	This study
pNZ-SI49	1.5-kb *uncA*(p) fragment in pAS3 with KpnI-EcoRI sites	This study
pNZ54	TlgB ORF fragment in pCR2.1-TOPO	This study
pNZ58	TlgB ORF fragment from pNZ54 in pCMB17apx, *pyroA4* instead of *pyr4* as marker	This study
pNZ59	GFP in pNZ58 (mRFP1-TlgB) replaced with mRFP1	This study

with the primers uncA_Asc_fwd1 (5-GGGCGCGCCCGGCATGGCGCCAG-GAGGTGGTG-3) and uncA_Pac_rev1 (5-CTTAATTAAACCTAGCACCGGT-GGCTCCAGTCG-3) and cloned into pCR2.1-TOPO, yielding pAS1. The restriction sites are underlined. The AscI-PacI fragment from pAS1 was subcloned into the corresponding sites of pCMB17apx, yielding pAS3. To create an N-terminal mRFP1 fusion construct of UncA, the GFP KpnI-AscI fragment from pAS3 was substituted by mRFP1 from pDM8, yielding pNZ9. To produce UncA N-terminally tagged with GFP under the native promoter, a 1.5-kb fragment of the putative *uncA* promoter was amplified from genomic DNA with the primers UncA nat(P) EcoRI fwd (5-GGA ATT CTC ATC ACC TAC TGG AGG CGC GC-3) and UncA nat(P) KpnI rev (5-CGG TAC CTT TGG CCT ATA GCC CAT ACA CC-3), digested with EcoRI and KpnI, and the two fragments were ligated with EcoRI-KpnI–digested pAS3, yielding pNZ-SI49 (*alcA* promoter replaced with the *uncA* promoter in pAS3).

Using the same approach as for UncA, N-terminal GFP fusion constructs of KinA and TlgB were created. The primer set used for KinA was KinA ATG AscI fwd (5-GGG CGC GCC CGG CAT GGC GTC CTC TAC-3) and KinA 1324bp Pac rev (5-CTT AAT TAA CAA GAA CGA TGC TGG GTG TGC-3). The PCR fragment was cloned into pCR2.1-TOPO and subsequently into pCMB17apx (*pyroA* as selection marker), yielding plasmid pCS2-NZ. The primer set used for TlgB was Tlg2nidulansAscI fwd (5-GGG CGC GCC CGG CAT GTG GCG GGA CCG-3) and Tlg2nidulansPacI rev (5-CTT AAT TAA CTA CGG GGC AAC GAT GCG GCC-3). The PCR fragment was cloned into pCR2.1-TOPO and subsequently into pDM8 (*pyroA* as selection marker), yielding pNZ58. All plasmids were transformed into the uracil- and pyrodoxin-auxotrophic strain TN02A3 (Δ*nkuA*). The integration events were confirmed by PCR and Southern blotting and microscopy (data not shown).

Creation of an *uncA*[rigor] and *kinA*[rigor] Mutant Allele

We changed the glycine residue 116 to glutamate by site-directed mutagenesis by using the oligonucleotides UncA P-Loop Gly fwd (5-GGT CAG ACC GGT TCG GAG AAG TCT TAC TCG-3) and UncA P-Loop Gly rev (5-CGAGTAA-GACTTCTCCGAACCGGTCTGACC-3), plasmid pAS3 as template, and the QuikChange XL site-directed mutagenesis kit (Stratagene, Heidelberg, Germany); this yielded plasmid pNZ15. We transformed strain TN02A3 and searched for transformants in which pNZ15 was homologously integrated at the *uncA* locus. Among 12 transformants, two (1 transformant named SNZ14) displayed the *uncA* deletion phenotype under both repressing and inducing conditions. PCR and Southern blot analysis confirmed that the construct was

integrated at the *uncA* locus in both transformants. The PCR fragments were sequenced to confirm the mutagenesis event.

The same was done for *kinA* using primer KinA Rigor P-Loop for (5-C GGT CAA ACC GGT GCA GAG AAG TCG TAT AC-3) and KinA Rigor P-Loop rev (5-GT ATA CGA CTT CTC TGC ACC GGT TTG ACC G-3) to change glycine residue 97 to glutamate using pCS2-NZ as template.

Light and Fluorescence Microscopy

For live-cell imaging of germlings and young hyphae, cells were grown on coverslips in 0.5 ml of MM 2% glycerol (derepression of the *alcA* promoter, moderate induction) or MM 2% glucose (repression of the *alcA* promoter). Cells were incubated at room temperature for 1–2 d. For pictures of young hyphae of each strain, the spores were inoculated on microscope slides coated with MM 2% glucose 0.8% agarose and grown at 30°C for 1 d. Images were captured at room temperature (200-ms exposure time) using an Axio Imager Z1 microscope (Carl Zeiss, Jena, Germany). Images were collected and analyzed with the AxioVision system (Carl Zeiss). Dynamic processes in the hyphae were quantified using the same software analyzing series of single pictures. We also used an SP5 laser scanning microscope (Lecia, Wetzlar, Germany).

N-[3-Triethylammoniumpropyl]-4-[p-diethylaminophenylhexatrienyl] Pyridinium Dibromide (FM4-64), Benomyl, and Cytochalasin A Treatment

FM4-64 was used at a concentration of 10 μM in the medium. Coverslips were incubated for 1–2 min and washed. Methyl 1-(butylcarbamoyl)-2-benzimidazole carbamate (benomyl; Aldrich Chemical, Milwaukee, WI) was used at a final concentration of 2.5 μg/ml in the medium from a stock solution of 1 mg/ml in ethanol. Cytochalasin A (Sigma Chemie, Deisenhofen, Germany) was used at a final concentration of 2 μg/ml in the medium from a stock solution of 100 mg/ml in dimethyl sulfoxide.

Immunostaining

We inoculated 10³ spores/ml with 0.5 ml MM on sterile coverslips for 12–24 h at room temperature (RT). Cells were fixed for 30 min with formaldehyde and digested for 1 h by using digestion solution (GlucanX; β-D-glucanase, zymolyase, and driselase in Na-phosphate buffer with 50% egg white),

washed with phosphate buffered saline (PBS), incubated in −20°C methanol for 10 min before and blocked with TBST + 5% skim milk before incubation with the first antibodies (anti-tubulin, 1:500) in Tris-buffered saline/Tween 20 (TBST) overnight at 4°C. Next, cells were washed and incubated with the secondary antibodies (1:200 in TBST) for 1 h at RT. Cells were washed and mounted on microscope slides (with mounting media with 4,6-diamidino-2-phenylindole [DAPI] and VECTORSHIELD [Vector Laboratories, Burlingame, CA]), sealed with nail polish, and stored at 4°C overnight in the dark before doing the microscopy. As monoclonal anti-α tubulin antibodies, we used the following clones from Sigma Aldrich: DM1A (anti-α tubulin), B3 (anti-polyglutamylated tubulin), 6–11B-1 (anti-acetylated tubulin), and TUB-1A2 (anti-tyrosinated tubulin). As secondary antibodies, we used fluorescein isothiocyanate (FITC)-conjugated anti-mouse immunoglobulin G (IgG) (Fab-specific) (Sigma Chemie), FITC-conjugated anti-mouse IgG (whole molecule) (Sigma Chemie), and Cy3 conjugated AffiniPure goat anti-mouse IgG (H+L) (Dianova, Hamburg, Germany).

RESULTS

Isolation of UncA and UncB

We identified eleven different kinesins in *A. nidulans*, with two members (named UncA and UncB) of the kinesin-3 family (formerly called *unc-104* family) (Rischitor *et al.*, 2004; Galagan *et al.*, 2005). The predicted structure of the *uncA* and the *uncB* genes were confirmed through amplification of small cDNAs and subsequent sequencing. The *uncA* gene contains an intron of 75 base pairs located between amino acid 21 and 22 of the open reading frame. The UncA protein is comprised of 1631 amino acids, with a calculated molecular mass of 182.7 kDa. The predicted motor domain starts two amino acids downstream of the initiation codon and consists of 361 amino acids. The ATP-binding motif (P-loop) starts at amino acid 111 (GQTGSGKS). The C-terminal half of the motor domain displays the highly conserved regions termed switch I (NETSSR), at amino acid position 224 and switch II (DLAGSE), at amino acid position 261, which are involved in nucleotide binding (ATP). Two microtubule-binding motifs were found, MT1 (RDLL) starting at amino acid position 170 and MT2 (VPYRDS) starting at amino acid position 312 (Song *et al.*, 2001).

Comparison of UncA with other Kin-3 proteins revealed 60% homology with *N. crassa* Nkin2, 48.1% with *U. maydis*, and 46.5% with *C. elegans* Unc104, but 80.8% homology with *Aspergillus oryzae*, and 88.1% with *Aspergillus fumigatus* (Figure 1). The homology between the proteins is much higher in the motor domains (Supplemental Figure 2). The C terminus of UncA exhibited very low sequence similarity to the corresponding regions of other Kin-3 family proteins, besides a forkhead-associated (FHA) domain at amino acid 496–596 and a pleckstrin homology (PH) domain at amino acid 1509–1615. The PH domain has been reported previously in Unc104-related kinesins in *C. elegans* where it has been proposed to bind lipids and lipid rafts to dock onto membrane cargoes (Klopfenstein *et al.*, 2002). The FHA domain is proposed to be involved in signaling and protein–protein interactions of kinesins (Westerholm-Parvinen *et al.*, 2000). In addition, a novel role for the FHA domain in the regulation of kinesin motors was discovered previously (Lee *et al.*, 2004).

The *uncB* gene contains an intron of 52 base pairs at position 112 of the open reading frame. The derived UncB protein is composed of 671 amino acids, with a calculated molecular mass of 75 kDa. The motor domain starts 116 amino acids downstream of the initiation codon and consists of 356 amino acids. The P-loop starts at amino acid 212 (GQTGSGKS). The C-terminal half of the motor domain displays the highly conserved regions termed switch I (NDTSSR), at amino acid 326 and switch II (DLAGSE) at amino acid 363, which are involved in nucleotide binding (ATP). Two microtubule-binding motifs were found, MT1
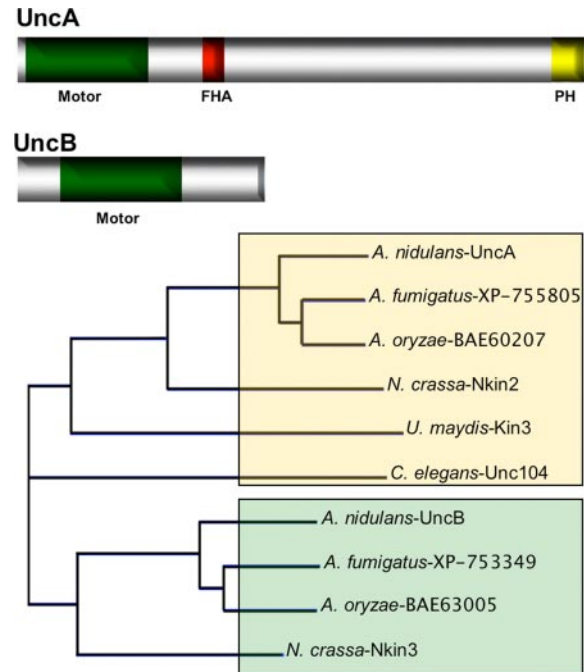
Figure 1. Scheme of UncA and UncB and relatedness analysis with other kinesins of the kinesin-3 family. The UncA (1631 amino acids) and UncB (671 amino acids) protein sequences were analyzed with SMART (http://smart.embl-heidelberg.de) and besides the kinesin motor domains a FHA and a PH domain were identified in UncA. The relatedness analysis was done with Vector NTI by using standard parameters. UncB groups with the fungal-specific subclass as indicated by green shading.

(RDLL) at amino acid position 268 and MT2 (VPYRDS) at amino acid 417 (Figure 1).

Comparison of full-length UncB with other Kin-3 proteins revealed 56.4% homology with *N. crassa* Nkin3, 83% with *A. oryzae*, and 75% with *A. fumigatus*. The N-terminal region starts with a short nonmotor sequence of 104 amino acids (Figure 1). The 195 amino acid-long part outside the motor domain exhibits very low sequence similarity to the corresponding regions of related proteins.

Deletion of uncA and uncB

We deleted the *uncA* open reading frame in strain *TN02A3* with *pyroA* as selection marker and confirmed the deletion event by diagnostic PCR (data not shown) and Southern blot (Figure 2 and Supplemental Figure 1). One of the strains 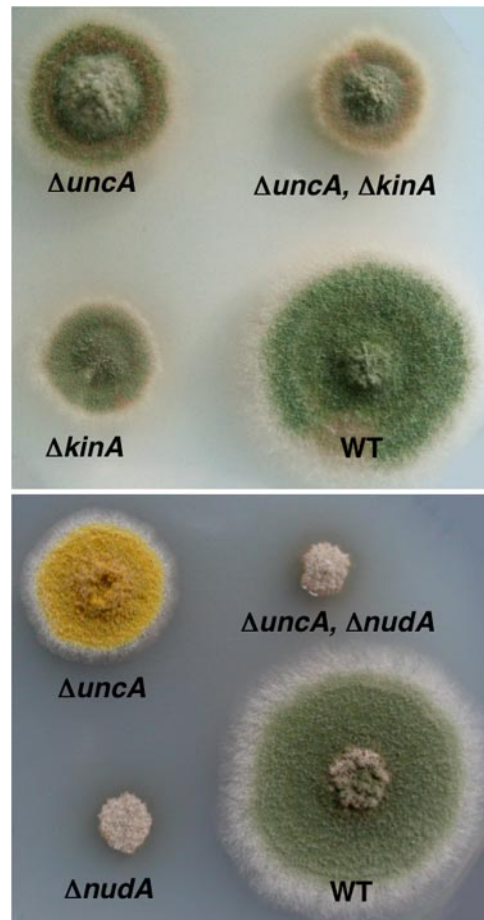(SNZ9) was used for further analysis and the construction of *uncA*-deletion strains in other genetic backgrounds. Colonies of this strain grew slower than wild-type colonies and seemed more compact. When we compared the distribution of nuclei or mitochondria, or the organization of the microtubule cytoskeleton, we did not observe any difference to wild-type (Supplemental Figure 3). However, we noticed more branching in the ΔuncA strain. At higher temperature, we observed a slight curved hyphal phenotype similar to the phenotype of cell end marker mutants (Takeshita *et al.*, 2008) (Figure 2B).

We deleted the *uncB* open reading frame in strain *TN02A3* with *pyr4* as selection marker and confirmed the deletion event by diagnostic PCR (data not shown) and Southern blot (Figure 2A and Supplemental Figure 1). One of the strains (SNZ3) was used for further analysis and the construction of
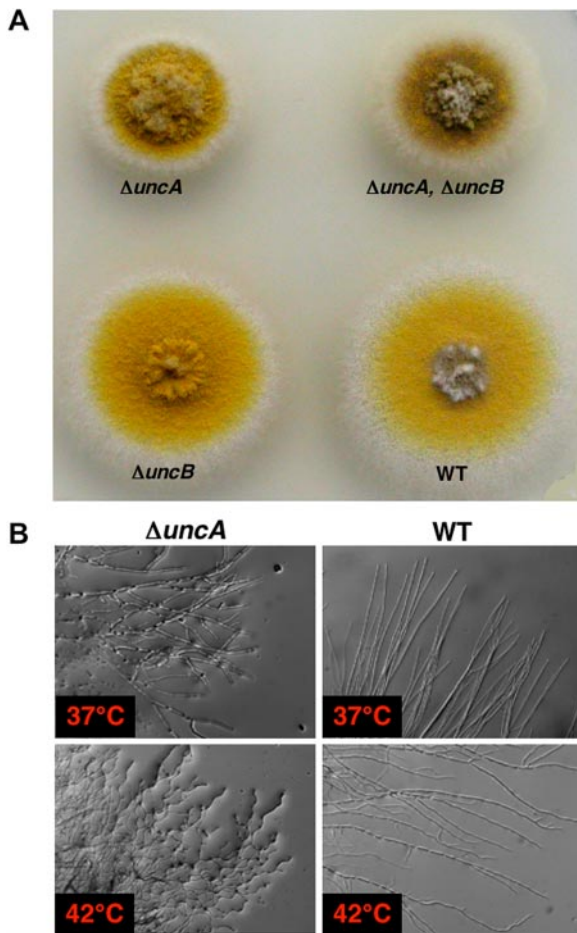
Figure 2. Phenotype of an *uncA*, an *uncB*, and a double-deletion strain. (A) Growth of the strains SNZ27 (Δ*uncA*), SNZ15 (Δ*uncB*), SNZ29 (Δ*uncA*, Δ*uncB*), and RMS011 on minimal medium for 3 d at 37°C. (B) Hyphal growth of the *uncA*-deletion strain and the wild type at 37 and 42°C grown on glycerol minimal medium for 2 d.

Figure 3. Comparison of colony growth of different mutants as labeled. Top, deletion strains of *uncA* (SNZ9) and conventional kinesin *kinA* (AnKin26) in comparison with the double deletion strain (SNZ36) and a wild type (TN02A3). Bottom, comparison of the colony phenotypes of the *uncA*-deletion strain (SNZ27) and the dynein-deletion strain (*nudA*) (XX60) and the corresponding double deletion (SNZ63). Colonies were grown for 3 d on glucose minimal medium at 37°C.

uncB-deletion strains in other genetic backgrounds. Colonies of this strain grew like wild-type colonies. We did not observe any difference to wild type with respect to nuclear or mitochondrial distribution, septum formation, or branching (data not shown).

To investigate whether UncA and UncB are functionally related, we constructed an *uncA/uncB* double deletion mutant (Figure 2A). It displayed the same compact growth phenotype than the *uncA*-deletion mutant. The analysis of nuclear and mitochondrial distribution, the organization of the microtubule (MT) cytoskeleton revealed no difference in comparison with the wild type (Suelmann and Fischer, 2000). This was unlike the situation in *N. crassa* (Fuchs and Westermann, 2005). Our results suggested that UncA and UncB act in different pathways. Therefore, we focused in this paper only on the molecular analysis of UncA.

To test whether deletion of *uncA* causes a more severe phenotype in the absence of other motor proteins involved in polarized growth, we constructed an *uncA/kinA* (conventional kinesin) and an *uncA/nudA* (heavy chain of dynein) double-deletion mutant (Figure 3). The growth defects of these strains were comparable to the growth defect of stains with single mutations in either *kinA* or *nudA*, respectively.

Localization of UncA along Microtubules

The UncA protein was visualized by fusion with a fluorescent protein (GFP or mRFP1 in the vector pMCB17apx). A 0.9-kb fragment from the *uncA* 5'-end was fused to GFP and under the control of the *alcA*-promoter (de-repressed with glycerol, induced with threonine, repressed with glucose). After homologous integration of the construct at the *uncA* locus, the 0.9-kb fragment becomes duplicated and the full-length *uncA*-open reading frame is fused to GFP and is under the control of the *alcA* promoter. The *uncA-GFP* strain (SNZ2), in which plasmid pAS3 is homologously integrated, grew like the *uncA*-deletion strain when grown on glucose medium and like wild type when grown on glycerol or threonine medium, showing that the GFP fusion protein was fully functional (Supplemental Figure 4). Under inducing conditions, GFP was visible as fast-moving spots and accumulated sometimes at the tips of the hyphae (Figure 4A and Supplemental Movie 1). They moved into two directions with speeds of up to 4 μm s^{-1}. The speed was determined as described in *Materials and Methods*. The GFP signal at the tip looked like an accumulation of dynamic vesicles. After addition of the microtubule-destabilizing drug benomyl,
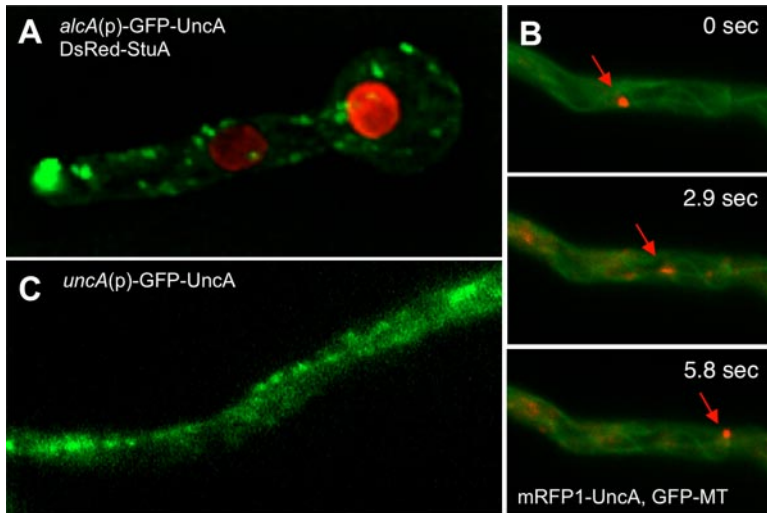
Figure 4. Localization of UncA. (A) UncA was labeled with GFP and nuclei with DsRed. UncA was under the control of the *alcA* promoter (SNZ4). (B) Movement of UncA along microtubules. Time-lapse analysis of mRFP1-UncA in a strain with GFP tagged microtubules (SNZ26). One spot (indicated with the arrow) was focused and followed over time. The time between the exposures of the pictures is indicated. (C) GFP-UncA expressed under the natural promoter (SNZ74). A pearl-string like arrangement of the signal is visible.

vesicle movement in the hyphae and at the tip stopped (Supplemental Figure 5), suggesting microtubule-dependent movement. This finding was supported by colocalization of GFP-labeled microtubules with mRFP1-labeled UncA (Figure 4B and Supplemental Movie 2). To exclude the possibility that the observed localization was due to *alcA*-driven expression (glycerol as carbon source) of the GFP-UncA fusion protein, we replaced the *alcA* promoter with a 1.5-kb DNA fragment derived from the region upstream of the *uncA* start codon. This construct was transformed into TN02A3. One strain with a homologous integration event at the *uncA* locus was selected for further analysis (SNZ74) (Supplemental Figure 6). The strain seemed like wild type, suggesting functionality of the GFP-UncA fusion protein. Although the GFP signal was weaker than in the previous strains, small moving spots were clearly visible (Figure 4C). These results suggested that in the above-described experiments *alcA*-driven expression with glycerol in the medium did not cause artifacts and/or mislocalization of the protein. Interestingly, the GFP-UncA protein preferred essentially one track in the cell (Supplemental Movie 1). This suggested a preference of UncA for a certain class of microtubules.

UncA Is Involved in Vesicle Transport

Because we excluded a role of UncA in mitochondrial movement (Supplemental Figure 7) and because Kin-3 of *U. maydis* localizes to early endosomes, we analyzed the association of UncA with vesicles. To this end, we stained the plasma membrane in *A. nidulans* strain (SNZ74, *uncA(p)::GFP::uncA*) with FM4-64. After internalization of the membrane, early endosomes were visible. The movement of the corresponding vesicles resembled the movement of GFP-UncA (Supplemental Movie 3). However, colocalization of the red FM4-64 and the green GFP signal proved to be difficult because of the high speed of the structures. This technical obstacle was overcome by generating a rigor variant of UncA by changing glycine residue 116 to a glutamate (see *Materials and Methods*). This modification of the P-loop allows binding of the motor to the microtubules but not their dissociation (Meluh and Rose, 1990; Nakata and Hirokawa, 1995). The movement of FM4-64–labeled vesicles was reduced and colocalization with GFP-UncA^{rigor} was observed in some cases (Figure 5A). Quantification was impossible, because of the alignment of the vesicles to a continuous structure (see below). That not all GFP signals colocalized

with FM4-64 suggests that UncA is not only associated with early endosomes but also with other vesicles. As a further proof for the binding of UncA to endosomes, we tagged a *S. cerevisiae* Tlg2 homologue, named TlgB in *A. nidulans*, with mRFP1 (see *Materials and Methods*). This protein was used before for endosome labeling in *A. oryzae* (Kuratsu *et al.*, 2007). TlgB (317 amino acids) displays 39.9% homology to
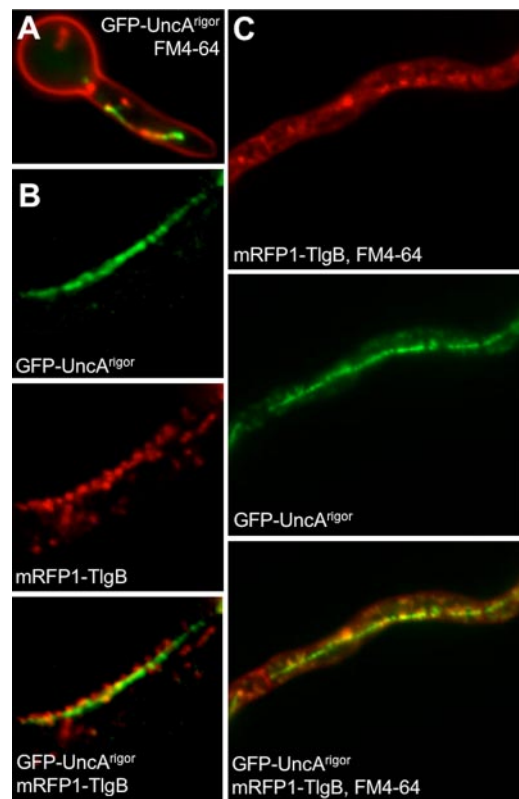
Figure 5. Colocalization of endosomes with UncA. (A) Endosomes were visualized with FM4-64 and UncA^{rigor} with GFP (SNZ14). UncA^{rigor} was expressed from the *alcA* promoter in the presence of glycerol. (B) Colocalization of mRFP1-TlgB and GFP-UncA^{rigor} (SNZ69). (C) Colocalization of mRFP1-TlgB and FM4-64 with GFP-UncA^{rigor}.
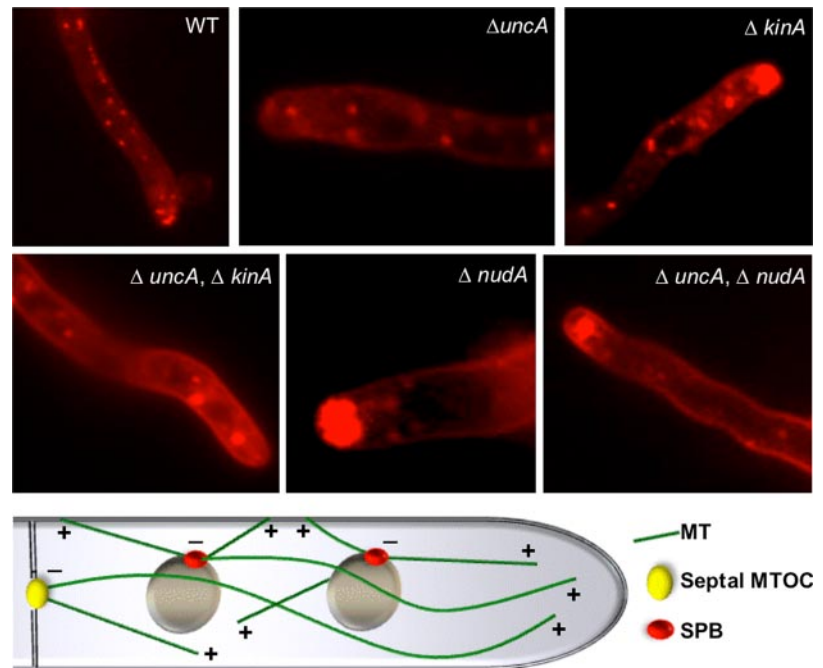
Figure 6. FM4-64 staining in the strains indicated in the pictures and scheme of microtubule organization in the hyphal tip of *A. nidulans*. The strains were the same as described in the legend for Figure 4. FM4-64 staining was done as described in *Materials and Methods*. The mixed polarity of MTs indicated in the scheme will be discussed in the first chapter of the Discussion section.

the *S. cerevisiae* Tlg2 protein (398 amino acids). Both proteins share a Syntaxin and target-soluble *N*-ethylmaleimide-sensitive factor attachment protein receptor domain. To localize TlgB, we cloned the full-length coding region downstream of mRFP1 in the vector pDM8 and integrated it ectopically into the genome of SNZ14 (GFP-UncA^rigor)(SNZ69). Southern blot analysis showed that the strain contained several integrations. Fluorescence microscopy revealed partial colocalization between UncA-GFP and mRFP1-TlgB (Figure 5B). Three other strains, also with integrations at different places in the genome, showed the same localization pattern, indicating that the localization was independent of the integration site. Strain SNZ69 was treated with FM4-64. Because in *S. cerevisiae* Tlg1 and Tlg2 endocytic vesicles were only transiently labeled with FM4-64 (Holthuis *et al.*, 1998), we anticipated that the combination of FM4-64 and mRFP1-TlgB would stain all GFP-UncA^rigor–labeled vesicles (Figure 5C). Indeed we detected more colocalization, but still some GFP signals did not localize at the same places as the red signals, again indicating that UncA is associated not only with endosomes.

To study whether the observed movement of FM4-64–labeled vesicles was due to UncA or another motor activity, we studied vesicle behavior (stained with FM4-64) in *uncA*-, *kinA*-, and *nudA*-deletion strains (Figure 6 and Supplemental Movies 4–8). It was clearly visible that the movement changed dramatically when UncA or dynein were absent or nonfunctional, respectively. Long-distance movement as observed in wild type was largely reduced in 28 out of 37 hyphae. In nine hyphae, one or two vesicles were observed moving long distances (2-min observation time). In addition to the reduced motility, an accumulation of vesicles was observed in the dynein mutant at the hyphal tip, suggesting that dynein is required for retrograde transportation. In the double mutant Δ*nudA*/Δ*uncA* the defect in vesicle movement was the same as in the dynein single mutant. In the *kinA*-deletion strain, long-distance vesicle movement occurred, and a vesicle accumulation was visible at the hyphal tip. The effect was not as strong as in the dynein mutant. This observation can be explained by the accumulation of

dynein at the microtubule plus end, and thereby the transportation to the tip zone, depending on conventional kinesin (Zhang *et al.*, 2003). Hence, the observed defect of vesicle movement in the *kinA* mutant is probably due to the lack of dynein at the tip. A double mutant between Δ*kinA* and Δ*uncA* displayed a similar phenotype as the Δ*uncA*-deletion strain, with some more accumulated vesicles at the tip (Figure 6).

UncA Localizes to a Subpopulation of Microtubules

In the above-described experiments, we found that a rigor mutation in the UncA motor reduced the movement of the vesicles, and most surprisingly, the GFP-UncA signal was aligned along a rod-like structure in the cell (Figure 7, A and B). This rod was a microtubule, as shown by disassembly with benomyl (Supplemental Figure 7). To analyze this phenomenon further, we stained the microtubules by secondary immunofluorescence by using anti-α-tubulin antibodies and compared them with the observed rod structure stained with mRFP1-UncA. Indeed, the red rod represented a subpopulation of microtubules (Figure 7C). Because UncA seemed to be a nice marker for this population of microtubules, we analyzed the occurrence in different developmental stages. We found the GFP-UncA labeled rod-like structures already in conidiospores, as well as in young germ tubes and older hyphal compartments. This suggests that the occurrence of this microtubule population is independent of the growth phase of the hyphae. In addition, we observed this rod during mitosis. In contrast, mitotic spindle microtubules were not labeled with mRFP1-UncA^rigor (Figure 8A). This suggests that UncA associates with the more stable cytoplasmic microtubules. This is in agreement with previous observations that not all microtubules are disassembled during nuclear division and are thus of different stability (Veith *et al.*, 2005).

To analyze the observed specificity of the UncA motor protein, we studied the presence of posttranslational modifications of tubulin in *A. nidulans*. One modification is the addition of glutamate residues near the carboxy terminus of α- and β-tubulin. Using anti-polyglutamylated tubulin anti-
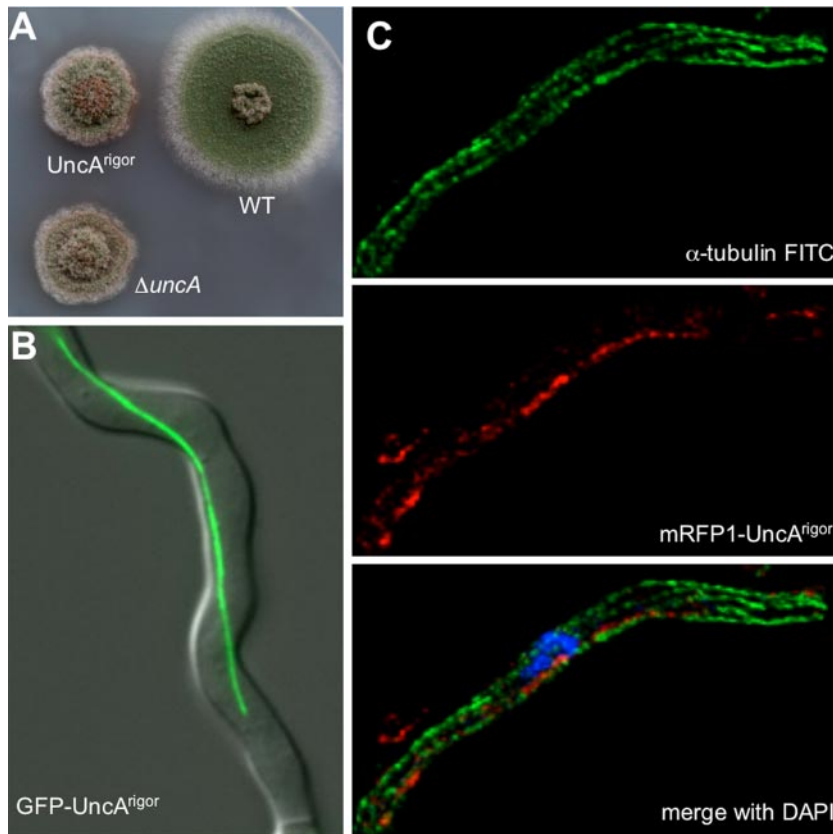
Figure 7. Localization of UncA[rigor] along a single microtubule. (A) The colony of an *uncA[rigor]* mutant (SNZ14) shows the same phenotype as an *uncA*-deletion strain (SNZ9). (B) GFP-UncA[rigor] localizes to a rod-like structure in a hyphal compartment. (C) Immunostaining of a tip compartment of an mRFP1-UncA[rigor] strain (SNZ54) with anti-α-tubulin antibodies and FITC-labeled secondary antibodies. Nuclei were stained with DAPI. Top, FITC fluorescence. Middle, mRFP1 fluorescence. Bottom, overlay with the DAPI channel.

bodies for immunostain experiments, we were not able to visualize microtubules (data not shown). It is possible, that these antibodies do not recognize the *A. nidulans* modified tubulin. However, it is also possible that this modification does not exist in *A. nidulans*. The same was true for the analysis of acetylated microtubules (data not shown). Another modification is a reversible removal of a terminal tyrosin residue of α-tubulin. In *A. nidulans* the C terminus of α-tubulin ends with the amino acids valin, glutamate, and tyrosine. We used monoclonal anti-tyrosine tubulin antibodies against the tyrosinated form of α-tubulin. These antibodies stained cytoplasmic and mitotic microtubules (Figure 8). In interphase cells, all microtubules were stained with the antibody, including the microtubule characterized by mRFP1-UncA[rigor] (Figure 8B). However, when we looked at mitotic cells, the mRFP1-UncA[rigor] rod was clearly visible and was not stained with the anti-tyrosin tubulin antibody (Figure 8A). In comparison, the mitotic spindle was stained. These findings suggest that UncA binds preferentially to detyrosinated microtubules. In interphase cells, tyrosinated and detyrosinated microtubules seem to exist in parallel in one microtubule bundle. During mitosis the tyrosinated cytoplasmic microtubule depolymerizes and the detyrosinated ones remain.

To test whether the observed behavior of the UncA[rigor] motor protein is specific for UncA, we compared the results to the binding of kinesin rigor variants of kinesin-1 (conventional kinesin, KinA) and kinesin-7 (KipA) (Seiler *et al.*, 1997; Requena *et al.*, 2001; Konzack *et al.*, 2005) (Figure 9). Kinesin-8 (KipB) was already studied in a previous article (Rischitor *et al.*, 2004) and did not show a preference for certain microtubules (Supplemental Figure 6). In KipA and KinA, we did not find any specificity either. Comparison of KinA[rigor]

with UncA[rigor] localization confirmed the specificity of UncA (Figure 9C). During our experiments, we made another interesting observation. We noticed that KinA[rigor] did not decorate microtubules, stained with the anti-tyrosin tubulin antibody, at the very tip of the hypha (Figure 9D).

DISCUSSION

In this article, we show that UncA is required for vesicle movement in *A. nidulans* and found that their transportation preferably occurs along a subpopulation of microtubules. This is in contrast to the finding in *N. crassa*, where this motor protein transports mitochondria (Fuchs and Westermann, 2005), but in agreement with our previous finding that in *A. nidulans* mitochondrial movement depends on the actin cytoskeleton (Suelmann and Fischer, 2000). We showed here that vesicle movement was dependent on the motor activity of UncA and occurred into both directions in the cell. This bidirectional movement and the accumulation of vesicles in the tip compartment of a dynein and a conventional kinesin mutant, is comparable with the situation in *U. maydis* and can be explained if UncA and dynein transport these vesicles into opposite directions, UncA toward the plus and dynein toward the minus end of microtubules (Wedlich-Söldner *et al.*, 2002). The lack of one motor causes an imbalance of the forces and an accumulation of the vesicles. However, first it was surprising that the vesicles only accumulated in the dynein mutant and not in the rear of the hypha in the *uncA*-deletion strain. To explain this, it has to be considered that in the tip compartment almost all microtubules are oriented with their plus ends toward the growing tip. In regions behind the first nucleus, however, the orientation is mixed and thus a single motor can transport
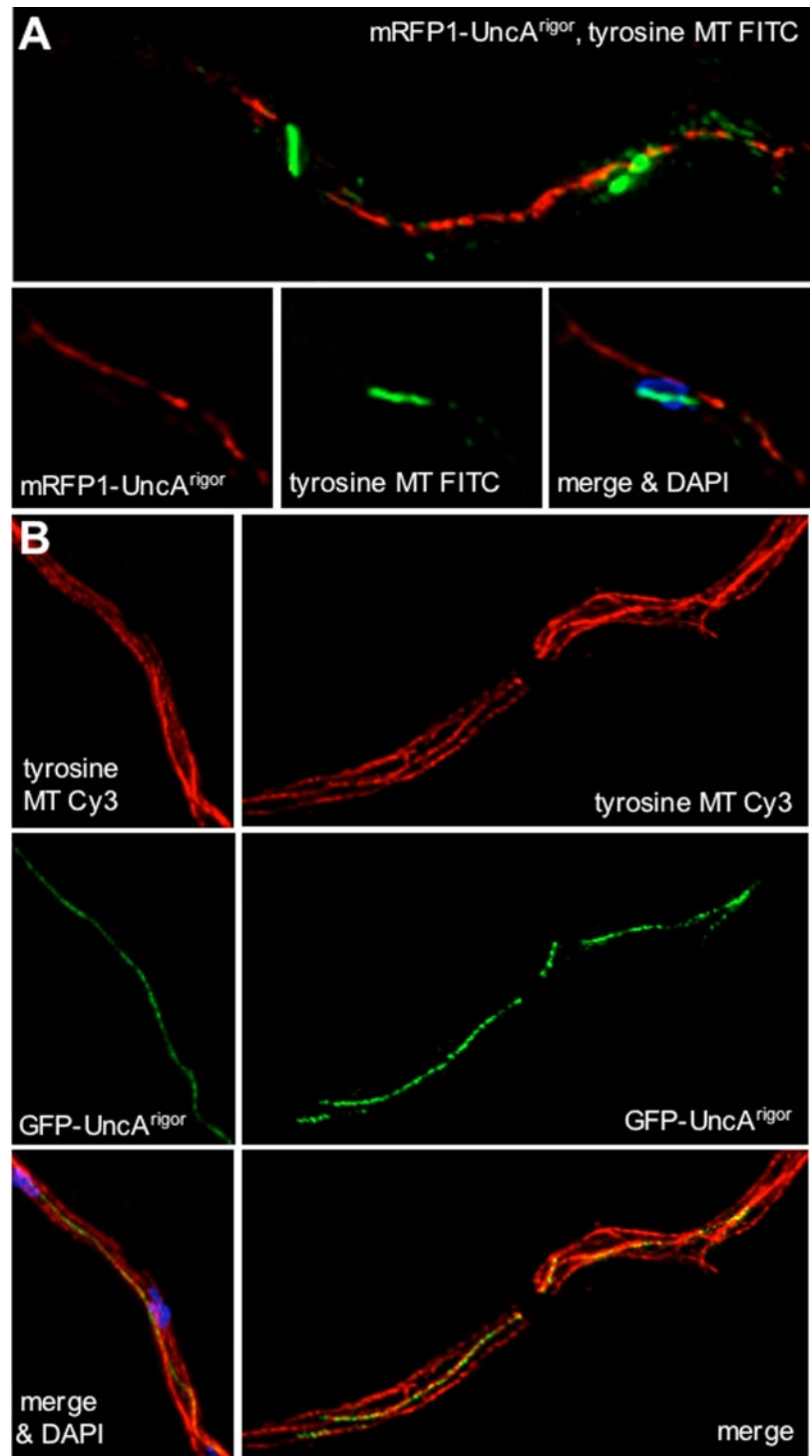
Figure 8. Immunostaining of mRFP1-UncA^rigor hyphae with anti-tyrosinated tubulin antibodies and FITC-labeled secondary antibodies. (A) Hyphal compartment during mitosis. mRFP1-UncA^rigor localizes to one MT in the cytoplasm but not to the two mitotic spindles, which are decorated with the green fluorescent FITC antibodies. The lower row of three pictures shows a second example and demonstrates that the anti-tyrosine antibody does not stain any microtubule in the cytoplasm (middle). Right, overlay of the mRFP1, FITC, and the DAPI channels. (B) Colocalization of GFP-UncA^rigor and tyrosinated microtubules (Cy3 stained) in interphase by laser scanning (left) and widefield fluorescence microscopy (right).

cargoes antero- and retrograde (Konzack *et al.*, 2005). This mixed orientation of microtubule polarities is due to overlapping microtubules emanating from neighbor nuclei and in addition, from septa (Veith *et al.*, 2005) (Figure 6). The effect of the deletion of conventional kinesin may be secondary, because KinA is required for dynein localization at the microtubule plus end (Zhang *et al.*, 2003).

One most surprising result of this study was the finding that UncA moved preferentially along one microtubule. This was in contrast to other kinesins, which did not prefer any

special microtubule. These findings suggest the existence of modified microtubules in *A. nidulans* and thereby most likely in other filamentous fungi. Already 30 years ago, a posttranslational modification at the C terminus of α-tubulin was detected in vertebrate brains (Arce *et al.*, 1975). This modification was a RNA-independent incorporation of tyrosine. In most eukaryotes, the C terminus of α-tubulin is characterized by two glutamate residues followed by an aromatic amino acid such as tyrosine in mammals and phenylalanine in *S. cerevisiae*. The last amino acid is subjected to
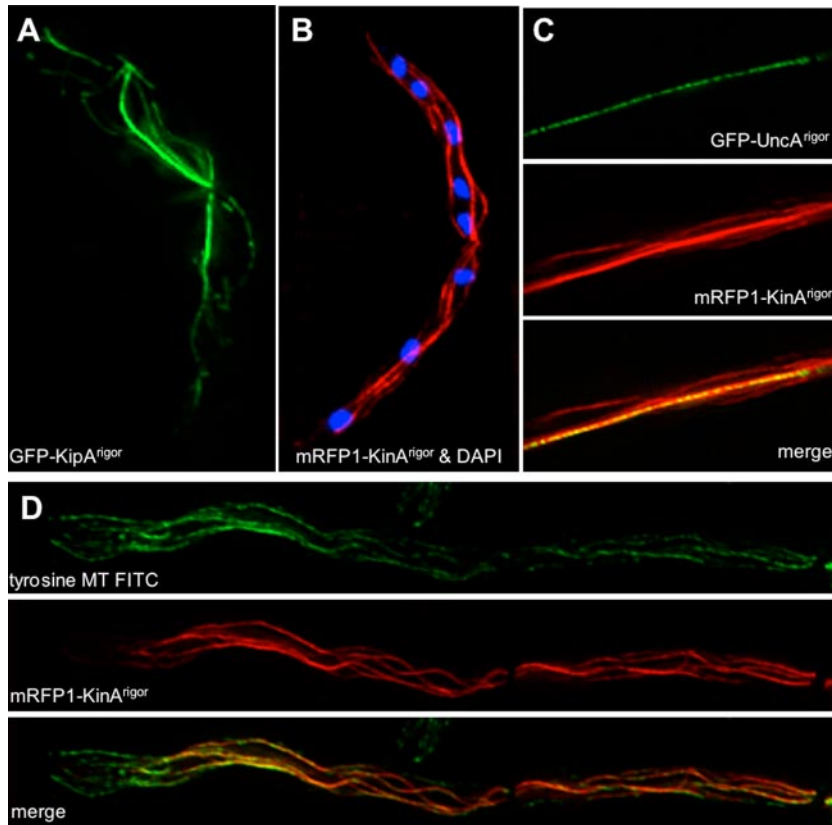
Figure 9. Comparison of the localization of three kinesin motor proteins in the rigor state. (A) GFP-KipA^rigor. (B) mRFP1-KinA^rigor overlaid with the DAPI channel. (C) Colocalization of GFP-UncA^rigor (top) with mRFP1-KinA^rigor (middle). Bottom, overlay. (D) Colocalization of mRFP1-KinA^rigor and tyrosinated microtubules in interphase. Top, FITC channel. Middle, mRFP channel. Bottom, overlay of the two channels.

a cyclic removal and readdition by a carboxypeptidase and a tubulin-tyrosin ligase. An equilibrium between the two modifying enzymes determines the status of the microtubule (Westermann and Weber, 2003). There is evidence that an accumulation of detyrosinated tubulin is associated with tumor growth (Mialhe *et al*., 2001). In *S. cerevisiae*, no cycling occurs, but detyrosinated microtubules are involved in nuclear oscillations (Badin-Larcon *et al*., 2004). Other modifications such as polyglutamylation, acetylation, and polyglycylation have not been reported in *S. cerevisiae* or filamentous fungi but in other eukaryotes including the most primitive eukaryote *Giardia lamblia* (Westermann and Weber, 2003). In this article, we showed that detyrosinated microtubules exist in *A. nidulans*, but we found no evidence for acetylated or polyglutamylated microtubules. To our knowledge, this is the first report of the existence of microtubule subpopulations in filamentous fungi.

There is increasing evidence that different modified microtubules play distinct roles in eukaryotic cells (Westermann and Weber, 2003). There was indirect evidence that Kif1A in mice binds preferentially to polyglutamylated microtubules (Ikegami *et al*., 2007). Our finding that UncA associated with detyrosinated microtubules is a second example for the specificity of kinesin-3 for certain microtubules and surprisingly, the specificity seems not to be evolutionarily conserved, given that the mice motor binds to polyglutamylated and the fungal one to detyrosinated microtubules. Another example for microtubule specificity was shown recently for conventional kinesin in neurites, where it binds preferentially to acetylated microtubules. Purified acetylated microtubules stimulated the kinesin activity (Reed *et al*., 2006). Furthermore, Dunn *et al*. (2007) found that kinesin-1 Kif5c binds preferentially to detyrosinated microtubules. In both cases these are

stable microtubules. In summary, microtubule modifications seem to act as traffic signs for certain microtubule-dependent motor proteins. However, the exact cellular function for that is largely enigmatic and whether detyrosination has any effect on the UncA motor activity remains to be shown.

We found that modified microtubules are more stable but that the modification is not the cause but instead the consequence for the increased stability (Gundersen *et al*., 1984, 1987; Schulze *et al*., 1987). Likewise, we observed previously that some microtubules are not depolymerized as most microtubules are during mitosis of fast-growing hyphae (Veith *et al*., 2005). Indeed, in this study we found the GFP-UncA–labeled microtubule intact in the cytoplasm during nuclear division (Figure 10). This could be the reason for the evolution of the preference of the kin-3 motor in *A. nidulans*. If we assume that transportation of vesicles is important during all stages of the cell cycle; it would explain why the organism would have an advantage if the motor transporting them would preferentially bind to the one remaining stable during mitosis. Because vesicle movement is important for fast polarized growth, this stable microtubule could be important for the maintenance of hyphal extension during mitosis (Riquelme *et al*., 2003).

The question of microtubule modifications and their roles in vivo raises another very interesting question about the specificity of different motors. Motors thus are not only specific for their cargoes but also apparently also for their tracks. Further experiments in *A. nidulans* and other eukaryotes are required to better understand the biological importance of microtubule modifications and their interactions with molecular motors.
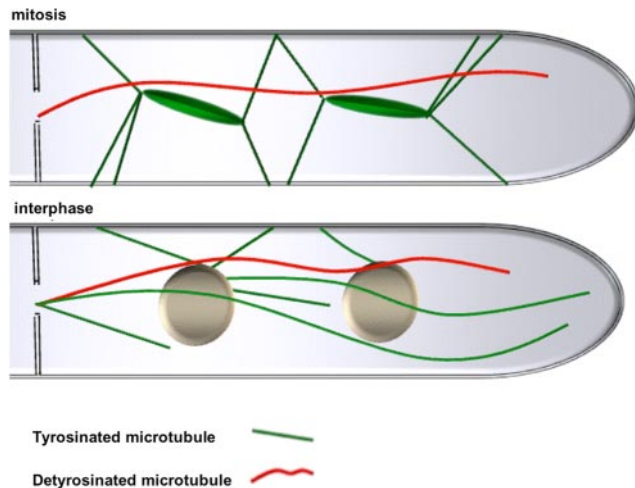
Figure 10. Proposed model for the arrangement of tyrosinated and detyrosinated microtubules during mitosis and during interphase in *A. nidulans*. For details, refer to *Discussion*.

ACKNOWLEDGMENTS

REFERENCES

Aramayo, R., Adams, T. H., and Timberlake, W. E. (1989). A large cluster of highly expressed genes is dispensable for growth and development in *Aspergillus nidulans*. Genetics *122*, 65–71.

Araujo-Bazan, L., Peñalva, M. A., and Espeso, E. A. (2008). Preferential localization of the endocytic internalization machinery to hyphal tips underlies polarization of the actin cytoskeleton in *Aspergillus nidulans*. Mol. Microbiol. *67*, 891–905.

Arce, C. A., Rodriguez, J. A., Barra, H. S., and Caputo, R. (1975). Incorporation of L-tyrosine, L-phenylalanine and L-3,4dihydroxyphenylalanine as single units into rat brain tubulin. Eur. J. Biochem. *59*, 145–149.

Badin-Larcon, A. C., Boscheron, C., Soleilhac, J. M., Piel, M., Mann, C., Denarier, E., Fourest-Lieuvin, A., Lafanechère, L., Bornens, M., and Job, D. (2004). Suppression of nuclear oscillations in *Saccharomyces cerevisiae* expressing Glu tubulin. Proc. Natl. Acad. Sci. USA *101*, 5577–5582.

Basu, R., and Chang, F. (2007). Shaping the actin cytoskeleton using microtubule tips. Curr. Opin. Cell Biol. *19*, 1–7.

Dunn, S., Morrison, E. E., Liverpool, T. B., Molina-Paris, C., Cross, R. A., Alonso, M. C., and Peckham, M. (2007). Differential trafficking of Kif5c on tyrosinated and detyrosinated microtubules in live cells. J. Cell Sci. *121*, 1085–1095.

Efimov, V., Zhang, J., and Xiang, X. (2006). CLIP-170 homologue and NUDE play overlapping roles in NUDF localization in *Aspergillus nidulans*. Mol. Biol. Cell *17*, 2021–2034.

Enke, C., Zekert, N., Veith, D., Schaaf, C., Konzack, S., and Fischer, R. (2007). *Aspergillus nidulans* Dis1/XMAP215 protein AlpA localizes to spindle pole bodies and microtubule plus ends and contributes to growth directionality. Eukaryot. Cell *6*, 555–562.

Fischer, R., Zekert, N., and Takeshita, N. (2008). Polarized growth in fungi—interplay between the cytoskeleton, positional markers and membrane domains. Mol. Microbiol. *68*, 813–826.

Fuchs, F., and Westermann, B. (2005). Role of Unc104/KIF1-related motor proteins in mitochondrial transport in *Neurospora crassa*. Mol. Biol. Cell *16*, 153–161.

Galagan, J. E. *et al.* (2005). Sequencing of *Aspergillus nidulans* and comparative analysis with *A. fumigatus* and *A. oryzae*. Nature *438*, 1105–1115.

Gundersen, G. G., Kalnoski, M. H., and Bulinski, J. C. (1984). Distinct populations of microtubules: tyrosinated and nontyrosinated alpha tubulin are distributed differently in vivo. Cell *38*, 779–789.

Gundersen, G. G., Khwaja, S., and Bulinski, J. C. (1987). Postpolymerization detyrosination of alpha-tubulin: a mechanism for subcellular differentiation of microtubules. J. Cell Biol. *105*, 251–264.

Hall, D. H., and Hedgecock, E. M. (1991). Kinesin-related gene *unc-104* is required for axonal transport of synaptic vesicles in *C. elegans*. Cell *65*, 837–847.

Hill, T. W., and Käfer, E. (2001). Improved protocols for *Aspergillus* minimal medium: trace element and minimal medium salt stock solutions. Fungal Genet. Newsl. *48*, 20–21.

Holthuis, J. C., Nichols, B. J., Dhruvakumar, S., and Pelham, H. R. (1998). Two syntaxin homologues in the TGN/endosomal system of yeast. EMBO J. *17*, 113–126.

Ikegami, K. *et al.* (2007). Loss of a-tubulin polyglutamylation in ROSA22 mice is assocated with abnormal targeting of KIF1A and modulated synaptic function. Proc. Natl. Acad. Sci. USA *104*, 3213–3218.

Klopfenstein, D. R., Tomishige, M., Stuurman, N., and Vale, R. D. (2002). Role of phosphatidylinositol(4,5)bisphosphate organisation in membrane transport by the Unc104 kinesin motor. Cell *109*, 347–358.

Konzack, S., Rischitor, P., Enke, C., and Fischer, R. (2005). The role of the kinesin motor KipA in microtubule organization and polarized growth of *Aspergillus nidulans*. Mol. Biol. Cell *16*, 497–506.

Kuratsu, M., Taura, A., Shoji, J.-Y., Kikuchi, S., Arioka, M., and Kitamoto, K. (2007). Systematic analysis of SNARE localization in the filamentous fungus *Aspergillus oryzae*. Fungal Genet. Biol. *44*, 1310–1323.

Lawrence, C. J. *et al.* (2004). A standardized kinesin nomenclature. J. Cell Biol. *167*, 19–22.

Lee, J., Shin, H., Choi, J., Ko, J., Kim, S., Lee, H., Kim, K., Rho, S., Lee, J., Song, H., Eom, S., and Kim, E. (2004). An intramolecular interaction between the FHA domain and a coiled coil negatively regulates the kinesin motor KIF1A. EMBO J. *23*, 1506–1515.

Meluh, P. B., and Rose, M. D. (1990). KAR3, a kinesin-related gene required for yeast nuclear fusion. Cell *60*, 1029–1041.

Mialhe, A. *et al.* (2001). Tubulin detyrosination is a frequent occurrence in breast cancers of poor prognosis. Cancer Res. *61*, 5024–5027.

Nakata, T., and Hirokawa, N. (1995). Point mutation of adenosine triphosphate-binding motif generated rigor kinesin that selectively blocks anterograde lysosome membrane transport. J. Cell Biol. *131*, 1039–1053.

Nayak, T., Szewczyk, E., Oakley, C. E., Osmani, A., Ukil, L., Murray, S. L., Hynes, M. J., Osmani, S. A., and Oakley, B. R. (2006). A versatile and efficient gene targeting system for *Aspergillus nidulans*. Genetics *172*, 1557–1566.

Okada, Y., and Hirokawa, N. (1999). A processive single-headed motor: kinesin superfamily protein KIF1A. Science *283*, 1152–1157.

Okada, Y., and Hirokawa, N. (2000). Mechanism of the single-headed processivity: diffusional anchoring between the K-loop of kinesin and the C terminus of tubulin. Proc. Natl. Acad. Sci. USA *97*, 640–645.

Okada, Y., Yamazaki, H., Sekine-Aizawa, Y., and Hirokawa, N. (1995). The neuron-specific kinesin superfamily protein KIF1A is a unique monomeric motor for anterograde axonal transport of synaptic vesicle precursors. Cell *81*, 769–780.

Otsuka, A. J., Jeyaprakash, A., García-Añoveros, J., Tang, L. Z., Fisk, G., Hartshorne, T., Franco, R., and Born, T. (1991). The *C. elegans* unc-104 gene encodes a putative kinesin heavy chain-like protein. Neuron *6*, 113–122.

Pollock, N., deHostos, E. L., Turck, C. W., and Vale, R. D. (1999). Reconstitution of membrane transport powered by a novel dimeric kinesin motor of the Unc104/KIF1A family purified from *Dictyostelium*. J. Cell Biol. *147*, 493–506.

Reed, N. A., Dawen, C., Blasius, T. L., Jih, G. T., Meyhofer, E., Gaertig, J., and Verhey, K. J. (2006). Microtubule acetylation promotes kinesin-1 binding and transport. Curr. Biol. *16*, 2166–2172.

Requena, N., Alberti-Segui, C., Winzenburg, E., Horn, C., Schliwa, M., Philippsen, P., Liese, R., and Fischer, R. (2001). Genetic evidence for a microtubule-destabilizing effect of conventional kinesin and analysis of its consequences for the control of nuclear distribution in *Aspergillus nidulans*. Mol. Microbiol. *42*, 121–132.

Riquelme, M., Fischer, R., and Bartnicki-Garcia, S. (2003). Apical growth and mitosis are independent processes in *Aspergillus nidulans*. Protoplasma *222*, 211–215.

Rischitor, P., Konzack, S., and Fischer, R. (2004). The Kip3-like kinesin KipB moves along microtubules and determines spindle position during synchronized mitoses in *Aspergillus nidulans* hyphae. Eukaryot. Cell *3*, 632–645.

Rivera, S. B., Koch, S. J., Bauer, J. M., Edwards, J. M., and Bachand, G. D. (2007). Temperature dependent properties of a kinesin-3 motor protein from *Thermomyces lanuginosus*. Fungal Genet. Biol. *44*, 1170–1179.

Sambrook, J., and Russel, D. W. (1999). Molecular Cloning: A Laboratory Manual, Cold Spring Harbor, New York: Cold Spring Harbor Laboratory Press.

Schliwa, M., and Woehlke, G. (2003). Molecular motors. Nature *422*, 759–765.

Schoch, C. L., Aist, J. R., Yoder, O. C., and Turgeon, B. G. (2003). A complete inventory of fungal kinesins in representative filamentous ascomycetes. Fungal Genet. Biol. *39*, 1–15.

Schuchardt, I., Aßmann, D., Thines, E., Schuberth, C., and Steinberg, G. (2005). Myosin-V, kinesin-1, and kinesin-3 cooperate in hyphal growth of the fungus *Ustilago maydis*. Mol. Biol. Cell *16*, 5191–5201.

Schulze, E., Asai, D. J., Bulinski, J. C., and Kirschner, M. (1987). Posttranslational modification and microtubule stability. J. Cell Biol. *105*, 2167–2177.

Seiler, S., Nargang, F. E., Steinberg, G., and Schliwa, M. (1997). Kinesin is essential for cell morphogenesis and polarized secretion in *Neurospora crassa*. EMBO J. *16*, 3025–3034.

Song, Y.-H., Marx, A., Müller, J., Woehlke, G., Schliwa, M., Krebs, A., Hoenger, A., and Mandelkow, E. (2001). Structure of a fast kinesin: implications for ATPase mechanism and interactions with microtubules. EMBO J. *20*, 6213–6225.

Steinberg, G. (2007). On the move: endosomes in fungal growth and pathogenicity. Nat. Rev. Microbiol. *5*, 309–316.

Stringer, M. A., Dean, R. A., Sewall, T. C., and Timberlake, W. E. (1991). *Rodletless*, a new *Aspergillus* developmental mutant induced by directed gene inactivation. Genes Dev. *5*, 1161–1171.

Suelmann, R., and Fischer, R. (2000). Mitochondrial movement and morphology depend on an intact actin cytoskeleton in *Aspergillus nidulans*. Cell Motil. Cytoskeleton *45*, 42–50.

Taheri-Talesh, N., Horio, T., Araujo-Bazan, L., Dou, X., Espeso, E. A., Penalva, M. A., Osmani, A., and Oakley, B. R. (2008). The tip growth apparatus of *Aspergillus nidulans*. Mol. Biol. Cell (*in press*).

Takeshita, N., Higashitsuji, Y., Konzack, S., and Fischer, R. (2008). Apical sterol-rich membranes are essential for localizing cell end markers that determine growth directionality in the filamentous fungus *Aspergillus nidulans*. Mol. Biol. Cell *19*, 339–351.

Toews, M. W., Warmbold, J., Konzack, S., Rischitor, P. E., Veith, D., Vienken, K., Vinuesa, C., Wei, H., and Fischer, R. (2004). Establishment of mRFP1 as fluorescent marker in *Aspergillus nidulans* and construction of expression vectors for high-throughput protein tagging using recombination in *Escherichia coli* (GATEWAY). Curr. Genet. *45*, 383–389.

Upadhyay, S., and Shaw, B. D. (2008). The role of actin, fimbrin and endocytosis in growth of hyphae in *Aspergillus nidulans*. Mol. Microbiol. *68*, 690–705.

Veith, D., Scherr, N., Efimov, V. P., and Fischer, R. (2005). Role of the spindle-pole body protein ApsB and the cortex protein ApsA in microtubule organization and nuclear migration in *Aspergillus nidulans*. J. Cell Sci. *118*, 3705–3716.

Waring, R. B., May, G. S., and Morris, N. R. (1989). Characterization of an inducible expression system in *Aspergillus nidulans* using *alcA* and tubulin coding genes. Gene *79*, 119–130.

Wedlich-Söldner, R., Straube, A., Friedrich, M. W., and Steinberg, G. (2002). A balance of KIF1A-like kinesin and dynein organizes early endosomes in the fungus *Ustilago maydis*. EMBO J. *21*, 2946–2957.

Westerholm-Parvinen, A., Vernos, I., and Serrano, L. (2000). Kinesin subfamily UNC104 contains a FHA domain: boundaries and physicochemical characterization. FEBS Lett. *486*, 285–290.

Westermann, S., and Weber, K. (2003). Post-translational modifications regulate microtubule function. Nat. Rev. Mol. Cell Biol. *4*, 938–947.

Wickstead, B., and Gull, K. (2006). A "Holistic" kinesin phylogeny reveals new kinesin families and predicts protein functions. Mol. Biol. Cell *17*, 1734–1743.

Xiang, X., Roghi, C., and Morris, N. R. (1995). Characterization and localization of the cytoplasmic dynein heavy chain in *Aspergillus nidulans*. Proc. Natl. Acad. Sci. USA *92*, 9890–9894.

Yelton, M. M., Hamer, J. E., and Timberlake, W. E. (1984). Transformation of *Aspergillus nidulans* by using a *trpC* plasmid. Proc. Natl. Acad. Sci. USA *81*, 1470–1474.

Zhang, J., Li, S., Fischer, R., and Xiang, X. (2003). The accumulation of cytoplasmic dynein and dynactin at microtubule plus-ends is kinesin dependent in *Aspergillus nidulans*. Mol. Biol. Cell *14*, 1479–1488.

Sterols Are Mainly in the Cytoplasmic Leaflet of the Plasma Membrane and the Endocytic Recycling Compartment in CHO Cells

Mousumi Mondal, Bruno Mesmin, Sushmita Mukherjee, and Frederick R. Maxfield

Transbilayer asymmetry is a general feature of most lipids in the plasma membrane and other post–endoplasmic reticulum organelles. This asymmetry has important consequences for membrane physical properties and cell signaling. Although cholesterol is a major lipid in these membranes, its transbilayer distribution is not well understood. Using fluorescent sterols (dehydroergosterol and cholestatrienol) and a variety of fluorescence quenchers, the authors determined that the majority of sterol is in the cytoplasmic leaflet of the plasma membrane and endocytic recycling compartment of CHO cells. Quenchers that are restricted to the exofacial leaflet of the plasma membrane reduce the fluorescence intensity by about 20%–30%, whereas microinjection of quenchers into the cytosol quenched the fluorescent sterols associated with the plasma membrane and endocytic recycling compartment by about 60%. The presence of high amounts of cholesterol in the cytoplasmic leaflet might have important implications for intracellular cholesterol transport and for membrane domain formation.
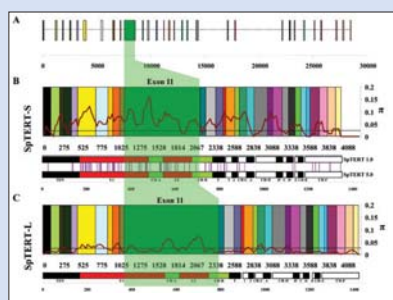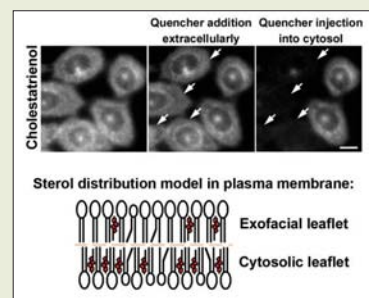
Genetic Hypervariability in Two Distinct Deuterostome Telomerase Reverse Transcriptase Genes and Their Early Embryonic Functions

Trystan B. Wells, Guanglei Zhang, Zenon Harley, and Homayoun Vaziri

Within a species of complex animals, genes for functional proteins are rarely variant. This constancy is thought to be required for the function of essential proteins. One such crucial protein is telomerase reverse transcriptase catalytic subunit (TERT). To study the function of TERT during early development, the authors cloned *SpTERT* from purple sea urchin embryos. Unexpectedly, they discovered two distinct telomerase genes named *SpTERT-S* and *SpTERT-L.* By cloning SpTERT from several individuals, they further discovered regions, especially exon 11 of *SpTERT-S,* with intraspecific germline hypervariability. Although the variant enzymes remained catalytically active, there were significant amino acid variations in multiple regions, including those involved in binding of TERT to its RNA component. The authors also uncovered a noncanonical essential function for telomerase that is required for embryo polarity at the mesenchymal blastula stage. These results suggest the presence of an active diversity-generation mechanism that has neofunctionalized telomerase throughout evolution.

The *Aspergillus nidulans* Kinesin-3 UNCa Motor Moves Vesicles along a Subpopulation of Microtubules

Nadine Zekert and Reinhard Fischer

The microtubule cytoskeleton is not as rigid and uniform as the name implies, but is characterized by its dynamic instability. In addition, microtubules can be made up of different tubulin isoforms and—to make a eukaryotic cell even more complex—of different posttranslationally modified tubulins. Microtubule modifications, such as acetylation or polyglutamylation, are evolutionarily old "inventions" and occur in primitive eukaryotes such as *Giardia lamblia,* whereas detyrosination appeared later during evolution. Although many modifications were discovered more than 20 years ago, their cellular functions are not well understood. Here, the authors show that in the filamentous fungus *Aspergillus nidulans* at least two different microtubule populations exist. This discovery came from studies of an unc-104–related motor protein that preferentially moves along detyrosinated microtubules and transports vesicles. These microtubules are more stable than the tyrosinated ones and even remain intact during mitosis when other cytoplasmic microtubules are degraded.
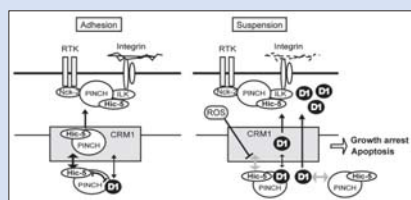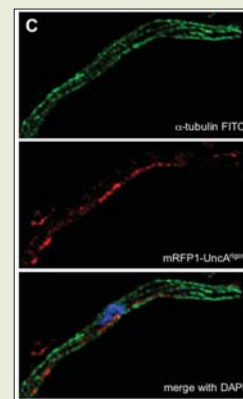
Competitive Nuclear Export of Cyclin D1 and Hic-5 Regulates Anchorage Dependence of Cell Growth and Survival

Kazunori Mori, Etsuko Hirao, Yosuke Toya, Yukiko Oshima, Fumihiro Ishikawa, Kiyoshi Nose, and Motoko Shibanuma

Anchorage dependence of cell growth is a critical trait that distinguishes nontransformed from transformed cells. The authors report a novel mechanism whereby anchorage-independent cell growth and survival is prevented. Cyclin D1 is a proto-oncogene that exhibits cell cycle– dependent nuclear localization. Its nuclear export is dependent on CRM1. The authors report that the nuclear localization of cyclin D1 is adhesion-dependent and regulated by the focal adhesion protein Hic-5 and its binding partner PINCH, which also cycle in and out of the nucleus. Hic-5 binds to CRM1 with high affinity and is a competitive inhibitor of CRM1-dependent cyclin D1 export in adherent cells. PINCH interacts with both cyclin D1 and Hic-5 and enhances the Hic-5–dependent inhibition of cyclin D1 export. Under nonadherent conditions, the cellular level of reactive oxygen species increases and inhibits the nuclear export of Hic-5, resulting in the nuclear export of cyclin D1. Consequently cells undergo growth arrest and apoptosis. *Ras* overexpression led to the anchorage-independent nuclear localization of cyclin D, revealing an interesting interdependence of the oncogenic potential of two oncogenes. ■

Interaction of the *Aspergillus nidulans* Microtubule-Organizing Center (MTOC) Component ApsB with Gamma-Tubulin and Evidence for a Role of a Subclass of Peroxisomes in the Formation of Septal MTOCs[▽]

Nadine Zekert,‡ Daniel Veith,†‡ and Reinhard Fischer*

Karlsruhe Institute of Technology, Institute for Applied Biosciences, Department of Microbiology, Hertzstrasse 16, D-76187 Karlsruhe, Germany

Peroxisomes are a diverse class of organelles involved in different physiological processes in eukaryotic cells. Although proteins imported into peroxisomes carry a peroxisomal targeting sequence at the C terminus (PTS1) or an alternative one close to the N terminus (PTS2), the protein content of peroxisomes varies drastically. Here we suggest a new class of peroxisomes involved in microtubule (MT) formation. Eukaryotic cells assemble MTs from distinct points in the cell. In the fungus *Aspergillus nidulans*, septum-associated microtubule-organizing centers (sMTOCs) are very active in addition to the spindle pole bodies (SPBs). Previously, we identified a novel MTOC-associated protein, ApsB (*Schizosaccharomyces pombe* mto1), whose absence affected MT formation from sMTOCs more than from SPBs, suggesting that the two protein complexes are organized differently. We show here that sMTOCs share at least two further components, gamma-tubulin and GcpC (*S. pombe* Alp6) with SPBs and found that ApsB interacts with gamma-tubulin. In addition, we discovered that ApsB interacts with the Woronin body protein HexA and is targeted to a subclass of peroxisomes via a PTS2 peroxisomal targeting sequence. The PTS2 motif was necessary for function but could be replaced with a PTS1 motif at the C terminus of ApsB. These results suggest a novel function for a subclass of peroxisomes in cytoskeletal organization.

Peroxisomes are ubiquitous organelles of eukaryotes which are surrounded by a single membrane (9, 30). They serve a variety of functions, depending on the species, the cell type, and the environmental or developmental conditions. In mammals, peroxisomes are involved in a number of catabolic and anabolic pathways, most importantly, peroxide metabolism, the β-oxidation of long-chain fatty acids, and the biosynthesis of ether phospholipids (17, 37). The vital importance of the organelle in humans is shown by the existence of a number of severe and often lethal disorders that occur when the biogenesis of the organelle is impaired (36). In plants, peroxisomes are involved in photorespiration and typically contain the glyoxylate cycle, as in protozoa and yeast (8).

Given the complexity of peroxisomal functions, it is obvious that a large number of proteins need to be targeted to these organelles. Peroxisomal membrane and matrix proteins are synthesized on free ribosomes in the cytosol and are imported posttranslationally into preexisting organelles (9). The apparatus of protein import is clearly distinct from the import machinery of other organelles because it translocates folded and even oligomeric proteins and there is evidence that they are descending from the endoplasmic reticulum (6). A large number of peroxisomal proteins employ a tripeptide sequence at the C terminus, PTS1 (S/A/C-K/R/H-L/M) (7). A second class of proteins uses a sequence close to the N terminus which is less conserved, consists of R/K-L/I/V-X$_5$-H/Q-L/A, and is called PTS2 (33). In both cases, complex protein machineries are employed and some of the components appear to be used in PTS1- and PTS2-dependent protein translocation (9).

A very distinct class of peroxisomes is represented by the fungal Woronin body. This structure is named after a Russian mycologist who reported the characteristics of a distinct type of organelle in the fungus *Ascobolus pulcherrimus* (1, 39). Woronin bodies have been described in more than 50 species of ascomycota and deuteromycota but are missing in single-cell yeasts such as *Saccharomyces cerevisiae* and *Schizosaccharomyces pombe*. Thus, their function appears to be important for the filamentous life style. In *Neurospora crassa*, they appear as hexagonal bodies in the cell and upon cell damage plug the septal pores after a few seconds (15). This sealing mechanism is very important in syncytial organisms to prevent loss of the entire cytoplasm and hence death of the entire mycelium after one hypha is damaged (20). Their exact composition, however, remained obscure for many decades until G. Jedd and N.-H. Chua purified the organelle from *N. crassa* and identified the main constituent as a single protein named Hex1 (15, 42), because it forms hexagonal crystals. The existence of a PTS1 peroxisomal targeting sequence at the C terminus of the protein indicated that the Woronin bodies represent specialized peroxisomes. Hex1 displays some sequence similarity to eIF5, and it is thought that Hex1 derived from eIF5 during evolution

* Corresponding author. Mailing address: Karlsruhe Institute of Technology, Institute for Applied Biosciences, Department of Microbiology, Hertzstrasse 16, D-76187 Karlsruhe, Germany. Phone: 49-721-608-4630. Fax: 49-721-608-4509. E-mail: reinhard.fischer@KIT.edu.
† Present address: Technologie-Lizenz-Büro (TLB) der Baden-Württembergischen Hochschulen GmbH, Ettlinger Str. 25, D-76137 Karlsruhe, Germany.
‡ Equal contribution.

by gene duplication and subsequent modification of its function (42). Another example of a peroxisome-associated function may be the Pro40 protein in *Sordaria macrospora* (5). This protein is implicated in the regulation of sexual development.

In addition to the Woronin body close to the septal pore (22), we had evidence in *Aspergillus nidulans* that microtubule (MT) polymerization is initiated at septa. Using an MT plus-end-associated protein, the kinesin motor KipA (kinesin-7), we showed that the cytoplasmic area close to septa acts as an active MT-organizing center (MTOC) (16). Furthermore, we identified a novel MTOC-associated protein, ApsB, and localized it to the spindle pole bodies (SPBs) and to septa (35). The presence of septal MTOCs is similar to that in *S. pombe*, but there is no evidence for such organelles in the *S. cerevisiae*-related filamentous fungus *Ashbya gossypii* (18, 19). Given that MTOCs are generally composed of a large protein complex with gamma-tubulin as one characteristic member, we anticipate that MT polymerization at septa also requires a protein complex (40). Here we show for the first time the presence of gamma-tubulin at septal MTOCs (sMTOCs) and that it physically interacts with ApsB. Surprisingly, ApsB is associated with a subclass of peroxisomes in the cytoplasm, and we propose that they are involved in septal MTOC formation.

MATERIALS AND METHODS

Strains, plasmids, and culture conditions. The preparation of the supplemented minimal and complete media used for *A. nidulans* and the standard strain construction procedures used are described in reference 11. To isolate total DNA and RNA, corresponding strains were grown in liquid culture for 16 h. Mycelium was harvested and immediately processed for total DNA (see below). A list of the *A. nidulans* strains used in this study is given in Table 1. Standard laboratory *Escherichia coli* strains (XL-1 blue and Top10) were used. The plasmids used are listed in Table 2.

Light and fluorescence microscopy. For live-cell imaging, cells were grown in glass-bottom dishes (FD35-100; World Precision Instruments, Berlin, Germany) in 2 ml of minimal medium (MM) containing either 2% glycerol or 2% glucose as a carbon source. Medium was supplemented with pyridoxine, *p*-aminobenzoic acid, biotin, arginine, uracil, or uridine, depending on the auxotrophy of the strains. Cells were incubated at room temperature for 1 to 2 days, and images were captured using an Axiophot microscope (Zeiss, Jena, Germany), a Plan-apochromatic 63× or 100× oil immersion objective lens, and an HBO50 Hg lamp. Alternatively, a Zeiss AxioImager Z1 with AxioVision software (V4.5) was used. Fluorescence was observed using standard Zeiss filter combinations no. 09 (fluorescein isothiocyanate, green fluorescent protein [GFP]) and no. 15 (monomeric red fluorescent protein 1 [mRFP1], DsRed). Laser images were obtained using the Zeiss Cell Observer SD, which combines the high-end Cell Observer microscopy platform and the CSU-X1 spinning-disc technology from Yokogawa for high-speed confocal microscopy. Images were collected and analyzed with a Hamamatsu Orca ER II camera system and the Wasabi software (version 1.2) or a Zeiss Axiocam and AxioVision software. Image and video processing was done with the Wasabi software from Hamamatsu, Adobe Photoshop, ImageJ (NIH, Bethesda, MD), and virtual dub (http://www.virtualdub.org).

Molecular techniques. Standard DNA transformation procedures were used for *A. nidulans* (41) and *E. coli* (27). For PCR experiments, standard protocols were applied using a Biometra Personal Cycler (Biometra, Göttingen, Germany) for the reaction cycles. DNA sequencing was done commercially (MWG Biotech, Ebersberg, Germany). Total DNA was extracted from *A. nidulans* in the following way. Spores were inoculated into liquid MM plus supplements and grown for 12 to 18 h at 30°C without shaking. Hyphal mats were harvested, dried with tissue paper, and ground in liquid nitrogen. The resulting powder was mixed with extraction buffer (50 mM EDTA, 0.2% sodium dodecyl sulfate [SDS]) and incubated for 30 min to 2 h at 68°C in a water bath. SDS and proteins were removed from the suspension by addition of potassium-acetate solution (8 M, pH 4.2) and centrifugation. Total DNA was precipitated from the supernatant with isopropanol, and the pellet was washed twice with 70% ethanol, air dried, resuspended in TE buffer with RNase A, and stored at 4°C. Southern hybridizations were performed according to the DIG Application Manual for Filter Hybridization (Roche Applied Science, Technical Resources, Roche Diagnostics GmbH, Mannheim, Germany).

Bimolecular fluorescence complementation assay (BiFC). The enhanced yellow fluorescent protein (eYFP)-tagged N-terminal half (YFP^N) was amplified using primers 5′-C*GGTACC*ATGGTGAGCAAGGGCGAGGAGCTG-3′ (fwd_Kpn_YFP-N) and 5′-C*GGCGCGCC*CGTGGCGATGGAGCGCATGATATAGACGTTGTGGCTGTTGTAG-3′. For the C-terminally eYFP-tagged (YFP^C) half, primers 5′-C*GGTACC*ATGGCCGACAAGCAGAAGAACGGCATCAAGG-3′ (fwd_Kpn_YFP-C) and 5′-C*GGCGCGCC*GTGGTTCATGACCTTCTGTTTCAGGTCGTTCGGGATCTTGCAGGCCGGGCGCTTGTACAGCTCGTCCATGCCGAGAGTGATCCC-3′ (rev_YFP-C_Li_Asc) were used. These primers introduced KpnI and AscI restriction sites (in italics) in addition to the protein linker sequences RSIAT (YFP^N) and RPACKIPNDLKQKVMNH (YFP^C) (underlined). eYFP was split at bp 460 to 462 by using the ATG codon as the start of the YFP^C half. PCR fragments were subcloned into pCR2.1-Topo (Invitrogen, Karlsruhe, Germany), subsequently released with KpnI and AscI, and used to replace GFP2-5 of pMCB17apx-apsB (35), giving pDV7 (YFP^N) and pDV8 (YFP^C). Full-length *apsB*$^{3.2}$ (3.2 kb) was taken from pDV21a and cloned into pDV7, giving pDV22b [*alcA(p)::YFP^N::apsB$^{3.2}$*], and full-length γ*tubulin*$^{1.8}$ was amplified using primers 5′-C*GGCGCGCC*CGGGATGCCTAGGTATACCCTC-3′ (Gamma_tub_Asc_fwd) and 5′-C*TTAATTAA*TTATACTCCAACTTCATCCTTTCC-3′ (Gamma_tub_Pac_rev) (the AscI and PacI restriction sites are in italics, and the start and stop codons are underlined) and cloned into pDV8, giving pDV50 [*alcA(p)::YFP^C::γtubulin$^{1.8}$*]. For BiFC analysis, pDV22 and pDV50 were combined and transformed into GR5, giving SNZ11. The cloned gene length is indicated as exponents; e.g., the length of the cloned gene *apsB*$^{3.2}$ is 3.2 kb. Similarly, *hexA* was amplified using primers 5′-C*GGCGCGCC*CGGGATGGGGTTACTACGACGACG-3′ (hexA_Asc_fwd) and 5′-C*TTAATTAA*TTATAGACGGGAAGAGTGGATGATC-3′ (hexA_Pac_rev1; 680 bp to stop codon) or 5′-G*TTAATTAA*CCTCAATCAAGTGCAAGGTTTCG-3′ [hexA_Pac_rev2; 1 kb, including the poly(A) site] and cloned into pDV8, giving pDV17 [*alcA(p)::YFP^C::hexA^{680}*], and into pDV7, giving pDV19a [*alcA(p)::YFP^N::hexA$^{1.0}$*]. For BiFC analysis, pDV17 and pDV22b were combined and transformed into GR5, giving SDV42, or pDV19a and pDV23a were combined, giving SDV43.

Protein extracts, immunoprecipitation, and Western blotting. To prepare protein extracts, *A. nidulans* strains SNZ-SI 42 [*alcA(p)::3×HA::apsB$^{3.2}$*], SNZ16 [*alcA(p)::GFP::γtubulin$^{1.8}$*], and SNZ37 [*alcA(p)::apsB$^{3.2}$::3×HA alcA(p)::GFP::γtubulin$^{1.8}$*] were incubated in liquid MM for 24 h at 37°C. The medium was supplemented with 0.2% glucose and 2% threonine to induce the *alcA* promoter. The mycelium was harvested by filtration through Miracloth (Calbiochem, Heidelberg, Germany), dried between paper towels, and immediately ground in liquid nitrogen. Afterwards, the mycelial powder was resuspended in protein extraction buffer (20 mM Tris-HCl, pH 8, 150 mM NaCl, 0.01% Triton X-100) containing protease inhibitor (2 mM phenylmethylsulfonyl fluoride [PMSF]) and vortexed for 5 min at 4°C. Cell debris was pelleted by two centrifugations (Eppendorf centrifuge 5403; Eppendorf, Hamburg, Germany) at 13,000 rpm at 4°C for 10 min. A volume of 1 ml protein extract was adjusted to 300 mM NaCl and incubated with monoclonal antibody HA.11 (dilution, 1:200; clone 16B12; Hiss Diagnostics, Freiburg, Germany). After 1 h of incubation at 4°C, 50 μl protein-G-agarose (Roche, Mannheim, Germany) was added and the mixture was incubated for an additional 3 h. Agarose beads were pelleted by centrifugation in an Eppendorf centrifuge at 15,000 rpm at 4°C for 30 s and washed three times with 1 ml extraction buffer containing protease inhibitor (2 mM PMSF) with different NaCl molarities (150 mM NaCl, 500 mM NaCl, and no NaCl). After the denaturation of the samples, protein extracts and coimmunoprecipitated pellets were loaded onto an 8% SDS-polyacrylamide gel. For Western blotting, a polyclonal antibody raised against GFP (product G1544; dilution, 1:4,000; Sigma-Aldrich, Munich, Germany) with anti-rabbit IgG peroxidase conjugate secondary antibody (product A0545; dilution, 1:4,000; Sigma-Aldrich, Munich, Germany) in the case of gamma-tubulin and the anti-HA antibody (clone 16B12; dilution, 1:1,000) with anti-mouse IgG peroxidase conjugate secondary antibody (product A2304; dilution, 1:10,000; Sigma-Aldrich, Munich, Germany) in the case of ApsB were used. Nitrocellulose membranes used for blotting were from Schleicher & Schuell (Dassel, Germany).

Yeast two-hybrid screen. A full-length cDNA fragment of *apsB* was amplified with primers 5′-G*GGATCC*GA ATGACTCTAAAAGAGC-3′ and 5′-G*TCGAC*TCAAACTTCGATATCAAC-3′ and cloned into the BamHI-SalI restriction sites of pGBT9 (Clontech), giving pRS89, and into pGAD424 (Clontech), giving pRS88. A cDNA fragment from a cDNA library containing the full-length *hexA* gene was cloned into of the yeast GAL4-Matchmaker system (Clontech), giving pRS91. Transformation of yeast strains, selection for diploids, a histidine growth assay, and a β-galactosidase (β-Gal) assay were done as described in reference 2.

TABLE 1. *A. nidulans*, *E. coli*, and *S. cerevisiae* strains used in this study

Strain	Genotype	Source
AJC1.5	*biA1 apsB6*	J. Clutterbuck (1969)
AJC1.7	*biA1 apsB10*	J. Clutterbuck (1969)
FGSC89	*biA1 argB2*	FGSC
GJA28	*biA1 ΔhexA::argB* (FGSC89 transformed with *ΔhexA::argB* deletion cassette)	G. Jedd, Singapore
GR5	*pyrG89 wA3 pyroA4*	38
MH11269	*biA1 niiA4 pyroA4 pexC::bar*	12
SDV38	*alcA(p)::GFP::hexA^{680} wA3 pyroA4* (GR5 transformed with pDV15)	This work
SDV42	*alcA(p)::YFP^N::apsB$^{3.2}$ alcA(p)::YFP^C::hexA^{680} wA3 pyroA4* (GR5 transformed with pDV17 and pDV22b)	This work
SDV43	*alcA(p)::YFP^N::hexA$^{1.0}$ alcA(p)::YFP^C::apsB$^{3.2}$ wA3 pyroA4* (GR5 transformed with pDV19a and pDV23a)	This work
SDV49-4	*alcA(p)::mRFP1::apsB$^{1.5}$ alcA(p)::GFP::hexA^{680} pyroA4 ΔnkuA::argB* (TN02A3 transformed with pDV15 and pDM8a)	This work
SDV70b	*yA1 pyroA4 riboB2 areA102 gpd(p)::GFP::acuE alcA(p)::mRFP1::apsB* (TALX207-10 transformed with pDV42a)	This work
SDV73	*alcA(p)::GFP::apsB$^{1.5}$ alcA(p)::mRFP1::hexA^{680} pyroA4 ΔnkuA::argB* [TN02A3 transformed with pDV39 and pMCB17apx(-apsB)]	This work
SDV77	*alcA(p)::GFP::apsB-PTS2.1 pyroA4 ΔnkuA::argB* (TN02A3 transformed with pDV43)	This work
SDV78c	*alcA(p)::mRFP1::hexA^{680} gpd(p)::GFP::acuE yA1 riboB2 areA102* (TALX207-10 transformed with pDV39 and pTN1)	This work
SDV79	*ΔhexA alcA(p)::GFP::apsB_PTS2^{mut}* (GJA28 crossed with SDV77a)	This work
SDV80	*apsB6 alcA(p)::GFP::apsB_PTS2^{mut}* (AJC1.5 crossed with SDV77)	This work
SDV88	*apsB6 alcA(p)::GFP::apsB$^{T.5}$* (AJC1.5 crossed with SEa3)	This work
SDV95	*ΔhexA ΔapsB alcA(p)::GFP::apsB_PTS2^{mut}* (SDV82 crossed with SRS25)	This work
SDV98	*apsB10 alcA(p)::GFP::tubA* (AJC1.7 crossed with SJW02)	This work
SDV103	*apsB10 alcA(p)::GFP::tubA alcA(p)::GFP::apsB_PTS2^{mut}* (SDV98 transformed with pDV43a)	This work
SEa3	*alcA(p)::GFP::apsB wA3 pyroA4*	35
SJW02	*alcA(p)::GFP::tubA ΔargB::trpCΔB wA3 pyroA4*	35
SNZ11	*alcA(p)::YFP^N::apsB$^{3.2}$ alcA(p)::YFP^C::γtubulin$^{1.8}$ wA3 pyroA4* (GR5 transformed with pDV22 and pDV50)	This work
SNZ16	*alcA(p)::GFP::γtubulin$^{1.8}$ pyroA4* (TN02A3 transformed with pNZ17)	This work
SNZ22	*alcA(p)::GFP::γtubulin$^{1.8}$ gpd(p)::DsRed::stuA(NLS)* (SNZ16 transformed with pJH19 and pTN1)	This work
SNZ34	*apsB10 alcA(p)::GFP::apsB_PTS2^{mut}_SRL* (AJC1.7 transformed with pNZ16)	This work
SNZ37	*alcA(p)::GFP::γtubulin apsB::3×HA* (SNZ16 transformed with pNZS23 and pTN1)	This work
SNZ59	*apsB(p)::GFP::apsB pyroA4* (TN02A3 transformed with pNZ-SI37)	This work
SNZ61	*γtubulin(p)::GFP::γtubulin pyroA4* (TN02A3 transformed with pNZ-SI36)	This work
SNZ94	*pabaA1 biA1 alcA(p)::GFP::apsB_PTS2^{mut}_SRL gpd(p)::GFP::stuA(NLS) ΔapsB::argB trpC801* (SRS24 transformed with pNZ16)	This work
SNZ-SH80	*alpB(p)::alpB::GFP pyroA4 ΔnkuA::argB* (SO451 transformed with *alpB::GFP::pyrG::RB-alpB* fusion PCR)	This work
SNZ-SI 42	*alcA(p)::3×HA::apsB pyroA4* (TN02A3 transformed with pSI-N4)	This work
SO451	*pyrG89 wA3 pyroA4 ΔnkuA::argB*	FGSC
SRS24	*gpd(p)::GFP::stuA(NLS) pabaA1 ΔapsB::argB trpC801*	31
TALX207-10	*yA1 pyroA4 areA102* transformed with *gpd(p)::GFP::acuE* and *riboB+* plasmid	M. Hynes and A. Andrianopoulos, Melbourne, Australia
TNO2A3	*pyrG89 pyroA4 ΔnkuA::argB*	S. Osmani
PJ69-4A	*MAT**a** trp1-901 leu2-3 ura3-52 his3-200 gal4Δ gal80Δ GAL2-ADE-LYS::GAL1-HIS3 met2::GAL7-lacZ*	2
AH109	*MAT**a** trp1-901 leu2-3,112 ura3-52 his3-200 gal4Δ gal80Δ LYS2::GAL1UAS-GAL1TATA-HIS3 GAL2UAS-GAL2TATA-ADE2 URA3::MEL1UAS-MEL1TATA-lacZ GAL2-ADE-LYS::GAL1-HIS3 met2::GAL7-lacZ*	13
Y187	*MATα ura3-52 his3-200 ade2-101 trp1-901 leu2-3,112 gal4Δ met-gal80Δ URA3::GAL1UAS-GAL1TATA-lacZ*	P. Uetz, Karlsruhe, Germany

^{a} FGSC, Fungal Genetics Stock Center.

The yeast strains used for transformation were AH109, Y187, and PJ69-4A (Clontech).

Site-directed mutagenesis. The peroxisomal target sequence of *apsB* was mutated using pDV21a as the template and the QuikChange XL site-directed mutagenesis kit from Stratagene. The last two amino acids were mutated using primer 5′-GCGATTTGGAGAAGCT̲ACG̲TAAGACCAGCAGTCAGATAA GGAG-3′ and the corresponding antiparallel primer, giving pDV43. Successful mutagenesis was confirmed by commercial sequencing (MWG Biotech, Ebersberg, Germany).

GFP or mRFP1 tagging of proteins. pMCB17apx was used as the basic vector for the tagging of *apsB* or *hexA* with GFP, and pDM8 was used for tagging with mRFP1 (see reference 35). Full-length *hexA* was amplified from genomic DNA using primers 5′-*CGGCGCGCCC*GGG̲ATG̲GGTTACTACGACGACG-3′ and 5′-*CTTAATTAA*TT̲A̲TAGACGGGAAGAGTGGGATGATC-3′.

To obtain *in vivo* protein expression levels, we expressed the proteins under the control of the corresponding natural promoters. The *apsB* promoter (1.33 kb) was amplified from genomic DNA using primers 5′-*GCCTAGG*CAAGC CGCAACTCCC-3′ (apsB_nat(p)_AvrII_fwd) and 5′-*CGGTACC*GGATCTG

TABLE 2. Plasmids used in this study

Plasmid	Construction	Source
pCR2.1-TOPO	Cloning vector	Invitrogen
pDM8a	GFP replaced with mRFP1 in pMCB17apx-apsB	35
pDV7	$alcA(p)::YFP^N::apsB^{1.5}$ pyr4 GFP of pMCB17apx-apsB replaced with YFP^N	This work
pDV8	$alcA(p)::YFP^C::apsB^{1.5}$ pyr4 GFP of pMCB17apx-apsB replaced with YFP^C	This work
pDV15	$alcA(p)::GFP::hexA^{680}$ pyr4 pMCB17apx with full-length hexA	This work
pDV17	$alcA(p)::YFP^C::hexA^{680}$ pyr4 apsB of pDV8 replaced with $hexA^{680}$	This work
pDV19	$alcA(p)::YFP^N::hexA^{1.0}$ pyr4 apsB of pDV7 replaced with full-length $hexA^{1.0}$	This work
pDV21a	pMCB17-apx containing full-length apsB of 3.2 kb between AscI and PacI restriction sites; $alcA(p)::GFP::apsB^{3.2}$ pyr4	This work; 35
pDV22b	$alcA(p)::YFP^N::apsB^{3.2}$ pyr4 apsB of pDV7 replaced with full-length $apsB^{3.2}$	This work
pDV23	$alcA(p)::YFP^C::apsB^{3.2}$ pyr4 apsB of pDV8 replaced with full-length $apsB^{3.2}$	This work
pDV39	$alcA(p)::mRFP1::hexA^{680}$ pyr4 apsB of pDM8a changed with $hexA^{680}$	35
pDV42a	$alcA(p)::mRFP::apsB^{3.2}$ pyr4 pDM8a with full-length $apsB^{3.2}$	35
pDV43	PTS2 of apsB in pDV21a is mutated $alcA(p)::GFP::apsB\_PTS2^{mut}$ pyr4	This work
pDV50	$alcA(p)::YFP^C::\gamma tubulin^{1.8}$ pyr4 apsB of pDV8 replaced with full-length $\gamma tubulin^{1.8}$	This work
pENTR^{MT}/D-Topo	Cloning vector	Invitrogen
pJH19	$gpd(p)::stuA(NLS)::DsRed$ argB	34
pMCB17apx(-apsB)	pMCB17 version for fusion of GFP to N termini of proteins of interest (with 1.5 kb of apsB)	35; V. P. Efimov
pMT-3 × HA	Gateway destination vector	34
pNZ16	PTS1 (SRL) added before stop codon of $apsB\_PTS2^{mut}$ in pDV43; $alcA(p)::GFP::apsB\_PTS2^{mut}\_SRL$ pyr4	This work
pNZ17	pMCB17-apx containing full-length $\gamma tubulin$ of 1.8 kb between AscI and PacI restriction sites; $alcA(p)::GFP::\gamma tubulin^{1.8}$ pyr4	This work
pNZ21	$apsB^{3.2}$ without stop codon in pENTR^{MT}/D-Topo	
pNZS23	$apsB^{3.2}$ from pNZ21 cloned into pMT-3 × HA $alcA(p)::apsB^{3.2}::3 × HA$ argB	This work
pNZ-SI36	$alcA(p)$ of pNZ17 replaced with 1.16-kb $\gamma tubulin(p)$ EcoRI and BsiwI restriction sites; $\gamma tubulin(p)::GFP::\gamma tubulin^{1.8}$ pyr4	This work
pNZ-SI37	$alcA(p)$ of pDV21 Replaced with 1.33-kb $apsB(p)$ AvrII and KpnI restriction sites; $apsB(p)::GFP::apsB^{3.2}$ pyr4	This work
pRS88	apsB in BamHI-SalI sites of pGAD424	This work
pRS89	apsB in BamHI-SalI sites of pGBT9	This work
pRS91	cDNA clone of hexA in pGAD424	This work
pSI-N4	pSM14 containing full-length apsB of 3.2 kb between AscI and PacI restriction sites; $alcA(p)::3×HA::apsB^{3.2}$ pyr4	This work
pSM14	GFP of pMCB17apx replaced with $3×HA$ between KpnI and AscI restriction sites	25
pTN1	pyroA from A. fumigatus	23

CCACTGCG-3′ (apsB_nat(p)_KpnI_rev) (the AvrII and KpnI restriction sites are in italics), cloned instead of $alcA(p)$ into pDV21, giving pNZ-SI37 [$apsB(p)::GFP::apsB$], and transformed into TN02A3, giving SNZ59. The gamma-tubulin promoter (1.16 kb) was amplified from genomic DNA using primers 5′-GGAATTCCATACCCAGCATAAATTCGG-3′ (Gamma_tub_nat(p)_EcoRI_fwd) and 5′-CCGTACGCTTTCTTGCTTGCCTTAAG-3′ (Gamma_tub_nat(p)_BsiwI_rev) (EcoRI and BsiwI restriction sites are in italics), cloned instead of $alcA(p)$ into pNZ17, giving pNZ-SI36 ($\gamma tubulin(p)::GFP::\gamma tubulin^{1.8}$), and transformed into TN02A3, giving SNZ61. AlpB AN4867 (S. pombe Alp6) was amplified via fusion PCR using primers 5′-GGGAGGACAAATACAAACTCG-3′ (Alp6_mitte_fwd) and 5′-ctccagcgcctgcaccagctccTTGCTCAGTCGAATCCTTC TTTTC-3′ (Alp6_linker_rev) to amplify the C-terminal fragment of AlpB without the stop codon and primers 5′-atcagtgcctcctctcagacagTAGCATACATGCA GTACATTTCTCG-3′ (Alp6_RB_link_fwd) (linkers in lower case letters) and 5′-ACCGTCATGGCAGAAACGAAG-3′ (Alp6_RB_rev) to amplify the right border of AlpB. The two PCR products were fused to a GFP-pyrG PCR cassette (kindly provided by S. Osmani, Ohio State University) to generate a 5.5 fusion PCR product using primers 5′-CCAGTCTCGGAACCTCAATT G-3′ (Alp6_Nprimer_fwd) and 5′-TTATCACCTGCTGGTTCTGAG-3′ (Alp6_Nprimer_rev). The fusion PCR product was transformed into A. nidulans strain SO451, giving SNZ-SH80 [$alpB(p)::alpB::GFP$].

Generation of the $apsB^{3.2}\_PTS2^{mut}\_SRL$ (PTS1) construct. A PTS1 targeting sequence (SRL) was added to the C terminus of ApsB by amplifying the full-length mutated gene $apsB^{3.2}\_PTS2^{mut}$ in pDV43 using primers 5′-TTTG GGCGCGCCCGGCATGACTCTAAAAGAGCAAAGTAGTACG-3′ (apsB_Asc_fwd) and 5′-CCTTAATTAATCAtagacgggaAACTTCGATATC-3′ (SRL_PTS1_PacI_rev) (PTS1 is in lowercase letters). The PCR product was cloned between the AscI and PacI restriction sites in the vector pMCB17apx and confirmed via sequencing, giving plasmid pNZ16, which was transformed into $apsB10$ mutant strain AJC1.7, generating strain SNZ34 [$apsB10$, $alcA(p)::GFP::$

$apsB\_PTS2^{mut}\_SRL$]. Ectopic integration of the construct and the presence of the mutated endogenous apsB locus were confirmed by PCR, Southern blotting, and sequencing of the PCR products. Likewise, transformation of the apsB construct was done with pNZ16 into apsB deletion strain SRS24, generating SNZ94 with the same rescue phenotype as in the case of AJC1.7.

Immunostaining. Spores (10^3/ml) were inoculated with 0.5 ml MM on sterile coverslips for 12 to 24 h at room temperature (RT). Cells were fixed for 30 min with formaldehyde and digested for 1 h using digestion solution (Glucanex, β-D-glucanase, lyticase, and Driselase in Na-phosphate buffer with 50% egg white), washed with PBS, incubated in −20°C methanol for 10 min, and blocked with Tris-buffered saline–Tween 20 (TBST) plus 5% skim milk before incubation with the first monoclonal antibody (anti-gamma-tubulin T6657 at 1:500; Sigma-Aldrich) in TBST overnight at 4°C. Next, cells were washed and incubated with the Alexa Fluor^{546}-labeled goat anti-mouse secondary antibody (A11003 at 1:200 in TBST; Molecular Probes) for 1 h at RT. Cells were washed and mounted on microscope slides (with VECTASHIELD mounting medium with DAPI [4′,6-diamidino-2-phenylindole]), sealed with nail polish, and stored at 4°C overnight in the dark before microscopy.

RESULTS

Identification of gamma-tubulin and GcpC^{Alp6} at septal MTOCs and interaction of ApsB with gamma-tubulin. A. nidulans ApsB has been localized at SPBs and at septa, suggesting the presence of MTOCs at septa (Fig. 1) (35). MTOCs are large protein complexes which consist of several proteins, gamma-tubulin, and associated gamma-tubulin complex proteins, which are mostly conserved from yeast to humans (26). Un-
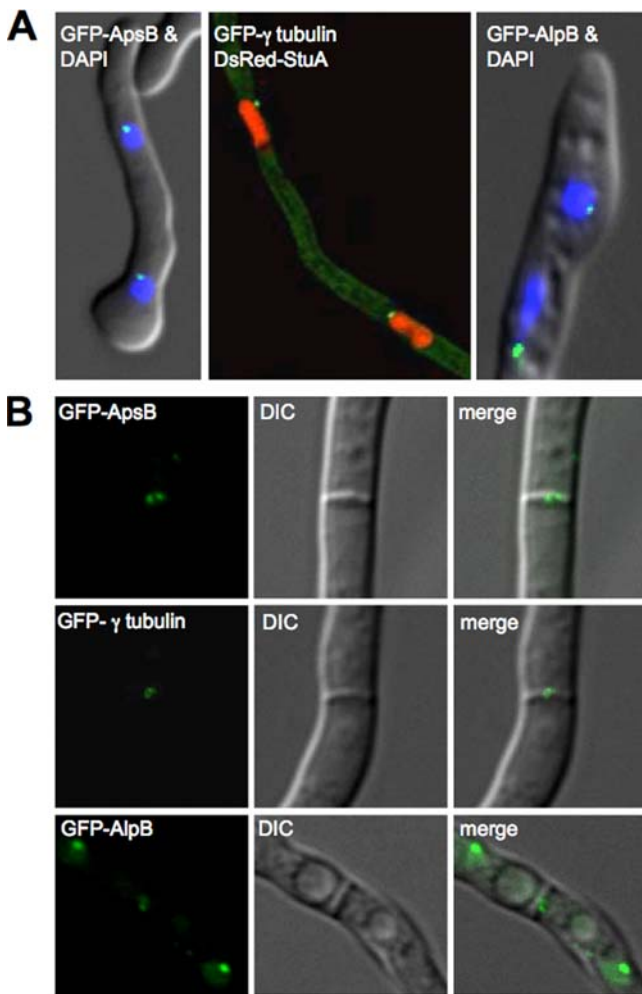
FIG. 1. Gamma-tubulin and AlpB localize to septal MTOCs. (A) GFP-ApsB, GFP–gamma-tubulin, and AlpB^Alp6-GFP localize to the SPBs. Nuclei are stained with DsRed-StuA(NLS) (SNZ22) or DAPI. (B) Localization of the same GFP-tagged proteins to the septal pore (two spots in the center). Fluorescence (left), differential interference contrast (DIC, middle), and merged (right) microscopic images are shown. The strains used were SNZ59 (GFP-ApsB), SNZ61 (GFP–gamma-tubulin), and SNZ-SH80 (AlpB^Alp6-GFP). All proteins were expressed from their natural promoters.

fortunately, the most important protein of MTOCs, gamma-tubulin, has not been identified at septa of *A. nidulans* before. In our own experiments, we were able to detect a very weak signal at septa when gamma-tubulin was expressed from its own promoter and fused to GFP. In *S. pombe*, it has also been reported that gamma-tubulin was present at nonnuclear MTOCs in very small amounts and thus was also not easy to detect (29). To further elucidate the composition of septal MTOCs, we searched the *A. nidulans* genome for a homologue of *S. pombe* Alp6 (*S. cerevisiae* Spc98, human Gcp3) and identified the open reading frame AN4867 (968 amino acids in length) with 35% identity to Alp6. In order to localize the corresponding protein, we constructed a C-terminal GFP fusion protein expressed from the native promoter and transformed it into *A. nidulans* (SO451). The protein localized to MTOCs at nuclei and at septa, indicating that the two MTOCs

also share this protein (Fig. 1). During the course of our experiments, this gene was analyzed in the laboratory of B. Oakley and was named *gcpC* (40).

In order to demonstrate that ApsB and gamma-tubulin colocalize at MTOCs, we visualized gamma-tubulin in a GFP-ApsB-expressing strain (Fig. 2A). Next, we showed that ApsB not only colocalizes but also interacts with gamma-tubulin. To this end, we applied the BiFC assay system and fused full-length ApsB with the N-terminal part of YFP and full-length gamma-tubulin with the C-terminal part of YFP. Corresponding *A. nidulans* strains showed a YFP signal at nuclei and at septa (Fig. 2B). Interestingly, we also found a fluorescence signal at the tips of all actively growing hyphae (Fig. 2C). Previously, ApsB had already been found at the hyphal tip and growing MTs were also reported to originate from the hyphal tip in some cases (16, 35). Gamma-tubulin alone was not visible at the hyphal tip, probably due to the high cytoplasmic background. Some cytoplasmic spots were also observed, as shown before for ApsB alone (35). Control experiments with ApsB or gamma-tubulin alone did not result in any fluorescence.

The ApsB–gamma-tubulin interaction result was confirmed by coimmunoprecipitation using hemagglutinin (HA)-ApsB and GFP–gamma-tubulin tagged proteins. Gamma-tubulin was detected in the precipitate obtained with anti-HA antibodies (Fig. 2D).

ApsB is associated with peroxisomes. To further analyze the role of ApsB, we employed a yeast two-hybrid analysis. The cDNA of *apsB* was cloned into pGBT9 (pRS89) and transformed into PJ69-4A. This strain was used as a recipient strain for a yeast two-hybrid gene bank kindly provided by S. Osmani (24). Besides ApsB itself, we identified five putative interacting clones (three unknown proteins, one Zn^{2+} finger protein, and one putative nucleoside transporter). The translation product of one of the clones displayed sequence identity to *A. nidulans* HexA, the homologue of the *N. crassa* Hex-1 protein (15). To prove the interaction between ApsB and HexA, we cloned the full-length *hexA* gene and tested it in the interaction screen. A yeast strain of mating type **a** (AH109) containing the GAL4 binding domain with *apsB* (Y2HapsB-BD) was crossed to a yeast strain of mating type α (Y187) containing the GAL4 activation domain with *apsB* (Y2HapsB-AD), *hexA* (Y2HhexA-AD), or just the empty vector (pGAD424) as a control. Diploids were identified by selective growth on YEPD agar medium lacking leucine and tryptophan (YEPD LT⁻) (Fig. 3A), as described by Cagney et al. (2). To look for positive protein-protein interactions, colonies were subsequently inoculated onto YEPD medium lacking leucine, tryptophan, and histidine (YEPD LTH⁻) (Fig. 3B). This medium allows growth only if the strains produce their own histidine due to a positive interaction of the respective proteins. Colonies with *apsB*/*apsB* and *apsB*/*hexA* grew well in comparison to the *apsB*/empty-vector combination. The weak background growth was reduced by the addition of 3 mM 3-amino-1,2,4-triazole (3-AT) (Fig. 3C). The positive interaction was confirmed with the β-Gal assay on membranes. ApsB interacted with itself, as well as with HexA, while in combination with the empty vector no reaction occurred (Fig. 3D). To exclude the possibility that neither HexA nor ApsB has an intrinsic affinity for other proteins and gives false positives in the yeast two-hybrid assay, we tested both of
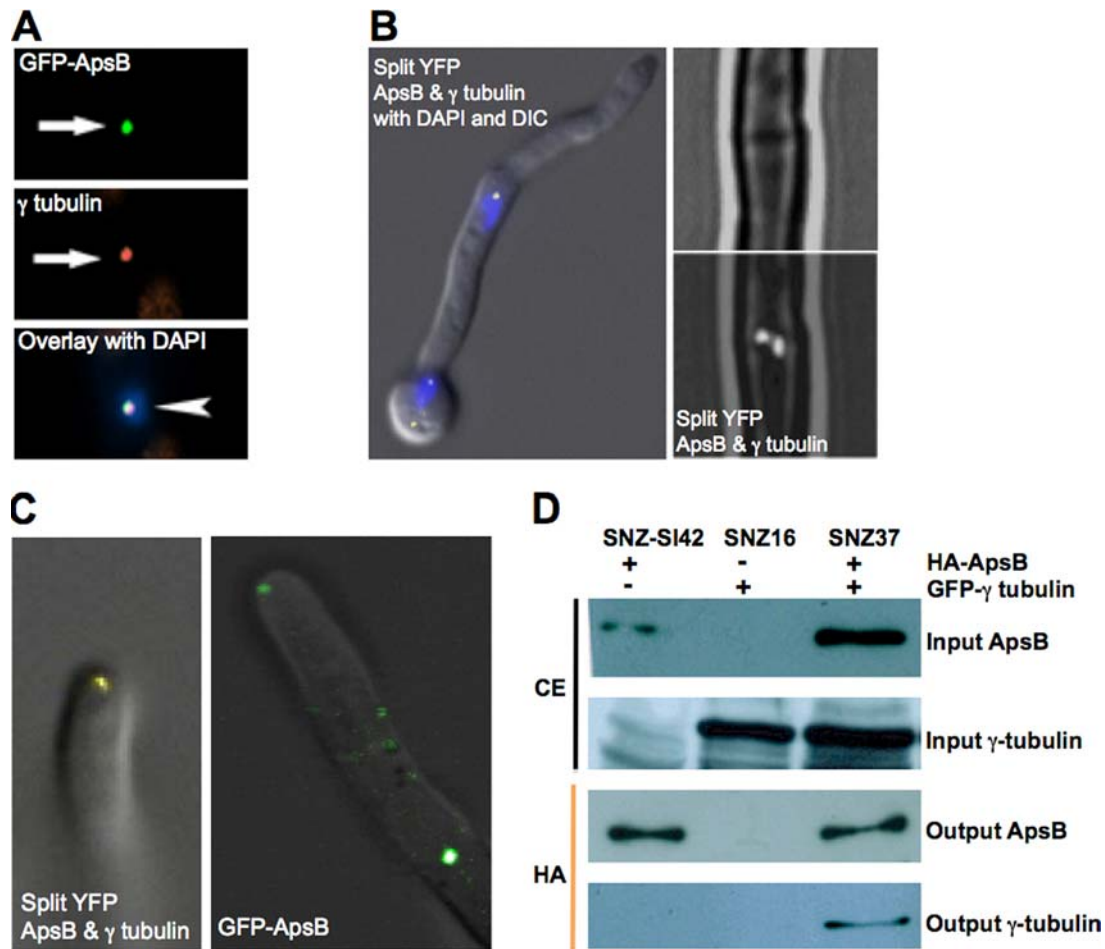
FIG. 2. Colocalization and interaction of ApsB with gamma-tubulin. (A) Colocalization of GFP-ApsB and gamma-tubulin using secondary immunofluorescence to detect gamma-tubulin with Alexa-Fluor[546]-labeled secondary antibodies. (B) BiFC of ApsB and gamma-tubulin (SNZ11). Fluorescent signals, indicating an interaction between ApsB and gamma-tubulin, were found at the SPBs (left) and to the center of septal pores as two spots (right). The upper image is a differential interference contrast (DIC) picture, and the lower image is a fluorescent picture merged with the upper DIC picture. (C) Fluorescent signals of interacting ApsB with gamma-tubulin (BiFC) and of GFP-ApsB in the hyphal tip. (D) Confirmation of the ApsB–gamma-tubulin interaction by coimmunoprecipitation. SNZ37 [*alcA(p)::apsB::3×HA alcA(p)::GFP::γtubulin*[1.8]] was used for this assay, and SNZ-SI 42 [*alcA(p)::3×HA::apsB*[3.2]] and SNZ16 [*alcA(p)::GFP::γtubulin*[1.8]] were the control strains. Anti-HA antibodies (clone 16B12 derived from a mouse; Hiss Diagnostics, Freiburg, Germany) were used for immunoprecipitation. Precipitation was performed in 1 ml crude extract (CE) of approximately 10 mg/ml total protein and 50 μl protein G-agarose (Roche, Mannheim, Germany). Western blot detection was done with anti-GFP antibodies (anti-GFP N terminus, derived from a rabbit, product G1544; Sigma-Aldrich, Munich, Germany) in the case of gamma-tubulin and with the anti-HA antibodies (clone 16B12) in the case of ApsB.

them and the empty vector against a library of *Treponema pallidum* with 73 different proteins (kindly provided by P. Uetz) (not shown). Growing on YPED LTH⁻, the empty vector produced three strains (4%) with a false-positive reaction, which were also seen for *apsB* and *hexA*. Despite these, no positive interaction with any of the remaining 70 *T. pallidum* proteins was found, indicating that neither ApsB nor HexA interacts randomly with given proteins and confirming that the HexA/ApsB interaction was specific. Sequence inspection of ApsB revealed a putative peroxisomal targeting sequence (PTS2), KIRDLEKQL, at amino acid positions 66 to 74. Likewise, proteins with sequence similarity to ApsB (29), such as mto1 (formerly known as mod20 or mbo1) and pcp1 (*S. pombe*), NCU02332.1 and NCU02411.1 (*N. crassa*), and AAH46878 (*Drosophila melanogaster*) and CDK5RAP2

(*Homo sapiens*) all have a possible PTS2, as identified with the software program psort (http://psort.hgc.jp/).

ApsB localizes to a subclass of peroxisomes. To obtain further proof of the peroxisomal localization of ApsB, we compared its localization with the localization of the peroxisomal enzyme AcuE (acetate-malate synthase). This protein was tagged with GFP (strain TALX207-10, kindly provided by M. Hynes and A. Andrianopoulos, Melbourne, Australia) and coexpressed in a strain with mRFP1-ApsB (strain SDV70b). Fourteen percent of the spots showed green and red fluorescence (Fig. 4A). In addition, we analyzed GFP-AcuE and mRFP1-tagged HexA (SDV78c), which confirmed the localization of mRFP1-HexA to peroxisomes (Fig. 4B). However, one important difference between ApsB and HexA was the frequency of colocalization with AcuE. While HexA and AcuE
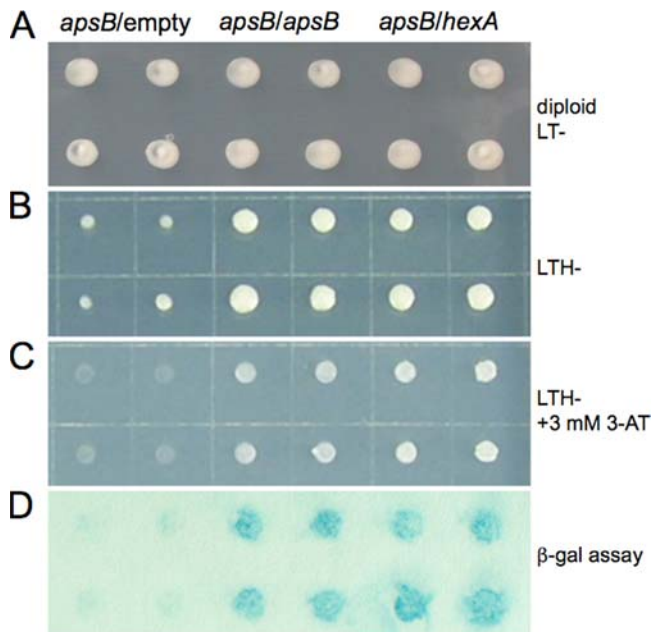
FIG. 3. Interaction of HexA and ApsB in the yeast two-hybrid system. (A) After crossing of Y2HapsB-BD with pGAD424 (empty vector), Y2HapsB-AD (*apsB*), or Y2HhexA-AD (*hexA*), diploids were grown on YEPD agar lacking leucine and tryptophan. Four colonies of each strain are shown for each combination. From here, colonies were inoculated onto selective YEPD medium lacking leucine, tryptophan, and histidine, which supports growth only in the case of interaction (B). (C) The same as in panel B but with the addition of 3 mM 3-AT to reduce background growth. (D) β-Gal assay of the colonies shown in panel A.

had about 95% hits, ApsB and AcuE showed only 14% colocalization, indicating that ApsB was transported only to a subclass of peroxisomes. In addition, we determined the frequency of mRFP1-ApsB and GFP-HexA colocalization to 10% (Fig. 4C). Similar results were obtained with *S. macrospora*, where Pro40 also colocalized only partially with HexA (5). An interaction between ApsB and HexA in *A. nidulans* was also shown *in vivo* using the BiFC assay system in strains coexpressing the N-terminal half of YFP (YN) fused to *hexA* and the C-terminal half of YFP (YC) fused to *apsB* or the other way around (Fig. 4D). ApsB-HexA colocalizing spots were found in the cytoplasm and at some septa (10%). To obtain a clearer picture of the ApsB and HexA structures at septa, we used deconvolution and laser-scanning spinning-disc microscopy. ApsB appeared normally as two spots in the center of the septal pore, whereas HexA localized normally on each side of the pore (Fig. 5). In three-dimensional (3D) reconstruction pictures, the spots appeared with a longer shape along the rim of the septum. Time course experiments revealed that ApsB colocalized with the constricting ring during septation (Fig. 6). These data show that at septa ApsB does not localize to peroxisomes or the Woronin body but rather the putative MTOC is embedded in the membrane of the septal pore.

Mutation of the peroxisomal target sequence in ApsB leads to HexA-like localization at septa. In order to test the functionality of the PTS2 sequence in ApsB, we mutated the consensus sequence ($Q^{73}L$ and $L^{74}R$) and fused the modified ApsB protein with GFP (pDV43). The construct (GFP-
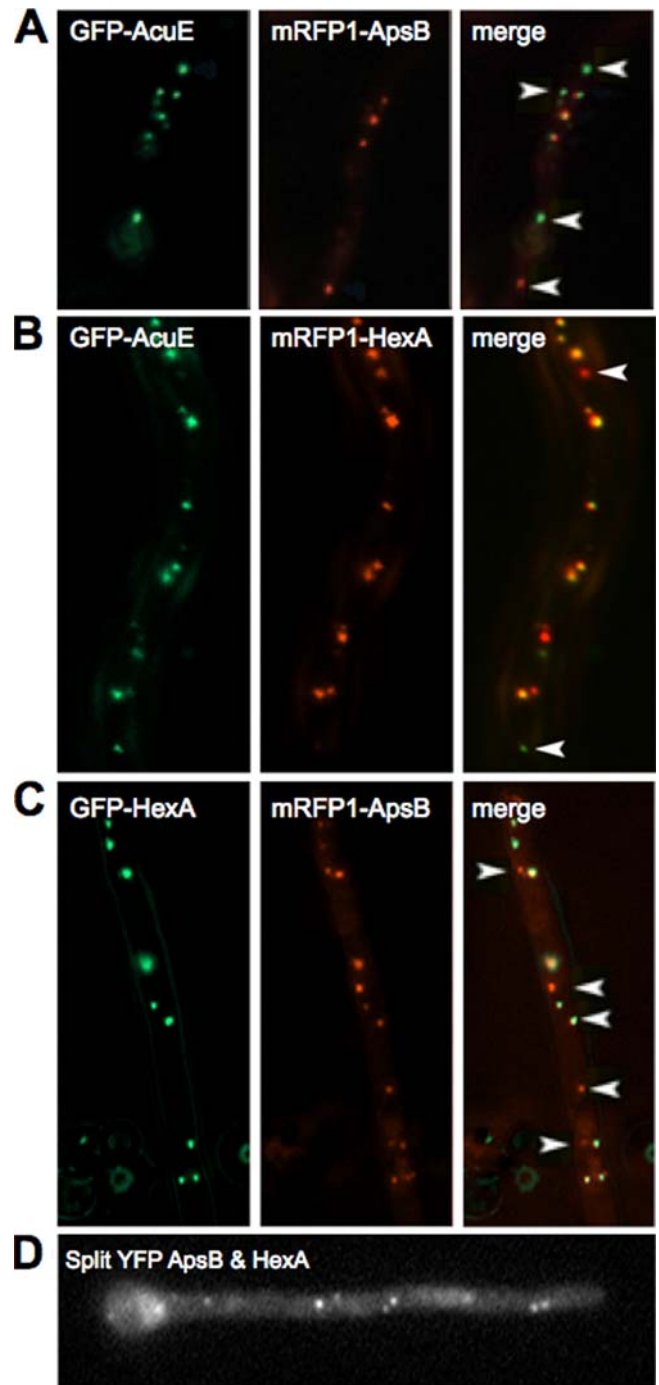

FIG. 4. ApsB localizes to a subclass of peroxisomes. (A) mRFP1-ApsB colocalized with GFP-AcuE, a peroxisomal enzyme, at a frequency of 14%, while the remaining 86% did not colocalize (arrowheads). The strain is SDV70b. (B) mRFP1-tagged HexA colocalized with GFP-tagged AcuE (SDV78c) in 95%. Only 5% of the spots were either GFP or mRFP1 labeled (arrowheads). (C) Colocalization of GFP-HexA and mRFP1-ApsB (SDV49-4). The frequency of colocalization was about 10%. (D) Bimolecular fluorescence complementation assay of HexA and ApsB (strain SDV42). Identical results were obtained with strain SDV43.
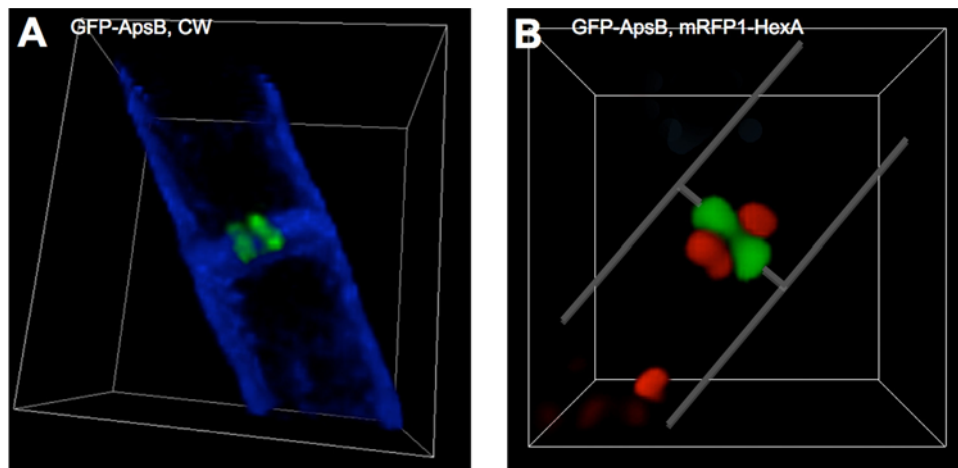
FIG. 5. Comparison of the septal localization of ApsB and HexA. (A) GFP-ApsB appeared as two spots in the center of the septal pore. The cell wall (CW) was stained with Calcofluor white M2R (fluorescent brightener 28 [F3543]; Sigma-Aldrich, Munich, Germany) at a 1:1,000 dilution for 5 min. A 3D view was captured with Zeiss AxioImager Z1 and AxioVision software (V4.5). (B) Double staining of ApsB and HexA. GFP-ApsB appeared as two spots in the center of the septal pore, whereas HexA localized on each side of the pore (three spots in the image). The cell wall is indicated by a line. A 3D view was captured with a Zeiss Cell Observer SD confocal microscope and AxioVision software (V4.5). The strains are SEa3 (A) and SDV73 (B).

ApsB_PTS2mut) was first transformed into wild-type *A. nidulans* strain TN02A3 (resulting in SDV77) and then introduced into strains in which either *hexA* was deleted (SDV79) or *apsB* was mutated (SDV80) or both *hexA* and *apsB* were deleted (SDV95). In strain SDV77, the localization pattern of GFP-ApsB_PTS2mut at SPBs and at cytoplasmic spots looked like that of wild-type GFP-ApsB (Fig. 7A). However, it was sur-
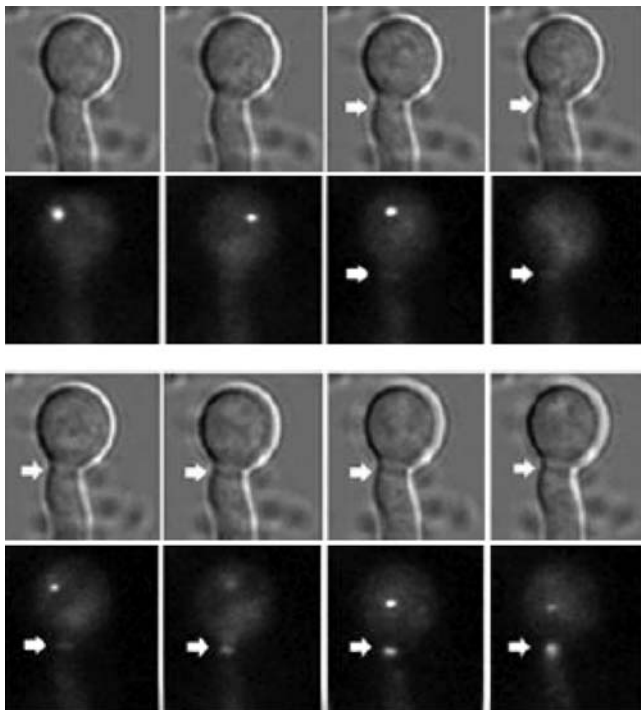

FIG. 6. ApsB follows the constricting ring during septum formation. Time course study of GFP-ApsB in strain SEa3 during septation. The pictures shown were taken at 5-min intervals.

prising to find that the localization of GFP-ApsB_PTS2mut at septa (Fig. 7C) did not show the normal localization of GFP-ApsB (Fig. 7B) but resembled in 70% of the cases the pattern of GFP-HexA (Fig. 7D), whereas in 22% of the cases it was similar to the GFP-ApsB localization. These localization patterns could be achieved through a piggyback import mechanism of GFP-ApsB_PTS2mut along with HexA or ApsB, which were still present as fully functional proteins in SDV77. Only in a strain lacking both ApsB and HexA (SDV95), the specific localization of the mutated ApsB protein was lost at septa (Fig. 7E). The results obtained with the last strain clearly argue for a role for peroxisomes in the transport of ApsB to septal MTOCs. It remains to be elucidated how the assembly of the MTOC at septa occurs.

The PTS2 motif of ApsB is important for asexual spore formation. To test whether the altered localization pattern of GFP-ApsB_PTS2mut at septa prevents its biological function, we analyzed if the mutated ApsB protein is able to complement the oligosporogenic phenotype produced by an *apsB* mutation. Therefore, we transformed ApsB [*alcA*(*p*)::*GFP*::*apsB*] and the PTS2-mutated ApsB protein (GFP-ApsB_PTS2mut) into strain AJC1.5 (*apsB6*). Under repressing conditions (glucose), all three strains showed brown colonies, due to the reduced numbers of spores, which is typical for *apsB* mutant strains (4, 32). Under inducing conditions (glycerol or sorbitol), however, wild-type ApsB protein was able to complement the oligosporogenic phenotype (spores were produced), while PTS2-mutated ApsB did not complement it (Fig. 8A and B).

As we previously described, ApsB is important for the production of MTs at sMTOCs (35). Therefore, we wanted to know if the failure of PTS2-mutated ApsB to complement the oligosporogenic phenotype was due to an inability to restore the MTOC activity at septa. In a GFP-ApsB_PTS2mut strain with GFP-labeled MTs and an *apsB6* background, the number of MTs was similar to the number of MTs in *apsB* mutant strains (data not shown). Therefore,
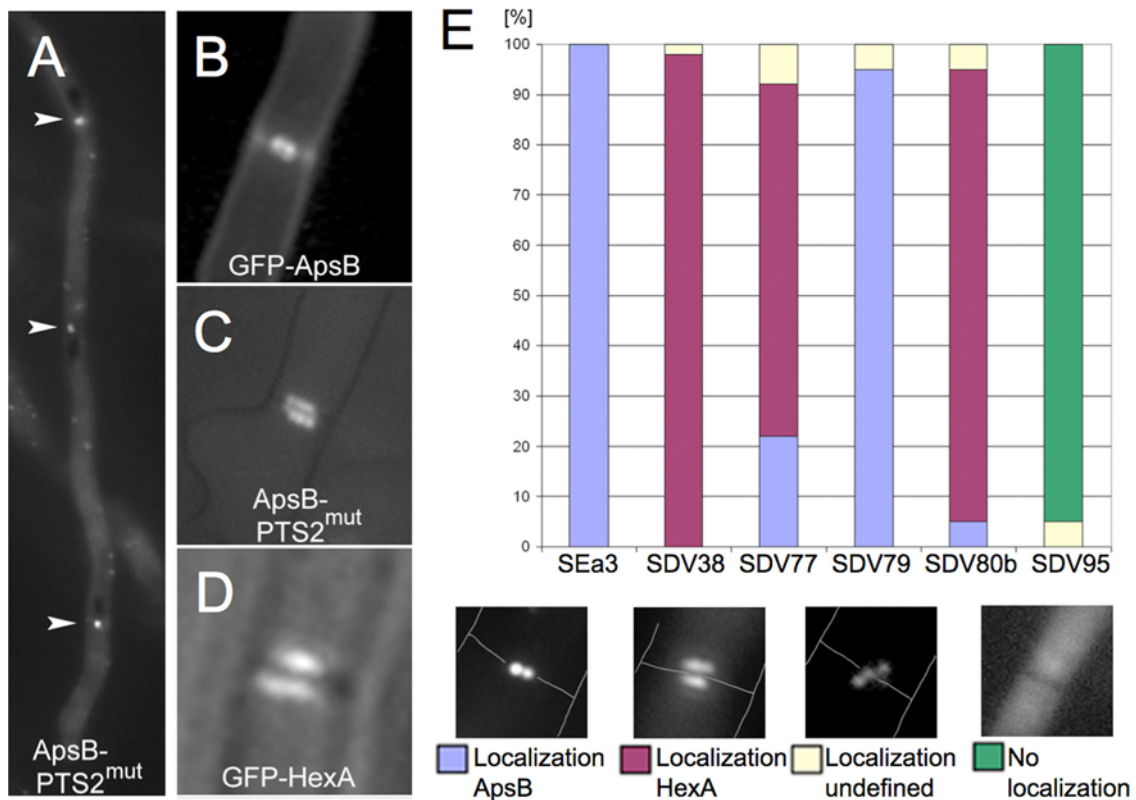
FIG. 7. Mutagenesis of PTS2 of ApsB. (A) GFP-ApsB_PTS2^{mut} localized to SPBs (arrowheads) and to cytoplasmic spots in SDV77 (genotype). At septa, the localization pattern resembled the pattern of GFP-ApsB or GFP-HexA, depending on the genetic background (B to E). (B) GFP-ApsB in the wild type (SEa3). (C) ApsB-PTS2^{mut} in SDV 77. (D) GFP-HexA in the wild type (SDV38). (E) Quantification of septal localization patterns. We determined the localization patterns of GFP-ApsB_PTS2^{mut} in the presence of a wild-type copy of ApsB and in the absence of HexA (SDV79), in the presence of a wild-type copy of HexA and a mutated copy of ApsB (*apsB6*) (SDV80b), in the presence of both proteins (SDV77), or in the absence of both proteins (SDV95). The pictures illustrate the localization patterns.

we assume that PTS2 of ApsB is important for its function at septa.

Next we tested if the function of PTS2-mutated ApsB can be restored by adding a PTS1 targeting sequence (SRL) at the C terminus of ApsB. We transformed PTS2-mutated ApsB with the PTS1 signal fused to the C-terminal part of the protein (GFP-ApsB_PTS2^{mut}_SRL) expressed from the *alcA* promoter into strain AJC1.7 (*apsB10*), resulting in SNZ34, and into *apsB* deletion strain (SRS24), resulting in SNZ94. The *apsB10* mutation converts codon 83 into a stop codon, and thus the mutant lacks most of the 1,052-amino-acid-long ApsB protein (data not shown). The transformed plasmids were integrated ectopically. Transformants of both strains (SNZ34 and SNZ94) appeared with the brown *apsB* mutant-like phenotype under repressing conditions (glucose) and a wild-type-like, spore-producing phenotype under inducing conditions (sorbitol). These results suggest that the ApsB-PTS1 protein was able to complement the developmental phenotype (Fig. 8).

DISCUSSION

In this paper, we show that ApsB interacts with gamma-tubulin at SPBs, at septa, at the tips of growing hyphae, and in spot-like structures in the cytoplasm. This is the first evidence

for the presence of gamma-tubulin at septa and in the hyphal tip region. We had evidence before that MTOCs exist at septa, but the nature of these MTOCs remained elusive (35). Our new results show that at least two other proteins associated with nuclear MTOCs exist in septal MTOCs, GcpC and the crucial protein gamma-tubulin. These findings are in agreement with the recent localization of GcpC (40). However, it is still unclear if sMTOCs share more or all proteins with nuclear MTOCs or whether specific proteins exist only at one or the other place. The biggest unsolved question is still the anchorage of sMTOCs. Structurally, the nuclear MTOC of *S. cerevisiae* has been studied the best and recently similar results were obtained with *A. gossypii* (14, 18, 19). It is likely that the situation is similar in *A. nidulans* and that nuclear MTOCs are embedded in the nuclear envelope. However, structural information about sMTOCs is still missing. Our fluorescence microscopy studies indicate that the MTOC appears as two dots inside the septal rim. The structure is clearly different from that of Woronin bodies at septa. Sometimes the two ApsB dots appeared to be connected through a third small dot. This has been described before in *S. pombe* for the equatorial MTOCs (eMTOCs), which are also characterized by the ApsB-homologous protein mto1 (formerly named mod20 or mbo1) (10, 29). In this yeast species, MTs are generated from nuclear MTOCs, eMTOCs, and interphase MTOCs (10, 28). The importance of
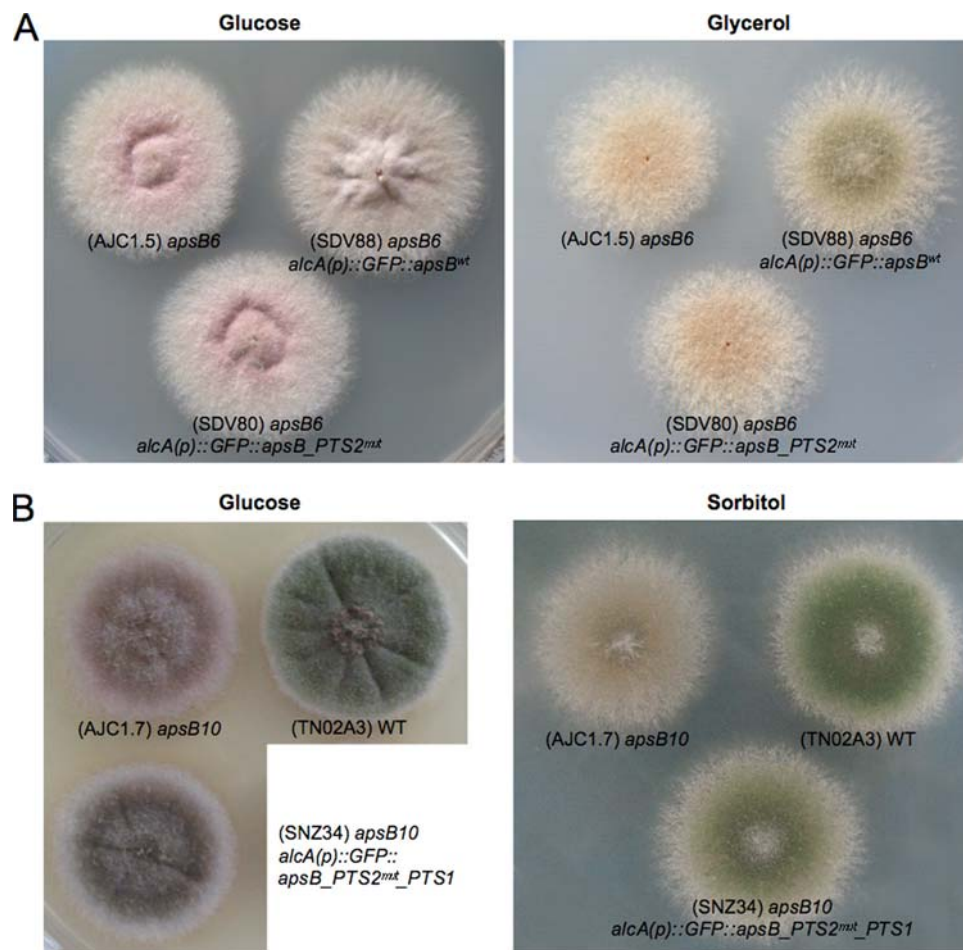
FIG. 8. The peroxisomal target sequence of ApsB is important for complementation of the oligosporogenic phenotype of *apsB* mutants. (A) Transformation of an *apsB6* mutant strain with wild-type *apsB* or the mutated *apsB* forms (strains SDV88 and SDV80, respectively). The constructs were expressed from the *alcA* promoter. It is repressed on glucose and derepressed on glycerol. (B) Transformation of an *apsB10* mutant strain with a mutated version of *apsB* in which a PTS1 sequence was added at the C terminus. Wild-type (WT) strain TN02A3, an *apsB* mutant strain (AJC1.7, *apsB10*), and the transformed strain (SNZ34) were grown on glucose and under inducing conditions on sorbitol.

non-nucleus-associated MTOCs was nicely demonstrated in enucleate cells (3).

We also identified the ApsB–gamma-tubulin interaction in the tips of growing hyphae. This is also the first evidence for gamma-tubulin in the hyphal tip. In comparison, in the chytridiomycete *Allomyces macrogynus*, gamma-tubulin has been identified as a component of the Spitzenkörper (21). Further evidence that gamma-tubulin may be functional in the hyphal tip comes from our observation that some MTs emanate from the hyphal tip and grow into the cytoplasm (16). We speculated at the time that either MTs which did not stop growth after reaching the hyphal tip or MT fragments close to the hyphal tip could be the origin of polymerization. However, our new results point to the possibility that MTOCs exist in the apical region of the hypha.

Several lines of evidence show that the spot-like appearance of ApsB and the ApsB–gamma-tubulin interaction are due to peroxisomal localization: colocalization with AcuE and HexA and the drastic reduction of the number of cytoplasmic spots in a *pexC* mutant. One very strong argument is the importance of the PTS2 sequence and the rescue of the PTS2 mutation by the

addition of a PTS1 sequence to the C terminus. The nonfunctionality of ApsB with a mutated PTS2 sequence could still be explained by the fact that this region appears to be evolutionarily conserved from yeast to humans (29), but the rescue of the mutation by the addition of the PTS1 sequence speaks clearly against this possibility. We envisage three possible explanations for the role of the peroxisomal localization. (i) Peroxisomes serve as hosts for sMTOCs. (ii) Peroxisomes catalyze a reaction that is required for MTOC function at the septum and is ApsB dependent. (iii) Peroxisomes serve as transport vehicles for sMTOC-associated proteins. Our results point to a transport function for peroxisomes. In agreement with such a role is the observation of fast-moving mto1 (ApsB) spots in *S. pombe* (29). These structures could represent peroxisomes. However, many open questions remain to be solved, e.g., how the proteins are further recruited from the peroxisomes to the sMTOCs. Against all three possibilities speaks the observation that the septal localization of ApsB and sMTOC function in mutants with defects in PTS1 or PTS2 peroxisomal protein import or in *pexC* mutants lacking peroxisomes appeared sim-

ilar to the situation in the wild type (results not shown). However, it has to be considered that the *pexC* mutant strain displays pleiotropic phenotypes and that the possibility of a piggyback import mechanism might mask the possible effects of PTS1 or PTS2 defects (12).

From our results we conclude that ApsB defines a new class of peroxisomes that is—besides the Woronin bodies—the second example of peroxisomes as organelles with a function beyond metabolic pathways (30).

REFERENCES

1. **Buller, A. H. R.** 1931. Researches on fungi. Hafner Publishing Co., New York, NY.
2. **Cagney, B., P. Uetz, and S. Fields.** 2000. High-throughput screening for protein-protein interactions using the two-hybrid assay. Methods Enzymol. **328:**3–14.
3. **Carazo-Salas, R. E., and P. Nurse.** 2006. Self-organization of interphase microtubule arrays in fission yeast. Nat. Cell Biol. **8:**1102–1107.
4. **Clutterbuck, A. J.** 1994. Mutants of *Aspergillus nidulans* deficient in nuclear migration during hyphal growth and conidiation. Microbiology **140:**1169–1174.
5. **Engh, I., C. Würtz, K. Witzel-Schlömp, H. Y. Zhang, B. Hoff, M. Nowrousian, H. Rottensteiner, and U. Kück.** 2007. The WW domain protein PRO40 is required for fungal fertility and associates with Woronin bodies. Eukaryot. Cell **6:**831–843.
6. **Gabaldón, T., B. Snel, F. van Zimmeren, W. Hemrika, H. Tabak, and M. A. Huynen.** 2006. Origin and evolution of the peroxisomal proteome. Biol. Direct **1:**8.
7. **Gould, S. J., G. A. Keller, N. Hosken, J. Wilkinson, and S. Subramani.** 1989. A conserved tripeptide sorts proteins to peroxisomes. J. Cell Biol. **108:**1657–1664.
8. **Hayashi, M., and M. Nishimura.** 2003. Entering a new era of research on plant peroxisomes. Curr. Opin. Plant Biol. **6:**577–582.
9. **Heiland, I., and R. Erdmann.** 2005. Biogenesis of peroxisomes. FEBS J. **272:**2362–2372.
10. **Heitz, M. J., J. Petersen, S. Valovin, and I. M. Hagan.** 2001. MTOC formation during mitotic exit in fission yeast. J. Cell Sci. **114:**4521–4532.
11. **Hill, T. W., and E. Käfer.** 2001. Improved protocols for *Aspergillus* minimal medium: trace element and minimal medium salt stock solutions. Fungal Genet. Newsl. **48:**20–21.
12. **Hynes, M. J., S. L. Murray, G. S. Khew, and M. A. Davis.** 2008. Genetic analysis of the role of peroxisomes in the utilization of acetate and fatty acids in *Aspergillus nidulans*. Genetics **178:**1355–1369.
13. **James, P., J. Halladay, and E. A. Craig.** 1996. Genomic libraries and a host strain designed for highly efficient two-hybrid selection in yeast. Genetics **144:**1425–1436.
14. **Jaspersen, S. L., and M. Winey.** 2004. The budding yeast spindle pole body: structure, duplication, and function. Annu. Rev. Cell Dev. Biol. **20:**1–28.
15. **Jedd, G., and N.-H. Chua.** 2000. A new self-assembled peroxisomal vesicle required for efficient resealing of the plasma membrane. Nat. Cell Biol. **2:**226–231.
16. **Konzack, S., P. Rischitor, C. Enke, and R. Fischer.** 2005. The role of the kinesin motor KipA in microtubule organization and polarized growth of *Aspergillus nidulans*. Mol. Biol. Cell **16:**497–506.
17. **Kovacs, W. J., S. Krisans, S. Hogenboom, R. J. Wanders, and H. R. Waterham.** 2003. Cholesterol biosynthesis and regulation: role of peroxisomes. Adv. Exp. Med. Biol. **544:**315–327.
18. **Lang, C., S. Grava, M. Finlayson, R. Trimble, P. Philippsen, and S. L. Jaspersen.** 2010. Structural mutants of the spindle pole body cause distinct alterations of cytoplasmic microtubules and nuclear dynamics in multinucleated hyphae. Mol. Biol. Cell **21:**753–766.
19. **Lang, C., S. Grava, T. van den Hoorn, R. Trimble, P. Philippsen, and S. L. Jaspersen.** 2010. Mobility, microtubule nucleation and structure of microtubule-organizing centers in multinucleated hyphae of *Ashbya gossypii*. Mol. Biol. Cell **21:**18–28.
20. **Maruyama, J., P. R. Juvvadi, K. Ishi, and K. Kitamoto.** 2005. Three-dimensional image analysis of plugging at the septal pore by Woroinin body during hypotonic shock inducing hyphal tip bursting in the filamentous fungus *Aspergillus oryzae*. Biochem. Biophys. Res. Commun. **331:**1081–1088.
21. **McDaniel, D. P., and R. W. Roberson.** 1998. γ-Tubulin is a component of the Spitzenkörper and centrosomes in hyphal-tip cells of *Allomyces macrogynus*. Protoplasma **203:**118–123.
22. **Momany, M., E. Richardson, C. Van Sickle, and G. Jedd.** 2002. Mapping Woronin body position in *Aspergillus nidulans*. Mycologia **94:**260–266.
23. **Nayak, T., E. Szewczyk, C. E. Oakley, A. Osmani, L. Ukil, S. L. Murray, M. J. Hynes, S. A. Osmani, and B. R. Oakley.** 2006. A versatile and efficient gene targeting system for *Aspergillus nidulans*. Genetics **172:**1557–1566.
24. **Osmani, A. H., J. Davies, C. E. Oakley, B. R. Oakley, and S. A. Osmani.** 2003. TINA interacts with the NIMA kinase in *Aspergillus nidulans* and negatively regulates astral microtubules during metaphase arrest. Mol. Biol. Cell **14:**3169–3179.
25. **Purschwitz, J., S. Müller, and R. Fischer.** 2009. Mapping the interaction sites of *Aspergillus nidulans* phytochrome FphA with the global regulator VeA and the white collar protein LreB. Mol. Genet. Genomics **281:**35–42.
26. **Raynaud-Messina, B., and A. Merdes.** 2007. Gamma-tubulin complexes and microtubule organization. Curr. Opin. Cell Biol. **19:**24–30.
27. **Sambrook, J., and D. W. Russell.** 2001. Molecular cloning: a laboratory manual, 3rd ed. Cold Spring Harbor Laboratory Press, Cold Spring Harbor, NY.
28. **Samejima, I., P. C. C. Laurenco, H. A. Snaith, and K. E. Sawin.** 2005. Fission yeast mto2p regulates microtubule nucleation by the centrosomin-related protein mto1p. Mol. Biol. Cell **16:**3040–3051.
29. **Sawin, K. E., P. C. C. Lourenco, and H. A. Snaith.** 2004. Microtubule nucleation at non-spindle pole body microtubule-organizing centers requires fission yeast centrosomin-related protein mod20p. Curr. Biol. **14:**763–775.
30. **Schrader, M., and H. D. Fahimi.** 2008. The peroxisome: still a mysterious organelle. Histochem. Cell Biol. **129:**421–440.
31. **Suelmann, R., N. Sievers, and R. Fischer.** 1997. Nuclear traffic in fungal hyphae: *in vivo* study of nuclear migration and positioning in *Aspergillus nidulans*. Mol. Microbiol. **25:**757–769.
32. **Suelmann, R., N. Sievers, D. Galetzka, L. Robertson, W. E. Timberlake, and R. Fischer.** 1998. Increased nuclear traffic chaos in hyphae of *apsB* mutants of *Aspergillus nidulans*: molecular characterization of *apsB* and *in vivo* observation of nuclear behaviour. Mol. Microbiol. **30:**831–842.
33. **Swinkels, B. W., S. J. Gould, A. G. Bodnar, R. A. Rachubinski, and S. Subramani.** 1991. A novel, cleavable peroxisomal targeting signal at the amino-terminus of the rat 3-ketoacyl-CoA thiolase. EMBO J. **10:**3255–3262.
34. **Toews, M. W., J. Warmbold, S. Konzack, P. E. Rischitor, D. Veith, K. Vienken, C. Vinuesa, H. Wei, and R. Fischer.** 2004. Establishment of mRFP1 as fluorescent marker in *Aspergillus nidulans* and construction of expression vectors for high-throughput protein tagging using recombination in *Escherichia coli* (GATEWAY). Curr. Genet. **45:**383–389.
35. **Veith, D., N. Scherr, V. P. Efimov, and R. Fischer.** 2005. Role of the spindle-pole body protein ApsB and the cortex protein ApsA in microtubule organization and nuclear migration in *Aspergillus nidulans*. J. Cell Sci. **118:**3705–3716.
36. **Wanders, R. J.** 2004. Metabolic and molecular basis of peroxisomal disorders: a review. Am. J. Med. Genet. **126A:**355–375.
37. **Wanders, R. J., and H. R. Waterham.** 2006. Biochemistry of mammalian peroxisomes revisited. Annu. Rev. Biochem. **75:**295–332.
38. **Waring, R. B., G. S. May, and N. R. Morris.** 1989. Characterization of an inducible expression system in *Aspergillus nidulans* using *alcA* and tubulin coding genes. Gene **79:**119–130.
39. **Woronin, M.** 1864. Entwicklungsgeschichte der *Ascobolus pucherrimus* Cr. und einiger Pezizen. Abh. Senkenb. Naturforsch. **5:**333–344.
40. **Xiong, Y., and B. R. Oakley.** 2009. *In vivo* analysis of the functions of gamma-tubulin-complex proteins. J. Cell Sci. **122:**4218–4227.
41. **Yelton, M. M., J. E. Hamer, and W. E. Timberlake.** 1984. Transformation of *Aspergillus nidulans* by using a *trpC* plasmid. Proc. Natl. Acad. Sci. U. S. A. **81:**1470–1474.
42. **Yuan, P., G. Jedd, D. Kumaran, S. Swaminathan, H. Shio, D. Hewitt, N.-H. Chua, and K. Swaminathan.** 2003. A Hex-1 crystal lattice required for Woronin body function in *Neurospora crassa*. Nat. Struct. Biol. **10:**264–270.